IL
NUOVO CIMENTO
ORGANO DELLA SOCIETÀ ITALIANA DI FISICA
SOTTO GLI AUSPICI DEL CONSIGLIO NAZIONALE DELLE RICERCHE

VOL. XVI, N. 3 *Serie decima* 1° Maggio 1960

Cloud Chamber Evidence for the Presence of Simultaneous High Energy Nuclear-Active Particles at Mountain Altitudes.

S. NARANAN, R. RAGHAVAN, P. V. RAMANAMURTHY, B. V. SREEKANTAN and A. SUBRAMANIAN

Tata Institute of Fundamental Research - Bombay

(ricevuto il 12 Novembre 1959)

Summary. — In an examination of twenty two thousand pictures of penetrating showers recorded with a multiplate cloud chamber, (60 cm × 60 cm × 20 cm), in a time of operation of 5 310 hours, at an altitude of 2.2 km, thirtytwo cases have been obtained in each of which two or more simultaneous parallel high energy nuclear-electromagnetic cascades, (~ 100 GeV), are seen developing in the plates of the chamber. The visible energy of the individual cores has been determined by the track length method. It is found that in most of the cases the visible energies of the parallel cascades in a picture are of comparable magnitude. The separation between the cores ranges from 5 to 40 cm, and the corrected distribution looks flat. There is clear indication that about half of the events are associated with dense air showers. The « unassociated » events have been interpreted in terms of local nuclear interactions of particles of energy ⩾ 450 GeV in air up to a height of 140 meters above the apparatus. The « associated » events have been explained as being parts of air showers containing about 100 nuclear-active particles of energy ⩾ 100 GeV near the core.

1. – Introduction.

While scanning pictures of penetrating showers obtained with a multiplate cloud chamber operated at an altitude of 2.2 km, several cases were noticed of « simultaneous » parallel high energy cascades which had developed in the

plates of the chamber. A detailed analysis of these photographs showed that the events, in many respects, were similar to the « structure bursts » recorded by GRIGOROV *et al.* [1], at an altitude of 3.2 km, with crossed layers of ionization chambers under lead. The main features that make these « double core » events observed in the cloud chamber important are:

1) the parallel cascades are due to interactions of high energy nuclear-interacting particles of *comparable* energies (~ 100 GeV);

2) the frequency of occurrence of events with a separation < 40 cm over an area of 0.11 m^2, which is the area of the chamber, is not negligibly small; and

3) about 50 per cent of the « double core » events are associated with dense air showers as shown by the cloud chamber photographs.

An attempt at even a semi-quantitative understanding of these features of the « double core » events has led us to the conclusions that:

a) in high energy interactions (≥ 450 GeV), most of the energy is carried away by few secondaries with a ratio of maximum to minimum energy less than 7 to 8 and

b) extensive air showers of energy $\geq 10^{15}$ eV at mountain altitudes contain a number of nuclear active particles of high energy (~ 100 GeV) of the order of 100.

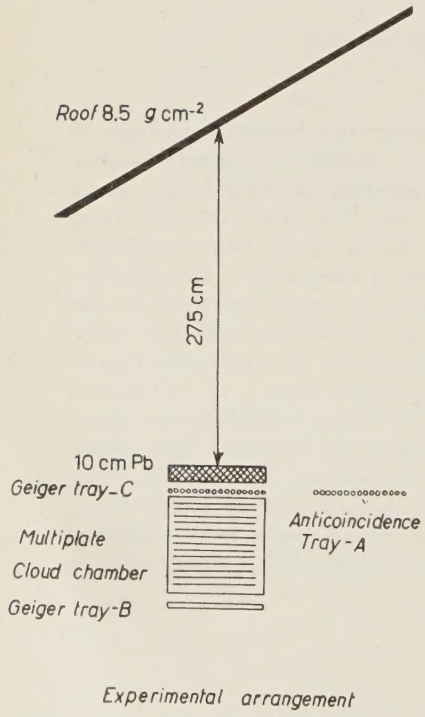

Fig. 1. – Experimental arrangement.

2. – Experimental arrangement.

The photographs were obtained with a multiplate cloud chamber of dimensions ($60 \times 60 \times 20$) cm^3, operated for a period of 2 years a Ootacamund at an altitude of 2.2 km above sea level. The chamber was triggered with a penetrating shower selection system. The details of the experimental arrangement are given in Fig. 1. The chamber was fitted with thirteen 1.25 cm lead plates for part of the time, and with thirteen 1.9 cm brass plates for the rest of the time.

[1] N. L. GRIGOROV, V. Y. SHESTOPEROV, V. A. SOBINYAKOV and A. V. POGURSKAYA: *Žu. Éksp. Theor. Phys.*, **33**, 1099 (1957).

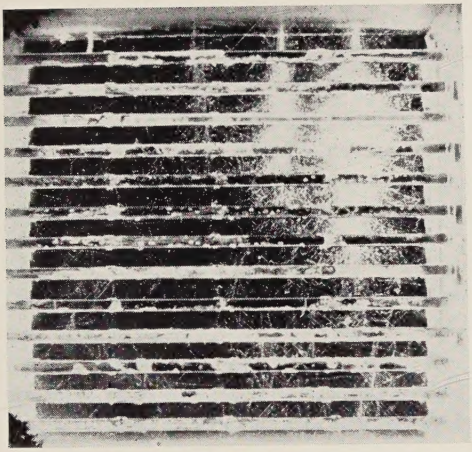

a)

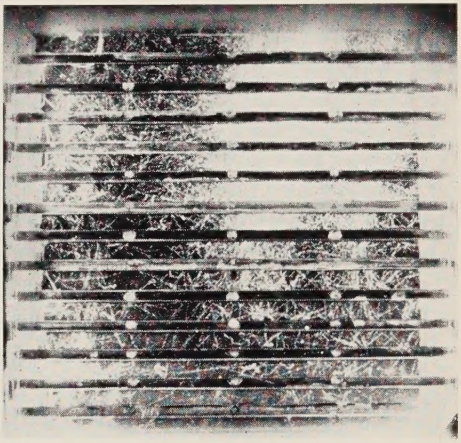

b)

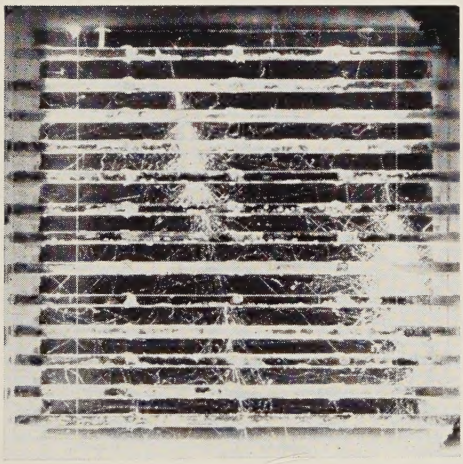

c)

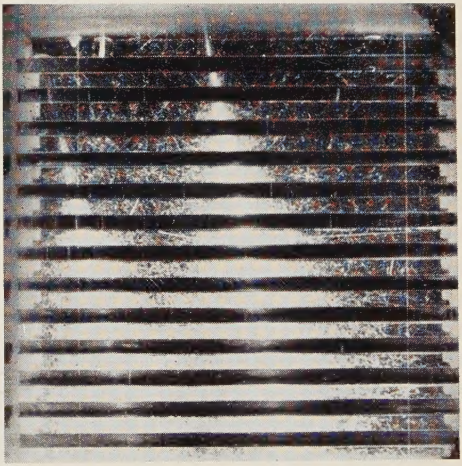

d)

Fig. 2. – *a*) Event No. OV 98. An event in which both the cores are in geometry and enter the chamber after being partly developed in the lead on the top. A third core of low energy can be seen on the left. Visible energy estimates: Left 26 GeV, Right 120 GeV. *b*) Event No. DM 32. An event in which both cores are in geometry and enter the chamber after being fairly well developed in the lead on top. Numerous electron tracks seen in the first few compartments, far from the cores, provide evidence for the association of the event with extensive air shower. Visible energy: Left 95 GeV, Right 55 GeV. *c*) Event No. TZ 143. An event in which both the nuclear-active particles interacted inside the chamber. Energy estimates: Left 21 GeV, Right 50 GeV. *d*) Event No. VI 100. A typical event in which the visible energies of the cores are very high. Visible energy estimates: Left 95 GeV, Right 185 GeV. (In this case the visible energies may be underestimated by as much as a factor 2. See text).

3. – Results.

3·1. *Frequency of events obtained.* – A total of 22 000 pictures of penetrating showers of energy ≥ 10 GeV were obtained. Nuclear interactions of energy ≥ 200 GeV were recorded with a frequency of about one a day. There were 32 cases in each of which two or more parallel high energy cascades were seen to have developed in the plates of the chamber; these are referred to hereafter as « double core » events (*). Cloud chamber photographs of four such typical events are shown in Fig. 2.

The total time of operation of the chamber was 5 310 h. For a period of 2 380 h, the chamber was operated in conjunction with an anticoincidence Geiger counter tray of area 0.3 m^2 placed at a distance of about a meter from the chamber. During this period 8 double core events were recorded. In the remaining 2 930 h, when the anti-tray was not in operation, as many as 24 such events were recorded.

3·2. *Lateral separation.* – The lateral separation of the cores varied from 5 cm to 40 cm, the mean value being 16 cm. The frequency distribution as a function of lateral separation looks flat, when corrected for the variation of the efficiency of detection with separation. Events with core separation less than 4 cm were discarded since in these cases the resolution into individual cores was difficult.

3·3. *Nature of the particles producing the cascade.* – Each event was examined stereoscopically to determine whether or not the axes of the cascades pass through the top 10 cm lead block (Fig. 1). All those cascades in which the axes were found to pass through 10 cm lead, were necessarily of nuclear origin, since in these cascades the number of electrons observed in the various compartments of the chamber were at wide variance with the number expected for remnants of pure electromagnetic cascades after 16 radiation lengths. In many of these cases, as also in most of the cases where the cores did not pass through the lead block, the emergence from the cores of heavily ionizing particles or penetrating particles provided direct evidence for the nuclear origin of the cascades.

3·4. *Energy estimates.* – The visible energies in the individual cores were estimated by the track-length method. The number of particles in each compartment was determined as follows: the *projected width* of complete saturation

(*) There are a few events with more than two cores. However, we designate all the events as double core events.

was first measured and a track density of 10 per mm was attributed to this width. For the other less dense regions, appropriate track densities were estimated visually and multiplied by the corresponding widths. The number of particles obtained by this method is naturally a lower limit, since the central saturated region for which a flat density has been ascribed may have a gradient. With a view to judge the extent of uncertainty due to this gradient, we re-evaluated the number of tracks assuming that they were distributed laterally as $1/r$ up to distances at which the number of tracks was small. For this case, it is easy to show that the total number of tracks in the shower in the compartment is given approximately by $2.5 w_i \cdot i$, where w_i is the width of the central region at the edge of which the projected ionization is i times the minimum ionization. This re-evaluation showed that, for cascades with a visible energy up 75 GeV, the correction needed was negligible compared to the uncertainties in the visual estimate, *i.e.* $\pm$ 25 per cent. In the case of very high energy cascades, (estimated visible energy $\geq$ 200 GeV), the estimated track length may be an underestimate by as much as a factor of two, and never more. However, we did not correct our visual estimates by the above method because it involves an assumption of a lateral distribution whose validity may be questioned.

To obtain the visible energies of the cascades, the track length was multiplied by 34 MeV per radiation length for lead plate pictures (*) and by 36 MeV per radiation length for brass plate pictures. Our energy estimates may be regarded as absolute lower limits and not likely to be in error in absolute values by more than a factor of two in the extreme cases. As we shall see later on, the conclusions drawn in this paper do not depend on the absolute values of energy so much as on the lower limits of the energy values. In the Table, we have listed the visible energies of the two cores for all the observed events.

There is no way of knowing whether a particular cascade had been initiated by a nucleon or a pion. So all the events were analyzed assuming the two possibilities. The energy of the particle was obtained by multiplying the visible

(*) There is some confusion in the literature about the value to be used for lead. According to BENDER [2] it is 34 MeV per radiation length. HAZEN [3] gives a value of 25 MeV per radiation length, which may be said to be not in disagreement with Bender's. But HINOTANI *et al.* [4] and DANILOVA *et al.* [5] arrive at a figure of 25 MeV per cm of lead, which means a value of about only 15 MeV per radiation length. However, in these latter experiments, the primary energies were obtained from calculated shower curves which may be in error.

(2) P. A. BENDER: *Nuovo Cimento*, **2**, 980 (1955).

(3) W. E. HAZEN: *Phys. Rev.*, **99**, 911 (1955).

(4) K. HINOTANI, K. SUGA and Y. TANAKA: *Journ. Phys. Soc. Japan*, **9**, 883 (1954).

(5) T. V. DANILOVA, O. I. DOVZHENKO, S. I. NIKOLSKI and T. V. RAKABOLSKAYA: *Žu. Éksp. Theor. Phys.*, **34**, 541 (1958).

TABLE. I. – *Visible energy estimates of cores.*

Event No.	Visible energy of cores in GeV		Remarks
	Higher	Lower	
UD 253	29	21	« Unassociated events »
XJ 40	84	41	
XS 64	58	21	
TS 81	33	31	
BB 128	90	55	
CL 35	63	49	
RP A	160	19	
YG 20	25	24	
BS 81	271	187	« Associated events »
BW 15	53	40	
CA 84	200	81	
WZ 96	36	13	
BN 53	68	56	
RQ 51	80	14	
TZ 143	50	21	
VI 100	185	95	
TG 94	40	21	
RZ 51	49	19	Both cores out of geometry.
DM 32	195	55	Events obtained with the anti-coincidence tray in operation.
OV 98	120	26	
OX 98	66	56	
SZ 288	39	21	
CT 81	36	14	Events which could arise from interactions in the roof.
IY 128	12	10	
IZ 174	36	12.5	
KB 18	40	9.5	
PW 51	28	9	
RC 127	10	10	
RD A	89	21	
SJ 144	25	10	
VD 74	9.2	5.3	
XV 18	6.6	5.7	

energy of the cascade by a factor of 4, when the particle producing the cascade was considered to be a nucleon, and by a factor of 2, when the particle was considered to be a pion. These factors were obtained on the assumption that the inelasticity is 0.5 in the collision of nucleons with lead or brass nuclei and 1 in the case of collisions of pions. The possible contribution to the visible energy from the π^0's produced by subsequent collisions of secondary charged pions was also taken into consideration, in arriving at these conversion factors.

3·5. *Classification of events.* – As shown in Fig. 1, there was a roof over the cloud chamber at a height of about 275 cm, with an equivalent thickness of 8.5 g cm^{-2}, and composed of only light elements. The cascades observed in the chamber were normally dense and broad and so the parallelism could be judged to an accuracy of only 2 to 3°. Therefore some of the cascades may in reality be slightly convergent and arise from the particles produced in high energy interactions in the roof. We have separated the possible « roof » events from those that have occurred outside from considerations of the estimated energy, the separation of the cores and *upper limits* to the transverse momenta, *i.e.* 1 GeV/c for pions and 3 GeV/c for nucleons. This classification is not sensitive to the nature of the particles producing the cores, whether they are pions or nucleons. It turns out that not more than 10 events can be attributed to secondaries arising from interactions in the roof. This category is mostly made up of the very low energy events (see Table).

Out of the remaining 22 events, 18 were obtained when the anti-tray was not in operation, and only 4 when the anti-tray was in operation. In order to avoid any bias due to the selection system, we shall, in what follows, consider only those events which were obtained when the anti-tray was not in operation. Out of the 18 events, 17 were such that at least one of the two cascades passed through the top lead block. There was only one case, in which neither of the cores passed through the top lead. We shall ignore this, since it does not satisfy the triggering requirement. Of the 17 events, in 9 cases the cloud chamber photographs showed association of the events with rather dense ($\geqslant 100$ particles m^{-2}) air showers. The air shower density is a conservative estimate in view of the presence of a 10.5 cm lead layer on top of the chamber. Hereafter, we shall refer to these events as « associated events ». In the remaining 8 events, either the association was weak (density $\leqslant 20$ particles m^{-2}) or there was no association at all. We shall call these as « unassociated events » for the purposes of discussion.

4. – Discussion.

4·1. « *Unassociated* » *double core events.* – As seen from the Table, the visible energies of individual cores of unassociated double core events vary from

19 GeV to 160 GeV. However, the ratio of the visible energies of simultaneous parallel cascades is in all cases less than 3, except in one instance in which the ratio is about 8. These cascades, as previousiy pointed out, cannot be pure electromagnetic cascades, and must arise as a result of the collision of nuclear interacting particles, like nucleons and pions, with lead or brass nuclei as the case may be. In order to release visible energies of more than 19 GeV, a nuclear-interacting particle must have an energy greater than 38 GeV if it is a pion and greater than 76 GeV if it is a nucleon, (see previous Section 3·4). These pions and nucleons may arise in collisions—hereafter referred to as *local interactions*—of higher energy primary particles with air nuclei in a layer of air above the chamber. The maximum separation of the cores, observable in this experiment, is about 40 cm; this naturally restricts the height at which the interaction could have occured in the air. We can, however, fix within broad limits, for each observed event, the potential range of heights in which the interaction could have taken place. For this we have used the estimated energies of the two cores and assumed values fo 270 MeV/c and 500 MeV/c (*) for the transverse momenta of pions and nucleons respectively. The broad limits defining the range of heights come from the limits ((4 ÷ 40) cm), for the observable separation of the cores. From this the mean height of interaction was obtained as 140 metres and the amount of matter for interaction ~ 14 g cm^{-2}. The question arises whether the observed number of unassociated double core events can be quantitatively explained in terms of interactions in this 14 g cm^{-2} of air; for this we need to know the efficiency for the detection of double core events and the flux of high energy particles at the level of observation. The efficiency depends on the separation between the cores and the probabilities of interaction in the lead block and in the plates of the chamber. The separation varies from 4 to 40 cm and the mean value is 16 cm. But as already pointed out, the frequency distribution of events as a function of lateral separation is flat and so the true mean separation of the double cores may be much larger than 16 cm. However, an upper limit to the efficiency of detection is obtained by considering the mean separation as 16 cm. Nuclear interactions taking place in the top few cm of the lead block will not be detected since the cascades produced will die down before reaching the chamber. We have considered therefore only 5 cm of lead immediately above the chamber as the effective producing layer, in addition

(*) The potential height at which interactions could have occured depends sensitively on the *lower limits* to the transverse momenta assumed. For the purposes of the present estimate, we have assumed that the distribution of transverse momenta for pions is flat between 200 MeV/c and 500 MeV/c which gives a weighted mean value of 270 MeV/c. For nucleons we have used an effective mean value of about twice the transverse momentum for pions, which we think is reasonable in the absence of more exact information on the transverse momenta for nucleons.

to the plates inside the chamber. For interactions in the plates, the survival probability through the top lead block has to be taken into account, for those cascades for which the axes pass through the top lead. From all such considerations we arrive at an upper limit of 0.06 for the overall efficiency for the detection of double core events in the chamber. This efficiency means that if 100 pairs of nuclear interacting particles arrive with a mean separation of ~ 16 cm, with one of the nuclear interacting particles in the solid angle defined by the chamber, then 6 cases of double events will be observed in the chamber. Actually 8 cases have been observed, in a time of operation of 2380 hours, over an area of 0.11 m^2, within a solid angle of 0.5 sr. This means there must have been at least 128 pairs of nuclear-interacting particles incident during this time. From this we can deduce the flux of particles that should have passed through the 14 g cm^{-2} of air and produced nuclear interactions which gave rise to these 128 pairs. This flux comes out to be $1.4 \cdot 10^{-3}$ m^{-2} s^{-1} sr^{-1}. This value corresponds to the flux of nuclear-active particles of energy $\geqslant 450$ GeV, at our height of observation, as deduced from the frequency of single interactions in the cloud chamber during the same operating period and as also deduced from the observations—at a higher altitude—of ČUDAKOV *et al.* [6] corrected suitably for the altitude difference. It was noted that about 15 per cent of the single nuclear interacting particles at these energies were associated with dense air showers. So, only 85 per cent of the flux was taken into account when making the comparison with the flux of particles responsible for the unassociated double core events.

If we now try to understand the double core events in terms of the interactions of particles of energy $\geqslant 450$ GeV we immediately come to the conclusion that this is possible only if in a majority of the collisions the primary energy is carried away by a few secondary particles (including the follow-through nucleon). Only then can we get particles of comparable energy (within a factor of 7) and of such high energy. This conclusion is valid whether the cores are assumed to be produced both by pions only, or one by a nucleon and the other by a pion. If one of the cores is due to the follow-through nucleon then the inelasticity in the primary interaction has necessarily to be $> 12\%$. It is unlikely that in the majority of cases both the cores are produced by nucleons, since this involves the production of nucleon and anti-nucleon pairs in local collisions, for which the primary energy has to be much higher and for which the flux would be too small. The possibility of closely spaced comparable energy nucleons coming from the fragmentation of heavy primaries, particularly α-particles, can also be ruled out purely from flux considerations. The conclusion drawn by us regarding the nature of inter-

[6] A. E. ČUDAKOV, N. A. DOBROTIN, N. L. GRIGOROV, G. N. VERNOV and G. T. ZACEPIN: *Suppl. Nuovo Cimento*, **2**, 737 (1958).

actions of particles of energy ≥ 450 GeV, *i.e.* that the energy must be carried away by a few secondaries in a majority of the collisions, finds support in the recent results on the analysis of high energy jets with nuclear emulsions (7).

4·2. *Associated double core events.* – The nine associated double core events cannot arise from *local interactions* (see Section **4**·1) of unassociated high energy nuclear interacting particles, since the observed density of the associated air showers cannot be developed in a few grams of air. As pointed out before, the flux of single nuclear-interacting particles associated with air showers is only 15 per cent of the total flux. So, not more than one or two events can arise from the *local interactions* of associated nuclear-active particles. The associated double core events must then essentially be due to the nuclear-interacting particles in the cores of air showers. We know that the particles responsible for the observed cores have energies of ~ 100 GeV. Purely from considerations of transverse momentum, nuclear-interacting particles of about this energy will be spread out in a circular area with a radius of ~ 3 metres around the core. This being the case, the probability of two nuclear active particles arriving with a separation less than 40 cm is quite small, unless the number of nuclear active particles of this energy is very high. This number may be estimated as follows:

Let A denote the area over which nuclear-active particles, with energy required to produce the observed cascades, are spread out in air showers. We shall assume that the density is uniform over this area; for the present calculations and magnitudes considered, this assumption is not greatly in error. Let σ be the area of detection of the chamber. If F is the number of air showers incident over the area in the period of operation, the number of single core events in the chamber is given by

$$S = F\varepsilon_s \exp\left[-\frac{\sigma n}{A}\right]\frac{\sigma n}{A},$$

where ε_s is the efficiency of detection of single core events and n is the number of nuclear-active particles in the air showers. The number of double core events (as defined previously by us) in the chamber will be given by

$$D = F\varepsilon_D\left\{1 - \exp\left[-\frac{\sigma n}{A}\right]\left(1 + \frac{\sigma n}{A}\right)\right\},$$

where ε_D is the efficiency for detecting double core events. Since we know the values of S, D, ε_s, ε_D and σ we can deduce the value of (n/A), the density

(7) C. F. Powell « *Nuclear Processes at super-high energies* », Mimeographed report, Kiev Conference on High Energy Physics (1959).

of nuclear-active particles necessary to account for the observed ratio of single core events to double core events. We get

$$n/A = 3.6^{+1.0}_{-1.25} \quad \text{particles/m}^2 .$$

From this, to get at the total number of nuclear-active particles contained in the showers, we have to fix A. If we assume that the high energy nuclear active particles are mostly pions, with an energy $\geqslant 100$ GeV—necessary to produce the observed cores—they will be spread over a circular area of radius ~ 3 metres for an assumed transverse momentum of 400 MeV/c. If the nuclear active particles are nucleons, their mean energy has to be 200 GeV and if we assume a transverse momentum of 1 GeV/c, they have to be distributed over an area of radius ~ 3.5 m. The value of A can therefore be taken as ~ 30 m^2 Then n will be $70 \div 140$.

This calculation is based on the average behaviour of air showers, *i.e.* that on the average the particles are spread over a circular area of certain radius and the showers contain a definite number of nuclear active particles n. However, there may be wide fluctuations in the nature of collisions, in the transverse momenta acquired by the particles and in the number of nuclear-interacting particles produced; it is also possible that there are close correlations at production between pairs of particles. Some of the double core events might as well be the result of such wide fluctuations. However, we find that the ratio of the number of double core events to the number of single core events, (after correcting for detection efficiencies) is as high as 0.4. This gives us confidence that the application of an average picture may not be wrong.

From the frequency of observed events we may say that showers containing about 100 high energy nuclear-active particles at a mountain altitude of 2.2 km, correspond to primary energies of $\geqslant 10^{15}$ eV at the top of the atmosphere. Unfortunately, there are no experimental results at mountain altitude which tell us the number of nuclear-active particles of high energy (~ 100 GeV), in air showers. The experiments of ABROSIMOV *et al.* [8] at sea level, show that showers of size $3 \cdot 10^5 < N < 2 \cdot 10^6$ contain as many as 55 nuclear-active particles of energy above 100 GeV within a radius of 6 metres from the core.

As pointed out in the introduction, GRIGOROV *et al.* [1] have observed the so-called « structure bursts » which are similar to our double-core events. However, the energies of the events observed by them are higher, as also the altitude of observation. They have interpreted their events in terms of purely local interactions of nuclear-active particles of energy ($10^{12} \div 10^{13}$) eV. The ob-

[8] A. T. ABROSIMOV, V. A. DMITRIEV, G. V. KULIKOV, E. I. MASSALSKY, K. I. SOLOVYOV and G. B. KHRISHTIANSEN: *Žu. Èksp. Theor. Phys.*, **36**, 751 (1959).

served association with dense air showers is attributed to the development of cascades which arise from the decays of π^0-mesons produced in the same local high energy interactions. In our case, all the events cannot be attributed to local interactions only since, as already emphasized, the observed densities of associated air showers cannot be developed in a few grams of air and the flux of high energy single nuclear-active particles associated with dense air showers is much too small to account for the associated double core events.

Regarding the nature of local interactions, the conclusions of GRIGOROV *et al.* are similar to ours, *i.e.* that in high energy collisions in air the primary energy is carried away by a few secondary particles.

* * *

We have great pleasure in thanking His Excellency BISHNURAM MEDHI, the Governor of Madras, for putting at our disposal laboratory space at Raj Bhavan, Ootacamund. We are thankful to Professor M. G. K. MENON for his interest in this investigation and for helpful discussions. The cloud chamber photographs used in this investigation were obtained in connection with an experiment on S-particles, and we are indebted to Mr. A. B. SAHIAR who initiated the project on S-particles in the Institute. We wish to express our thanks to Mr. SIDDESWAR LAL for his valuable help during the course of the experiment and the analysis. Our thanks are also due to Messrs. A. R. APTE and K. F. DINSHAW for their help in running the chamber.

RIASSUNTO (*)

Esaminando 22 000 fotografie di un uno sciame penetrante ottenute con una camera a nebbia con molte lastre (60 cm × 60 cm × 20 cm), in 5313 ore di funzionamento, ad una altitudine di 2200 m, si sono riscontrati 32 casi in ciascuno dei quali si vedono svilupparsi nelle piastre della camera una o più cascate nucleari-elettromagnetiche parallele simultanee di alta energia (~ 100 GeV). L'energia visibile dei singoli cores è stata determinata col metodo della lunghezza della traccia. Si trova che nella maggioranza dei casi le energie delle cascate parallele visibili nella stessa fotografia sono di grandezza paragonabile. La separazione fra i cores va da 5 a 40 cm, e la distribuzione corretta appare piana. Vi sono chiare indicazioni che circa la metà degli eventi sono associati a sciami densi dell'aria. Gli eventi « non-associati » sono stati interpretati in termini di interazioni nucleari locali di particelle di energia ≥ 450 GeV in aria sino ad un'altezza di 140 m al di sopra dell'apparecchio. Gli eventi « associati » sono stati interpretati come facenti parte di sciami dell'aria contenenti circa 100 particelle nucleari attive di energia $\geqslant 100$ GeV vicino al core.

(*) *Traduzione a cura della Redazione.*

IL NUOVO CIMENTO Vol. XVI, N. 3 1° Maggio 1960

Cloud Chamber Study of Extensive Air Showers.

T. Gémesy, T. Sándor and A. Somogyi

Central Research Institute of Physics of the Hungarian Academy of Sciences - Budapest

(ricevuto il 16 Novembre 1959)

Summary. — Measurements were carried out by means of a multi-plate cloud chamber controlled by an extensive air shower arrangement in order to check the authors' earlier results concerning the transition effect of the extensive air showers as well as to determine a more precise value of the photon/electron ratio.

Introduction.

A few years ago we started measurements by means of GM-counters of the transition effect of extensive air showers in lead in order to determine the photon/electron ratio in extensive air showers.

Investigated the transition effect turned out, however, to depend markedly on the dimensions and geometry of the apparatus. As a consequence the transition effect cannot give but a rough information on the photon/electron ratio in air showers ([1,2]).

For this reason we began measurements with a cloud chamber so as to check the results obtained with the GM-counter method and to determine at the same time more precisely the photon/electron ratio in question.

The cylindrical cloud chamber with an effective area of 300 cm² was con-

([1]) L. Jánossy, T. Sándor and A. Somogyi: *Acta Phys. Hung.*, **6**, 455 (1957).
([2]) A. Somogyi: *Acta Phys. Hung.*, **7**, 189 (1957).

trolled by the four-fold coincidence system of four GM-counters, each having an effective surface of 320 cm^2.

The geometry of the system is to be seen in Fig. 1.

Inside the chamber there were 7 lead plates, the three upper ones had a thickness of 3 mm, the four lower ones that of 6 mm each.

Some of the preliminary results have already been published ([3]). The results obtained this way may be summarized as follows.

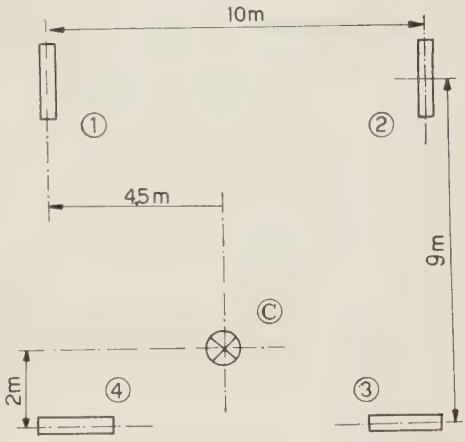

Fig. 1. – General layout of the apparatus.
① ② ③ ④: GM-counters;
©: cloud chamber.

1. – The photon-electron ratio.

The number of electron pairs counted on the photographs gave the number of the incident photons on the chamber, and the single tracks starting outside the number of electrons. Among the 4342 photographs evaluated we found in this way the total number of photons to be 3521 and that of electrons 3164. Accordingly we obtained for the photon/electron ratio

$$\alpha = 1.13 \pm 0.03 .$$

Considering as photons also single tracks emerging from one of the lead plates without any visible track entering, the ratio becomes

$$\alpha = 1.44 \pm 0.07 .$$

The latter result is based on the evaluation of 820 photographs only.

The errors given above are exclusively of statistical nature. According to a rough calculation the errors due to the geometry of the apparatus may be neglected. We estimated also the number of photons penetrating all the seven plates without giving rise to any visible secondary particle.

([3]) I. Dohán, T. Gémesy, T. Sándor and A. Somogyi: *Acta Phys. Hung.*, **9**, 97 (1958).

Assuming each of the photons to have an energy equal to the critical energy in air, *i.e.* 84 MeV, the numerical values of the photon/electron ratio given above increase by about 3% .

The agreement between the experimental data and the figures predicted by the electromagnetic cascade theory is remarkable.

We also studied the question whether the photon/electron ratio is dependent on the shower density. No significant dependence was found in the density range (30÷200) particles/m².

2. – The transition effect.

We investigated the transition effect in two different ways.

a) We plotted the number N_i of the photographs showing at least one visible track between the plates i and $i-1$ against i (Fig. 2). (Numerical values of N_i are shown in Table I.) This curve ought to be of the same shape as the transition curve. The cloud chamber curve in Fig. 2 has no maximum whereas the curves obtained in the earlier measurements with the same four sets of GM-counters in the same position showed a pronounced maximum at about 7 mm of lead (1).

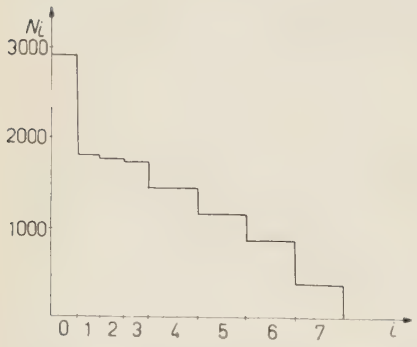

Fig. 2. The number of photographs (N_i) which show at least one ionizing particle between the plates i and $i+1$, plotted against i.

b) We counted the number of particle groups between the plates i and $i+1$ on each photograph taking as an « electron group » a group of tracks which originates from a single electron and as a « photon group » particles originating from a single electron pair.

Denoting the total number of « electron-groups » and of « photon-groups » on the 4342 evaluated photographs by E_i and P_i respectively, we obtained the results given in Table I.

TABLE I.

$i=$	0	1	2	3	4	5	6	7
$N_i=$	2918	1811	1756	1735	1432	1150	855	366
$E_i=$	3967	2122	1506	1041	601	393	270	121
$P_i=$	—	998	1431	1735	1483	1158	883	282
$E_i+P_i=$	3987	3120	2937	2776	2084	1551	1103	403

The values $E_i + P_i$ are plotted in Fig. 3. Apart from statistical fluctuations they are proportional to the probabilities $e_i + \alpha p_i$, here e_i represents the probability that an electron entering the top plate penetrates i lead plates or produces a secondary ionizing particle penetrating the lead plate i. Similarly, p_i stands for the probability of a photon-produced secondary ionizing particle penetrating plate i.

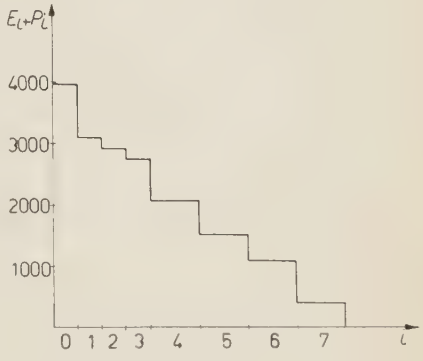

Fig. 3. – The total number of electron- and photon-produced particle groups $(E_i + P_i)$ between the plates i and $i+1$, obtained from all photographs, plotted against i.

According to GM-counter measurements the expression $e(d) + \alpha p(d)$ shows a maximum at about $d = 7$ mm of lead, in contrast to the curve of Fig. 3, which does not reveal any maximum. (If a maximum existed at all, it should belong to a thickness $d < 3$ mm of lead.)

No definite answer could be given hitherto as to the reason for these contradictions. Perhaps they are due to the experimental conditions being quite different in the case of the cloud chamber and GM-counters, resp. Recently, a new type of measurement was started to check this assumption. Another explanation would be the existence of low-energy electrons visible on the cloud chamber photographs but not detected by the GM-counters. Indeed, the cloud chamber has a lower energy threshold for electrons than have the GM-counters used in our experiments. It does not seem, however, probable that the whole discrepancy can be explained in this way.

RIASSUNTO (*)

Si sono effettuate misurazioni a mezzo della sistemazione di una camera a nebbia con molte lastre pilotata da un dispositivo per sciami estesi dell'aria per controllare i precedenti risultati degli autori relativi all'effetto di transizione degli sciami estesi dell'aria e per determinare un valore più preciso del rapporto fotone/elettrone.

(*) *Traduzione a cura della Redazione.*

IL NUOVO CIMENTO Vol. XVI, N. 3 1° Maggio 1960

On the Physical Interpretation of Complex Poles of the S-Matrix - I.

G. Beck

Centro Brasileiro de Pesquisas Físicas - Rio de Janeiro

H. M. Nussenzveig (*)

Instituut voor Theoretische Fysica - Utrecht

(ricevuto il 16 Dicembre 1959)

Summary. — To improve the usual treatment of the transient behaviour of continuous systems by the « method of complex eigenvalues », it is necessary to take into account the excitation conditions. This is done by considering initial-value problems. Three examples are investigated: 1) a harmonic oscillator coupled with a vibrating string; 2) the electromagnetic oscillations of a perfectly conducting spherical antenna; 3) the scattering of Schrödinger particles by a hard sphere. In each case, the general solution of the initial-value problem is related to the « method of complex eigenvalues » by associating a propagator with each pole of the S-matrix. In this way, the difficulty of exponential growth, which occurs in the usual treatment, is eliminated, and the dependence of the decay law on the excitation is exhibited. For Schrödinger particles, the spreading of wave packets restricts the domain of validity of the exponential decay law. The origin of the « transient modes » which are associated with the poles of the S-matrix is discussed. It is shown that the antenna modes originate from the effect of inertial forces. The limitations on the physical interpretation in the case of short-lived modes are emphasized.

1. – Introduction.

It is well known that the transient behaviour of a discrete system, such as an electric network with lumped parameters or a mechanical system with a finite number of degrees of freedom, is closely related to the « complex eigen-

(*) On leave of absence from Centro Brasileiro de Pesquisas Físicas.

frequencies » of the system. Let us consider, for instance, an electric network with lumped parameters. Its response to a time-harmonic excitation may be described by giving a characteristic function of the network (steady-state admittance or impedance) as a function of the frequency. This function usually has an analytic continuation with poles in the « complex-frequency » plane. The poles are associated with the « free modes of oscillation » of the network. The response of the network to inhomogeneous initial conditions (given charges in the capacitors or currents in the inductors), in the absence of external driving functions, is a superposition of these modes, with amplitudes determined by the initial conditions. The poles also play an important role in the determination of the response of the network to an arbitrary excitation, including external driving functions [1].

The « method of complex eigenvalues » is also employed in the theory of transients in continuous systems, but the situation is far less satisfactory in this case. Perhaps the earliest example is Thomson's treatment [2] of the electromagnetic oscillations of a perfectly conducting sphere. Thomson's « natural modes of oscillation » satisfy the requirement of containing only outgoing radiation. They are associated with the « complex eigenfrequencies » $\omega_n = \omega_n' - i\gamma_n$, $\gamma_n > 0$ $(n = 1, 2, ...)$, with a corresponding time factor $\exp[-i\omega_n t]$. According to Thomson, ω_n' represents the frequency, and γ_n the damping constant, associated with the n-th natural mode. All the modes are strongly damped. The same method was applied by Abraham [3] to a thin, perfectly conducting, prolate spheroid. The damping is much weaker in this case.

Thomson's method was criticized by Lamb [4], on the ground that the solutions are not bounded at infinity. In fact, Thomson's modes behave like $r^{-1} \exp[-i\omega_n(t - r/c)]$ at large distances from the sphere, so that they increase exponentially for $r \to \infty$. This « exponential catastrophe » is a characteristic feature of such damped, purely outgoing waves, since the field at large distances was in the neighbourhood of the source at a correspondingly remote time. As was pointed out by Lamb, the difficulty is related to the unphysical assumption that the modes have been in existence for an indefinitely long time. It may be overcome by taking into account the excitation conditions, as was shown by Lamb in an example.

Some illustrations of this point in connection with Thomson's problem were given by Love [5]. He considered the case in which the initial field around

---

[1] M. F. Gardner and J. L. Barnes: *Transients in Linear Systems* (New York, 1942).
[2] J. J. Thomson: *Proc. Lond. Math. Soc.*, **15** (1), 197 (1884).
[3] M. Abraham: *Ann. Phys.*, **66**, 435 (1898).
[4] H. Lamb: *Proc. Lond. Math. Soc.*, **32** (1), 208 (1900).
[5] A. E. H. Love: *Proc. Lond. Math. Soc.*, **2** (2), 88 (1904).

the sphere is identical to an electrostatic multipole field. This gives rise to an outgoing disturbance with a sharp front, which travels with the velocity of light. It was shown by LOVE that the field beyond the wave front remains undisturbed (so that there is no exponential catastrophe), whereas the field behind the wave front is a superposition of Thomson's modes with constant amplitudes. Thus, LOVE's paper shows the way to find a proper physical interpretation of Thomson's modes, for a particular type of excitation. However, it does not indicate how the results depend on the excitation.

The solution of Thomson's problem for an arbitrary initial field was given by HILL and GELBAUM ([6]), in the form of an expansion in stationary states. However, the connection between this form of the solution and Thomson's modes was not discussed.

The method of complex eigenvalues was introduced in quantum mechanics by GAMOW ([7]), in connection with the theory of α-decay. The « complex-energy wave functions » which correspond to Thomson's modes are associated with « decaying states ». The exponential catastrophe is also found in this case. Methods for dealing with this difficulty have been suggested in many papers. The usual method ([8-12]) is to consider the decay of a wave packet which is initially concentrated within the nucleus. For a Schrödinger particle, in contrast with the electromagnetic case, there is no limiting velocity, and an outgoing wave packet with a sharp front is impossible ([13]). What one tries to show, then, is that the wave function is very small for $r \gg vt$, and differs very little from the « wave function of a decaying state » for $r \ll vt$, where v is a mean velocity associated with the emitted particle. This has been done, however, only for special choices of the wave packet, and the approximations are valid only for long-lived and widely separated « decaying states ».

A general relation between the decay law and the energy spectrum of the initial state was given by KRYLOV and FOCK ([14]). However, their definition of « decay law » cannot be accepted without restrictions.

A time-dependent theory of resonance reactions was given by MOSHINSKY ([15]),

([6]) E. L. HILL and B. GELBAUM: unpublished (1954). We are indebted to Professor W. B. CHESTON for bringing this paper to our attention. We wish to thank Professor E. L. HILL for sending us a copy of the manuscript.

([7]) G. GAMOW: *Zeits. Phys.*, **51**, 204 (1928).

([8]) O. K. RICE: *Phys. Rev.*, **35**, 1538 (1930).

([9]) H. B. G. CASIMIR: *Physica (Haag)*, **1**, 193 (1934).

([10]) G. BREIT and F. L. YOST: *Phys. Rev.*, **48**, 205 (1935).

([11]) G. BREIT: *Handb. d. Phys.*, Bd. XLI/1 (Berlin, 1959), p. 28.

([12]) A. M. LANE and R. G. THOMAS: *Rev. Mod. Phys.*, **30**, 257, 343 (1958).

([13]) N. G. VAN KAMPEN: *Phys. Rev.*, **91**, 1267 (1953).

([14]) N. S. KRYLOV and V. A. FOCK: *Žurn. Eksp. Teor. Fiz.*, **17**, 93 (1947). See also L. A. KHALFIN: *Sov. Phys. Journ. Exp. Theor. Phys.*, **6**, 1053 (1958).

([15]) M. MOSHINSKY: *Phys. Rev.*, **84**, 525 (1951).

and applied by LOZANO to the problems of decay ([16]) and of scattering by a potential ([17]). The connection between Moshinsky's approach and that of the present paper will be discussed later.

Complex eigenvalues have also been employed in the theory of emission of light ([18]) and in the theory of unstable elementary particles ([19]), but these problems will not be considered here.

In the present paper, we shall investigate three examples of transients in continuous systems. The excitation conditions will be taken into account by looking for the general solution of the initial-value problem. The treatment is based on an extension of the standard methods which are employed in the case of discrete systems. In this way, it is possible to obtain a rigorous foundation for the method of complex eigenvalues. The « complex eigenvalues » are the poles of the S-matrix. Thus, the main questions to be considered are: *a*) What is the relation between the transient behaviour of the system and the poles of the S-matrix? *b*) How does the behaviour of the system depend on the excitation?

The first example (Section 2) is the problem of a harmonic oscillator coupled with a vibrating string, a special case of which was solved by LAMB ([1]). This is one of the simplest illustrations of the theory, and it is particularly suitable for explaining the method. The second example (Section 3) is Thomson's problem of the perfectly conducting sphere, which is of special interest in connection with antenna theory. The third example (Section 4) is the analogue of Thomson's problem in non-relativistic quantum mechanics, *i.e.* the initial-value problem for a hard sphere.

In each case, we shall find the general solution of the initial-value problem. The solution will be expressed in terms of propagators, which are very convenient for visualizing the results. The only parameters which appear in the solution are the poles of the S-matrix. Their role is similar to that of the « complex eigenfrequencies » of discrete systems. A propagator may be associated with each pole of the S-matrix. These « propagators of transient modes » are closely related to the « complex-frequency wave functions » which are employed in the method of complex eigenvalues, but the excitation at a definite instant introduces a cut-off factor, which eliminates the exponential catastrophe.

The idea of exponential decay, which is usually associated with the method of complex eigenvalues, may be applied, in general, only to the propagators,

---

([16]) J. M. LOZANO: *Rev. Mex. Fis.*, **3**, 63 (1954).

([17]) J. M. LOZANO: *Rev. Mex. Fis.*, **2**, 155 (1953).

([18]) V. F. WEISSKOPF and E. P. WIGNER: *Zeits. Phys.*, **63**, 54 (1930); **65**, 18 (1930); W. HEITLER: *The Quantum Theory of Radiation*, 3rd ed. (Oxford, 1954).

([19]) See G. HÖHLER: *Zeits. Phys.*, **152**, 546 (1958), where further references are given.

and not to the actual wave function. In the case of short-lived modes (*e.g.* in Thomson's problem or in the hard-sphere problem), the decay law depends very strongly on the excitation. In the Schrödinger case, one must also take into account the effect of the spreading of wave packets; as will be shown in Section 4, this introduces further limitations on the domain of validity of the exponential decay law.

The origin of the « transient modes » will also be discussed. It will be seen that there are significant differences, in this respect, between the first example and the others.

It will be shown in the second part that the « expansion in transient modes » introduced in this paper may have as a limiting case an expansion in stationary states. In general, however, the transient modes are not even approximately orthogonal, and one cannot ascribe an independent physical meaning to each term in the expansion.

2. – Vibrating string and oscillator.

The problem which will be treated in this section may be formulated as follows: *a harmonic oscillator is attached to the extremity of a semi-infinite string; given the initial displacement and velocity of the oscillator and the string, it is required to determine the subsequent motion.* This differs only slightly from Lamb's example ([1]). However, while LAMB restricted himself to the case in which the string is at rest, and a sudden blow is given to the oscillator, we shall consider an arbitrary initial excitation.

Let the rest position of the string coincide with the positive x-axis, and let $y(x, t)$ denote the transverse displacement of the string. We shall assume that the oscillator is constrained to move only in the y direction, so that $y(0, t)$ represents the displacement of the oscillator. Let m denote the mass of the oscillator, and ω_0 its natural frequency. Let T be the tension of the string, and let us define $\gamma = T/m$. If we take the wave velocity in the string to be unity, its equation of motion is

$$\frac{\partial^2 y}{\partial x^2} - \frac{\partial^2 y}{\partial t^2} = 0 \qquad (x > 0). \tag{1}$$

The equation of motion of the oscillator

$$\left(\frac{\mathrm{d}^2}{\mathrm{d}t^2} + \omega_0^2\right) y(0, t) = \gamma \frac{\partial y}{\partial x}(0, t)\,, \tag{2}$$

may be considered as a boundary condition for the motion of the string. Let the initial conditions be

$$y(x, 0) = u(x) \; ; \quad \frac{\partial y}{\partial t}(x, 0) = v(x) \qquad (x \geqslant 0). \tag{3}$$

The stationary solutions of (1) and (2) may be written as (up to a constant factor)

$$y(x, t, \omega) = \exp\left[-i\omega(x + t)\right] - S(\omega) \exp\left[i\omega(x - t)\right], \tag{4}$$

where

$$S(\omega) = \frac{\omega^2 - \omega_0^2 - i\gamma\omega}{\omega^2 - \omega_0^2 + i\gamma\omega} = \frac{(\omega + \omega_1)(\omega + \omega_2)}{(\omega - \omega_1)(\omega - \omega_2)} \tag{5}$$

is the S-matrix (in this case, an ordinary function of ω), which satisfies the well-known unitarity and symmetry conditions. The parameters

$$\omega_{1,2} = \pm (\omega_0^2 - \tfrac{1}{4}\gamma^2)^{\frac{1}{2}} - \tfrac{1}{2} i\gamma \tag{6}$$

are the poles of $S(\omega)$, which, in agreement with causality, are located in the lower half of the complex ω-plane. According to the method of complex eigenvalues, they represent the « complex eigenfrequencies » of the system.

The general solution of (1) and (2) may be expressed as a superposition of stationary solutions (Fourier integral). The expansion coefficients have to be determined by the requirement that the solution must satisfy the initial conditions (3). It may be seen that, although the stationary solutions do form a complete set ([20]), they are not orthogonal in this case. The physical reason for this is the additional degree of freedom due to the presence of the oscillator. In spite of the non-orthogonality, however, it is still possible to find formulae for the evaluation of the expansion coefficients.

Perhaps the most obvious way of finding the connection with the method of complex eigenvalues would be to deform the path of integration in the Fourier integral into the complex ω-plane. The connection would appear by taking the residues of the integrand at the poles of $S(\omega)$. We shall, however, follow a different procedure, which, besides being much simpler, leads more directly to the physical interpretation. This procedure is an extension of d'Alembert's classical solution of the Cauchy problem for the vibrating string.

The general solution of (1) is

$$y(x, t) = f(x - t) + g(x + t) \, , \tag{7}$$

([20]) N. G. VAN KAMPEN: *Physica*, **21**, 127 (1955).

where f and g are arbitrary functions of their arguments. To satisfy the initial conditions (3), it suffices to take

$$f(x)=\frac{1}{2}u(x)-\frac{1}{2}\int_0^x v(x')\,dx' \qquad (x\geqslant 0), \tag{8}$$

$$g(x)=\frac{1}{2}u(x)+\frac{1}{2}\int_0^x v(x')\,dx' \qquad (x\geqslant 0). \tag{9}$$

We may add an arbitrary constant to f, and subtract the same constant from g, without modifying the results. However, the choice of the lower limit 0 in the above integrals simplifies the subsequent calculations.

Since we are interested in the solution of the initial-value problem for $t>0$, the function $g(x+t)$ in (7) is completely defined by (9). However, $f(x-t)$ is defined by (8) only if $x\geqslant t$. In this case (7) becomes

$$y(x,t)=\frac{1}{2}[u(x+t)+u(x-t)]+\frac{1}{2}\int_{x-t}^{x+t} v(x')\,dx' \qquad (x\geqslant t), \tag{10}$$

which is the well-known d'Alembert solution, corresponding to free propagation in the string.

In order to determine the solution for $x<t$, we need the continuation of f to negative values of its argument. Physically, this means that we must find the « reflected wave », *i.e.* that part of the outgoing wave which has interacted with the oscillator. For this purpose, we must employ the boundary condition. Replacing (7) in (2), and introducing the notation $\bar{f}(t)=f(-t)$, we find

$$\bar{f}''(t)+\gamma\bar{f}'(t)+\omega_0^2\bar{f}(t)=-g''(t)+\gamma g'(t)-\omega_0^2 g(t) \qquad (t>0) \tag{11}$$

where the primes stand for derivatives with respect to the argument. According to (9), the second member of (11) is known, so that this is an ordinary differential equation for the unknown function $\bar{f}(t)$.

Since the displacement of the oscillator is given by $y(0,t)=y_0(t)=\bar{f}(t)+g(t)$, (11) may be rewritten as

$$y_0''(t)+\gamma y_0'(t)+\omega_0^2 y_0(t)=2\gamma g'(t)=\gamma[u'(t)+v(t)]\,. \tag{12}$$

This is the equation of motion of a damped harmonic oscillator, with natural frequency ω_0 and damping constant γ, subject to the external driving force

$2m\gamma g'(t)$ (*). Thus, *the effect of the coupling to the string on the motion of the oscillator is equivalent to a damping term (radiation damping) and a given external force, due to the incoming waves.*

Introducing the notations $u(0) = u_0$ and $v(0) = v_0$ for the initial displacement and initial velocity of the oscillator, respectively, we find from (8) and (9)

$$\bar{f}(0) = g(0) = \tfrac{1}{2}u_0\,; \qquad \bar{f}'(0) = \tfrac{1}{2}[v_0 - u'(0)]\,; \qquad g'(0) = \tfrac{1}{2}[v_0 + u'(0)]\,. \tag{13}$$

The solution of (11) subject to the conditions (13) is a typical problem of the theory of transients in discrete systems, to which the standard Laplace transformation method (1) may be applied. If $F(p)$, $G(p)$, denote the Laplace transforms of $\bar{f}(t)$, $g(t)$, respectively, the Laplace transform of (11) becomes

$$F(p) = -\frac{(p+p_1)(p+p_2)}{(p-p_1)(p-p_2)}\,G(p) + \frac{pu_0 + v_0}{(p-p_1)(p-p_2)} = \tag{14}$$

$$= \left[-1 + \sum_{j=1}^{2}\frac{a_j}{(p-p_j)}\right]G(p) - \frac{1}{2}(p_1+p_2)^{-1}\sum_{j=1}^{2}\frac{a_j}{(p-p_j)}\left(u_0 + \frac{v_0}{p_j}\right),$$

where

$$p_j = -i\omega_j \qquad (j = 1, 2), \tag{15}$$

and

$$a_j = -2p_j(p_j+p_k)(p_j-p_k)^{-1} = i\cdot\text{residue}\,[S(\omega)]_{\omega=\omega_j} \qquad (j = 1, 2;\ k \neq j). \tag{16}$$

The inverse Laplace transform of (14) is

$$\bar{f}(t) = -g(t) + \sum_{j=1}^{2} a_j \exp[p_j t] * g(t) - \tag{17}$$

$$-\frac{1}{2}(p_1+p_2)^{-1}\sum_{j=1}^{2} a_j\left(u_0 + \frac{v_0}{p_j}\right)\exp[p_j t],$$

where

$$f_1(t) * f_2(t) = \int_0^t f_1(t')\,f_2(t-t')\,\mathrm{d}t' = \int_0^t f_1(t-t')\,f_2(t')\,\mathrm{d}t' \tag{18}$$

is the convolution product.

(*) The parameter γ plays the role of a coupling constant between the oscillator and the string. According to (6), for $\gamma \ll 2\omega_0$ (weak coupling), the poles of $S(\omega)$ are located very close to the real axis, below the points $\pm\omega_0$. When γ increases from 0 to $2\omega_0$, they approach the negative imaginary axis (moving along the half-circle of radius ω_0 and center at the origin), joining each other at the point $-i\omega_0$ for $\gamma = 2\omega_0$ (critical damping). For $\gamma > 2\omega_0$, the poles move in opposite directions along the negative imaginary axis; one of them approaches the origin, while the other tends to $-i\,\infty$.

It follows from (7), (9) and (17) that

$$(19)\qquad y(x,t)=\frac{1}{2}\left[u(t+x)-u(t-x)\right]+\frac{1}{2}\int_{t-x}^{t-x}v(x')\,\mathrm{d}x'+\frac{1}{2}\sum_{j=1}^{2}a_j\exp\left[p_j(t-x)\right]\cdot$$

$$\cdot\left\{\int_0^{t-x}\exp\left[-p_jx'\right]\left[u(x')+\frac{v(x')}{p_j}\right]\mathrm{d}x'-(p_1+p_2)^{-1}\left(u_0+\frac{v_0}{p_j}\right)\right\}\qquad(0\leqslant x<t).$$

Equations (10) and (19) give the general solution of the problem. The case treated by LAMB, in which the string is initially at rest and an impulse is given to the oscillator, corresponds to the initial conditions

$$(20)\qquad u(x)=0\quad(x\geqslant 0)\,;\qquad v(x)=0\quad(x>0)\,;\qquad v_0\neq 0\,.$$

Substituting this in the solution, we find, in exact agreement with Lamb's result,

$$(21)\qquad y(x,t)=-\frac{1}{2}(p_1+p_2)^{-1}v_0\sum_{j=1}^{2}\frac{a_j}{p_j}H(t-x)\exp\left[p_j(t-x)\right],$$

where $H(t)$ denotes Heaviside's step function, $H(t)=0\quad(t<0)$; $H(t)=1\quad(t>0)$. For $x<t$, each term of (21) is of the form usually associated with a « complex-frequency wave function ». However, there is no exponential catastrophe, because the step function introduces a sharp cut-off at the wave front. This corresponds to the excitation at a definite instant.

We may consider the situation described by (21) as the analogue of an emission process, in which the kinetic energy initially concentrated in the oscillator is gradually propagated to the string.

According to (12), the terms which contain u_0 and v_0 in (19) may be regarded as the ordinary transients associated with the initial displacement and velocity of the oscillator, which are transmitted to the string. To interpret the remaining terms, which arise from the forced motion of the oscillator, it suffices to consider the case in which $u_0=v_0=0$. Under these circumstances, (10) and (19) may be rewritten as follows:

$$(22)\qquad y(x,t)=\int_0^{\infty}\left[G_-(x,x',t)\,f(x')+G_+(x,x',t)\,g(x')\right]\mathrm{d}x'\,,$$

where f and g are given by (8) and (9),

$$(23)\qquad G_-(x,x',t)=\delta(x-x'-t)\,,$$

$$(24)\qquad G_+(x,x',t)=\delta(x-x'+t)-\delta(x+x'-t)+$$

$$+\sum_{j=1}^{2}a_jH(t-x-x')\exp\left[p_j(t-x-x')\right],$$

and $\delta(x)$ is Dirac's δ-function.

By means of (8) and (9), the initial wave function is decomposed into an « outgoing part » f and an « incoming part » g. The subsequent behaviour of f and g is determined by the kernels G_- and G_+ of the integral transformation (22). For this reason, we shall call G_- the *propagator of the outgoing part*, and G_+ the *propagator of the incoming part* (*).

If we take the special (purely symbolic) initial conditions

$$u(x) = \delta(x - x_0) \; ; \qquad v(x) = 0 \, , \tag{25}$$

(22) becomes

$$y(x, t) = \tfrac{1}{2} G_-(x, x_0, t) + \tfrac{1}{2} G_+(x, x_0, t) \, . \tag{26}$$

Thus, in this case, the initial pulse splits into two identical pulses, which move in opposite directions. According to (23), the outgoing pulse propagates freely (as it would do in an unlimited string), as ought to be expected. According to (24), the same applies to the incoming pulse before it strikes the oscillator ($t < x_0$). For $t > x' = x_0$ the first term in the second member of (24) vanishes. The remaining terms represent the reflected wave, which consists of two parts: *a*) an inverted « mirror image » of the incoming pulse; *b*) an « exponential tail », similar to (21), which is due to the excitation of the oscillator transients by the incoming pulse (**).

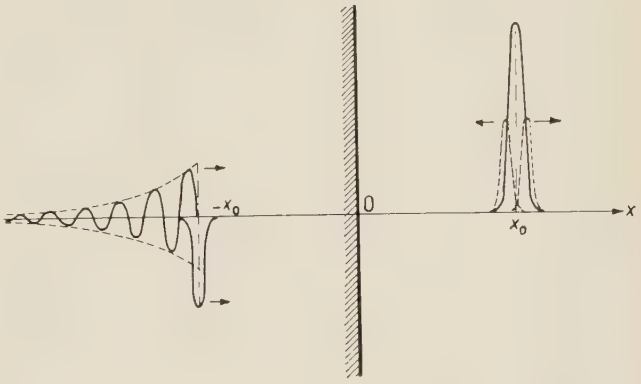

Fig. 1. – An initial pulse at x_0 in real space splits into two equal pulses which propagate in opposite directions; the incoming pulse gives rise in image space to a mirror image at $-x_0$, followed by an exponential tail.

These results may also be visualized by introducing an « image space », *i.e.* a fictitious continuation of the string for $x < 0$. The initial situation in real space and in image space corresponding to (26) is depicted in Fig. 1, which shows the break-up of the initial

(*) It should be understood that the names « outgoing » and « incoming » refer only to the initial situation; subsequently, the « incoming part » gives rise to an outgoing (reflected) wave.

(**) It may readily be verified that, in the limiting case $m \to \infty$ ($m \to 0$), which corresponds to a fixed extremity (free extremity), we obtain from (24) the ordinary reflection with change of sign (without change of sign). In the case $m \to 0$, we must employ the relation: $\lim_{\gamma \to \infty} [\gamma H(z) \exp(-\gamma z)] = \delta(z)$.

pulse at x_0, and the mirror image of the incoming pulse at $-x_0$, followed by the exponential tail. If we let the different parts of this initial configuration propagate freely (in the direction of the arrows in Fig. 1), the resulting wave function in real space is identical to (26).

According to (24), to each pole ω_j of $S(\omega)$ corresponds a term of the form

$$G_j(x, x', t) = a_j H(t - x - x') \exp [p_j(t - x - x')] \tag{27}$$

in the propagator of the reflected wave. We shall call $G_j(x, x', t)$ the *propagator of the transient mode* associated with the pole ω_j. Notice that, according to (16), the factor a_j is completely determined by the poles of the S-matrix. The remarks which were made in connection with (21) may be applied just as well to (27). In this way, we may give a rigorous meaning to the method of complex eigenvalues, for an arbitrary initial excitation: the « *complex-frequency wave functions* », *with a suitable cut-off factor* (*which eliminates the exponential catastrophe*), *correspond precisely to the propagators of the transient modes.*

Owing to the « exponential tail » in (24), *the form of the reflected wave at a given moment depends on the whole previous history, i.e. on the entire portion of the incoming wave which has stricken the oscillator up to that moment.* It is only in very special cases that terms of the form of (27) will appear in the reflected wave. This happens in Lamb's illustration of an « emission process » (cf. (21)). According to (25) and (26), it also happens in the case of excitation by a very sharp pulse. More generally, if the initial disturbance vanishes for $x > x_0$, the reflected wave will be of this form for $t - x > x_0$, *i.e.* after the whole incoming wave packet has stricken the oscillator. However, these are special cases, and we may conclude that, as a rule (for an arbitrary excitation), no trace of exponential behaviour will appear in the reflected wave.

3. – Spherical antenna.

The next problem which we shall consider is Thomson's problem of the « free oscillations » of a perfectly conducting spherical antenna. We shall study the decay of an arbitrary initial field. Our problem is therefore *to find a solution of Maxwell's equations in the exterior of a perfectly conducting sphere, which satisfies the boundary conditions on the surface of the sphere and given initial conditions.*

The electromagnetic field outside the sphere may be represented in terms of two scalar functions, the well-known Debye potentials ([21,22]). The general

([21]) P. J. W. DEBYE: *Ann. Phys.*, **30**, 57 (1909).

([22]) C. J. BOUWKAMP and H. B. G. CASIMIR: *Physica*, **20**, 539 (1954).

solution of Maxwell's equations in free space is a superposition of « electric » (E) and « magnetic » (M) solutions, corresponding to the Debye potentials $\Pi^E(\boldsymbol{r}, t)$ and $\Pi^M(\boldsymbol{r}, t)$, respectively. The general form of the E-solution is (we take $c = 1$)

$$\boldsymbol{E}(\boldsymbol{r}, t) = \operatorname{rot}\operatorname{rot}(\boldsymbol{r}\Pi^E) \; ; \quad \boldsymbol{H}(\boldsymbol{r}, t) = \frac{\partial}{\partial t}\operatorname{rot}(\boldsymbol{r}\Pi^E) \, . \tag{28}$$

The general form of the M-solution is obtained from (28) by substituting:

$$\Pi^E \to \Pi^M \; ; \qquad \boldsymbol{E} \to \boldsymbol{H} \; ; \qquad \boldsymbol{H} \to -\boldsymbol{E} \, . \tag{29}$$

Both Debye potentials satisfy the scalar wave equation

$$(\Delta - \partial^2/\partial t^2)\Pi^{E,M}(\boldsymbol{r}, t) = 0 \, . \tag{30}$$

We shall employ spherical co-ordinates, $\boldsymbol{r} = (r, \theta, \varphi)$, with origin at the center of the sphere. Let a be the radius of the sphere. The boundary condition at the surface of the sphere (vanishing of the tangential component of the electric field) may be expressed as follows:

$$\Pi^M(\boldsymbol{r}, t) = 0 \qquad \text{for } r = a, \tag{31}$$

$$\frac{\partial}{\partial r}[r\Pi^E(\boldsymbol{r}, t)] = 0 \qquad \text{for } r = a. \tag{32}$$

According to (30), the initial-value problem is determined by the following initial conditions:

$$\Pi^{E,M}(\boldsymbol{r}, 0) = U^{E,M}(\boldsymbol{r}) \; ; \quad \frac{\partial \Pi^{E,M}}{\partial t}(\boldsymbol{r}, 0) = V^{E,M}(\boldsymbol{r}) \qquad (r \geqslant a). \tag{33}$$

Let us introduce the multipole expansion of the Debye potentials

$$\Pi^{E,M}(\boldsymbol{r}, t) = \sum_{l=1}^{\infty} \sum_{m=-l}^{l} \psi_{lm}^{E,M}(r, t)\, Y_{lm}(\theta, \varphi) \, . \tag{34}$$

It follows from (28) and (29) that

$$rE_r(\boldsymbol{r}, t) = \sum_{l=1}^{\infty} \sum_{m=-l}^{l} l(l+1)\, \psi_{lm}^{E}(r, t)\, Y_{lm}(\theta, \varphi) \, , \tag{35}$$

$$rH_r(\boldsymbol{r}, t) = \sum_{l=1}^{\infty} \sum_{m=-l}^{l} l(l+1)\, \psi_{lm}^{M}(r, t)\, Y_{lm}(\theta, \varphi) \, , \tag{36}$$

so that the initial-value problem may be formulated just as well in terms of the radial components of $\boldsymbol{E}$ and $\boldsymbol{H}$, which are closely related to the Debye potentials ([22]).

The initial values (33) have corresponding expansions

$$(37)\quad U^{E,M}(\boldsymbol{r}) = \sum_{l=1}^{\infty} \sum_{m=-l}^{l} u_{lm}^{E,M}(r)\, Y_{lm}(\theta, \varphi)\ ; \qquad V^{E,M}(\boldsymbol{r}) = \sum_{l=1}^{\infty} \sum_{m=-l}^{l} v_{lm}^{E,M}(r)\, Y_{lm}(\theta, \varphi)\ ,$$

provided that we restrict ourselves to functions having zero mean value when averaged over all solid angles (*). This restriction, as well as the corresponding omission of the term $l = 0$ from (34) to (37), is related to the non-existence of radiating monopoles ([22]).

Substituting (34) and (37) in (30) to (33), we find separate initial-value problems for each value of l and m. We may restrict ourselves in what follows to one particular value of l and m. In order not to encumber the notation, we shall omit both of these subscripts. We shall also omit the superscripts E and M, except where it is necessary to draw the attention to differences between electric and magnetic multipoles; most of the results apply equally well to both cases.

The initial-value problem for an electric or magnetic multipole of order l then becomes:

$$(38)\quad \left[\frac{\partial^2}{\partial r^2} - l(l+1)r^{-2} - \frac{\partial^2}{\partial t^2}\right][r\psi(r, t)] = 0 \qquad (r > a);$$

$$(39)\quad \psi(r, 0) = u(r)\ ; \quad \frac{\partial \psi}{\partial t}(r, 0) = v(r) \qquad (r \geqslant a);$$

$$(40)\quad \psi^M(a, t) = 0\ ;$$

$$(41)\quad \left\{\frac{\partial}{\partial r}[r\psi^E(r, t)]\right\}_{r=a} = 0\ .$$

The normalized stationary solutions of (38) which satisfy the boundary conditions are

$$(42)\quad F(k, r)\exp[-ikt] = (2\pi)^{-\frac{1}{2}}[h_l^{(2)}(kr) + S(k)\,h_l^{(1)}(kr)]\exp[-ikt]\ ,$$

where $h_l^{(1)}(z)$, $h_l^{(2)}(z)$ are the spherical Hankel functions ([23]). The S-functions

(*) We thereby exclude from our consideration the trivial case of the electrostatic field due to a charged sphere.

([23]) P. M. Morse and H. Feshbach: *Methods of Theoretical Physics* (New York, 1953), p. 1573.

for magnetic and electric multipoles are given by

$$S^M(k) = -[h_l^{(2)}(ka)]/[h_l^{(1)}(ka)], \tag{43}$$

$$S^E(k) = -[kah_l^{(2)}(ka)]'/[kah_l^{(1)}(ka)]', \tag{44}$$

where the primes stand for derivatives with respect to ka.

The well-known relations

$$S^*(k)\,S(k^*) = S(k)\,S(-k) = 1 \tag{45}$$

follow from (43) and (44) and from the properties of the spherical Hankel functions.

We have

$$h_l^{(1)}(z) = z^{-1}\exp[iz]\sum_{n=0}^{l}\frac{i^{n-l-1}(l+n)!}{n!\,(l-n)!}(2z)^{-n} = z^{-l-1}p_l(z)\exp[iz], \tag{46}$$

where $p_l(z)$ is a polynomial of degree l in z. Similarly,

$$[zh_l^{(1)}(z)]' = z^{-l-1}q_{l+1}(z)\exp[iz], \tag{47}$$

where $q_{l+1}(z)$ is a polynomial of degree $l+1$ in z.

It follows from (43) to (47) that $S^M(k)$, $S^E(k)$ are meromorphic functions of the complex variable k. Their poles are roots of the equations

$$h_l^{(1)}(ka) = 0 \qquad (M), \tag{48}$$

$$[kah_l^{(1)}(ka)]' = 0 \qquad (E). \tag{49}$$

According to (46) and (47), (48) has exactly l roots, and (49) has exactly $l+1$ roots.

It will be shown in Appendix A that all the roots of (48) and (49) are simple, and that they are located in the lower half of the k-plane. Therefore, $S^M(k)$ *has exactly l poles and $S^E(k)$ has exactly $l+1$ poles; all the poles are simple and lie in the lower half-plane.* The non-existence of poles in the upper half-plane also follows from the causality condition [24]. According to (45), if k_n is a pole, so is $-k_n^*$, while k_n^* and $-k_n$ are zeros. Therefore, the poles lie symmetrically with respect to the imaginary axis (*).

---

[24] N. G. VAN KAMPEN: *Phys. Rev.*, **89**, 1072 (1953).

(*) The results which have been proved so far on the poles of $S^M(k)$ are particular cases of general theorems on the zeros of $H_\nu^{(1)}(z)$ for $\nu \neq 0$, which are due to H. FALKENBERG and E. HILB (*Gött. Nachr.*, 190 (1916)) and H. FALKENBERG (*Math. Zeits.*, **35**, 457 (1932)). It also follows from their investigations that $S^M(k)$ has no poles on the negative imaginary axis for even l, whereas, for odd l, it has one and only one negative imaginary pole.

Let k_j^M $(j=1, 2, ..., l)$ and k_j^E $(j=1, 2, ..., l+1)$ be the poles of $S^M(k)$ and $S^E(k)$, respectively. Then, it follows from (43) to (47) that

$$S^M(k) = (-1)^l \exp[-2ika] \prod_{j=1}^{l} (k + k_j^M)(k - k_j^M)^{-1}, \tag{50}$$

$$S^E(k) = (-1)^{l+1} \exp[-2ika] \prod_{j=1}^{l+1} (k + k_j^E)(k - k_j^E)^{-1}. \tag{51}$$

These are the canonical product expansions of the S-function, for a scatterer of range a and a finite number of poles ([24]).

The poles of $S^M(k)$ and of $S^E(k)$ for the first few values of l are given in Table I ([25]).

TABLE I. – *The poles of $S^M(k)$ and of $S^E(k)$.*

$l=$	1	2	3
$ak_j^M=$	$-i$	$\pm\frac{1}{2}\sqrt{3}-\frac{3}{2}i$	$-2.26i$ $\pm 1.75-1.87i$
$ak_j^E=$	$\pm\frac{1}{2}\sqrt{3}-\frac{1}{2}i$	$-1.60i$ $\pm 1.81-0.70i$	$\pm 0.87-2.17i$ $\pm 2.77-0.83i$

The functions $krF(k, r)$ $(0 \leqslant k < \infty)$, where $F(k, r)$ has been defined in (42), form a complete orthonormal set in $a \leqslant r < \infty$. This allows us to solve the initial-value problem by means of an expansion in stationary states. The general solution of (38) which satisfies the boundary conditions is

$$\psi(r, t) = \int_0^\infty [a(k)\cos(kt) + b(k)\sin(kt)]F(k, r)k^2\,\mathrm{d}k\,. \tag{52}$$

The initial conditions (29) will be satisfied if we take

$$a(k) = \int_a^\infty u(r')F^*(k, r')r'^2\,\mathrm{d}r'\,, \qquad kb(k) = \int_a^\infty v(r')F^*(k, r')r'^2\,\mathrm{d}r'\,. \tag{53}$$

Replacing these results in (52), we get

$$\psi(r, t) = \frac{1}{2}\int_{-\infty}^{+\infty}\mathrm{d}k\int_a^\infty \mathrm{d}r'(kr')^2[u(r') + ik^{-1}v(r')]F^*(k, r')F(k, r)\exp[-ikt]\,. \tag{54}$$

([25]) J. A. STRATTON: *Electromagnetic Theory* (New York, 1941), p. 559. A graphical representation of the poles of $S^M(k)$ may be found in E. JAHNKE and F. EMDE: *Tables of Functions* (New York, 1945), p. 243, fig. 129.

This is equivalent to the result obtained by HILL and GELBAUM ([6]).

The connection with the method of complex eigenvalues may be found by inverting the order of integration in (54) and evaluating the integral with respect to k by contour integration; this gives rise to residues at the poles of $S(k)$. It is much simpler, however, to apply the method of Section 2, which leads to an extension of Love's treatment ([5]).

The general solution of the multipole wave equation (38) is ([26])

$$\psi(r, t) = r^l D_r^l [r^{-1} \varphi(r, t)] , \tag{55}$$

where D_r^l is the differential operator

$$D_r^l = \left(\frac{\partial}{r \partial r} \right)^l \tag{56}$$

and $\varphi(r, t)$ is the general solution of the one-dimensional wave equation,

$$\varphi(r, t) = f(r - t) + g(r + t) . \tag{57}$$

Equation (55) is related to the well-known process of generating a multipole by repeated differentiation of a monopole.

The function $\varphi(r, t)$ is not uniquely determined by (55), for we may add to it an arbitrary solution $\chi(r, t)$ of the homogeneous equation

$$D_r^l [r^{-1} \chi(r, t)] = 0 . \tag{58}$$

The general solution of this equation is

$$\chi(r, t) = \sum_{n=0}^{l-1} A_n(t) r^{2n+1} , \tag{59}$$

where $A_0(t)$, ..., $A_{l-1}(t)$ are arbitrary functions of t. If we restrict ourselves to solutions of the form (57), there is still some arbitrariness in the choice of the functions f and g. In fact, according to (59), the pair $f(r - t)$, $g(r + t)$ is equivalent to the pair

$$f(r - t) + \sum_{n=0}^{2l} (-1)^{n+1} C_n (r - t)^n , \qquad g(r + t) + \sum_{n=0}^{2l} C_n (r + t)^n , \tag{60}$$

where C_0, ..., C_{2l} are $2l+1$ arbitrary constants. We may take advantage of this arbitrariness to choose the functions f and g in such a way that the solu-

([26]) H. LAMB: *Hydrodynamics*, 6th ed. (Cambridge, 1953), p. 522.

tion takes the simplest possible form. We shall determine these functions by the following $2l+1$ conditions:

$$f^{(j)}(a) = g^{(j)}(a) = 0 \quad (j = 0, 1, \ldots, l - 1); \qquad f^{(l)}(a) - g^{(l)}(a) = 0 , \tag{61}$$

where $f^{(j)}(a)$ denotes the j-th derivative of f, evaluated at the point a, and similarly for $g^{(j)}(a)$.

Replacing (55) to (57) in the initial conditions (39), we get

$$D_r^l\{r^{-1}[f(r) + g(r)]\} = r^{-l}u(r) \qquad (r \geqslant a), \tag{62}$$

$$D_r^{l+1}[g(r) - f(r)] = r^{-l}v(r) \qquad (r \geqslant a). \tag{63}$$

The choice of the homogeneous conditions (61) greatly simplifies the solution of these equations. If we define the operator D_r^{-l} applied to a function $w(r)$ by

$$D_r^{-l}[w(r)] = \int_a^r r_1 \, dr_1 \int_a^{r_1} r_2 \, dr_2 \ldots \int_a^{r_{l-1}} w(r_l) r_l \, dr_l \qquad (l \text{ integrations}), \tag{64}$$

it follows from (61) to (63) that

$$f(r) = \tfrac{1}{2} r D_r^{-l}[r^{-l}u(r)] - \tfrac{1}{2} D_r^{-l-1}[r^{-l}v(r)] \qquad (r \geqslant a) \tag{65}$$

$$g(r) = \tfrac{1}{2} r D_r^{-l}[r^{-l}u(r)] + \tfrac{1}{2} D_r^{-l-1}[r^{-l}v(r)] \qquad (r \geqslant a). \tag{66}$$

Equation (66) determines the function $g(r+t)$ for all $t \geqslant 0$, whereas $f(r-t)$ is determined by (65) only for $r - t \geqslant a$. To find the « reflected wave » $f(r-t)$ $(r - t < a)$, we must apply the boundary condition.

It follows from (55) to (57) that

$$\psi(r, t) = \sum_{n=0}^{l} (-1)^n c_{ln} r^{-n-1}[f^{(l-n)}(r - t) + g^{(l-n)}(r + t)] , \tag{67}$$

where

$$c_{ln} = [2^n n! \, (l - n)!]^{-1} (l + n)! . \tag{68}$$

In the case of magnetic multipoles, we must apply (40), which gives

$$\sum_{n=0}^{l} c_{ln} a^{-n-1} \bar{f}^{(l-n)}(t) = (-1)^{l+1} \sum_{n=0}^{l} (-1)^n c_{ln} a^{-n-1} g^{(l-n)}(t) , \tag{69}$$

where

$$\bar{f}(t) = f(a-t)\ ; \qquad \bar{g}(t) = g(a+t)\ . \tag{70}$$

According to (61), $\bar{f}(t)$ and $\bar{g}(t)$, as well as their derivatives up to the order $l-1$, vanish for $t=0$. To solve (69) under these conditions, we shall apply the Laplace transformation. Let $F(p)$, $G(p)$, be the Laplace transforms of $\bar{f}(t)$, $\bar{g}(t)$. Then, according to (43) and (46), the Laplace transform of (69) may be written as follows:

$$F(p) = -\exp[-2ap]\, S^M(iap)\, G(p)\ . \tag{71}$$

Taking into account (50), we get

$$\exp[-2ap]\, S^M(iap) = (-1)^l \prod_{j=1}^{l} (p+p_j^M)(p-p_j^M)^{-1} = \tag{72}$$

$$= (-1)^l - \sum_{j=1}^{l} a_j^M (p-p_j^M)^{-1}\ ,$$

where

$$p_j^M = -ik_j^M\ , \tag{73}$$

$$a_j^M = (-1)^{l+1} 2p_j^M \prod_{k\neq j}^{l} (p_j^M + p_k^M)(p_j^M - p_k^M)^{-1} = \tag{74}$$

$$= i\cdot \text{residue}\,\left(\exp[2ika]\, S^M(k)\right)_{k=k_j}\ .$$

Replacing (72) in (71), and applying the inverse Laplace transformation we finally obtain

$$\bar{f}^M(t) = (-1)^{l+1}\bar{g}^M(t) + \sum_{j=1}^{l} a_j^M \exp[p_j^M t] * \bar{g}^M(t) \qquad (t>0), \tag{75}$$

where we have employed the notation for the convolution product, defined in (18). Equations (66), (70) and (75) determine the reflected wave.

An entirely similar calculation gives, for electric multipoles,

$$\bar{f}^E(t) = (-1)^l \bar{g}^E(t) + \sum_{j=1}^{l+1} a_j^E \exp[p_j^E t] * \bar{g}^E(t) \qquad (t>0) \tag{76}$$

where p_j^E and a_j^E may be obtained from (73) and (74) by replacing M by E and l by $l+1$ (cf. (51)).

Equations (55) to (57), (65), (66), (75) and (76) give the general solution of our initial-value problem. As was done in the previous section, we may

rewrite the solution in terms of propagators:

$$\varphi(r, t) = \int_a^\infty [G_-(r-a,\ r'-a,\ t) f(r') + G_+(r-a,\ r'-a,\ t) g(r')]\, \mathrm{d}r' \,, \tag{77}$$

where the « outgoing part » f and the « incoming part » g are defined by (65) and (66), and the corresponding propagators G_- and G_+ are given by

$$G_-(r, r', t) = \delta(r - r' - t) \,, \tag{78}$$

$$G_+^M(r, r', t) = \delta(r - r' + t) + (-1)^{l+1} \delta(r + r' - t) + \sum_{j=1}^{l} G_j^M(r, r', t) \,, \tag{79}$$

$$G_+^E(r, r', t) = \delta(r - r' + t) + (-1)^l \delta(r + r' - t) + \sum_{j=1}^{l+1} G_j^E(r, r', t) \,, \tag{80}$$

with

$$G_j(r, r', t) = a_j H(t - r - r') \exp[p_j(t - r - r')] \,. \tag{81}$$

These results may again be visualized by means of an « image space » ($r < a$), in which the role of the mirror is played by the surface of the sphere. An incoming pulse gives rise to a « mirror image » (the sign of which depends on the type and order of the multipole), followed by an « exponential tail » of transient modes. The expression (81) for the propagator of a transient mode is similar to that found in the previous section; according to (73) and (74), it is entirely determined by the poles of the S-matrix. Thus, it is possible to give a rigorous meaning to Thomson's « natural modes of oscillation » (cf. Section 1), by introducing a cut-off factor (which eliminates the exponential catastrophe) and identifying them with the propagators of the transient modes.

The apparent lack of symmetry in the propagators is due to the fact that (78) to (81) apply only for $t > 0$. For $t < 0$, the unknown in (69) is $g(a+t)$, whereas $f(a-t)$ is given by (65). The complete expression for the propagators, valid both for $t > 0$ and for $t < 0$, is easily found. The result is that (79) to (80) remain unchanged, while

$$G_-(r, r', t) = G_+(r, r', -t) \,, \tag{82}$$

so that the symmetry of the propagators is restored. The solution for $t < 0$ is related to the solution for $t > 0$ by time inversion, so that the « emission modes » are replaced by « absorption modes ».

The results obtained in the present problem show a close formal analogy with those obtained in Section 2. It must be emphasized, however, that, from the physical point of view, the transient phenomena found in these two problems have essentially different origins. In the case of Section 2, we have to deal with an interaction between a field (string) and a discrete mechanical system (oscillator). As a consequence of the energy exchange between string and oscillator, part of the energy localized in the field may become temporarily stored in the mechanical system. This process is easy to visualize and does not require any further explanation.

In the case of the perfectly conducting sphere, however, the field forms a closed system, which can be described by a complete orthogonal set of stationary wave functions. Thus, the transient modes which have been found in this case cannot be attributed to an interaction with another system (such as the oscillator in the former example). As will be shown below, we have to deal with an interaction between different regions of the field.

It might appear, at first sight, that the surface currents and charges on the sphere should be considered as an independent part of the system, which may absorb field energy and store it for some time. However, since the sphere is a perfect conductor, the normal component of Poynting's vector on its surface must vanish, and no energy can be accumulated on the surface. The energy accumulation which gives rise to the transient modes must therefore be localized in the field itself. Thus, we are led to look for the physical process by means of which energy can temporarily be stored outside of the sphere, apparently in free space. We shall refer to this phenomenon as « antenna effect ».

In order to understand the antenna effect, it should first be observed that energy can be accumulated in those regions of a wave field where « repulsive forces » act upon it, *i.e.* where the « refractive index » decreases or becomes imaginary. This occurs, for instance, in the interior of a potential barrier (*) or in the interior of a superconductor.

In the present case, the repulsive forces (which act in the neighbourhood of the sphere) are centrifugal forces, which correspond to the « centrifugal potential » $l(l+1)r^{-2}$ in the multipole wave equation

$$\left[\frac{\partial^2}{\partial r^2} - l(l+1)r^{-2} + k^2\right][r\psi(k, r)] = 0 \,. \tag{83}$$

It can easily be verified that the antenna modes occur only in frequency re-

(*) A characteristic example of energy accumulation inside a potential barrier has recently been studied by M. Malogolowkin (to be published).

gions which satisfy the condition

$$k^2 \ll l(l+1)/a^2 \,, \tag{84}$$

which means that the centrifugal forces must be taken into account. In particular, as will be seen in the next section, no antenna modes appear in the case of s-waves ([27]).

Centrifugal forces give rise to « non-asymptotic » terms in the solutions of the field equations. In the case of an electric dipole wave, for instance, the solution of Maxwell's equations corresponding to an incoming spherical wave packet has the form

$$E_r = 2r^{-2}[g'(r+t) - r^{-1}g(r+t)]\cos\theta \,, \tag{85}$$

$$E_\theta = -r^{-1}[g''(r+t) - r^{-1}g'(r+t) + r^{-2}g(r+t)]\sin\theta \,, \tag{86}$$

$$H_\varphi = r^{-1}[g''(r+t) - r^{-1}g'(r+t)]\sin\theta \,. \tag{87}$$

As long as the wave packet is at large distances from the sphere, only asymptotic terms (in r^{-1}) have to be considered, and both the energy density and the Poynting vector are proportional to $\sin^2\theta$, so that they vanish at the poles ($\theta = 0, \pi$). As the wave packet approaches the sphere, however, non-asymptotic terms become increasingly more important and the energy current is deviated towards the polar regions, where an energy storage takes place.

In general terms, the deviation of Poynting's vector under the action of inertial forces can be considered as a consequence of Einstein's conservation laws for the electromagnetic field in curvilinear co-ordinates

$$\frac{\partial\sqrt{-g}\,S_\mu^\nu}{\partial x^\nu} = \frac{1}{2}\frac{\partial g_{\lambda\nu}}{\partial x^\mu}\sqrt{-g}\,S^{\lambda\nu} \,,$$

where $g_{\lambda\nu}$ and S_μ^ν are the components of the metric tensor and of the electromagnetic energy-momentum tensor, respectively. It follows from this that the way in which inertial forces act on the electromagnetic field is very similar to the way in which they act on a mechanical system. We conclude, therefore, that the antenna effect is a direct consequence of the inertia of the electromagnetic field, and that it results from the action of the inertial field.

The antenna effect is a very general phenomenon, which comes into play whenever a propagating field meets obstacles with curved surfaces. It also plays a role in diffraction phenomena, giving rise to optical border effects in

([27]) Cfr. also H. M. NUSSENZVEIG: *Nucl. Phys.*, **11**, 499 (1959), Sect. 4.2 (*b*).

the neighbourhood of sharp edges. A more detailed discussion of the general character of the antenna effect and its connection with inertial forces will be given in another paper.

It must be strongly emphasized, in connection with the physical interpretation of the transient modes, that no special significance can be attached, in general, to the « amplitude of excitation » of each separate mode. In fact, the transient modes are not orthogonal, so that the total energy is not a sum of terms associated with the separate modes, and it is not possible to excite one particular mode independently of the others. A similar situation exists in the case of transients in discrete systems.

The remarks which were made at the end of Section 2 concerning the dependence of the decay on the excitation may be extended to the present case.

The perfect conductor, which we have considered in this section, is an ideal limiting case, which may be approximately realized by a superconductor or by a very good normal conductor. In the latter case, however, the presence of the ohmic losses renders the problem considerably more complicated, and additional effects, which are not apparent in the limit of infinite conductivity, may have to be taken into account.

4. – Hard sphere.

The counterpart in non-relativistic quantum mechanics of the problem treated in Section 3 is the following problem: *given an arbitrary (normalizable) initial wave packet in the exterior of a « hard sphere » of radius a, it is required to determine its subsequent behaviour.* The solution of this problem for s-waves has been given by MOSHINSKY ([28]); however, as will be seen below, the S-function has no poles in this case, so that we shall be interested in higher angular momenta.

The initial-value problem may be formulated as follows: to find a solution of Schrödinger's equation (we take $\hbar = m = 1$)

$$-i\frac{\partial}{\partial t}\Psi(\boldsymbol{r}, t) = \frac{1}{2}\Delta\Psi(\boldsymbol{r}, t) \tag{88}$$

which satisfies the boundary condition

$$\Psi(\boldsymbol{r}, t) = 0 \qquad \text{for } r = a, \tag{89}$$

and the initial condition

$$\Psi(\boldsymbol{r}, 0) = U(\boldsymbol{r}) \qquad (r \geqslant a). \tag{90}$$

([28]) M. MOSHINSKY: *Rev. Mex. Fis.*, **1**, 28 (1952).

If we expand the wave function and its initial value in partial waves,

$$\Psi(\boldsymbol{r}, t) = \sum_{l=0}^{\infty} \sum_{m=-l}^{l} \psi_{lm}\, \delta(r, t)\, Y_{lm}(\theta, \varphi)\,, \tag{91}$$

$$U(\boldsymbol{r}) = \sum_{l=0}^{\infty} \sum_{m=-l}^{l} u_{lm}(r)\, Y_{lm}(\theta, \varphi)\,, \tag{92}$$

we find the following initial-value problem for the l-th partial wave:

$$\left[\frac{\partial^2}{\partial r^2} - l(l+1)r^{-2} + 2i\frac{\partial}{\partial t}\right][r\psi(r, t)] = 0\,, \tag{93}$$

$$\psi(a, t) = 0\,, \tag{94}$$

$$\psi(r, 0) = u(r)\,, \qquad (r \geqslant a), \tag{95}$$

where the subscripts l and m have been dropped for convenience.

The stationary scattering states are given by

$$F(k, r)\exp[-iEt] = (2\pi)^{-\frac{1}{2}}[h_l^{(2)}(kr) + S(k)\,h_l^{(1)}(kr)]\exp[-iEt]\,, \tag{96}$$

where

$$E = \tfrac{1}{2}k^2 \tag{97}$$

and

$$S(k) = -[h_l^{(2)}(ka)]/[h_l^{(1)}(ka)]\,, \tag{98}$$

which is identical to the S-function for *magnetic* multipole waves of order l (cf. (43)). The only difference is that $l = 0$ is allowed here. The corresponding S-function is

$$S(k) = \exp[-2ika] \qquad (\text{for } l = 0), \tag{99}$$

which has no poles.

The solution of the initial-value problem by means of the stationary-state expansion is similar to that given in the previous section. The main differences are the dispersion formula (97) and the absence of a condition on the initial time derivative. The result may be obtained by means of an appropriate modification of (54):

$$\psi(r, t) = \frac{1}{2}\int_{-\infty}^{+\infty} dk \int_{a}^{\infty} dr'(kr')^2 u(r')\, F^*(k, r')\, F(k, r)\exp\left[-\frac{1}{2}ik^2t\right]. \tag{100}$$

The connection with the method of complex eigenvalues may be found by an extension of the treatment given in Section 3.

The general solution of the radial equation (93) is

$$\psi(r, t) = r^l D_r^l[r^{-1}\varphi(r, t)] , \tag{101}$$

where D_r^l is the differential operator (56), and $\varphi(r, t)$ is the general solution of the one-dimensional free-particle Schrödinger equation, which is given by [29]

$$\varphi(r, t) = \int_{-\infty}^{+\infty} U(r - r', t) f(r')\, \mathrm{d}r' = \int_{-\infty}^{+\infty} U(r', t) f(r + r')\, \mathrm{d}r' , \tag{102}$$

where $f(r')$ is an arbitrary function, and

$$U(r, t) = \exp\,[-i\pi/4]\,(2\pi t)^{-\frac{1}{2}} \exp\,[ir^2/2t] \tag{103}$$

is the free-particle Schrödinger propagator (« heat pole » solution). We have

$$\lim_{t \to 0} U(r, t) = \delta(r) , \tag{104}$$

so that the initial condition (95) becomes

$$D_r^l[r^{-1} f(r)] = r^{-l} u(r) \qquad (r \geqslant a). \tag{105}$$

The function $f(r)$ is not uniquely determined by (101) and (102); we may add to it any solution of the equation

$$D_r^l\{r^{-1}[f(r + r') + f(r - r')]\} = 0 . \tag{106}$$

The general solution of this equation is

$$f(r) = \sum_{n=0}^{l-1} C_n r^{2n+1} , \tag{107}$$

where C_0, C_1, ..., C_{l-1} are arbitrary constants. We may profit from this to choose f in such a way that the solution takes the simplest possible form.

---

[29] W. Pauli: *Handbuch der Physik*, **24**/1, 2. Aufl. (Berlin, 1933), p. 103.

This is achieved by imposing the supplementary conditions (*)

$$f^{(j)}(a) = 0 \qquad (j = 0, 1, ..., l-1). \tag{108}$$

The solution of (105) subject to these conditions is

$$f(r) = rD_r^{-l}[r^{-l}u(r)] \qquad (r \geqslant a), \tag{109}$$

where D_r^{-l} is defined by (64). The problem is now reduced to the determination of the «reflected wave» $f(r)$ $(r < a)$ in (102). Substituting (101) and (102) in the boundary condition (94), we obtain the differential equation

$$\sum_{n=0}^{l} (-1)^n c_{ln} a^{-n-1}[f^{(l-n)}(a-r) + f^{(l-n)}(a+r)] = 0 \qquad (r > 0), \tag{110}$$

where $f(a-r)$ is the unknown, and c_{ln} is defined by (68).

Equation (110) is identical to (69), with t replaced by r and $f = g$ (but not $\bar{f} = \bar{g}$!). The supplementary conditions (108) are related in the same way to (61). Therefore, according to (75), the solution of (110) is

$$f(a-r) = (-1)^{l+1} f(a+r) + \sum_{j=1}^{l} a_j \exp[p_j r] * f(a+r) \qquad (r > 0), \tag{111}$$

where p_j and a_j are given by (73) and (74), respectively.

Equations (101), (102), (109) and (111) give the general solution of the initial-value problem. The solution may be rewritten in the following form:

$$\varphi(r, t) = \int_a^\infty G(r-a, r'-a, t) f(r')\, dr', \tag{112}$$

where $f(r')$ is given by (109), and $G(r, r', t)$, which may be called the propagator of the φ-wave, is given by

$$G(r, r', t) = U(r-r', t) + (-1)^{l+1} U(r+r', t) + \sum_{j=1}^{l} G_j(r, r', t), \tag{113}$$

where

$$G_j(r, r', t) = a_j M(r+r', k_j, t), \tag{114}$$

(*) These conditions do not exclude the possibility that terms of the form of (107), which would give rise to singular integrals in (102), may appear in the solution. However, according to (106), such terms may be dropped.

and

$$M(x, k, t) = \int_{-\infty}^{\infty} H(x' - x) \exp [ik(x - x')] U(x', t) \, dx' . \tag{115}$$

If we introduce an « image space », so that (113) is defined for $-\infty < r < +\infty$, it follows from (104) and (112) to (114) that $G(r, r', t)$ is that solution of the one-dimensional free-particle Schrödinger equation which, for $t = 0$, reduces to

$$G(r, r', 0) = \delta(r - r') + (-1)^{l+1} \delta(r + r') + \sum_{j=1}^{l} a_j H(-r - r') \exp [ik_j(r + r')] . \tag{116}$$

According to (79) and (81), this is identical to $G_+^M(r, r', 0)$. Thus, we may say again that a pulse in « real space » at $t = 0$ gives rise in « image space » to a mirror image, followed by an exponential tail of transient modes. If we let this initial configuration propagate freely (according to Schrödinger's equation), the result is described by $G(r, r', t)$.

There is a far-reaching formal analogy between the present problem and that of the previous section (for magnetic multipoles). The main difference lies in the nature of free propagation, which is described in one case by the wave equation, and in the other by Schrödinger's equation. Notice that, since there is no limiting velocity for Schrödinger particles, the « reflected pulse » in this case appears at once in real space, whereas in the electromagnetic case it appears only after the incident pulse has stricken the surface of the sphere.

The propagator associated with a pole of the S-matrix,

$$k = k' - iK \qquad (K > 0) \tag{117}$$

is given by (114) and (115). The function $M(x, k, t)$ was introduced by MOSHINSKY ([15]). It may be expressed in terms of the error function of a complex argument, by means of the formula

$$M(x, k, t) = \tfrac{1}{2} v(x, k, t) \operatorname{erfc} (\exp [-i\pi/4] w) , \tag{118}$$

with

$$w = (2t)^{-\frac{1}{2}} (x - kt) , \tag{119}$$

$$\operatorname{erfc} (z) = 2\pi^{-\frac{1}{2}} \int_{z}^{\infty} \exp [-\zeta^2] \, d\zeta , \tag{120}$$

and

$$v(x, k, t) = \exp[i(kx - Et)], \tag{121}$$

where E is the « complex energy », given by

$$E = E' - \tfrac{1}{2}i\Gamma = \tfrac{1}{2}k^2 = \tfrac{1}{2}(k'^2 - K^2) - ik'K. \tag{122}$$

According to (115), $M(x, k, t)$ is that solution of the free-particle Schrödinger equation which, for $t = 0$, reduces to

$$M(x, k, 0) = H(-x)\exp[ikx], \tag{123}$$

which is a wave packet with a sharp front. For $t > 0$, the front becomes diffuse, and is replaced by a transitional region, in which $|w| \leqslant 1$. According to (119), the width of this region is given by $|x - kt| \leqslant (2t)^{\frac{1}{2}}$ (or, in ordinary units, $(2ht/m)^{\frac{1}{2}}$). This « blurring » of the initially sharp edge is a purely quantal « diffraction » effect (*). We shall be interested in the behaviour of $M(x, k, t)$ outside of the transitional region, *i.e.* either beyond or behind the wave front, but not very close to it. Thus, we want to find the behaviour of (118) for $|w| \gg 1$. For this purpose, we shall employ the asymptotic expansion of the error function, which is given in Appendix B.

Let A and B denote the regions of the complex plane *above* and *below* the second bisector, respectively, so that $-\pi/4 < \arg w < 3\pi/4$ if $w \in A$, and $3\pi/4 < \arg w < 7\pi/4$ if $w \in B$. Then, it follows from (118) and from the results given in Appendix B that

$$M(x, k, t) = M_A(x, k, t) = it(x - kt)^{-1}U(x, t)\cdot$$
$$\cdot\left[1 - \tfrac{1}{2}iw^{-2} + \ldots + (-\tfrac{1}{2}i)^n(2n-1)!!\, w^{-2n} + R_n(w)\right] \qquad \text{if } w \in A, \tag{124}$$

$$M(x, k, t) = M_B(x, k, t) = v(x, k, t) + M_A(x, k, t) \qquad \text{if } w \in B, \tag{125}$$

(*) For real k, (123) may be thought of as representing a beam of particles of « velocity » k confined to the half-space $x < 0$ by a perfectly absorbing shutter, which is suddenly removed at $t = 0$. According to classical mechanics, the behaviour of the current at a point $x > 0$ as a function of time would be given by a step function, with a sharp rise at $t = x/k$ (time of flight). For Schrödinger particles, the current begins to rise immediately after $t = 0$, and approaches the classical value for $t \gg x/k$. In the neighbourhood of $t = x/k$, there appear oscillations in the current, which resemble the Fresnel diffraction pattern of a straight edge in optics. MOSHINSKY has called this effect « diffraction in time » (M. MOSHINSKY: *Phys. Rev.*, **88**, 625 (1952)).

where $U(x, t)$ and $v(x, k, t)$ are defined by (103) and (121), respectively, and

$$|R_n(w)| \leqslant \pi^{\frac{1}{2}} 2^{-n-1}(2n+1)!!\,|w|^{-2n-1} \qquad (n = 0, 1, \ldots). \tag{126}$$

For $|w| \gg 1$, $M_A(x, k, t)$ differs from the free-particle propagator essentially by a factor of squared modulus

$$t^2[(x - k't)^2 + (Kt)^2]^{-1}, \tag{127}$$

which has a peak of width Kt around the point $x = k't$. M_B differs from M_A by the additional term $v(x, k, t)$. *This term corresponds to the « complex-energy wave function » which is usually associated with a « decaying state » in the method of complex eigenvalues.* However, it appears in the propagator only for a special class of poles, and only for a limited range of values of x and t.

To show this, let us consider the behaviour of $M(x, k, t)$ in « real space » ($x > 0$) as a function of x, for fixed t ($t > 0$). It may be seen in Fig. 2 that, if $k \in B$, then $w \in A$ for all $x > 0$. On the other hand, if $k \in A$, then $w \in B$ if

$$0 < x < (k' - K)t, \tag{128}$$

and $w \in A$ if $(k' - Kt) < x$. Thus, *it is only in the case of poles located above the second bisector, and only within the range of values of x and t defined by* (128), *that the term usually associated with a « decaying state » appears in the propagator.*

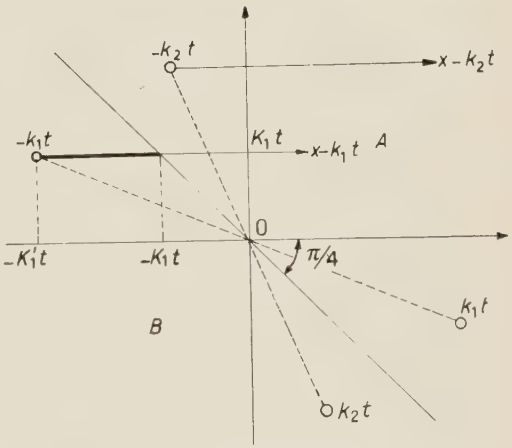

Fig. 2. – For a pole k_2 belonging to B, $x - k_2 t$ lies in A. For a pole k_1 belonging to A, $x - k_1 t$ lies in B within the range indicated by the thick line, and it lies in A outside of this range.

It is readily verified that the real part of the exponent in (121) is always negative within the range (128), so that there is no exponential catastrophe. This also follows from the conservation of probability, since (123) is a normalizable wave packet. The essential point is the presence of the cut-off factor in (123).

The distinction between poles located above or below the second bisector is implicitly contained in HEITLER and HU's criterion ([30]), according to which

([30]) W. HEITLER and N. HU: *Nature*, **159**, 776 (1947).

only those poles for which the real part E' of the « complex energy » (122) is positive give rise to « decaying states ». It has been pointed out elsewhere ([31]) that Heitler and Hu's justification of this criterion is not satisfactory.

In fact, according to (128), there is a continuous transition between poles belonging to A and poles belonging to B, the range (128) becoming smaller and smaller as the second bisector is approached. Moreover, if we compare the order of magnitude of the two terms of (125) as a function of time, within the range (128), we find that $M_A(x, k, t)$ always predominates over $r(x, k, t)$ after a sufficient lapse of time. Since

$$|v(x, k, t)| = \exp[K(x - k't)], \tag{129}$$

we may say that the term $r(x, k, t)$ is associated with the propagation of the initial wave packet, without change of shape (with velocity k'). However, as is well known, a free-particle Schrödinger wave packet always undergoes a broadening in the course of time. This « spreading effect » is contained in the term $M_A(x, k, t)$ of (125). It follows from (123) that the width of the initial wave packet is of the order of K^{-1}. According to the uncertainty relation, this corresponds to a momentum spread of the order of K, so that the wave packet will have spread by an amount of the order of Kt after a time t (cf. (127)). The effect of spreading becomes important when this quantity is comparable with the initial width, *i.e.* for $t \gtrsim t_s = K^{-2}$. On the other hand, according to (129), the « lifetime » is given by $\tau = \Gamma^{-1} = \frac{1}{2}(k'K)^{-1}$. It follows that, as we approach the second bisector, t_s and τ become of the same order, so that the spreading effect predominates over the exponential decay within a single half-life. There is no time, so to speak, for the exponential law to manifest itself. This explains the special role which is played by the second bisector.

It also follows from the above discussion that, no matter what may be the position of the pole, *the exponential law cannot remain valid for arbitrarily large times*: it must ultimately be superseded by the decay law for a free-particle wave packet. In this case, as is well known ([32]), the probability distribution at a fixed point behaves like t^{-3} for $t \to \infty$. This may be verified in the present example; similar results have been obtained by other authors ([19,33]).

In the case of a pole which is close to the real axis (« long-lived » transient mode), a careful discussion is required to determine the range of validity of the exponential decay law and the dependence of the decay on the excitation.

([31]) H. M. NUSSENZVEIG: *Nucl. Phys.*, **11**, 499 (1959).
([32]) W. BRENIG and R. HAAG: *Fortschr. Phys.*, **7**, 183 (1959).
([33]) J. PETZOLD: *Zeits. Phys.*, **155**, 422 (1959).

However, in the hard-sphere problem, there are no poles satisfying this condition. Although there are poles above the second bisector for $l > 1$, they are still far from the real axis (see JAHNKE-EMDE ([25])). This may be understood by considering the origin of the transient modes in this case. They are clearly related to the presence of the « centrifugal barrier »: for sufficiently large angular momentum, it is possible for a wave packet to remain « trapped » near the surface of the sphere for a short time (cf. the discussion on the role of the centrifugal forces at the end of Section 3). However, the centrifugal barrier alone is too transparent to allow the formation of long-lived modes.

So far, we have considered only the behaviour of the propagator for $t > 0$. However, (112) to (115) may be applied just as well for $t < 0$. According to (103), we may take

$$U(r, -t) = U^*(r, t) . \tag{130}$$

It follows from (115) and (130) that

$$M(x, k, -t) = M^*(x, -k^*, t) , \tag{131}$$

so that poles which are symmetrically placed with respect to the imaginary axis exchange their roles under time inversion. In particular, for $t < 0$, the term (121) may appear in the propagator only in the case of poles located above the *first bisector* (*). It corresponds to the reverse of an « emission mode », so that it may be called an « absorption mode » ([30]). Thus, the absorption modes appear in connection with « final-value problems », *i.e.* when we want to describe how a given situation was built up.

Taking into account the symmetry of the pole distribution about the imaginary axis, it follows from (113) to (115), (130) and (131) that

$$G(r, r', -t) = G^*(r, r', t) . \tag{132}$$

If we denote the solution of the initial-value problem, which is a functional of the initial value $u(r)$, by $\psi(r, t, [u])$, it follows from (101), (112) and (132) that

$$\psi(r, -t, [u]) = \psi^*(r, t, [u^*]) . \tag{133}$$

The second member of (133) describes the « time-reversed motion » corres-

(*) We are indebted for this remark to Professor L. VAN HOVE.

ponding to the solution for $t > 0$ ([34]). This result could of course have been anticipated.

By going over from the stationary-state expansion (100) to the « expansion in transient modes » (113), we have effectively replaced a function given on the real axis, the S-function, by a set of complex parameters, the poles of the S-function. This transformation may be very useful: it gives us greater insight into the behaviour of the solution, and it clearly displays the role of the excitation conditions. However, it must be stressed that, on account of the non-orthogonality of the transient modes, *it is not possible, in general, to ascribe an independent physical meaning to each term of the expansion.* Thus, the price that has to be paid for what is accomplished by this transformation is the loss of some definiteness in the physical interpretation.

The transient modes occupy an intermediate position between stationary states and free-particle wave packets, sharing some of the properties of both. In the case of poles which are far from the real axis, the free-particle features predominate. On the other hand, in the case of poles which are close to the real axis, it may be possible to give an approximate description of the system, during a long time interval, by means of concepts taken over from the theory of stationary states. A more complete discussion of this case will be given in the second part.

* * *

The authors wish to thank Professor C. J. Bouwkamp and Professor N. G. Van Kampen for valuable discussions. One of us (H.M.N.) is indebted to the National Research Council of Brazil for award of a fellowship. He also wishes to thank Professor L. Van Hove for the hospitality of the Institute of Theoretical Physics, Utrecht.

Appendix A

The roots of equations (48) and (49).

In this Appendix, we shall prove the following results:

a) The roots of the equations

$$(M) \qquad h_l^{(1)}(ka) = 0\,,$$

$$(E) \qquad [kah_l^{(1)}(ka)]' = 0\,,$$

([34]) E. P. Wigner: *Göttinger Nachrichten*, **31**, 546 (1932).

are located in the lower half of the k-plane; b) all the roots are simple.

To prove *a*), we start from the following identity, which results from the differential equation of the spherical Hankel functions:

$$(A.1)\quad (k^2-k^{*2})r^2\,|h_l^{(1)}(kr)|^2=\frac{\mathrm{d}}{\mathrm{d}r}\left\{r^2 h_l^{(1)}(kr)\frac{\mathrm{d}}{\mathrm{d}r}[h_l^{(1)}(kr)]^*-r^2[h_l^{(1)}(kr)]^*\frac{\mathrm{d}}{\mathrm{d}r}[h_l^{(1)}(kr)]\right\},$$

and we integrate both members over the interval from a to r. If k is a root of (M) or (E), the contribution to the second member from the lower limit a vanishes, and we are left with

$$(A.2)\quad (k^2-k^{*2})\int_a^r |h_l^{(1)}(kr')|^2 r'^2\,\mathrm{d}r'-r^2\left\{h_l^{(1)}(kr)\frac{\mathrm{d}}{\mathrm{d}r}[h_l^{(1)}(kr)]^*-[h_l^{(1)}(kr)]^*\frac{\mathrm{d}}{\mathrm{d}r}[h_l^{(1)}(kr)]\right\}.$$

For sufficiently large r, we have $|kr|\gg l$, so that the spherical Hankel functions in the second member of (A.2) may be replaced by their asymptotic expansions, leading to

$$(A.3)\quad (k^2-k^{*2})\int_a^r |h_l^{(1)}(kr')|^2 r'^2\,\mathrm{d}r'\approx -i\,|k|^{-2}(k+k^*)\exp[i(k-k^*)r].$$

Let us assume first that $k=k'-iK$, with $k'\neq 0$. Then, it follows from (A.3) that

$$(A.4)\quad K\approx\frac{1}{2}\,|k|^{-2}\exp[2Kr]\left[\int_a^r |h_l^{(1)}(kr')|^2 r'^2\,\mathrm{d}r'\right]^{-1}>0,$$

so that *a*) is proved, except in the case of purely imaginary roots. To compleet the proof, we must show that there cannot be any roots on the positive imaginary axis. This follows from the fact that, for $v>0$, $ip_l(iv)$ in (46) and $-iq_{l+1}(iv)$ in (47) are polynomials in v with real positive coefficients.

To prove statement *b*), it suffices to show that $[h_l^{(1)}(ka)]'\neq 0$ or $[kah_l^{(1)}(ka)]''\neq 0$, if k is a root of (M) or (E), respectively. This follows from the non-vanishing of the Wronskian determinants

$$(A.5)\quad h_l^{(2)}(z)h_l'^{(1)}(z)-h_l^{(1)}(z)h_l'^{(2)}(z)=2iz^{-2},$$

$$(A.6)\quad [zh_l^{(2)}(z)]'[zh_l^{(1)}(z)]''-[zh_l^{(1)}(z)]'[zh_l^{(2)}(z)]''=2i[1-l(l+1)z^{-2}].$$

Appendix B

Asymptotic expansion of the error function (*).

The function erfc (z), where z is a complex variable, is defined by

$$\text{(B.1)} \qquad \operatorname{erfc}(z) = 2\pi^{-\frac{1}{2}} \int_z^\infty \exp[-\zeta^2]\,\mathrm{d}\zeta\,.$$

The path of integration in (B.1) may be deformed in an arbitrary way, provided that it remains within the quadrant $-\pi/4 \leqslant \arg\zeta \leqslant \pi/4$ for $|\zeta| \to \infty$. We have

$$\text{(B.2)} \qquad \operatorname{erfc}(z) + \operatorname{erfc}(-z) = \operatorname{erfc}(-\infty) = 2\,,$$

so that it suffices to consider the half-plane $\operatorname{Re} z \geqslant 0$.

To find the asymptotic expansion of erfc (z) in this half-plane, we choose as path of integration a straight line parallel to the real axis. A straightforward application of the method of integration by parts yields

$$\text{(B.3)} \qquad \operatorname{erfc}(z) = \pi^{-\frac{1}{2}} z^{-1} \exp[-z^2] \cdot \left[1 - \frac{1}{2} z^{-2} + \frac{1\cdot 3}{2^2} z^{-4} - \ldots + \left(-\frac{1}{2}\right)^n (2n-1)!!\, z^{-2n} + R_n(z)\right],$$

where

$$\text{(B.4)} \qquad (2n-1)!! = 1\cdot 3\cdot 5 \ldots (2n-1)\,,$$

$$\text{(B.5)} \qquad R_n(z) = \left(-\frac{1}{2}\right)^n (2n+1)!!\, z \exp[z^2] \int_z^{\infty + i \operatorname{Im} z} \exp[-\zeta^2]\zeta^{-2n-2}\,\mathrm{d}\zeta\,.$$

It follows from (B.5) that

$$\text{(B.6)} \qquad |R_n(z)| \leqslant \pi^{\frac{1}{2}} 2^{-n-1}(2n+1)!!\, |z|^{-2n-1} \qquad (\operatorname{Re} z \geqslant 0).$$

The asymptotic expansion of erfc (z) in the left half-plane follows from (B.2) and (B.3).

(*) The results of this appendix have been given in a less complete form by Moshinsky [15].

RIASSUNTO (*)

Per migliorare la trattazione usuale del comportamento transitorio dei sistemi continui col « metodo degli autovalori complessi », è necessario tener conto delle condizioni di eccitazione. Ciò si fa prendendo in considerazione i problemi del valore iniziale. Si analizzano tre casi: 1) un oscillatore armonico accoppiato ad una corda vibrante; 2) le oscillazioni elettromagnetiche di un'antenna sferica perfettamente conduttrice; 3) lo scattering di particelle di Schrödinger su una sfera rigida. In ogni caso la soluzione generale del problema del valore iniziale viene messo in relazione col « metodo degli autovalori complessi » associando un propagatore a ciascun polo della matrice S. In questa maniera la difficoltà dell'aumento esponenziale, che si ha nella trattazione usuale, è eliminata, e si mette in evidenza la dipendenza della legge di decadimento dalla eccitazione. Per le particelle di Schrödinger la dispersione dei pacchetti d'onde restringe il dominio di validità della legge esponenziale del decadimento. Si discute l'origine dei « modi transitori » che sono associati ai poli della matrice S. Si dimostra che i modi dell'antenna hanno origine negli effetti delle forze d'inerzia. Si sottolineano le limitazioni dell'interpretazione fisica nel caso dei modi a vita breve.

(*) *Traduzione a cura della Redazione.*

Cross Section for $^{31}P(n, p)^{31}Si$ Reaction up to 5 MeV (*).

P. Cuzzocrea, G. Pappalardo and R. Ricamo

Istituto di Fisica dell'Università - Catania
Centro Siciliano di Fisica Nucleare - Catania

(ricevuto il 21 Dicembre 1959)

Summary. — The cross section for the reaction $^{31}P(n, p)^{31}Si$ has been measured by the activation method. The average behaviour of the cross section is the same that was found by others, but our measurements have put in evidence many details and a wide but well defined peak at 3.72 MeV. We have observed again the resonance peaks at 2.84 and 3.13 MeV found before by R. Ricamo. There is also evidence of other resonances around 4.5 MeV.

1. – Introduction.

The interaction mechanism of (n, p) reactions has become interesting in recent years because data ([4-6]) taken at a neutron energy of 14 MeV are in partial disagreement with the simple classical statistical evaporation theory ([7-10]).

(*) Work sponsored in part by the U.S.A. Air Force.

([1]) J. A. Grundl, R. L. Henkel and B. L. Perkins: *Phys. Rev.*, **109**, 425 (1958).
([2]) S. Morita: *Journ. Phys. Soc. Japan*, **13**, 431 (1958).
([3]) R. Ricamo: *Nuovo Cimento*, **8**, 383 (1951).
([4]) V. V. Verbinski, T. Hurlimann, W. E. Stephens and E. J. Winhold: *Phys. Rev.*, **108**, 779 (1957).
([5]) L. Colli, U. Facchini, I. Ioei, M. G. Marcazzan and A. M. Sona: *Nuovo Cimento*, **13**, 730 (1959).
([6]) R. F. Coleman, B. E. Hauker, L. O. O'Connor and J. L. Perkins: *Proc. Phys. Soc.*, **73**, 215 (1959).
([7]) N. Austern S. T. Butler and H. Mc Manus: *Phys. Rev.*, **92**, 350 (1953).
([8]) J. R. Lamarsh and H. Feshbach: *Phys. Rev.*, **104**, 1633 (1956).
([9]) G. Brown and H. Muirhead: *Phil. Mag.*, **2**, 473 (1957).
([10]) S. T. Butler: *Phys. Rev.*, **106**, 272 (1957).

In particular, the angular distributions from heavy nuclei are peaked forward.

We propose to extend the study to the (n, p) reaction mechanism in intermediate mass nuclei using neutrons in the energy region $(2 \div 5)$ MeV, where there are data on only a few elements ([16,17-21,22]).

The form of the (n, p) cross-section as a function of neutron energy should give a first indication of the interaction mechanism; proton angular distributions, and data for competing reactions should allow a more complete description of the (n, p) process.

In the present work phosphorus was chosen for its low threshold for the (n, p) reaction ($Q = -0.68$ MeV), relatively low excitation energy of the compound nucleus ^{32}P ($E^* = (10 \div 13)$ MeV) ([11]), and for the fact that the β energy and half life of the residual nucleus ^{31}Si are suited for the measurement of the (n, p) cross section by the activation method.

The (n, p) cross-section for ^{31}P was recently measured in its average behaviour by GRUNDL *et al.* ([1]) from 1.6 to 14 MeV, and by MORITA ([2]) up to 5.2 MeV. More detailed measurements between 1.9 and 3.6 MeV were made previously by RICAMO ([3]). This paper concerns measurements between 3 and 5 MeV using the activation method.

2. – Neutron source and phosphorus irradiations.

As a monochromatic neutron source we have used a heavy ice target bombarded with deuterons. The heavy ice target has been obtained by condensing a D_2O vapor stream on a copper tube opportunely shaped and cooled with liquid air. The deuterons produced by ionizing D_2 gas in an RF source were accelerated by a HVEC 2 MeV Van de Graaff electrostatic accelerator to energies of 1.8 and 2.0 MeV. The deuteron beam was deflected by 25° and focused on the ice target.

The target thickness was about $\frac{1}{4}$ of the saturation value and the deuteron current was 5 μA. In this condition the neutron intensity remained constant within a few per cent for some hours.

The neutron energy from the D(d, n)^{3}He reaction, was varied by changing the angle θ between the deuteron direction and the neutron accepted direction. With the deuteron energies used, the emerging neutron energy E_n was varied from 2.8 to 5.23 MeV by changing the angle θ from 0° to 90°.

During the course of the measurements we have repeatedly tested the Van de Graaff generator voltage, with H^- ions accelerated against LiOH and CaF_2 thin targets and have observed the resonance peaks of the (p, γ) and (p, $\alpha\gamma$)

([11]) P. M. ENDT and C. M. BRAAMS: *Rev. Mod. Phys.*, **29**, 683 (1957).

reaction in ^{7}Li and ^{19}F. The threshold for the ^{7}Li(p, n) reaction was also measured.

The accelerator voltage stability was 1‰.

Phosphorus samples were obtained compressing pure red phosphorus, mixed with a 1% colophony alcohol solution, in a plexiglass plate with a cavity (44×28) mm wide and 4 mm deep.

The average surface density was 650 mg/cm², corresponding to the saturation thickness for β self-absorption. To avoid air moisture absorption, samples were painted with 6 mg/cm² thick varnish.

Samples to be irradiated were mounted at the inner surface of an Al hollow cylinder 153 mm in radius, with its center at the neutron source (Fig. 1).

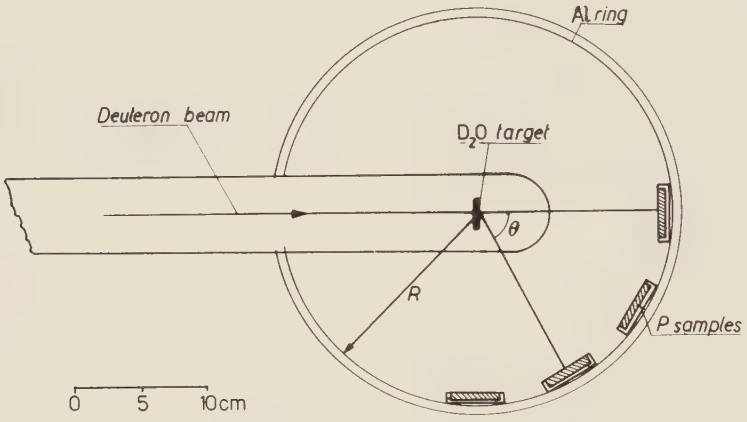

Fig. 1. – Experimental arrangement for phosphorus irradiation.

In each irradiation four samples were exposed for four hours in the neutron flux. The sample irradiation was repeated five times at $E_d = 1.8$ MeV, and two times at $E_d = 2$ MeV shifting each time some samples to cover the entire neutron energy range from 2.8 to 5.23 MeV. One sample was always irradiated at 0° as a monitor of the neutron flux.

3. – Beta activity measurements and σ(n, p) calculation.

^{31}Si is β active with $T = 157$ min and $E_\beta = 1.48$ MeV. For a target relatively thin for neutrons, one has for the number N of ^{31}Si nuclei produced per second per cm²:

$$N = \eta\,\sigma(\mathrm{n},\,\mathrm{p})(E_n)\cdot\varphi\,, \tag{1}$$

where η is the number of ^{31}P nuclei per cm^2, $\sigma(n, p)(E_n)$ is the total cross-section for the (n, p) reaction, and φ the number of neutrons per cm^2 per second at the sample.

If A is the measured activity of ^{31}Si after a time t_2 from the end of an irradiation, the cross-section for the (n, p) reaction is:

$$\sigma(n, p) = h \frac{A \exp[\lambda t_2]}{\sigma(\theta)}, \tag{2}$$

where h is a constant, λ the decay constant for ^{31}Si and $\sigma(\theta)$ the differential cross section for the neutron production in the D(d, n)^{3}He reaction.

The β activities of the four samples from each irradiation were measured at the same time with four 18505 Philips G.M. mica window β counters, whose entrance windows were limited by Al openings 3 mm thick, 20 mm long and 10 mm wide.

The four counters were fixed side by side and the four samples, carried by an iron slide,were explored each by one counter in steps of 4 mm length through the 10 mm wide counter window. In this way we obtained nine points of the excitation curve for each sample.

The measured half life was 157 min and we did not find indication of the ^{32}P, 14.3 d half life.

The average statistical counting errors were 4%.

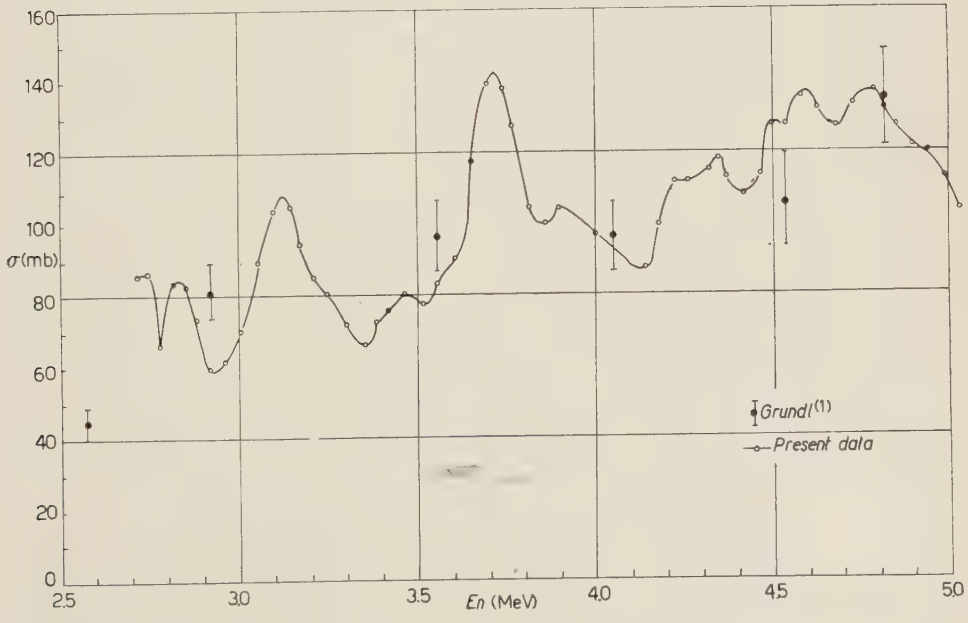

Fig. 2. – Cross section for $^{31}P(n, p)^{31}Si$ reaction normalized to GRUNDL *et al.* (1).

The relative cross-section was then obtained from the measured activities from each of seven runs reduced at $t_2 = 0$ using the D(d, n) laboratory system differential cross-section $\sigma(\theta)$ given by FOWLER and BROLLEY [12] deduced from BLAIR *et al.* [13].

The five (at $E_d = 1.8$ MeV) and the two (at $E_d = 2$ MeV) relative cross-sections obtained in this way were then normalized for the neutron flux variation in different irradiations using the activities of the $\theta = 0°$ samples. An average relative cross section σ' was then obtained showing maximal standard errors of 5%.

The absolute cross-section σ(n, p) was obtained by normalization of our results to the value of GRUNDL *et al.* [1] at 4.82 MeV (Fig. 2).

4. – Discussion and conclusion.

Recoil protons observed in nuclear photoplates exposed to the neutron flux at 0° allowed us to evaluate the neutron energy spectrum. The measured half widths were 300 keV for $E_n = 5$ MeV and 100 keV at $E_n = 2.5$ MeV. The neutron energy variation due to deuteron voltage instability was less than 3 keV.

The 10 mm width of the β counter window corresponded to 3°.7 angle at the neutron source giving a neutron energy spread of about 100 keV. The exploration of samples in 4 mm steps ($\Delta E_n \simeq 40$ keV), however, allowed indication of details with corresponding better resolution as is to be seen from the cross-section curve in Fig. 2 especially in the energy region $(4 \div 5)$ MeV.

The differential cross-section $\sigma(\theta)$ for neutrons from the d, d reaction at $E_d = 1.6$ MeV was recently remeasured in this laboratory and found very similar to that given by FOWLER and BROLLEY [12] in their report. We hope, therefore, to have not introduced noticeable errors using the known angular distribution of d, d neutrons in the calculation of the relative cross-section.

In Fig. 2 the experimental points of GRUNDL *et al.* [1] are indicated, and they fit our curve very well. Some discrepancies are found comparing our results with those of MORITA [2] expecially at $E_n = 4.7$ MeV.

Our measurements are the first to show a marked fine structure in the σ(n, p) cross-section for ^{31}P in the energy range from 3.6 to 5 MeV.

The pronounced maxima at 3.13 and 3.72 MeV are probably not due to single levels in ^{32}P as such levels at $E_n < 1$ MeV are already spaced only about 25 keV [14].

[12] J. L. FOWLER and J. E. BROLLEY: *Rev. Mod. Phys.*, **28**, 103 (1956).

[13] J. M. BLAIR, G. FREIER, E. LAMPI, W. SLEATOR jr. and J. H. WILLIAMS: *Phys. Rev.*, **74**, 1599 (1948).

[14] K. F. HANSEN, R. M. KIEHN and C. GOODMAN: *Phys. Rev.*, **92**, 652 (1953).

However, because of the marked structure observed in the $\sigma(n, p)$ reaction, we intend to study energy spectra and angular distributions of protons and the σ_t and $\sigma(n, \alpha)$ cross-sections.

To have a more complete presentation of the whole $\sigma(n, p)$ curve we normalized the values of RICAMO [3] around 3.0 and 3.5 MeV at those of GRUNDL *et al.* [1].

The Fig. 3 shows this. It is to be seen that present measurements fit very well those of RICAMO in the energy region (2.7 ÷ 3.6) MeV.

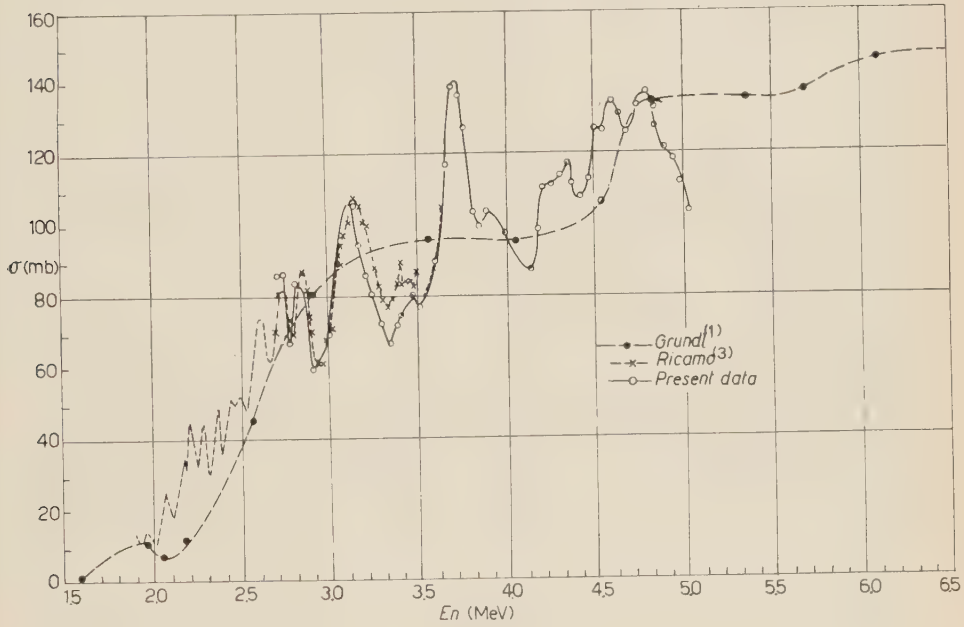

Fig. 3. – Cross sections for $^{31}P(n, p)^{31}Si$.

The curve of Ricamo taken with $E_d = 0.6$ MeV is higher than that of GRUNDL *et al.* in the energy region (2.0 ÷ 2.7) MeV. However, one observes the same discrepancy for the $^{32}S(n, p)^{32}P$ reaction in the same neutron energy region. The curve of LUSCHER *et al.* [15] for sulphur obtained with the activation method using d, d neutrons at $E_d = 0.61$ MeV is identical for $E_n = (2 \div 3.5)$ MeV to that obtained in another laboratory [16] five years later in similar conditions, but the two curves differ in the energy region $E_n = (2.0 \div 2.6)$ MeV from the

[15] E. LÜSCHER, R. RICAMO, P. SCHERRER and W. ZÜNTI: *Helv. Phys. Acta*, **23**, 561 (1950).

[16] P. HUBER and T. HÜRLIMANN: *Helv. Phys. Acta*, **28**, 33 (1955).

values of ALLEN *et al.* ([17]) in the same way as does the RICAMO $^{31}P(n, p)^{31}Si$ curve relative to the Grundl *et al.* cross-section at low energy.

Two explanations are possible:

a) the differential cross-section for the $D(d, n)^3He$ reaction at $E_d = (0.6 \div 1)$ MeV should have a less pronounced anisotropy then that given by HUNTER and RICHARDS ([18]), CHAGNON and OWEN ([19]), FULLER *et al.* ([20]);

b) the fission cross-section of ^{238}U used in the works ([1]) and ([17]) is unreliable in the energy interval $E_n = (2.0 \div 2.6)$ MeV.

We intend to measure the $D(d, n)^3He$ differential cross-section at deuteron energy lower than 1 MeV with photoplates whose energy response, is of course, well known.

* * *

We are indebted to R. M. WILLIAMSON (Duke University, Durham, N.C.) for many helpful discussions, and we like to thank him here.

([17]) L. ALLEN jr., W. A. BIGGERS, R. J. PRESTWOOD and R. K. SMITH: *Phys. Rev.*, **107**, 1363 (1957).
([18]) G. H. HUNTER and H. T. RICHARDS: *Phys. Rev.*, **76**, 1445 (1949).
([19]) P. R. CHAGNON and G. E. OWEN: *Phys. Rev.*, **101**, 1798 (1956).
([20]) J. C. FULLER, W. G. DANCE and D. C. RALPH: *Phys. Rev.*, **108**, 91 (1957).
([21]) M. J. SCOTT and R. E. SEGEL: *Phys. Rev.*, **102**, 1557 (1956).
([22]) J. B. MARION, R. M. BRUGGER and R. A. CHAPMAN: *Phys. Rev.*, **101**, 247 (1956).

RIASSUNTO

È stata misurata la sezione d'urto della reazione $^{31}P(n, p)^{31}Si$ nell'intervallo di energia $E_n = (2.7 \div 5)$ MeV con neutroni della reazione $D(d, n)^3He$ determinando l'attività del ^{31}Si ottenuta a varie energie di neutroni. I risultati si accordano molto bene con l'andamento medio determinato da altri autori mettendo però in evidenza una nuova risonanza molto marcata a 3.7 MeV. La $\sigma(n, p)$ presenta inoltre vari picchi non risolti attorno a 4.5 MeV.

Relativistic Observations and the Clock Problem (*).

J. Terrell

Los Alamos Scientific Laboratory, University of California - Los Alamos, N. Mex.

(ricevuto il 21 Dicembre 1959)

Summary. — Relativistic observational data are discussed, with the purpose of clarifying some aspects of the clock problem, usually called the « clock paradox » or « twin paradox ». Einstein's position, that an ideal clock which moves in a closed curve with respect to an unaccelerated clock will indicate the passage of less time, is supported. It is pointed out that the sets of observational data of two observers who take the place of the clocks in the above situation will not be at all similar. Furthermore, the data of the accelerated observer, obtained by means of single Doppler shift and visual observational methods, will be highly implausible and inconsistent with data obtained by radar and double Doppler shift methods. Thus the accelerated observer will be under no temptation to consider himself in a situation equivalent with that of the unaccelerated observer, and should not be surprised to discover upon returning that he has aged less than the other observer. It is pointed out that the accelerated observer will see striking effects due to relativistic aberration which will not be seen by the other observer, but that neither observer will be able to see or photograph the Lorentz contraction. Only the special theory of relativity is necessary in these calculations, since no genuine gravitational fields, produced by massive bodies, are involved.

1. – Introduction.

More than fifty years ago, in his original paper on the special theory of relativity (1), Einstein stated that an ideal clock which is moved in a closed curve with respect to an unaccelerated reference system will be found, at the end of its journey, to have lost time with respect to a clock stationary in that

(*) Work performed under the auspices of the U.S. Atomic Energy Commission.

(1) A. Einstein: *Ann. Phys.*, **17**, 891 (1905).

system. This statement is usually called the « clock paradox » or « twin paradox » (in reference to accelerated and unaccelerated observers). During the last twenty years the clock problem has been much discussed by DINGLE ([2]), who believes that EINSTEIN made a « regrettable error », and by many other writers who have responded in defense ([3-23]) of Einstein's statement. All standard textbooks on relativity and innumerable papers not mentioned here have supported Einstein's view; however, a few writers ([24-26]) appear to have accepted Dingle's views.

The basic reasons for the continuing controversy include the following:

1) The use of the word « paradox », which implies a contradiction between two correct statements and leaves the impression that the matter is not well understood. It is probably unfortunate that the clock problem has been referred to as an « apparent paradox ».

([2]) H. DINGLE: *Nature*, **144**, 888 (1939); **145**, 427, 626 (1940); **146**, 391 (1940); *The Special Theory of Relativity* (New York, 1941; also later editions); *Amer. Journ. Phys.*, **10**, 203 (1942); **11**, 228 (1943); *Nature*, **177**, 782 (1956); **178**, 680 (1956); *Proc. Phys. Soc. (London)*, A **69**, 925 (1956); *Nature*, **179**, 865, 1129, 1242 (1957); **180**, 500, 1275 (1957); *Austral. Journ. Phys.*, **10**, 418 (1957); *Science*, **127**, 158 (1958); *Bull. Inst. Phys.*, **9**, 314 (1958).

([3]) J. W. CAMPBELL: *Nature*, **145**, 426 (1940).

([4]) F. C. POWELL: *Nature*: **145**, 626 (1940).

([5]) P. S. EPSTEIN: *Amer. Journ. Phys.*, **10**, 1, 205 (1942).

([6]) L. INFELD: *Amer. Journ. Phys.*, **11**, 219 (1943).

([7]) W. H. MCCREA: *Nature* **167**, 680 (1951); **177**, 784 (1956); **178**, 681 (1956); *Proc. Phys. Soc. (London)*, A **69**, 935 (1956); *Nature*, **179**, 909 (1957); *Discovery*, **18**, 175 (1957).

([8]) H. E. IVES: *Nature*, **168**, 246 (1951).

([9]) G. THOMSON: *The Foreseeable Future* (Cambridge, 1955), pp. 88-89.

([10]) F. S. CRAWFORD, Jr.: *Nature*, **179**, 35, 1071 (1957).

([11]) S. F. SINGER: *Nature*, **179**, 977 (1957).

([12]) W. COCHRAN: *Nature* **179**, 977 (1957); *Proc. Camb. Phil. Soc.*, **53**, 646 (1957).

([13]) J. H. FREMLIN: *Nature*, **180**, 499 (1957).

([14]) C. G. DARWIN: *Nature*, **180**, 976 (1957).

([15]) J. D. ROBINSON and E. FEENBERG: *Amer. Journ. Phys.*, **25**, 490 (1957).

([16]) E. M. MCMILLAN: *Science*, **126**, 381 (1957); **127**, 160 (1958).

([17]) R. M. FRYE and V. M. BRIGHAM: *Amer. Journ. Phys.*, **25**, 553 (1957).

([18]) G. BUILDER: *Austral. Journ. Phys.*, **10**, 246, 424 (1957); **11**, 279 (1958); **12**, 300 (1959); *Phil. of Science*, **26**, 135 (1959); *Bull. Inst. Phys.*, **8**, 210 (1957).

([19]) C. B. LEFFERT and T. M. DONAHUE: *Amer. Journ. Phys.*, **26**, 515 (1958).

([20]) A. D. FOKKER: *Physica*, **24**, 1119 (1958).

([21]) R. H. ROMER: *Amer. Journ. Phys.*, **27**, 131 (1959).

([22]) E. FEENBERG: *Amer. Journ. Phys.*, **27**, 190 (1959).

([23]) C. C. MACDUFFEE: *Science*, **129**, 1359 (1959).

([24]) E. L. HILL: *Phys. Rev.*, **72**, 236 (1947).

([25]) L. ESSEN: *Nature*, **180**, 1061 (1957).

([26]) E. G. CULLWICK: *Electromagnetism and Relativity* (New York, 1957).

2) The incorrect belief that the statement « all motion is completely relative » is consistent with the special theory. Associated with this belief is a philosophical reluctance to accept relativistic aging differences. These are Dingle's basic tenets. However, the special theory predicts symmetry of observation for unaccelerated observers only; this symmetry is by no means true of other reference frames. The general theory of relativity makes no statements about symmetry of observations by two observers.

3) The incorrect belief that the clock problem cannot be handled by the special theory because of the accelerations. Accelerations were treated by use of the special theory in Einstein's first paper ([1]). Apparently it is now recognized by most writers, including DINGLE, that the general theory is not necessary in this matter. Both MOLLER ([27]) and MCMILLAN ([16]) have used special relativity to treat continuous acceleration in the clock problem. The general theory would be necessary only if genuine gravitational fields produced by massive bodies were involved.

4) Insufficient, and in some cases inaccurate, discussion of what the two observers (« twins ») will be able to observe. It appears that this matter has not been thoroughly considered. For instance, it was pointed out only very recently ([28]) that neither observer would be able to see or photograph the Lorentz-Fitzgerald contraction.

It is the purpose of this paper to discuss, in more detail than has previously been given, precisely what observations could be made by the accelerated and unaccelerated observers. It is hoped that this will make it clear in what ways the two observers are not equivalent.

2. – Unaccelerated case.

The simplest clock problem which has figured in the controversy involves three observers, A, B, and C, none of whom is accelerated; all are moving with uniform relative velocities along a single straight line in field-free space. In order to avoid discussing infinite sets of observers in each co-ordinate system, it will be assumed here and in other cases that each observer is equipped with radar, radio, and optical equipment for the purpose of measuring distances and relative velocities and synchronizing clocks. The radar method of measuring distance does not differ in principle from the optical methods discussed by EINSTEIN ([1]); it involves a signal moving at the velocity of light c, which is transmitted by observer A to observer B (for instance) and either reflected or retransmitted back to A. Observer A then plots the distance to B as $c(t_r - t_t)/2$ at the time $t_A = (t_r + t_t)/2$, where t_t and t_r are the times of trans-

([27]) C. MØLLER: *The Theory of Relativity* (Oxford, 1955), p. 258.

mission and reception as measured by A. In addition, B transmits to A the reading of B's clock at the time the signal is received by B (telescopic observation by A would give the same result), and A plots this reading (t_B) also for the time t_A.

It is postulated that the situation as observed by A with his equipment is this: B passes him with relative velocity v at the time $t_A = 0 = t_B$, synchronizing his clock in passing. Observer B attains a distance L at time $t_A = L/v$ and simultaneously passes observer C, travelling in the opposite direction, also with velocity v relative to A. Observer C synchronizes his clock to that of B at the moment of passing; there is no difficulty in doing this when the distance between them is vanishingly small. Finally C passes the position of A at $t_A = 2L/v$ and A and C compare clocks.

The result is unambiguous if the postulates of special relativity are accepted. Observer A observes the clocks of both B and C to be running uniformly slower than his, with the relation being $t_B = t_C = \alpha t_A$ according to the data of A, where $\alpha = \sqrt{1 - v^2/c^2}$. He will thus observe the reading $t_C = 2\alpha L/v$ on C's clock at the moment of passing, when $t_A = 2L/v$. It cannot be correctly argued that A would observe C synchronizing his clock with that of B, but somehow making a mistake in the process (as observed by A) of just enough to make $t_C = t_A$ at the moment when A and C pass. If this were so, another observer with zero velocity relative to A, located at the point where B and C pass, would have to observe the same thing, and this is not possible if B and C see their synchronization as correct. It is a standard result in the special theory of relativity that two observers in the same inertial system, even though widely separated, can synchronize their clocks with no difficulty and will then obtain exactly the same observations of phenomena occurring in other systems.

Since A, B, and C are all assumed to be in inertial systems of co-ordinates, there is no reason to prefer the observations of A to those of B or C. Observer B, for instance, observes A's clock to be too slow by the same factor, α, that A observes for B's clock, and observes C's clock to be even slower than that of A, since B measures C's velocity to be $2v/(1 + v^2/c^2)$, which is greater than v. Hence B agrees that C's clock reads less than that of A when C passes A. Similarly, the data of observer C indicate that A's clock is slow by the factor α, but that B's clock is even slower, thus accounting for the fact that C's clock, having been synchronized to that of B, still reads less time than A's when A passes C.

3. – Accelerated case.

In the situation just described, A, B, and C are equally good as observers. Their observations are different, but this fact is a basic phenomenon of special

relativity. As long as they continue their uniform, unaccelerated, velocities, there is no basis for saying that anyone's clock is « really » indicating the passage of less time than another's clock; to do so would be to give preference to one of the three co-ordinate systems, However, such a statement does become possible if the observers are not in equivalent situations. The unaccelerated situation becomes the familiar clock problem if one change is made, substituting observer B for observer C at the time of their meeting. Thus we deal only with observers A and B; as observed by A, B synchronizes his clock in passing, travels with velocity v to a distance L, then reverses direction in a time negligible with respect to L/v and returns to the position of A. The observations of A are essentially the same as in the unaccelerated case, so that B's clock will read less than A's upon the second meeting. The observations of B, who does not remain in a single inertial system, will be confusing and apparently internally inconsistent, as will be discussed later. Thus the acceleration which B undergoes makes a real difference in the status of the two observers.

The acceleration period of observer B has been assumed to be short enough that it need not be considered in the calculations. The clock problem may be solved for lengthy periods of acceleration, but the calculations are also more lengthy ([16,27]), though straightforward. In no case does it become necessary to use the general theory, although the clock problem may be discussed from this point of view ([17,19,27,29]) if desired. In all calculations it is necessary to assume that the clocks are ideal clocks, which run during acceleration at the same rate as unaccelerated clocks with respect to which they are momentarily stationary. Actual clocks may not be ideal; they may, for instance, stop permanently under acceleration. Neither the general nor special theories of relativity can predict fully the behavior of actual clocks ([30]).

We thus have to assume, if the problem deals with actual clocks, that B's clock does not change reading in an essentially discontinuous way during the short acceleration period. It is not physically reasonable that another observer, stationary with respect to A and located in the small area of B's acce-

---

([28]) J. Terrell: unpublished paper on *The Clock « Paradox »* (1957); *Bull. Am. Phys. Soc.*, **4**, 294 (1959); *Phys. Rev.*, **116**, 1041 (1959).

([29]) R. C. Tolman: *Relativity, Thermodynamics, and Cosmology* (Oxford, 1934) p. 194.

([30]) The assumption of ideal clocks, or that actual clocks may be so corrected as to substitute for ideal clocks, is essential to the treatment of acceleration in either the special or general theories. However, accelerations observed in studies of fundamental particles can be so great that no conceivable clock would be ideal, as even the fundamental particles are disrupted. Without a complete theory of the constitution of such particles no completely accurate description can be given for such high accelerations. With lesser accelerations fundamental particles should be exceedingly good approximations to ideal clocks.

leration, would observe such a jump in B's clock reading. It would be completely unreasonable to assume that the jump would be just enough to make the clocks of A and B coincide at the end of the journey, since the jump would then depend on the distance of A from the additional observer. The third observer has been momentarily introduced merely to forestall doubts about observations at a distance; according to the special theory his observations would be identical with those of A, after the usual corrections for time lags.

CRAWFORD [10] has pointed out that the assumption of no jump in clock reading is experimentally correct for μ-mesons (one type of physical « clock »). Cosmic-ray data indicate [31-33] that μ-mesons have a much longer observed lifetime at relativistic velocities than at rest, as expected, and that the ages of μ-mesons which come to rest at different altitudes above sea level are not equalized by any anomalous disintegration rates during deceleration.

The difference in clock readings of observers A and B may be discussed very simply in terms of Minkowski's four-dimensional space-time. One of the basic results of special relativity is that the four-dimensional interval s between two events, defined by $s^2 = c^2t^2 - \sigma^2$, is an invariant quantity, the same for all unaccelerated (« Galilean » or inertial) co-ordinate systems. In this equation t and σ are the measured intervals in time and space. If the departure, turnaround, and return of B are designated by subscripts 1, 2, and 3, the interval between events 1 and 2 (or between 2 and 3) is given, in terms of A's data, as $s_{12} = s_{23} = \sqrt{(cL/v)^2 - L^2} = (Lc/v)\sqrt{1 - v^2/c^2}$. Since observer B is physically present at events 1 and 2 (and is in an inertial system during this time), he will measure the interval as entirely timelike, the time interval being $\tau_{12} = (L/v)\sqrt{1 - v^2/c^2}$. He obtains the same result for τ_{23}; thus he measures the time interval for his entire journey as $(2L/v)\sqrt{1 - v^2/c^2}$, while observer A measures it as $2L/v$, a longer time.

It is true in general that an observer who is physically present at two events (and unaccelerated during this interval) will measure less time between the two events than any other observer who is in a different inertial system and hence observes a space interval between the two events. This statement, of course, follows immediately from the definition of the invariant space-time interval s.

4. – Data of the two observers.

The non-equivalence of observers A and B becomes quite clear when their sets of data on measured distances and times are compared, as McCREA [7]

(31) B. ROSSI, N. HILBERRY and J. B. HOAG: *Phys. Rev.*, **57**, 461 (1940).
(32) F. RASETTI: *Phys. Rev.*, **60**, 198 (1941).
(33) H. TICHO: *Phys. Rev.*, **72**, 255 (1947).

has done. In order to make the situation slightly more general, it is now assumed that B comes to rest with respect to A and remains at rest for a time Δ before beginning the return trip. This situation then covers several different types of clock problems simultaneously; the simpler problem discussed in the previous section is, of course, obtained by setting $\Delta = 0$.

We postulate, then, that A, making radar measurements of distance as a function of time, observes B to synchronize his clock in passing, proceed at velocity v to a distance L, pause at this distance for a time Δ, and return at velocity v. He also observes B's clock to be losing time during the periods of relative motion, so that at the second meeting B's clock reads $2\alpha L/c + \Delta$, while A's clock reads $2L/c + \Delta$. What B observes, using similar equipment, may be calculated by use of the Lorentz transformation or by the elementary

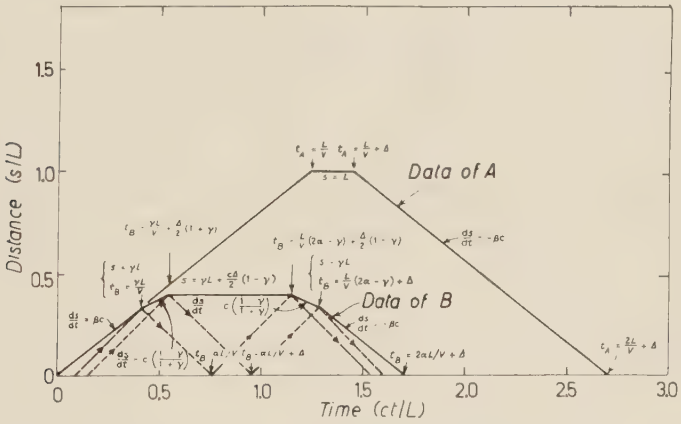

Fig. 1. – Data of observers A and B on relative distance as a function of time, obtained by radar or double Doppler shift methods, and in the case of observer A also by the use of single Doppler shift or visual observations. Paths of a few light or radar signals as plotted by B are shown as dashed lines. In this and the other figures it is assumed for illustrative purposes that $\beta = v/c = 0.8$, $\alpha = \sqrt{1-\beta^2} = 0.6$, $\gamma = \sqrt{(1-\beta)/(1+\beta)} = \frac{1}{3}$, and $\Delta = 0.2L/c$.

process of tracing the interchange of signals, and is shown in Fig. 1. For the purpose of drawing the figure the choices $\beta = v/c = 0.8$ and $\Delta = 0.2L/c$ have been made, so that $\alpha = \sqrt{1-\beta^2} = 0.6$ and the Doppler shift factor $\gamma = \sqrt{(1-\beta)/(1+\beta)} = \frac{1}{3}$. This numerical value of relative velocity is also the one chosen by DARWIN [14], to avoid « tiresome irrationalities ». The postulated observations of A are also shown, and it is seen that the two sets of observations are not at all similar.

The radar measurements of distance which B makes during the initial

stage of his journey, with transmission and reception both occurring before B undergoes acceleration, indicate a relative velocity v, the same result obtained by A. The same result is also obtained during the last stage of B's journey. Those radar measurements for which reception (or transmission) occurs during the « pause » of time Δ indicate a smaller relative velocity given by $v(1-\gamma)/(1+\gamma)$. Those radar measurements made by B for which transmission occurs on the outward journey and reception occurs on the return trip take a constant time, as measured by B, and indicate that A, is for a time, at a constant distance less than L, given by $\gamma L+\Delta(1-\gamma)/2$. It is assumed here that $\Delta \leqslant 2L/c$, so that B could not send and receive the same radar signal during the « pause » (for larger values of Δ observer B would observe the distance of A to increase continuously to the value L and then remain constant for a time).

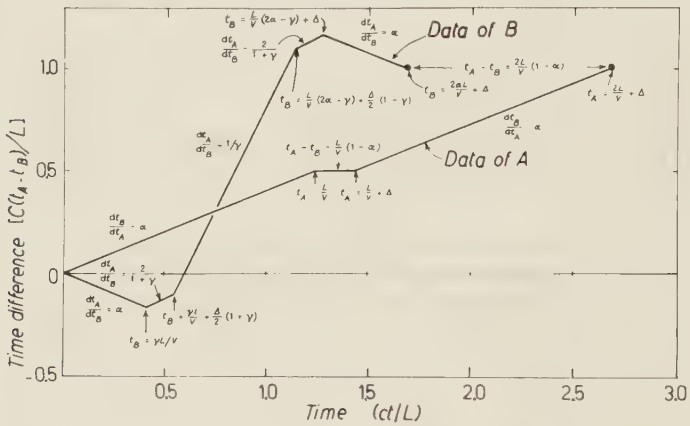

Fig. 2. – Data of observers A and B on differences in clock readings as functions of time. Both sets of data have been corrected by means of the distance observations of Fig. 1.

Fig. 2 shows the two sets of data on the difference in readings of the two clocks, as observed after correction for the time which light (or radio) signals take to reach the observers. As in the case of the distance measurements, those measurements completed within the first part (or the last part) of B's journey give the usual result, that B observes A's clock to be losing time the ratio of rates being α. However, the data received by B during the « pause » show A's clock to be gaining time at a rate given by $\mathrm{d}t_A/\mathrm{d}t_B = 2/(1+\gamma)$; this is also true for data received at a later time, corresponding to radar transmission during the time Δ. Moreover, for the first part of B's return journey the incoming corrected time data of B indicate that A's clock is running

extremely fast, by the factor $1/\gamma$. Naturally, these points are automatically plotted for an earlier time than that of reception of data. Finally, B observes A's erratic clock to be ahead of his on the occasion of reunion, which is at a time $2L/v+\Delta$ for A and $2\alpha L/v+\Delta$ for B.

It is possible for observers A and B to take additional data on their relative velocities by measuring the Doppler shift of radar signals. If they observe the frequency f_r of their own radar signals (originally at frequency f_t) as returned to them by reflection, special relativity predicts that this «double Doppler shift» will be given by $f_r/f_t=\gamma^{\pm 2}$ for inertial reference frames; the minus sign is to be used for the case of decreasing distance between the observers. The velocity may be calculated from the relation $v/c=(1-\gamma^2)/(1+\gamma^2)$, and the distance may be obtained by integration of velocity. If observer A chooses to measure the Doppler shift of the radar signals transmitted by observer B, he must use the equation $f_r/f_0=\gamma^{\pm 1}$ and solve for v in the same way. Here the negative exponent is once again to be used for the case of relative motion toward the observer; f_0 is the transmitted frequency as measured in the rest system of the transmitter, presumed to be known to A.

Observer A would obtain exactly the same set of data in either of these ways as with his radar measurements. Observer B would verify his radar data by measurement of the Doppler shift of his own reflected signals, but from single Doppler shift data would obtain a conflicting and nonsensical set of data as to velocity, which would, however, be consistent with his visual observations, to be discussed. He could obtain agreement between both types of Doppler data only by first correcting the rest-calibrated frequency f_0 of A's transmitter to a presumed frequency f_t as measured in B's co-ordinate system, using his data on the rate of A's clock, and then applying the appropriate equation ([34]), $f_r/f_t=(1\pm v/c)^{-1}$. On this last basis his single Doppler shift data would give him no independently useful data, requiring both radar distance and clock observations for corrections.

It has become apparent that observer B is in trouble if he attempts to apply the simple equations given by special relativity for unaccelerated observers, and most of his difficulties have not yet been mentioned. If he should have the point of view that his situation is precisely equivalent to that of observer A, his confidence might be shaken by the strong accelerations which he, and not observer A, will feel. In any case, B observes at these times a sudden and permanent (until the next acceleration) change in the apparent

([34]) This equation is correct relativistically, and may be applied by observer A without difficulty. The relativistic Doppler shift may be derived as the product of the non-relativistic shift for stationary observer, as given here, and the relativistically reduced rate of a moving clock. A similar statement may be made for the assumption of stationary transmitter.

directions of stars and other external objects, a shift which A does not see. This is the optical phenomenon of aberration, the expression for which, derived ([1]) from the Lorentz transformation, is $\sin\theta = (\alpha \sin\theta')/(1 - \beta\cos\theta')$. Here θ is the polar angle of an object as seen by any observer, *i.e.*, the apparent visual direction of the object, and θ' is the apparent direction of the same object as seen simultaneously by another observer at the same location but moving in the direction $\theta = 0 = \theta'$ with relative velocity $v = \beta c$. If an observer at the point of acceleration, stationary with respect to A, sees a star at 90° to the path of B, for example, B will see it somewhat ahead at about 37° (for $\beta = 0.8$; in general the angle would be given by $\sin\theta = \alpha$) during the first part of his journey, at 90° while he is at rest with respect to A, and at 143° during the last part of his trip.

It should be noted, however, that neither observer A nor B will see or photograph any Lorentz-Fitzgerald contractions of stars or groups of stars at any time. As has been recently pointed out ([28]), the contraction due to relativistic motion is optically invisible. In effect, aberration is equivalent to a conformal transformation on the surface of a sphere centered at the point of observation, on which are plotted the apparent directions of distant objects. If a distant object is seen by one observer to have a particular outline, circular for instance, it will be seen with precisely the same outline (for sufficiently small subtended angle ([35])) by any other observer in relative motion but simultaneously at the same point. He will, however, see it at a different angle and apparent distance (the ratio of apparent distances is just the Doppler shift ratio), and there will be curious distortions of perspective, or of appearance with the use of stereoscopic vision ([28]). The visual data of any observer will lead to the well-known contraction only when corrected for the finite velocity of light.

If B observes A through a telescope, he will see sudden changes in the apparent distance of A at the times of acceleration; that is, the angle subtended by the face of A's clock or meter stick will suddenly change. The aberration equation yields the result that, when B comes to rest with respect to A, B observes A suddenly to shrink in apparent subtended angle, the ratio of change being γ. The effect is that A, apparently at distance γL, suddenly appears to be at distance L. As soon as B begins to move toward A (from the point of view of A), B observes a further apparent shrinkage of A, the ratio again being γ, so that A now appears to be at a distance L/γ. Observer B, knowing the finite velocity of light, naturally ascribes these events to times

([35]) R. Penrose: *Proc. Cam. Phil. Soc.*, **55**, 137 (1959), has recently shown that for the special case of a circular outline there is no restriction as to subtended angle. Spheres will be seen as having circular outlines by all observers, regardless of relative velocities and subtended angles.

earlier than those of observation. By observing the angle subtended by A throughout his journey, B has a perfectly valid way of plotting the distance of A as a function of (corrected) time. That is, the method is valid for an inertial system of co-ordinates, and A would merely verify his radar measurements in this way. However, B's data, shown in Fig. 3, will give B the

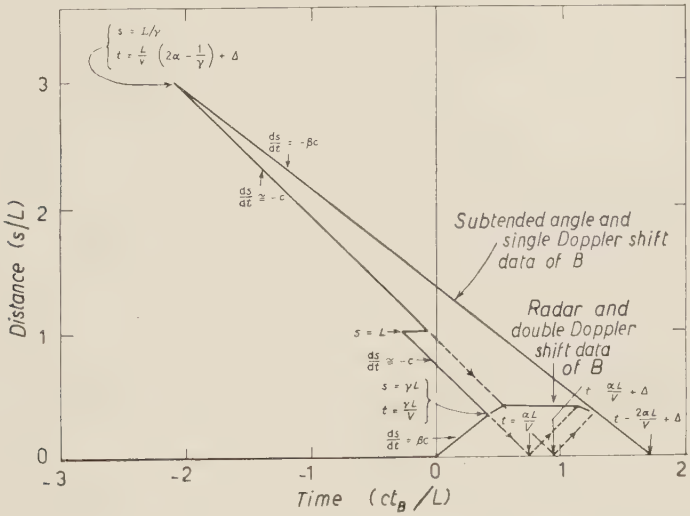

Fig. 3. – Data of observer B on the distance of A, as taken in several different ways. Paths of a few light or radar signals as plotted by B are shown as dashed lines.

problem of deciding how A can move at speeds slightly greater than the speed of light and travel alternately backward and forward in time, thereby existing in three or occasionally five places simultaneously. Observer B will also have to decide why these data differ from his radar and double Doppler shift data; as mentioned earlier, his single Doppler shift data could be interpreted as being consistent with his visual observations.

The simplest solution to the difficulties facing observer B would be that he decide that he has changed velocity and has not remained in a single inertial system. He can then correct his data to obtain a consistent set for some unaccelerated co-ordinate system. An alternative which B could choose is to apply the general theory of relativity and assume himself to have been unaccelerated throughout these events. He could, because of the principle of equivalence, account for all observed effects by introducing moving gravitational fields having the nature of plane shock waves, which passed him coincidentally with his application of rocket power (or whatever produced his accelerations as observed by A). Thus observer B could assume himself to have remained stationary while A and the rest of the universe were accelerated.

However, this would be a somewhat complicated, coincidental, and physically implausible explanation, although it would agree with the general theory of relativity and would account for all the observations discussed.

5. – Conclusion.

It is the intent of this paper to clarify some features of the clock problem, in particular what the accelerated observer could actually observe by the use of conceivable equipment, and to show that in all aspects the problem can be handled by the tools of special relativity alone. The result is that the accelerated observer will definitely observe less elapse of time than the unaccelerated observer. No paradox, in the sense of a contradiction, is involved since the two observers cannot be considered, and cannot consider themselves, to be in equivalent situations.

* * *

I am indebted to many persons at this Laboratory for informative discussions, and in particular to Drs. A. W. Schardt and A. M. Lockett for careful examination of some of the points discussed in this paper. I am grateful to Drs. C. G. Darwin, W. H. McCrea, J. A. Wheeler, and H. A. Wilson for helpful advice, and to Dr. H. Dingle for pointing out some ambiguities of language in an earlier version of this paper (with which he disagrees).

RIASSUNTO (*)

Si discutono i dati relativistici delle osservazioni con lo scopo di mettere in chiaro alcuni aspetti del problema dell'orologio, detto di solito « il paradosso dell'orologio » o « il paradosso dei gemelli ». Si sostiene la posizione di Einstein, secondo la quale un orologio immaginario che si muova su una curva chiusa rispetto ad un orologio non soggetto ad accelerazioni indicherà il trascorrere di un tempo minore. Si sottolinea che i gruppi di dati d'osservazione di due osservatori che prendono il posto degli orologi nella suddetta situazione non saranno per nulla simili. Per altro i dati dell'osservatore sottoposto ad accelerazione, ottenuti a mezzo dei metodi di un singolo spostamento di Doppler e dell'osservazione visuale, saranno del tutto implausibili e non coerenti con i dati ottenuti a mezzo dei metodi del radar e del doppio spostamento di Doppler. Cosicchè l'osservatore sottoposto ad accelerazione non sarà tentato a considerarsi in una situazione equivalente a quella dell'osservatore non sottoposto ad accelerazione, e non sarebbe sorpreso nello scoprire al ritorno che è invecchiato meno dell'altro osservatore. Si sottolinea che l'osservatore sottoposto all'accelerazione vedrà effetti impressionati dovuti all'aberrazione relativistica, che non saranno visti dall'altro osservatore. ma nessuno dei due sarà in grado di vedere o fotografare la contrazione di Lorentz, Per questi calcoli è sufficiente la teoria ristretta della relatività, perchè non vengono interessati genuini campi gravitazionali, prodotti da corpi di massa notevole.

(*) *Traduzione a cura della Redazione.*

Cosmic Ray Investigations with an Airborne Neutron Monitor (*).

M. A. Pomerantz, V. R. Potnis and S. P. Agarwal

Bartol Research Foundation of the Franklin Institute - Swarthmore, Penna.

(ricevuto l'8 Gennaio 1960)

Summary. — A neutron monitor has been in operation aboard a magnetic survey aircraft. During a cruise in November, 1958, the latitude effect of the nucleonic component was measured over the same route between Tokyo and the Aleutian Islands as that covered by Sandström in February, 1957. Although the two sets of data normalized at Tokyo are in agreement up to approximately 43° N (modified geomagnetic latitude), a change in the shape of the curve had occurred at higher latitudes. The intensity at 55° N had decreased by 13%, and the «knee» had shifted from 47° N to 43° N. The latitude variation of the absorption mean free path was determined from intensity *vs.* altitude curves at geomagnetic latitudes 50° N, 37° N, 25° N, and 13° N. A change of roughly 10% over a range of primary cut-off rigidity from 2 GV to 15 GV was indicated. Comparison with earlier results of others revealed no appreciable variation of the mean free path during the solar cycle.

1. – Introduction.

In order to investigate in a comprehensive manner the relationship between the spatial distribution of cosmic ray intensities and the magnetic field of the earth, a neutron monitor has been installed aboard a Super Constellation aircraft specifically equipped for conducting magnetic surveys, and operating under the technical direction of the Hydrographer of the United States Navy. This preliminary report of some of the results obtained during the initial flights, however, does not pertain to the magnetic measurements, but rather is concerned with two particular aspects of the cosmic ray investigations which do not involve the simultaneous magnetometer recordings: *a*) the time variation of the latitude effect of the nucleonic component, and *b*) the latitude-dependence of the atmospheric absorption of the nucleonic component.

(*) Supported by the Office of Naval Research. Reproduction in whole or in part is permitted for any purpose of the United States Government.

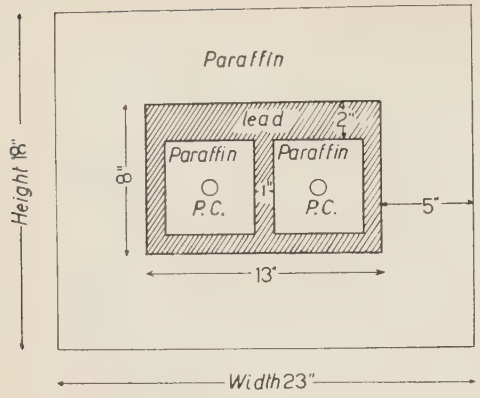

Fig. 1. – Arrangement of pile aboard project magnet aircraft. Length of pile: 25 inch. Diameter of counters: 2.5 inch. Active length of counters: 20 inch. Length of lead: 20 inch.

2. – Experimental details.

The arrangement of the airborne pile is shown schematically in Fig. 1. The paraffin is contained in sealed magnesium tanks, and the entire pile is enclosed inside a welded aluminum box secured to the deck of the Super Constellation aircraft. The counter walls are aluminum. Two completely independent sets of associated electronic circuits and printout recorders permit continuous internal consistency checks. Calibra-

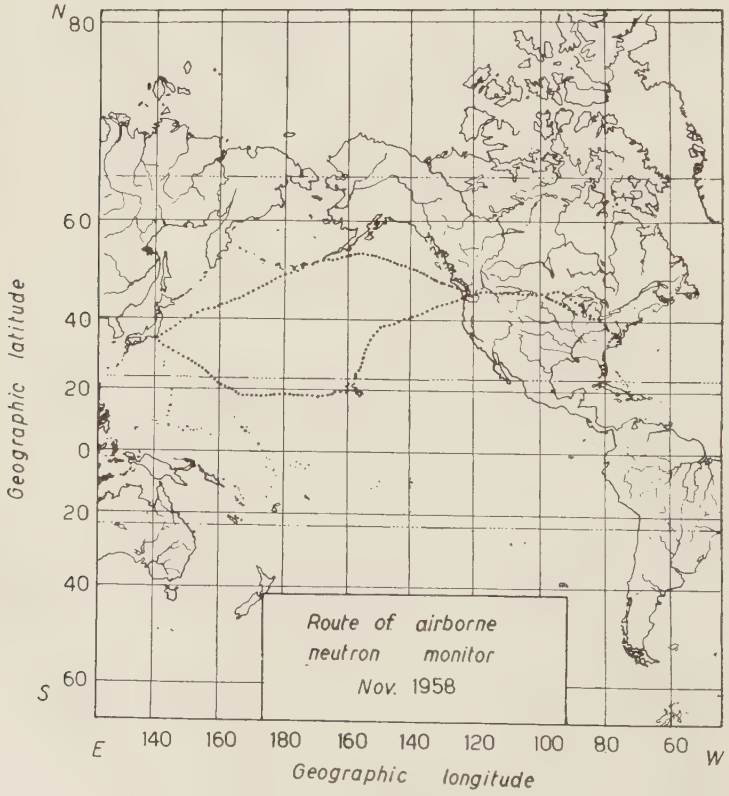

Fig. 2. – Route of project magnet airborne neutron monitor during November, 1958.

tion runs with a Ra-Be neutron source are conducted immediately prior to takeoff, and upon landing.

The data presented in the following sections were obtained in November, 1958, during the course of flights over the routes indicated in Fig. 2.

3. – Latitude effect of nucleonic component.

The track between Tokyo and the Aleutian Islands practically overlapped the route over which similar measurements were obtained by SANDSTRÖM (1) twenty-one months earlier. In Fig. 3, both sets of data have been plotted as a function of modified geomagnetic latitude, $\bar{\lambda}$ (2). The normalization con-

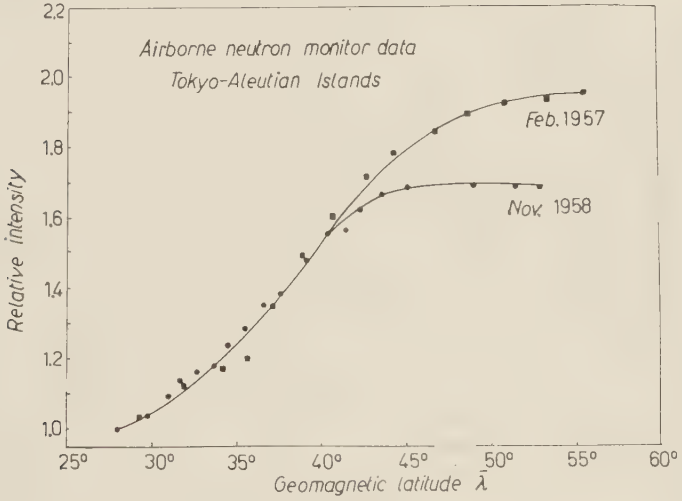

Fig. 3. – Relative intensity of the nucleonic component in February, 1957 (1), and in November, 1958, plotted as a function of modified geomagnetic latitude, $\bar{\lambda}$ (2).

stant for reducing the counting rates to the same relative intensity scale was computed for Tokyo ($\bar{\lambda} = 28°$ N). During Sandström's flight, the Mount Norikura neutron monitor indicated no fluctuations exceeding 1%, and no correction was applied to the data (1). The present data have been corrected for similar fluctuations during the flight although variations in the fixed station counting rate did not exceed 1% (3).

(1) A. E. SANDSTRÖM: *Suppl. Nuovo Cimento*, **8**, 263 (1958).
(2) J. J. QUENBY and W. R. WEBER: *Phil. Mag.*, **4**, 90 (1959).
(3) We wish to thank Dr. Y. MIYAZAKI for promptly supplying the Mt. Norikura data.

It is clear that the two sets of data are in agreement up to approximately 43° N, within the statistical and systematic uncertainties. Although during February, 1957, the intensity at high latitude had exhibited a slow increase, a plateau of constant counting rate appeared north of 45° in November, 1958. On the basis of the indicated normalization, the nucleonic flux decreased by 13% at 55° N.

Although there is considerable ambiguity in the definition of the knee of latitude effect, if the procedure generally followed by other investigators is adopted, it may be stated that the knee in February, 1957, (if indeed the term is applicable) occurred at 47° N and has shifted to 43° N in November, 1958.

In any event, the fact that the curves in Fig. 3 coincide at lower latitudes appears to indicate that the *shape* of the primary rigidity spectrum at higher rigidities (> 4.4 GV) was essentially unaffected by the modulation mechanism compared with the low rigidity end.

4. – Atmospheric absorption of nucleonic component.

An accurate determination of the atmospheric absorption coefficients is required for reducing data obtained with airborne instruments to a standard pressure-altitude, since unavoidable changes in cruising altitude are imposed by weather conditions and other considerations beyond internal control. Furthermore, direct measurement, with a detector aboard an aircraft, of the dependence of intensity upon height yields a much more precise coefficient for correcting ground-station neutron monitor data for variations in barometric pressure than does the usual statistical analysis of the correlation of counting rates with barometer readings. In the latter case, intensity variations not associated with atmospheric absorption complicate the situation, particularly during periods of solar maximum.

The latitude-variation of the mean free path of atmospheric neutrons was measured previously with fast neutron detectors aboard an aircraft ([4]). However, determinations of the atmospheric absorption of the nucleonic component with airborne piles were confined to high latitudes ([1,5]).

In view of the foregoing considerations, it is of interest to examine in detail data obtained during ascents and descents, as well as periods of level flight at different altitudes above a fixed station. In Fig. 4, the counting rates per counter at geomagnetic latitudes 50° N, 37° N, 25° N, and 13° N respectively are plotted on a logarithmic scale as a function of pressure-altitude (NACA

([4]) J. A. SIMPSON: *Phys. Rev.*, **83**, 1175 (1951).
([5]) J. A. SIMPSON and W. C. FAGOT: *Phys. Rev.*, **90**, 1068 (1953).

standard atmosphere). The statistical standard deviations are smaller than the symbols except where indicated. The straight lines represent the best fit determined by the method of least squares with appropriate weighting of the various points.

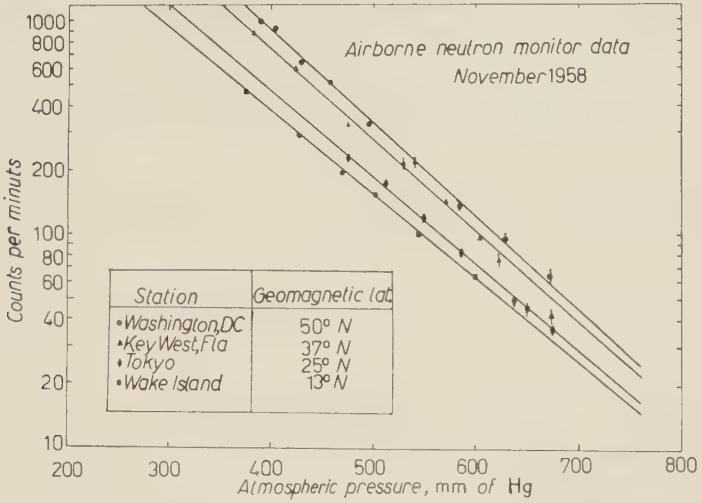

Fig. 4. – Atmospheric absorption curves at different latitudes. The corresponding mean free paths are listed in Table I.

Table I summarizes atmospheric absorption measurements obtained with airborne piles. The tabulated results of the present experiment are derived from the slopes of the curves in Fig. 4.

The latitude variation of the atmospheric absorption coefficient is considerably smaller than that observed earlier with fast neutron detectors ([3]). The present results indicate a change in the absorption mean free path of roughly 10% over a range of primary cut-off rigidity from 2 GV to 15 GV.

The generally-accepted barometer coefficient for the nucleonic component ($(-0.96 \pm 0.06)\%$/mm of Hg as determined by SIMPSON *et al.* ([6]) from neutron monitor data at Climax), corresponds to an absorption mean free path of (142 ± 9) g/cm², in agreement with the value determined with airborne neutron monitors.

The fact that the present results are in accord with previous measurements indicates that the mean free path has not changed appreciably during the solar cycle.

([6]) J. A. SIMPSON, W. FONGER and S. B. TREIMAN: *Phys. Rev.*, **90**, 934 (1953).

TABLE I. – *Summary of atmospheric absorption measurements with airborne neutron monitor.*

Date	Location	Geo-magnetic latitude	Absorption mean free path, g/cm²	Range of atmospheric depth, g/cm²	Reference
Nov., 1958	Washington, D.C.	50° N	136 ± 7 (*)	550 ÷ 950	Present paper
Nov., 1958	Key West, Florida	37° N	139 ± 1	550 ÷ 950	Present paper
Nov., 1958	Tokyo, Japan	25° N	147 ± 9	650 ÷ 950	Present paper
Nov., 1958	Wake Island	13° N	152 ± 5	550 ÷ 950	Present paper
Jan., 1957	Sweden	65° N	131 ± 5	570 ÷ 680	SANDSTRÖM (1958)
Jan., 1957	Sweden	58° N	133	300 ÷ 600	SANDSTRÖM (1958)
Aug., 1952	United States	52° N	141 ± 2	530 ÷ 750	SIMPSON and FAGOT (1953)
Aug., 1952	Mobile, Alabama	41° N	141 ± 4	580 ÷ 770	SIMPSON and FAGOT (1953)

(*) If measurements obtained in March, 1959, are combined with the November, 1958, data the absorption mean free path becomes (136 ± 3) g/cm².

* * *

It is a pleasure to express our appreciation to the Hydrographer, United States Navy, for accommodating the neutron monitor aboard the Project Magnet aircraft. Hydrographic Office personnel, particularly WILBURT GEDDES, have co-operated wholeheartedly in solving the technical problems in connection with the installation and operation of the equipment. Finally, we wish to thank the pilot, Lieutenant Commander J. H. BRADY, and the members of the crew who have been so helpful throughout the entire operation.

RIASSUNTO (*)

Un rivelatore di neutroni è stato installato su un aereo adibito al rilevamento magnetico. Durante un volo nel Novembre 1958 l'effetto di latitudine sulla componente nucleonica fu misurato lungo lo stesso percorso da Tokyo alle Aleutine effettuato da Sandström nel Febbraio 1957. Sebbene i due gruppi di dati normalizzati per Tokyo si accordino sino a circa 43° N (latitudine geomagnetica modificata), a latitudini più alte si è rilevata una modificazione nella forma della curva. L'intensità a 55° N è diminuita del 13%, ed il « ginocchio » della curva si è spostato da 47° N a 43° N. La variazione con la latitudine del percorso libero medio di assorbimento venne determinato in base alle curve intensità-altitudine alle latitudini geomagnetiche 60° N, 37° N, 25° N e 13° N. Si è rilevata una variazione di circa il 10% su un campo di rigidezza di cut-off primario fra 2 GV e 15 GV. Il confronto con i precedenti risultati ottenuti da altri non ha rivelato variazioni del cammino libero medio durante il ciclo solare.

(*) *Traduzione a cura della Redazione.*

On the Interaction of (200÷300) MeV K^+-Mesons in Emulsion.

D. Evans, F. Hassan (*), K. K. Nagpaul (**) and N. Shafi (***)

H. H. Wills Physical Laboratory - University of Bristol

(ricevuto il 14 Gennaio 1960)

Summary. — The mean free path for (200÷300) MeV K^+-meson reactions with emulsion nuclei (other than hydrogen) is found to be (60±6) cm. One scatter from hydrogen in 92 m of track length is described and the data on elastic and inelastic reactions are given. No evidence of π-meson production was seen. The nuclear effects of the inelastic reactions are discussed.

1. – Introduction.

The study of K^+-meson reactions with emulsion nuclei has now been extended into the (200÷300) MeV region by a number of workers [1-3]. Part of the results reported in the present paper were combined with preliminary work by the Los Angeles group and appeared in Helmy *et al.* [3]. Assuming the K-mesons of positive strangeness to form a charge doublet with isotopic spin $\frac{1}{2}$, and a simple nuclear model, preliminary analysis of the experimental data shows an increasing contribution with energy of a p-wave in the $T=0$ state for scattering [2,3]. The analysis was only expected to give a qualitative result since crude assumptions had to be made for simplicity, and a more complete assessment is being made by the group in Los Angeles. Ceolin *et al.* [4] have

(*) Now at the Ministry of Education training College, Cairo.

(**) Now at the Panjab University, Chandigarh.

(***) Now at the Muslim University, Aligarh, U.P.

[1] G. T. Zorn and B. Sechi Zorn: *Bull. Am. Phys. Soc.*, Ser. II, **3**, 24 (1958).

[2] D. Keefe, A. Kernan, A. Montwill, M. Grilli, L. Guerrieso and G. A. Salandin: *Nuovo Cimento*, **12**, 241 (1959).

[3] D. Evans, F. Hassan, K. K. Nagpaul, Md. Shafi, E. Helmy, J. H. Mulvey, D. J. Prowse and D. H. Stork: *Nuovo Cimento*, **10**, 168 (1958).

[4] C. Ceolin, N. Dallaporta, L. Guerrieto, I. Laboragine, G. A. Salandin and L. Taffara: *Nuovo Cimento*, **43**, 818 (1959).

used the nuclear effects observed, in an attempt to determine the angular distribution for charge exchange scattering independently of assumptions about the isotopic spin classification of the positive and neutral K-meson with strangeness +1. They conclude that the charge exchange scattering distribution is more backward peaked that that of the inelastic scattering, which is in disagreement with the prediction of the preliminary phase shift analysis ([3]).

The present communication gives the full experimental results obtained at Bristol in analysing the interactions in emulsion of K^+-mesons of (200 ÷ 300) MeV and investigates critically the information that can be obtained from the nuclear products of the reactions.

2. – Experimental details.

The experiment was done in part of a stack of Ilford 600 μm G-5 emulsions (K_4^+ stack) which was exposed to the separated 625 MeV/c positive K-meson beam from the Bevatron, and subsequently shared between University College, Dublin, the University of Padua, and the University of Bristol.

2·1. *Scanning for and analysis of inelastic reactions.* – An unbiased sample of interactions was found by scanning along the tracks of the K^+-mesons. Tracks within 3° of the beam direction, were selected for following by an initial count of 400 blobs, the value of the blob density to be expected for the K-mesons (24÷28/100) μm having been found by making counts on the tracks of all particles entering the plates. The selected tracks were then followed for 10 cm or until they stopped, entered a star, appeared to undergo a scatter of $\geqslant 6°$ or showed a sudden change in grain density. The primaries of all interactions were subjected to an ionization measurement based on at least 1000 blobs, and a measurement of $p\beta$. Fig. 1 shows a random sample of the results. In the total number of interac-

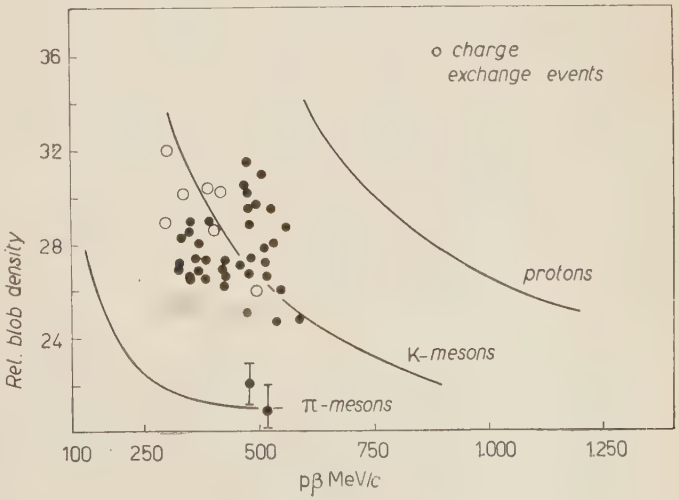

Fig. 1. – Blob density, βp plot for primaries of a sample of interactions.

tions only 4 due to π-mesons were observed (2 are seen in Fig. 1). Taking 30 cm as the mean free path of the π-mesons in emulsion, this would indicate only $\sim 1\%$ contamination in the tracks selected by the above procedure. The small value of the contamination was further confirmed by accurate ionization and $p\beta$ measurements on a sample of tracks that had been chosen for following. These measurements gave no evidence of the presence of protons.

All tracks from stars were followed as far as was possible and the presence of K^+-mesons detected either by their decay effects or by measurements of ionization, $p\beta$ and range. In 153 events, 7 were found not to be completely analysable. Care was taken that cases of π-meson production would not be missed, but no distinction was made between the hydrogen isotopes and α-particles making up the low energy interaction products. The scattering events (*i.e.* no other prongs associated) were investigated for a change in ionization by counting another 1000 blobs after the scatter. This enabled a classification into the categories *a*) elastic scatters, *b*) inelastic events (ΔE 30 MeV) and *c*) decays in flight. Decays in flight usually show a sudden decrease in ionization, and could thus also be detected when the change in direction of the track was $< 6°$. The angles between the directions of the primary K-mesons and those of the outgoing mesons and any protons of $\cdot 30$ MeV, were respectively measured. Two prong stars were carefully investigated for compatibility with the interpretation as K-meson collisions with hydrogen.

The value of the incident beam energy is discussed in [3] and was used in deducing the energy at which a meson underwent an interaction. An error of ~ 15 MeV in the estimate may be expected.

2·2. *Recording of elastic scatters.* – Since most of the elastic scatters are less than 10°, care has to be taken to ensure as little scanning loss as possible at small angles. A little more than half the total track length was scanned to give the elastic scattering data. All changes in direction $\geqslant 1°$ in the emulsion plane were recorded, and for space angles $\geqslant 6°$ ionization measurements were made before and after the scatter. It was generally found impracticable to count more than 1000 blob after the scatter, and taking into account normalization uncertainties when the track after changing its direction had to be measured in more than one plate, it was concluded that energy losses < 30 MeV could not be detected.

3. – Results.

In a K^+-meson path length of 92 m, 152 inelastic events (not including 1 scatter from hydrogen) were observed. In 94 cases the K-meson was seen to re-emerge while in 51 cases no scattered meson was found. No evidence of

π-meson production was seen. 7 stars could not be analysed completely because of the steepness of secondary tracks. The mean free path for reactions other than with hydrogen, of K^+-mesons having a mean energy of 270 MeV, is thus found to be (60 ± 6) cm and is in agreement with the previous work (see Section 1).

One event was found which could be interpreted as an elastic scatter from free hydrogen. The K-meson was scattered through 45° while the proton recoiled at an angle of 54° and had an energy of 96 MeV. The meson left the stack before coming to rest, but ionization measurements indicated its energy after the scatter to be (185 ± 20) MeV. Hence the event can be interpreted as a scatter of 74° in the centre of mass, of a K-meson of 281 MeV primary energy.

Table I shows the frequency of observation of elastic scatters in a path length of 51.5 m. The number of scatters is shown corrected for unobserved solid angle when different plane angle cut-offs are employed. No significant change in statistics occurs for any cut-off $\gtrsim 2°$ and the cross-sections given are based on a 2° minimum plane angle.

TABLE I. – *In space angle interval.*

Plane angle cut-off	4° ÷ 6°		6° ÷ 10°		10° ÷ 20°	
	No. observed	No. corrected	No. observed	No. corrected	No. observed	No. corrected
1°	23	26	31	34	17	18
2°	22	31	29	35	17	19
3°	18	32	27	37	17	20
4°	10	31	23	36	15	19

Space angle interval

	4° ÷ 6°	6° ÷ 10°	10° ÷ 13°	15° ÷ 20°
Cross-section mb/sr	8450 ± 1700	2490 ± 450	520 ± 145	136 ± 70

The results are independent of and in agreement with those published in HELMY *et al.* [3].

The Appendix tabulates the full details of the inelastic reactions. The distribution of energy loss as a function of scattering angle and the value of the charge-exchange to non-charge-exchange ratio show the same features as have already been observed [2,3].

4. – Discussion.

It is assumed that the K-meson reactions can be described using an independent particle model of the nucleus. The mean energy loss of a K^--meson in an inelastic scatter is 148 MeV; the mean energy of knock on protons (energy > 20 MeV) is 52 MeV. Hence, a considerable secondary cascade is initiated inside the nucleus by the initial scatter. Fig. 2*a* compares the distribution of energy taken by protons > 20 MeV from inelastic scatters and charge exchanges respectively. It is seen that there is no significant difference; the respective mean energies are 52^{+5}_{-1} and 58^{+9}_{-1} MeV. The distributions of number of « black tracks » (*i.e.* equivalent to protons < 20 MeV, but with range $\geqslant 5$ μm to exclude recoils) per star for the two classes of event is shown in Fig. 2*b*. They are typical of what would be expected from an evaporating

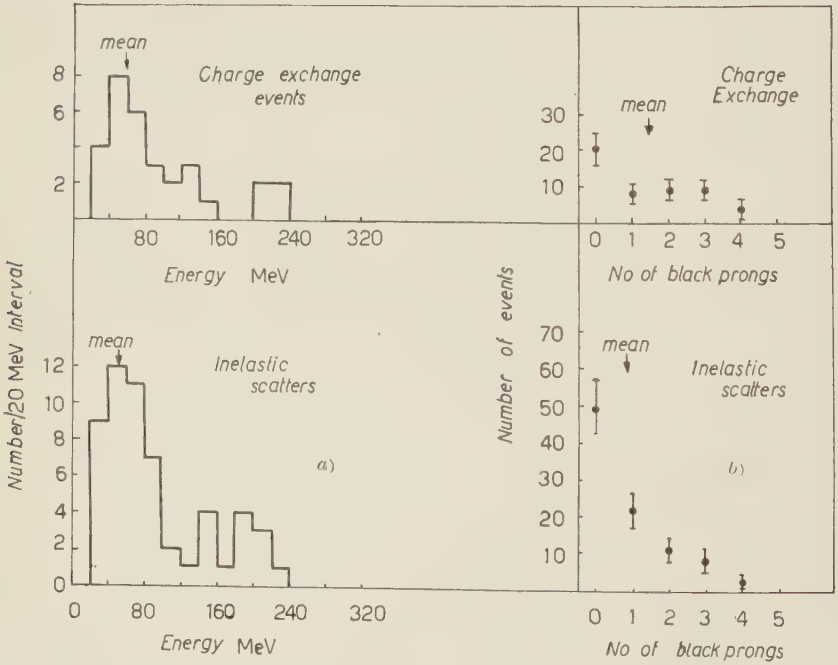

Fig. 2. – *a*) Energy frequency distribution of protons with energy > 20 MeV; *b*) Frequency distribution of black prongs ($\geqslant 5$ μm).

nucleus; the mean numbers of black prongs per star associated with inelastic scatters and charge exchanges are 0.9 ± 0.2 and 1.5 ± 0.2 respectively. The greater number of black prongs for charge exchanges ((0.6 ± 0.3) per star) can be explained as being due to the increased charge of the nucleus in the latter reaction. The knock-on cascade is hardly affected by the extra charge, but the evaporating nucleus with little excitation preferentially emits the

extra loosely bound proton. Thus the nuclear excitation energy associated with inelastic scatters and charge exchanges are seen to be very similar and not characteristic of larger momentum transfers in the latter type of reaction.

In their investigation of the angular distribution of the charge exchange scattering, CEOLIN *et al.* [4] used the distribution of resultant momentum of the charged nuclear products, which was shown in the case of inelastic scattering to be on average correlated with the momentum of the scattered meson if the absolute value of the observed momentum were doubled. A similar analysis has been done with the present results for events where a proton with energy $\geqslant 30$ MeV is emitted. Fig. 3*a* shows the distribution of the quantity $\theta_0 - \theta_r$ for inelastic scatters where θ_0 is the observed angle of scatter of the meson and θ_r is that to be expected in order to balance twice the momentum of the knock on protons. It is seen that on average, the calculated angle is a reasonable estimate with a spread of $\sim 60^\circ$ on a single result. This compares well with the correlation obtained by CEOLIN *et al.* Fig. 3*b* compares the distribution in θ_r for the inelastic scatters and charge exchange events respectively. The forward peaking of the former, obtained by CEOLIN *et al.*, does not seem to be present. It must be borne in mind here, that the presence of the knock on proton determines that an appreciable momentum transfer has occurred. One might therefore expect that a larger number of the remaining events are due to forward scattered K-mesons. The fraction of events without knock on protons is respectively 0.45 ± 0.09 and 0.45 ± 0.06 for charge exchanges and inelastic scatters. It is therefore difficult to deduce from the present analysis any difference in the two scattering distributions. This is perhaps not very surprising in view of the degeneracy of the nuclear effects.

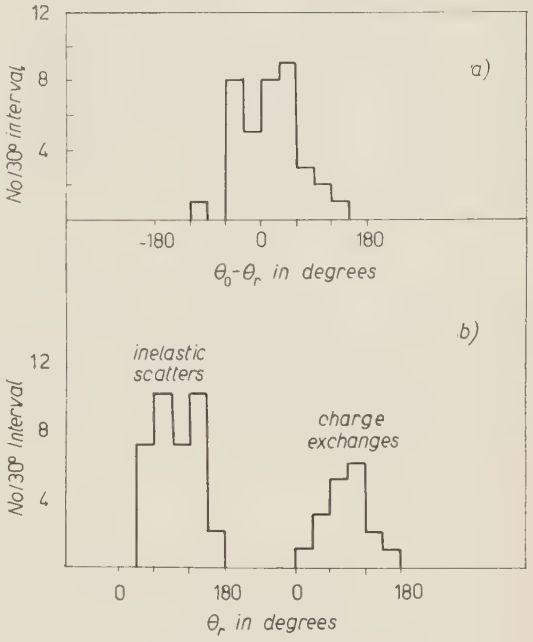

Fig. 3. – *a*) Difference between observed (θ_0) and calculated (θ_r) angle of scatter for inelastic scattering events; *b*) Comparison of calculated angle of scatter (θ_r) for inelastic scatters and charge exchanges.

5. – Conclusions.

The mean free path for (200 ÷ 300) MeV K^+-meson reactions with emulsion nuclei (excluding hydrogen) is (60 ± 6) cm. One scatter from hydrogen and no π-meson production was observed in a track length of 92 m. An analysis of the nuclear effects produced does not lead to any indication that the charge exchange scattering is more strongly peaked backward than that in which the K-meson remains in the same charge state. Rather than a confirmation of the predictions of the phase shift analysis on the inelastic scatters, this is probably only an indication that the nuclear effects are too insensitive a measure of the initial scattering process.

* * *

We are very grateful to Dr. E. J. LOFGREN and the Bevatron staff for the exposure of the stack and to Professor C. F. POWELL for the use of the facilities in the laboratory at Bristol. We acknowledge with pleasure the collaboration with the group at U.C.L.A. and the help afforded by the exchange of information that has taken place between us, the University College, Dublin, and the University of Padua.

APPENDIX

E_1 energy (MeV) *of primary to interaction; ΔE loss of energy* (MeV) *of* K; *θ_K angle of scatter of* K *in degrees; N_G number of protons* > 20 MeV; *N_B number of other tracks* ($\geqslant 5$ μm); *R recoils* < 5 μm *range.*

Charge exchange.

Event	E_1	N_G+N_B	Event	E_1	N_G+N_B	Event	E_1	N_G+N_B
1	296	$1+0R$	18	280	$0+0$	35	262	$1+0$
2	296	$1+1$	19	277	$2+0$	36	260	$1+2$
3	296	$1+0$	20	277	$0+2R$	37	258	$1+1$
4	295	$0+1$	21	276	$1+3R$	38	258	$1+0$
5	292	$1+1$	22	274	$1+0$	39	255	$0+3$
6	292	$1+3$	23	272	$1+0$	40	253	$1+4$
7	291	$0+3$	24	272	$1+3$	41	251	$2+1R$
8	288	$1+0$	25	270	$1+4$	42	250	$1+0$
9	287	$1+0$	26	270	$2+2$	43	249	$0+3$
10	287	$1+0$	27	270	$0+0$	44	257	$0+2$
11	287	$0+0$	28	269	$0+3$	45	245	$1+1$
12	286	$0+0$	29	267	$2+4$	46	245	$0+3$
13	285	$1+0$	30	267	$0+5$	47	243	$1+1$
14	283	$2+2$	31	266	$2+3$	48	242	$1+0$
15	282	$1+0$	32	265	$1+2$	49	240	$0+0$
16	280	$0+1$	33	264	$1+2$	50	240	$0+0$
17	280	$0+4$	34	263	$0+2$	51	235	$0+2$

Non charge exchange.

Event	E_1	ΔE	θ_K	N_G+N_B	Event	E_1	ΔE	θ_K	N_G+N_B
1	296	101	22	0+0	48	276	205	166	1+0
2	295	140	88	0+1	49	274	198	129	1+0
3	295	75	17	0+1	50	273	218	79	1+0
4	295	95	178	0+4	51	273	180	66	0+0
5	293	171	74	1+2	52	272	190	153	1+2
6	292	169	74	1+3	53	271	113	65	0+1
7	292	167	97	1+0R	54	270	80	4	1+0
8	292	220	54	1+2R	55	270	197	119	1+1R
9	291	238	68	0+1	56	279	238	17	2+0
10	291	159	91	1+2	57	269	74	106	0+1R
11	291	138	34	0+0	58	269	163	129	1+0
12	291	229	38	1+0	59	269	239	141	1+0
13	290	185	94	1+0	60	268	178	80	2+1
14	290	253	156	0+4	61	267	191	77	1+1
15	290	240	77	1+1	62	265	75	61	1+1
16	290	237	8	1+0	63	265	189	75	0+1
17	289	99	37	1+1	64	265	226	60	0+2
18	289	9	91	1+0	65	263	145	87	1+0
19	289	39	15	0+0	66	262	107	72	0+0
20	288	98	69	0+0	67	261	200	91	1+0
21	288	171	90	1+2	68	260	65	17	0+0
22	288	75	41	1+0	69	260	63	36	1+0
23	287	97	47	1+0	70	260	215	123	0+0
24	286	203	110	2+0	71	258	130	24	1+1
25	286	240	154	1+2	72	258	211	104	1+0
26	285	165	108	1+2	73	258	215	44	1+0
27	284	199	106	0+0	74	255	0	9	0+1
28	284	99	78	0+ZR	75	255	105	14	1+4
29	284	207	102	1+0	76	255	35	60	0+3
30	283	156	61	1+0	77	255	153	82	2+0R
31	283	235	119	0+0R	78	255	162	90	1+0
32	283	178	93	0+0	79	255	80	31	1+0
33	283	93	56	0+0	80	253	168	50	1+0
34	282	190	144	1+0	81	252	212	124	0+3
35	282	159	62	0+0	82	250	90	71	0+1
36	280	175	145	1+0R	83	250	184	94	2+2
37	280	90	42	1+0	84	249	153	27	1+0
38	280	173	87	0+1R	85	249	199	120	1+0
39	280	125	135	2+0	86	247	75	66	1+1R
40	279	96	25	1+0	87	246	112	24	0+1
41	278	148	60	0+3R	88	243	174	86	1+0R
42	278	155	98	0+3	89	242	106	110	1+0
43	277	242	124	2+1	90	283	83	51	0+1
44	277	122	30	0+1	91	235	173	110	1+3
45	276	224	142	0+3	92	235	68	11	0+0
46	276	−11	33	0+2R	93	234	152	74	1+3
47	276	0	37	0+0R	94	234	78	31	0+1R

RIASSUNTO (*)

Si è trovato che il percorso libero medio per le reazioni dei mesoni K^+ a (200÷300) MeV con nuclei dell'emulsione diversi dall'idrogeno è (60±6) cm. Si descrive uno scatter da idrogeno su 92 m di lunghezza di traccia e si danno i dati sulle reazioni elastiche ed anelastiche. Non si è trovato prova di produzione di mesoni π. Si discutono gli effetti nucleari delle reazioni anelastiche.

(*) *Traduzione a cura della Redazione.*

The Superconducting State in the Bethe-Goldstone Approximation.

A. Katz, A. de-Shalit and I. Talmi

Department of Physics, The Weizmann Institute of Science - Rehovoth

(ricevuto il 15 Gennaio 1960)

Summary. — Using a soluble model for the many body problem it is shown that the Cooper-type solution to the Bethe-Goldstone equation yields the exact value for the ground state energy of the system. The BCS method yields the ground state energy to order $1/\Omega$.

Systems of many interacting fermions have been treated by the Brueckner method, which is essentially an improved version of perturbation theory. In this method it is possible to sum up a selected type of graphs, of various orders which are believed to represent the major contribution to the energy from two-particle correlations. Higher order correlations are neglected. It has been shown by Bethe and Goldstone [1] that Brueckner's method is equivalent to an independent pair approximation with a pair-interaction modified to take into account the occupation of some states by the other fermions. Thus, in the treatment of Bethe and Goldstone the many-fermion problem is reduced to a two body problem with a modified interaction.

For a special class of attractive interactions Bardeen, Cooper and Schrieffer [2] have suggested another method for calculating energies and eigenfunctions. Their method also limits its considerations to pair-correlations and ignores correlations of higher order. Instead of summing however, over different terms in the perturbation expansion, it starts with a wave function which has a built-in pair correlation. This wave function is chosen so as to

(1) H. A. Bethe and J. Goldstone: *Proc. Roy. Soc.* (*London*), A **238**, 551 (1957).
(2) J. Bardeen, L. N. Cooper and J. R. Schrieffer: *Phys. Rev.*, **108**, 1175 (1957).

diagonalize that part of the interaction which scatters pairs with total momentum coupled to zero near the top of the Fermi sea. In infinite systems the ground state energy obtained this way is non-analytic in the interaction strength and cannot, therefore, be obtained by a perturbation expansion or its equivalent.

K. GOTTFRIED, ([3]) in an unpublished report, discussed the possibility that the BCS result could be derived from the Bethe-Goldstone equation. The aim of this note is to show that there exists, at least in one simple case, a close connection between the Bethe-Goldstone and the BCS treatment of many-fermion systems.

To obtain Brueckner's solution from the Bethe-Goldstone (BG) equation one has to take that solution of the BG equation which approaches the non-interacting pair wawe-function for large relative separations of the two particles. The BG equation has, however, also a Cooper-type ([4]) solution which describes a «bound» pair. We shall show in the following, using a simple well known soluble model ([5]), that by taking the Cooper solution in the BG equation we obtain the exact energy of the system. The BCS theory, applied to this model, leads to the same energy up to order $1/\Omega$, where Ω is the number of available states.

We consider a system of N fermions governed by a Hamiltonian $H_0 + H'$ H_0 is a single particle Hamiltonian which has a set of 2Ω degenerate eigenstates $|k\rangle$, with $k = \pm k_1, \pm k_2, ..., \pm k_\Omega$ $(k_i > 0)$. The interaction H', defined to be effective only between these 2Ω states, is given by

$$H' = -G \sum_{kk'} a_k^\dagger a_{-k}^\dagger a_{-k'} a_{k'} \qquad k > 0,\ k' > 0, \tag{1}$$

where $a_k^\dagger$ is the creation operator for a fermion in the state k.

A convenient example for our system is a j-shell in a spherically symmetric field. In this case k can be the z component of the angular momentum of the fermion. It then takes on the values: $\pm\frac{1}{2}, \pm\frac{3}{2}, ..., \pm j$, with $2\Omega = 2j+1$. Our considerations are, however, more general.

If the system contains only two particles we choose for our basis the functions

$$|k, k'\rangle = a_k^\dagger a_{k'}^\dagger |0\rangle\ , \tag{2}$$

where $|0\rangle$ is the vacuum (no particle in any of the 2Ω states). We normalize

([3]) K. GOTTFRIED: unpublished.

([4]) L. N. COOPER: *Phys. Rev.*, **104**, 1189 (1956).

([5]) See for instance Y. WADA, F. TAKANO and N. FUKUDA: *Progr. Theor. Phys.*, **19**, 597 (1958).

the energy so that the 2Ω states $|k\rangle$ belong to the eigen-value $E_0 = 0$ of H_0.

Hence

$$(k_1, k_2|H|k_1', k_2') = -G\,\delta_{k_1,-k_2}\delta_{k_1',-k_2'}\,. \tag{3}$$

Since the interaction is assumed to be attractive it is clear that the ground state must be constructed from functions in which $k+k'=0$. In the subspace of the Ω functions $|k, -k\rangle$ the matrix of the Hamiltonian has all its elements equal to $-G$. It is a matrix of order Ω and rank 1, and therefore all its eigenvalues except one are zero. The only non vanishing eigenvalue which gives the ground state energy, is equal to the trace of this matrix *i.e* $-\Omega G$. The corresponding eigenvector is (1, 1, ..., 1), which is obtained by applying the operator $\sum_{k>0} a_k^\dagger a_{-k}^\dagger$ to the vacuum.

If the system contains an even number N of fermions, we may obtain the energy spectrum with the help of a method used by WADA, TAKAÑO and FUKUDA [4] and also independently by KERMAN (unpublished). Defining operators s_{kx}, s_{ky}, s_{kz}, S_x, S_y, S_z, as

$$\begin{cases} s_{kx} = \tfrac{1}{2}(a_k^\dagger a_{-k}^\dagger + a_{-k}a_k)\,, & S_x = \sum_{k>0} s_{kx}\,, \\ s_{ky} = -\tfrac{1}{2}i(a_k^\dagger a_{-k}^\dagger - a_{-k}a_k)\,, & S_y = \sum_{k>0} s_{ky}\,, \\ s_{kz} = -(a_k^\dagger a_k + a_{-k}^\dagger a_{-k} - 1)\,, & S_z = \sum_{k>0} s_{kz} = \tfrac{1}{2}(N-\Omega)\,, \end{cases} \tag{4}$$

we note that they obey the commutation relations of the components of angular momentum. The Hamiltonian (1) can be expressed in terms of the operators (4) as

$$H' = -G(S_x + iS_y)(S_x - iS_y) = -G\,[S(S+1) - S_z(S_z-1)]\,. \tag{5}$$

Here $S(S+1)$ is the eigenvalue of $S_x^2+S_y^2+S_z^2$. From the commutation relations of S we know that S must be a positive integer or half integer. Noting that the possible eigenvalues of s_{kz} are 0, $\pm\frac{1}{2}$ we see that our system is equivalent to an ensemble of spin $\frac{1}{2}$ or spin 0 particles corresponding to any k. Therefore the maximum value for S is $\frac{1}{2}\Omega$ and it can assume also the values $\frac{1}{2}\Omega-1$, $\frac{1}{2}\Omega-2$ down to $|S_z| = \frac{1}{2}(\Omega - N)$. The lowest energy and the corresponding eigenstate are given by the largest S. They are

$$E_G = -G\left[\frac{1}{2}\Omega\left(\frac{1}{2}\Omega+1\right) - \frac{1}{2}(N-\Omega)\left\{\frac{1}{2}(N-\Omega)-1\right\}\right] = \tag{6}$$

$$= -G\,\frac{N}{2}\left(\Omega - \frac{N}{2} + 1\right)$$

and

$$\psi_{g.s.} = \left(\sum_{k>0} a_k^\dagger a^\dagger{}_k\right)^{N/2} 0)$$

as can be easily checked. The Hamitonianl (1) is proportional to Racah's seniority operator ([6]). The result (6) could therefore be deduced from Racah's eq. (50) with $v = 0$.

Eq. (6) gives the exact ground state energy of (1). In the Bethe-Goldstone ([1]) approach we consider the equation of motion of one pair to which there are available the $\Omega - (N/2)$ unoccupied pair states plus its own unperturbed state. The problem is thus similar to the problem of a single pair treated above except that we have to replace Ω by $(\Omega - (N/2) + 1)$. The solutions to the Bethe-Goldstone equation are therefore: a ground state with an energy $-G(\Omega - (N/2) + 1)$, and all the rest of the states having vanishing interaction energy. The eigenvector of the ground state has equal components in all unoccupied pair states. If the representation from which we start is a momentum representation our solution describes a highly localized « bound pair » which is formed in the medium of the other particles. The existence of such bound pair solutions was pointed out by COOPER ([4]). The Cooper type solutions are usually ignored in the Bethe-Goldstone procedure (by the requirement of suitable boundary conditions) because they violate the assumption that the particles maintain the Fermi distribution even under the influence of the interaction. Ascribing the Cooper solution and its energy $-G(\Omega - (N/2) + 1)$ to each of the $N/2$ interacting pairs we obtain again the exact result (6).

In the BCS treatment one starts with the trial function

$$\psi = \prod_k (U_k + V_k a_k^\dagger a^\dagger{}_{-k}) |0\rangle ,$$

where U_k and V_k are the variation parameters and $U_k^2 + V_k^2 = 1$. The projection of this wave function onto the space of N particles (not normalized) is given by an expression similar to (4) ([7])

$$\left(\sum_k \frac{V_k}{U_k} a_k^\dagger a^\dagger{}_k\right)^{N/2} 0 \quad .$$

The values of U_k and V_k as determined from the variation principle depend only on the unperturbed energy of the state. In a degenerate shell they are therefore the same for all states. Since $2\sum_{k>0} V_k^2 = N$, we have

$$V_k^2 = \frac{N}{2\Omega} \qquad \text{and} \qquad U_k^2 = 1 - \frac{N}{2\Omega} . \qquad \text{for } k \gtrless 0 . \tag{7}$$

([6]) G. RACAH: *Phys. Rev.*, **63**, 367 (1943).

([7]) B. MOTTELSON: *Lectures at the Les Houches Summer School* (Paris, 1958), p. 299.

The Bardeen-Cooper-Schrieffer expression for the ground state energy can be taken from Belyaev's eq. (22) and (20) [8]

$$E_G = 2 \sum E_k V_k^2 - G\{(\sum U_k V_k)^2 + 2 \sum V_k^4\} \tag{8}$$

(E_k is the unperturbed energy of the k states. In our case $E_k = 0$). Substituting (7) in (8) and multiplying by Ω instead of summing over k, we arrive at

$$E_G = - G \frac{N}{2}\left(\Omega - \frac{N}{2} + \frac{N}{\Omega}\right). \tag{9}$$

Eq. (9) agrees very well with (6) since the difference between N/Ω and 1 is negligeable in comparison with $\Omega - N/2$ in most cases of interest.

We should emphasize that the agreement between the results of Bardeen-Cooper-Schrieffer and Bethe-Goldstone could only be obtained by taking specifically the Cooper-type solution of the Bethe-Goldstone equation. Brueckner's theory is obtained from the « normal » solutions of the Bethe-Goldstone equation and would have generally led to a higher energy in our model. In some circumstances, therefore, one may have to use the Cooper-type solution rather than the « normal » solutions, in order to describe the pair correlations in the ground state of many fermion systems.

One must also remember, however, that the coincidence in energies does not imply a coincidence of wave functions. In the Bardeen-Cooper-Schrieffer wave function the particles are equally distributed over all states (as in the exact wave function). The Bethe-Goldstone method does not give a unique prescription for the wave function of the N-particle system.

---

[8] S. T. Belyaev: *Mat. fys. Medd.*, **31**, no. 11.

RIASSUNTO (*)

Con l'uso di un modello risolvibile del problema dei molti corpi si dimostra che la soluzione del tipo di Cooper alla equazione di Bethe-Goldstone dà il valore esatto della energia dello stato base del sistema. Il metodo BCS dà l'energia dello stato base sino all'ordine $1/\Omega$.

(*) *Traduzione a cura della Redazione.*

IL NUOVO CIMENTO Vol. XVI, N. 3 1° Maggio 1960

A New Measurement of the Mean Life of the Positive Pion.

J. Ashkin (*), T. Fazzini, G. Fidecaro, Y. Goldschmidt-Clermont, N. H. Lipman, A. W. Merrison and H. Paul (**)

CERN - Geneva

(ricevuto il 25 Gennaio 1960)

Summary. — The mean life of the positive π-meson has been determined from about 8000 $\pi\mu$ decay events recorded by photographing pulses on an oscilloscope. The pictures were measured with an instrument originally developed for the evaluation of bubble chamber pictures, and the data were analysed using a fast computer. The value obtained for the mean life of the π-meson is $\tau_\pi = 25.46 \pm 0.32$ ns.

1. – Introduction.

The mean life of the positive pion has been measured by several groups [1], and the result of averaging their measurements has been given by Crowe [2] as (25.6 ± 0.5) ns. In these measurements the grand total of all pion decays recorded was about 11000. We have observed a similar number of decays by photographing pulses displayed on an oscilloscope, and have subsequently analysed these traces by making extensive use of an instrument designed to

(*) Ford Foundation Fellow, on leave from Carnegie Institute of Technology, Pittsburgh.

(**) Ford Foundation Fellow, on leave from Institut für Radiumforschung, Vienna.

(1) W. L. Kraushaar, J. E. Thomas and V. P. Henri: *Phys. Rev.*, **78**, 486 (1950); W. L. Kraushaar: *Phys. Rev.*, **86**, 513 (1952); O. Chamberlain, R. F. Mozley, J. Steinberger and C. E. Wiegand: *Phys. Rev.*, **79**, 394 (1950); C. E. Wiegand: *Phys. Rev.*, **83**, 1085 (1951); M. Jakobson, A. Schulz and J. Steinberger: *Phys. Rev.*, **81**, 894 (1951); L. Lederman, E. T. Booth, H. Byfield and J. Kessler: *Phys. Rev.*, **83**, 685 (1951); R. P. Durbin, H. H. Loar and W. W. Havens: *Phys. Rev.*, **88**, 179 (1952).

(2) K. M. Crowe: *Nuovo Cimento*, **5**, 550 (1957).

measure bubble chamber photographs (IEP) and of a high-speed electronic computer (a Ferranti « Mercury »). In this way a large amount of data could be easily recorded, analysed and checked for systematic errors. As will be apparent, the analysis represents the major part of the experiment. The actual cyclotron time used for recording the data was about half an hour.

2. – Experimental method.

The layout of the experiment is essentially that used in a previous experiment ([3]) and is shown in Fig. 1. The 127 MeV positive pions from the CERN synchrocyclotron were first filtered by 2 cm of polyethylene to remove protons of the same momentum. They then passed through the monitor counters 1 and 2, which were 5 cm high, 3 cm wide, and 1 cm thick, mounted on either side of a thick lead collimator. The hole in the collimator was the same size as these counters. The pions were then slowed down in a block of copper and about 30% came to rest in counter 3. Counter 3 was 5 cm high, 6 cm wide and 2 cm thick. It was inclined at an angle of about 45° to the beam, in this way presenting an effective thickness of about 3 cm to the beam. To identify particles stopping in counter 3, counters 1, 2, 3 were in fast (9 ns) coincidence, and counter $\bar{4}$ in anticoincidence. Counter $\bar{4}$ was $(10\times12\times1)$ cm^3. The intensity of the meson beam was reduced to obtain an average rate of about 16 pions per second stopping in counter 3.

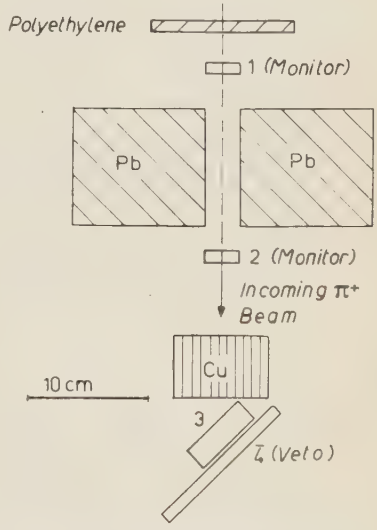

Fig. 1. Experimental arrangement.

The coincidence 1 2 3 $\bar{4}$ triggered the sweep of an Edgerton, Germeshausen and Greer travelling-wave oscilloscope on which the pulses from counter 3 were displayed. These pulses were clipped at the photomultiplier with a 0.75 ns cable terminated by an 18 Ω resistor to avoid undershoot. The resistor chain in the photomultiplier was chosen to reduce saturation effects as described previously ([3]), and this meant that time measurements could be made with very small separations between pion and muon pulses. The length of the oscilloscope sweep was 430 ns, and the pion pulse appeared 110 ns after

([3]) J. Ashkin, T. Fazzini, G. Fidecaro, A. W. Merrison, H. Paul and A. V. Tollestrup: *Nuovo Cimento*, **13**, 1240 (1959).

the start. This left a useful sweep length, within which pulses could be measured, of 320 ns after the pion pulse, *i.e.* about 13 pion mean lives. Only one in 10 000 π mesons survives for more than nine mean lives, so examining this long period of time enabled us to evaluate the background properly. The time-calibration of the sweep was obtained by displaying every 10 seconds a 100 MHz sine-wave which was accurate to better than one part in 10^4.

We recorded about 20 000 events, on 35 mm Eastman-Kodak Linagraph Pan film.

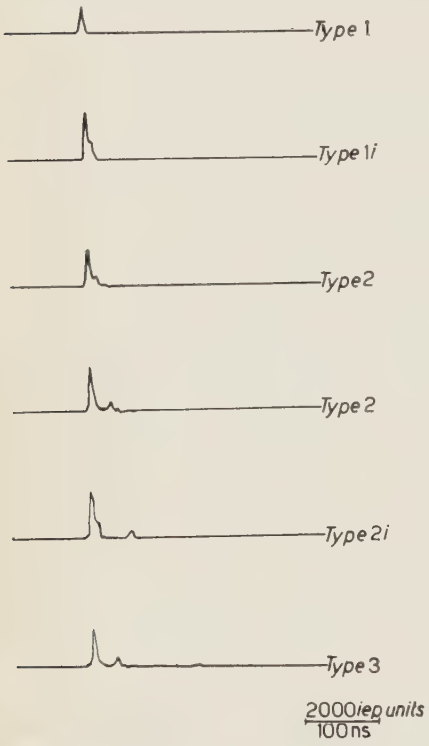

Fig. 2. Facsimile drawing of several oscilloscope traces, with classification.

3. – Evaluation of photographs.

The first version of the instrument for evaluation of photographs (IEP 1) was used to extract the required information from the pictures ([4]). The method has been described elsewhere ([5]) in some detail. The IEP projects a chosen part of the film onto a screen. By means of two micrometer screws, the operator can move the objective in two perpendicular directions (X and Y) to bring any desired point of the projection in coincidence with a fixed cross hair. The two perpendicular displacements are digitized (1 unit $=2.69 \cdot 10^{-4}$ cm on the film) and counted by electronic scalers. The co-ordinates can be punched on paper tape by pressing a pedal. In addition, information for the identification of the measured points on the tape (such as the event classification) can be punched by pressing a key of an electric typewriter which provides also a printed record.

For each event, the operator measured the co-ordinates of the start of the trace, of the highest point on each pulse peak, and of the end of the trace. As it is not evident *a priori* that the measurement of the pulse peaks corresponds to an unbiased measurement of time, the influence of pulse height on pulse time was investigated as discussed below.

([4]) Y. GOLDSCHMIDT-CLERMONT, G. VON DARDEL, L. KOWARSKI and C. PEYROU: *Nucl. Instr.*, **2**, 146 (1958); G. VON DARDEL, Y. GOLDSCHMIDT-CLERMONT and F. ISELIN: *Nucl. Instr.*, **2**, 154 (1958).

([5]) Y. GOLDSCHMIDT-CLERMONT and H. PAUL: *CERN Report* 59-28, August 11, 1959.

As soon as the co-ordinates of an event were measured, the operator typed a label to identify it. The events were classified by the operator not according to physical interpretation, but rather according to the number of pulses on the trace (mostly 1, 2, 3) and this classification number was the label typed after each event. If a second pulse was not clearly separated but visible on the falling edge of the first, the letter « *i* » was typed after the classification figure (cf. Fig. 2). In case of doubt, the letter « *a* » was used. The labels were used to steer the computer into the channels of calculation appropriate to each type of event. These were devised so as to incorporate a certain amount of checking in the computer programme, to guard against instrumental and operator errors. The labelling scheme was such that simple rules could be given to the operators.

TABLE I. – *Labelling of events.*

Type 1 :	Mostly pions which decayed so early that the muon pulse is buried within the pion pulse. It also includes scattered-out particles, etc. These latter amounted to 2% of the incoming beam.
1*i*:	Pion with indication of a muon that is visible as a change of slope on the falling edge, but not measurable.
1*a*:	A doubtful type 1 event (1 or 1*i*).
2 :	Mostly π-μ events. Includes also π-μ-e decays where the μ is buried within the π, or, rarely, within the e (false π-μ).
2*i*:	π-μ-e events, with the muon pulse occuring early on the tail of the π.
2*a*:	A doubtful type 2 event (2 or 2*i*).
3 :	π-μ-e decays where all three pulses are measurable.
3*i*:	π-μ-e decays where the μ is just visible, with an additional random pulse (quite rare).
3*a*:	A doutbful type 3 event (3 or 3*i*).
4 :	Only one such event was found, apparently a π-μ-e decay with an early random particle. No events with more than 4 pulses were found.

All types of classification are listed in Table I, together with their possible physical interpretations. Since random events are quite rare, the π-μ-e decays, where the three pulses are visible on the photograph (type 3), are

unambiguous. Most of the pion decays, however, appear as type 2, a class that contains

a) genuine $\pi \to \mu$ decays;

b) $\pi \to \mu \to$ e decays for which the μ-meson pulse is buried within the π-meson pulse;

c) π-μ-e decays for which the μ-meson pulse is buried within the positron (quite rare).

In cases *a*) and *c*), the second pulse on the scope corresponds to the μ-meson and the pulse separation is determined by the π life-time. In case *b*), the second pulse is the positron and the μ-meson life-time determines the pulse separation. The *b*) events, that we shall call « False π-μ events » constitute the main source of background in our experiment.

The total time spent by the operator in reading the films was about 250 hours.

4. – Analysis of the data.

The computer programme read the tape in event by event, and first performed a number of consistency checks detailed in Table II. The limits of acceptance of these consistency criteria were obtained in a preliminary com-

TABLE II. – *Rejection criteria with nomenclature used in computer print-out.*

Error:	printed if the operator has made a mistake and detected it before starting the next measurement. (Label: e). The event was re-measured correctly afterwards.
IEP $\neq 8$:	this indicates a IEP mistake, cf. Ref. ([5]).
No measure:	event consisted of a label, but of no co-ordinates. This occurs mostly in connection with *IEP* $\neq 8$.
Wrong class:	the label does not correspond to the number of points measured.
Jump:	inclination of trace not within limits.
Jump X:	length of the sweep not within required limits.
Chance:	first pulse not within (98 ÷ 118) ns from the beginning of the trace (see Fig. 6).
Zero:	the scalers indicated a too large value when the measuring stage was returned to the origin. When this error was found, the measurements were repeated.

puter run. The events which did not meet these requirements were rejected (Table III). The number of events rejected because of the Jump and Jump X criteria was rather large. This was due solely to the very narrow limits we

TABLE III. – *Rejected events.*

Errors	Jump X	Jump	Wrong class	Chance	No measure	$IEP \neq 8$
192	21	482	89	13	31	113

placed in applying these criteria. All the information about the accepted events was obtained in the form of histograms. The numbers of accepted events of different types are given in the second column of Table IV.

TABLE IV. – *Classification of accepted events.*

Label	First classification	After re-examination	After muon pulse height selection
1	3 704	3 704	—
1*a*	20	20	—
1*i*	1 116	1 116	—
2	10 419	10 608	—
2*a*	28	—	—
2*i*	357	196	—
3	1 133	1 153	—
3*a*	3	—	—
3*i*	21	4	—
4	1	1	—
2 and 3	—	11 761	11 352

Before preparing time distributions, it was essential to check the linearity of the time base of the oscilloscope. The measurements of the time calibration traces indicated, in fact, an appreciable non-linearity of the sweep velocity, as well as changes from one section of the film to another. By use of auxiliary computer programmes, appropriate averages were made over film sections, and empirical functions were defined to correct for the non-linearity. The final time distributions were prepared using these functions. For a discussion of the errors involved in the distance to time conversion, see below Section 7*c*.

It can be seen that in the first classification of events detailed in the second column of Table IV, there was a total of 385 events classified by the operator as $2i$ or $2a$. These events were individually re-examined and 146 of them were accepted as type 2 events. The time distribution of the remaining 239 events was then examined. It indicated the presence of 43 type 2 events and 196 type $2i$ events. The final total of 10 608 type 2 events (π-μ) was arrived at by adding to the already identified type 2 events these 43 events. The assignment of these events in the time histogram was, of course, somewhat arbitrary. A re-examination was made also of the $3a$ and $3i$ events and left only four events finally classified as $3i$. This number was, of course, too small to analyse further on the basis of a time distribution, so all four remaining events were accepted as $3i$. The details of the second classification are shown in the third column of Table IV. The total number of π-μ events resulting from this classification (*i.e.* the sum of type 2 and 3 events) is 11 761.

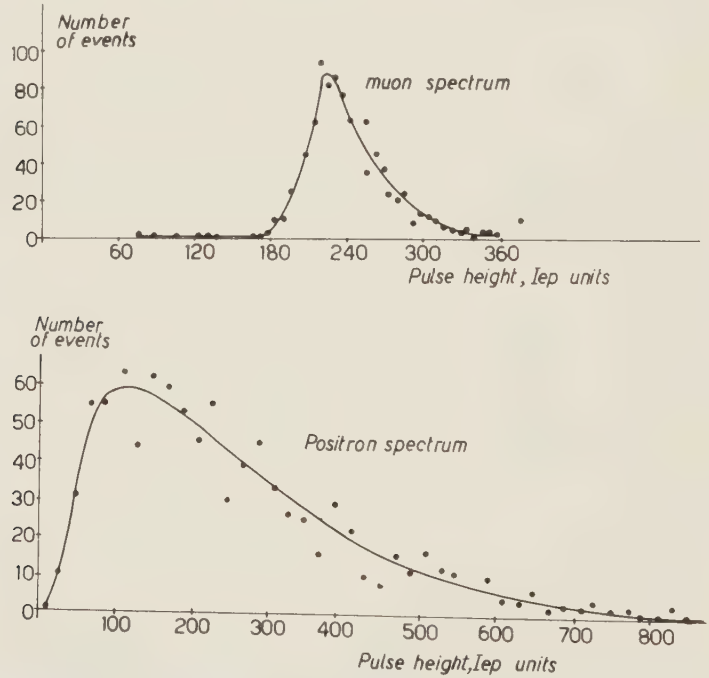

Fig. 3. – Pulse height distributions of second pulse (muon) and third pulse (positron), from 940 events of type 3 (π-μ-e).

These events were then subjected to pulse heightanalys is. The muon and electron spectra for the events of type 3, for which there is no ambiguity of interpretation, are shown in Fig. 3. As the range of the mono-energetic muon is small with respect to the dimensions of the counter, one expects a

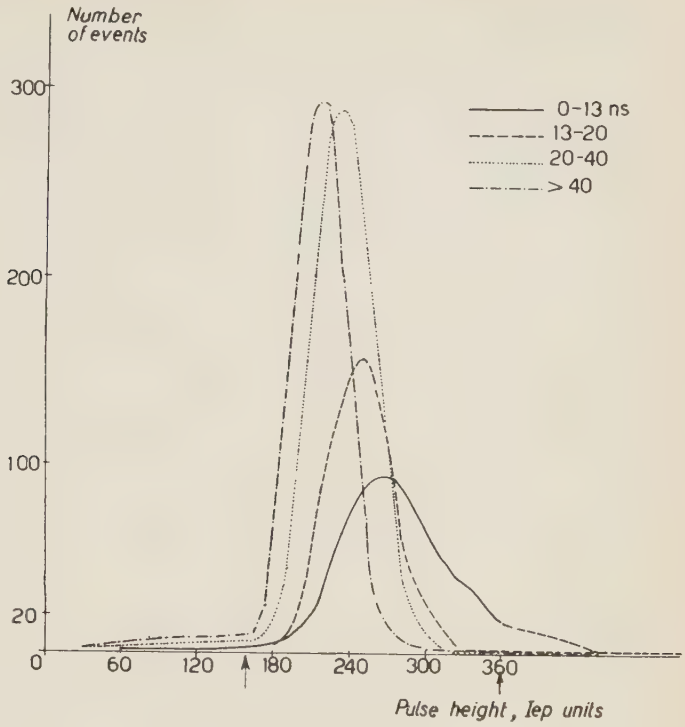

Fig. 4. – Pulse height spectra of muons pulses, within selected time intervals, for events of type 2. The arrows show the final limits of acceptance.

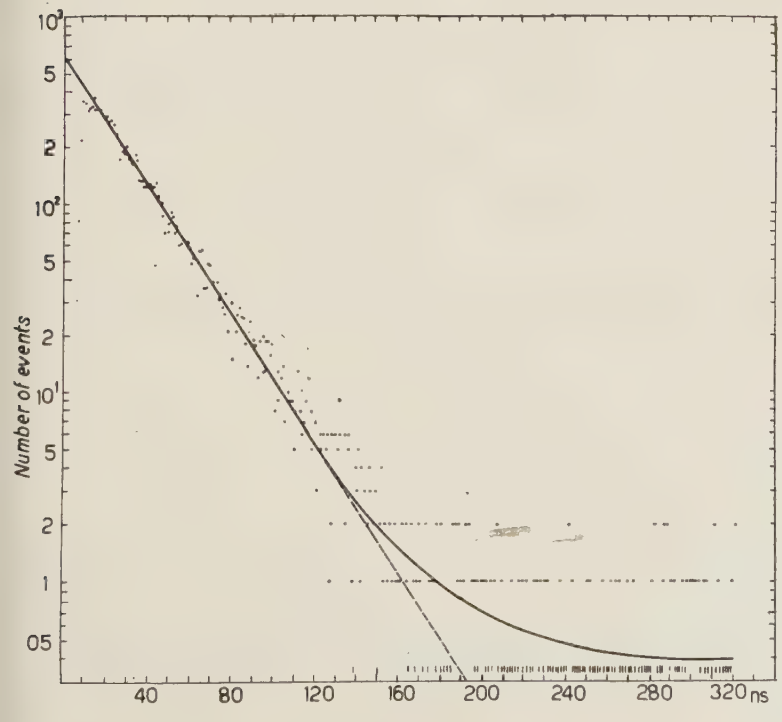

Fig. 5. – Final differential histogram of the 11 352 selected events. Boxes containing zero events are indicated by a stroke. The full line is the curve fitted by least-squares (cut-off at 16 ns). The exponential part is shown by the dotted line ($\tau = 25.46$ ns).

constant pulse height. It can be seen from the comparison of the two spectra in Fig. 3 that by imposing a height selection for the second pulses, it is possible to eliminate a sizeable fraction of the false π-μ events. However, this height selection could not be based on a very narrow part of the muon spectrum, as it was found that the muon pulse height depends on the muon time, as indicated in Fig. 4, where the muon pulse height distributions of type 2 events are shown. The early muon pulses tend to be higher, as they sit on the tail of the nearby pulse, and so would be rejected by a low upper limit on the pulse height. The limits of acceptance of muon pulse heights used in the final run of the programme were thus chosen as indicated by the arrows in Fig. 4. It can be seen that with these limits there is a negligible influence on muons appearing after 13 ns. This pulse height selection rejected 409 type 2 events and reduced the background of false π-μ events by a factor 2.3. This left 11352 π-μ events (see Table IV) for the final time analysis. The final histogram of the time intervals between pions and muons of these 11352 events, grouped in 320 boxes of 1 nanosecond length, is shown in Fig. 5.

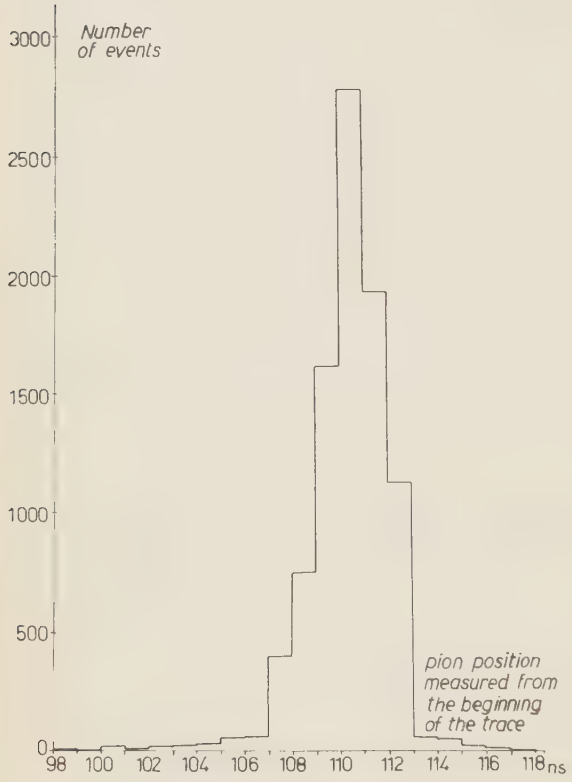

Fig. 6. – Time distribution of the first pulse.

The time distribution of pion pulses measured from the start of the trace is shown in Fig. 6.

5. – Least square fit to the decay curve.

Two statistical analyses were performed to extract the value of the pion mean life from the final time distribution histogram. In both these methods the calculations were performed with different lower time-limits for the ac-

ceptance of muons (« cut-offs »). The choice of the final cut-off is discussed in Section 8.

The first analysis was made with the usual method of least squares to fit to the histogram an exponential decay curve with added background. The background arises from residual false π-μ events. The background is thus assumed to follow an exponential also, but with the muon mean life.

A computer programme was written which fits a curve of the form:

$$(1) \qquad y_i = N(1 - \exp[-\lambda \Delta t]) \exp[-\lambda t_i] + B\lambda' \Delta t \left| 1 - \lambda' \left(t_i + \frac{\Delta t}{2} \right) \right| .$$

to a histogram f_i $(i = 0, 1, 2, \ldots, n-1)$ which contains the number of decays in the interval (t_i, t_{i+1}), where

$n = 320$

$\Delta t = t_{i+1} - t_i$ is the width of the histogram boxes

N is the initial source strength

λ is the decay constant of the source

B is the initial background strength

λ' is the decay constant of the background (assumed to be known and equal to 1/2220).

The source and background terms in Eq. (1) are both corrected for decay within a histogram box.

The programme adjusts N, λ and B, so as to make:

$$(2) \qquad S = \sum_{i=h}^{n-1} w_i (f_i - y_i)^2$$

a minimum, where the weights w_i are given by:

$$(3) \qquad w_i = \frac{1}{y_i}$$

and h is the lower limit, or cut-off, for the time-values used which may be chosen at will. The programme requires some initial estimates N_0, λ_0 and B_0. It then finds the increments of N, λ and B necessary to minimize S. Since starting from good initial estimates the increments will be small, the problem can be linearized and solved by standard iterative techniques. The iteration converges quite rapidly; it is stopped when the increment to λ has become less than 0.1%. The computer gives the errors derived from the residuals $f_i - y_i$.

This programme was checked on artificial spectra of known source strength, background strength, and life-time, generated by the computer using a Monte-Carlo method.

6. – A maximum likelihood estimate.

In order to verify that no error was introduced in the least square fit by the fact that in the late channels there were very few events, or none at all, a maximum likelihood method, described in more detail elsewhere (6), has also been used to estimate the mean life.

The time base was divided into 1 ns boxes as for the previous analysis. The probability that f_i particles are observed between t_i and t_{i+1} is given by the Poisson law:

$$(4) \qquad P(f_i) = \frac{1}{f_i!}\left\{\int_{t_i}^{t_{i+1}} [N\lambda \exp[-\lambda t] + B\lambda' \exp[-\lambda' t]]\,\mathrm{d}t\right\}^{f_i} \cdot \cdot \exp\left[-\int_{t_i}^{t_{i+1}} \{N\lambda \exp[-\lambda t] + B\lambda' \exp[-\lambda' t]\}\,\mathrm{d}t\right].$$

With some obvious approximations, the total likelihood function is thus proportional to:

$$(5) \qquad P = \exp\left[-\int_{t_h}^{t_n} \{N\lambda \exp[-\lambda t] + B\lambda' \exp[-\lambda' t]\}\,\mathrm{d}t\right] \cdot \cdot \prod_{i=h}^{n-1} \left\{N\lambda \exp\left[-\lambda\left(t_i + \frac{\Delta t}{2}\right)\right] + B\lambda' \exp\left[-\lambda\left(t_i + \frac{\Delta t}{2}\right)\right]\right\}^{f_i},$$

where again h is the cut-off.

Assuming λ' to be known, the maximum of the likelihood function was found on the computer by an iterative solution of the three equations obtained differentiating the logarithm of Eq. (5). The iteration was stopped when the simultaneous increments for the mean life, N and B were smaller than 0.001 ns, 0.1 particle and 0.1 particle respectively. There was no difficulty at all in getting the convergence of the iteration.

The programme, which has also been tested with the Monte Carlo sequences of decay times mentioned in the previous section, has given a perfect agreement with the least square fit for the values of λ, N and B.

(6) G. FIDECARO: to be published.

For example, the mean life of the positive pion, for a cut-off of 16 ns, obtained with the maximum likelihood method was 25.47 ns, while the least square gave 25.46. Similarly, the maximum likelihood method gave $N = 15317$ and $B = 1053$, while the least square fit gave $N = 15321$ and $B = 1078$.

7. – Discussion of the errors.

The most important decision which had to be made in the treatment of the results was the choice of cut-off, and this is discussed separately in Section **8**. We discuss in this section other possible sources of error and their treatment.

a) *Chance coincidences.* We ran at a sufficiently low rate, so that the probability of a second particle arriving while we were examining the decay of the first was negligible. This was confirmed by the fact that in the photographs we found no more than six events which could perhaps be classified as randoms. These were made up of the one type 4 event, one of the 13 rejected events labelled « Chance » (see Table II), and, possibly, some of the four type $3i$ events . The effect of such low chance rates upon the final result is completely negligible.

b) *Identification of events.* It was checked that the procedure we had used in Section **4** for the final assignment of the residual 43 type $2i$ and $2a$ events to the time histogram, on the basis of their time distribution, had a negligible influence on the final result.

Although, of course, the assignment of the four remaining $3i$ events was doubtful, their small number means they too have no influence on the final result.

c) *Distance to time conversion.* The setting error of the individual pulse measurements (accuracy of centering the instrument on the pulse maxima) was found to be ± 4 iep units, or ± 0.2 ns.

The interpolation functions were accurate to 0.3% on the average, and none of them could be wrong by more than 1%. As the errors are random and each of them applied only to a fraction of the data, the effect on the mean life is of no importance and the effect on its error is small.

d) *Pulse height.* To check that no systematic error was introduced by the choice of the limits of acceptance of the muon pulse heights, the mean life was estimated with varied limits, using separate histograms constructed with an additional computer run. For example, by comparing the results of evaluating the mean life with and without muon height selection, it was found that the selection did not affect the value of the mean life by more than 0.2%, for values of the cut-off larger than 8 ns.

The influence of pion pulse height on mean life was investigated by evaluating separately the mean life for three different pion pulse heights (Fig. 7). It is evident from the figure that large pion pulses give a longer mean life, if early muon pulses are included by using a cut-off earlier than 12 ns. This is because it is easier to obscure early muon pulses with large pion pulses.

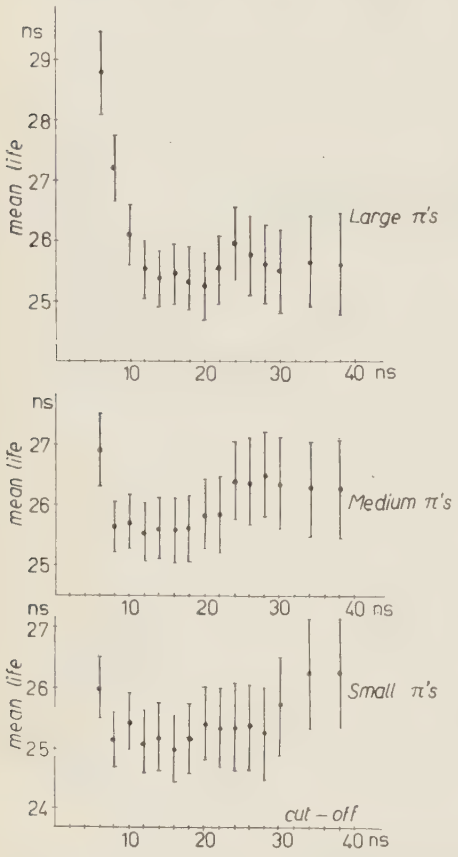

Fig. 7. – Estimated pion mean life as a function of cut-off for selected muon pulse heights and selected pion pulse heights.

e) *Effect of anticoincidence.* A positron arising from an early decaying muon may trigger the anticoincidence counter and bias against such events. As the resolving time was quite small (10 ns), the effect for later cut-offs is zero.

f) *Background.* As already indicated, the only appreciable source of background arises from false π-μ events. To check that the statistical method used took this effect into account correctly, an artificial background was added to the final histogram, so as to increase the background source strength (B in eq. (1)) by a factor of three. The mean life result was altered by less than 0.3%. Similarly, the mean life was also estimated from a histogram without muon pulse height discrimination as mentioned in Section 7*d*. The background source strength was larger by a factor of 2.3, but the value of the mean life differed by less than 0.2%. The statistical error on the mean life, however, was increased from 1.18% to 1.25%.

8. – The choice of the time cut-off.

One would like to choose the time cut-off for muons, already introduced in Section 5, as early as possible, so that very few events are rejected for the final evaluation of the mean life. There is a danger, however, in taking the

cut-off too close to the pion pulse, because of the systematic errors introduced by the loss of early muons. In this Section, we give the arguments which led to our final choice of the time cut-off.

i) The time at which the muon pulse begins to be observable as a change in slope on the tail of the pion pulse is 3.7 ns. This number was estimated by comparing the total number of events of types $1i$, 2, $2i$, 3 and $3i$ (Table IV, column 3) to the source strength N obtained from the fit. Similar comparisons based on events of type $1i$ and 2, and $2i$ and 3, gave the same results.

ii) The time at which the muon pulse begins to be measurable as a distinct peak is 7.7 ns, evaluated in a similar way.

iii) The most important criteria, however, are those concerned with the pulse height selection procedures already discussed in Sections **4** and **7***d*. It will be recalled that correlations existed between pulse heights and mean lives, for cut-offs earlier than 8 ns for muons and 12 ns for pions.

Taking a margin of safety over the limits discussed above, a somewhat arbitrary choice of 16 ns was made for the cut-off and used in the final evaluation. With this value of the cut-off the number of events used in this evaluation was 8307.

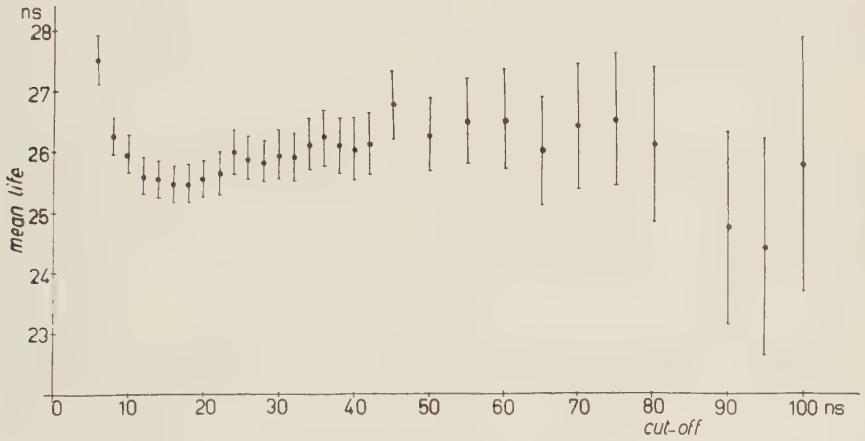

Fig. 8. – Estimated mean life as a function of cut-off for selected muon pulse height, but for all pion pulse heights.

In Fig. 8, which shows the value of the life-time plotted against cut-off, there appears to be a systematic decrease, although within the statistical errors, of the mean life at cut-offs between 18 and 24 ns. It should be kept in mind, however, that the successive points are not statistically independent, as each value includes all the measurements used to obtain the results to its

right. This decrease, therefore, cannot be considered as a genuine systematic effe t.

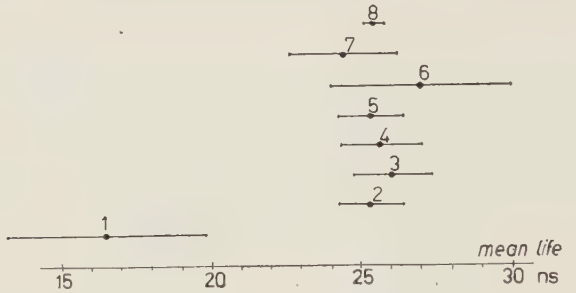

Fig. 9. – Comparison with the mean life values obtained in previous experiments: 1) W. L. KRAUSHAAR, J. E. THOMAS and V. P. HENRI: *Phys. Rev.*, **78**, 486 (1950); 2) W. L. KRAUSHAAR: *Phys. Rev.*, **86**, 513 (1952); 3) O. CHAMBERLAIN, R. F. MOZLEY, J. STEINBERGER and C. E. WIEGAND: *Phys. Rev.*, **79**, 394 (1950); 4) C. E. WIEGAND: *Phys. Rev.*, **83**, 1085 (1951) (Using the same data as 3); 5) M. JAKOBSON, A. SCHULZ and J. STEINBERGER: *Phys. Rev.*, **81**, 894 (1951); 6) L. LEDERMAN, E. T. BOOTH, R. BYFIELD and J. KESSLER; *Phys. Rev.*, **83**, 685 (1951); 7) R. P. DURBIN, H. H. LOAR and W. W. HAVENS: *Phys. Rev.*, **88**, 179 (1952); 8) Present experiment.

9. – Final result.

The value of the mean life of the positive pion obtained from the final histogram with a cut-off of 16 ns is:

$$\tau = (25.46 \pm 0.32) \text{ ns} .$$

This is based on 8307 events, 136 ± 18 of which are attributed to false π-μ background by the least square fit. The R.M.S. error includes a statistical error of 1.18% and an estimated residual systematical error 0.5%.

This value of the mean life is compared to the previously published results in Fig. 9.

* * *

We wish to express our gratitude to Mrs. BOVARD, Mrs. DANJEAN and Miss LAIDERRIER, who took the measurements on the IEP instrument with skill and patience.

RIASSUNTO

La vita media del mesone π^+ è stata determinata da circa 8000 decadimenti $\pi\mu$ fotografati su un oscillografo. Le fotografie sono state misurate con uno strumento destinato ad analisi di fotografie in camera a bolle ed i dati ottenuti sono stati elaborati su una calcolatrice elettronica rapida. Il valore ottenuto per la vita media del mesone π è $\tau_\pi = (25.46 \pm 0.32)$ ns.

Vapour Pressure of Isotopic Liquids.

II - Ne and A above Boiling-Point (*).

G. Boato, G. Casanova and M. E. Vallauri

Istituto di Fisica dell'Università - Genova
Istituto Nazionale di Fisica Nucleare - Sezione di Genova

(ricevuto il 25 Gennaio 1960)

Summary. — In order to extend previous studies of vapour pressure of isotopic liquids in a wider temperature range, a new cryostat was built. The single stage separation factor α of the isotopic pairs ^{36}A—^{40}A and ^{20}Ne—^{22}Ne was measured up to a vapour pressure of 12 atmospheres, using natural isotopic mixtures. The logarithm of the vapour pressure ratio of the pure isotopes was derived from α and found to be linearly dependent on $1/T$ within the experimental error, which amounts to less than 2‰ at boiling temperature of neon. The dependence on $1/T$ is given numerically by $\ln(p_{36}/p_{40}) = 1.31(1/T) - 8.95 \cdot 10^{-3}$ for argon, from 83 °K to 120 °K, and by $\ln(p_{20}/p_{22}) = 2.510(1/T) - 5.673 \cdot 10^{-2}$ for neon, from 25 °K to 40 °K. A brief discussion of the results is given.

1. – Introduction.

The static equilibration method already used for measuring the single stage separation factor

$$(1) \qquad \frac{(N_A/N_B)_{\text{vap.}}}{(N_A/N_B)_{\text{liq.}}} = \alpha \qquad \left[\begin{matrix} A \text{ lighter} \\ B \text{ heavier} \end{matrix}\right\} \text{ isotopic species}\Bigg]$$

of isotopic simple liquids below boiling-point [1], has been extended to cover a wider temperature range. Using a metallic equilibration cell specially de-

(*) Presented at the Congresso della S.I.F., Pavia, October 1959.
[1] G. Boato, G. Scoles and M. E. Vallauri: *Nuovo Cimento*, **14**, 735 (1959).

signed, vapour pressure of 12 atmospheres were attained. Argon and neon were chosen as the first systems to be studied as in this case it is easier to draw theoretical conclusions from the results.

A vapour bath cryostat was used, the cryogenic liquid being nitrogen in the case of argon and hydrogen in the case of neon. Since at this Institute liquid hydrogen is not available, the neon experiments were carried out at the Cryogenic Laboratory of the «Sincrotrone Nazionale» in Frascati (Rome).

2. – Experimental equipment.

The apparatus used is schematically shown in Fig. 1.

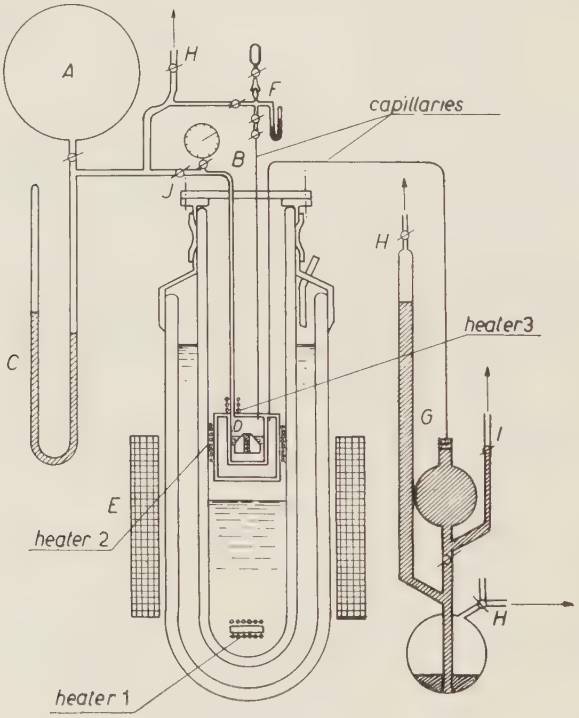

Fig. 1. – Diagram of the apparatus. A=10.7 l. storage flask; B=precision Bourdon gauge; C=precision mercury manometer; D=equilibration cell with metal floating stirrer; E=coil to move stirrer; F=sampling line; G=gas thermometer; H=to vacuum lines; I=to helium reservoir; J=metal vacuum-pressure valve.

2·1. *The measuring cell.* – The equilibration-and-measuring cell, 40.1 cm³ in volume, is contained in a larger cell, acting as a thermometric bulb, filled with helium. Both cells are made of pure electrolytic copper, owing to its good

heat conductivity. A hollow metal floating stirrer, 7 cm³ in volume, is used to agitate the liquid inside the equilibration cell, through the action of an intermittent magnetic field. The cell is connected with the gas reservoir by means of a german silver tube (0.5 cm internal diameter) and with the sampling system by means of a stainless steel capillary (0.02 cm internal diameter). The connections of the metallic high pressure side of the apparatus with the glass low pressure side are made through slightly modified Edwards' vacuum valves. The Dewar vessel containing the apparatus was made vacuum tight in order both to avoid hydrogen losses when working with neon and to allow pumping over liquid nitrogen when working with argon. The vessel is surrounded by a larger container, to be filled with liquid nitrogen.

2·2. *Thermoregulation and temperature measurement.* – As the measurements were to be carried out in a wide range of temperatures, a vapour cryostatic bath was employed. When the level of the cryogenic liquid is brought somewhat below the bottom of the copper cell, owing to the heat transfer from above, the cell will reach an equilibrium temperature which is nearer to room than to fluid temperature. However any lower temperature may be attained by boiling off the cryogenic fluid at a given rate with the aid of a heat source put inside the fluid (heater 1 in Fig. 1). Because of the refrigerating action of the vapour and the good thermal conductivity of copper, a sufficiently constant temperature can thus be maintained inside the equilibration cell.

To measure the temperature of the cell, a helium gas thermometer is used. As already mentioned, the thermometric bulb, 45 cm³ in volume, surrounds the measuring cell; the connection with the mercury measuring device is made by a thin capillary, 0.04 cm internal diameter, as shown in Fig. 1.

The gas thermometer acts also as a thermoregulating unit, in that the mercury can operate a relay when in contact with the stainless steel needle used to determine the reference position of the mercury level in the manometer, as shown in Fig. 1. If operated, the relay switches off the heater 1, thus permitting the cell temperature to rise; if not operated, the refrigerating action of the vapour prevails and the temperature decreases.

The temperatures determined by the gas thermometer agreed, within the error of measurement, with the temperatures calculated by the vapour pressures of argon and neon measured by manometers B and C, thus assuring both the purity of employed gases and the good performance of the gas thermometer. The sensitivity of the thermometer is constant at all temperatures owing to the negligible amount of dead spaces. The sensitivity depending from the amount of helium filling was given by

$$\sigma = (3.065 \pm 0.003)\ ^\circ\mathrm{K/cm}$$

for argon measurements, and by

$$\sigma = (0.998 \pm 0.001) \ ^\circ\mathrm{K/cm}$$

for neon measurements, thus allowing for the determination of absolute temperature with a precision of about 1‰ in both cases.

3. – Experimental procedure.

3·1. *Employed gases.* – Tank argon and neon of good purity were used; the argon was supplied by the Rivoira Co. of Turin and was assured to be 99.99% pure, the impurities being only N_2, H_2O and CO_2. The neon was kindly sent to us by the Kamerlingh Onnes Laboratory of Leiden and was seen to contain no O_2, N_2 and A, but remarkable amounts of H_2O, CO_2 and He (or H_2). A rough purification of neon was performed by condensing H_2O and CO_2 with liquid nitrogen and by pumping off the volatile fraction at boiling hydrogen temperature. The final purity was controlled by the mass spectrometer and by checking the triple point pressure.

3·2. *Filling of the measuring cell.* – The gas, initially contained in the storage flask A, was condensed directly inside the cell; before condensation, the cryogenic fluid was brought to a level a few centimetres above the top of the cell. In the case of argon, the nitrogen bath was cooled down by pumping to a temperature corresponding to an argon vapour pressure of about 10 cm Hg. In the case of neon no pumping was necessary, since at the hydrogen boiling point the neon vapour pressure is sufficiently low (about 4 cm Hg). Heater 3 was used to prevent some solid inert gas from condensing in the cell filling tube. In order to avoid isotopic fractioning, care was taken to stop condensation before the lowest possible vapour pressure was reached.

3·3. *Isotopic equilibration.* – Once the filling was completed, the metallic valve *J*, situated in the proximity of the cell, was closed. During the measurements, no use of vapour pressure thermometers was made, since the temperature could be exactly determined by the gas thermometer alone. In this way we were able to minimize the errors brought about by manometric spaces; it is evident that the larger are the dead spaces and the higher is the vapour pressure, the larger become these errors.

The next step was to boil away as much cryogenic liquid as to bring its level several centimeters under the cell; the temperature of the cell was raised to the desired value with the aid of heater 2 and thermoregulation was set on. To obtain a satisfactory thermal stability, the power consumption of the bath

heater was 2.5 W in the case of nitrogen and 0.4 W in the case of hydrogen, the corresponding fluid evaporation rate being capable of restoring the regulated temperature in cycles of about one minute.

A comment has to be made with respect to the temperature gradient along the cell. In the first apparatus (1) the gradient was directed from the top to the bottom, because of the continuous pumping over the bath. In the present apparatus the situation is reversed, since the heat flux coming from the connecting tubes generally makes the upper part of the equilibration cell warmer; only during the short time heater 1 is on, that is when the cold vapour hits the external cell, is it possible for the temperature to be lower at the top than at the bottom of the internal measuring cell. In the apparatus used in the present work a noticeable improvement was therefore accomplished as far as liquid-vapour equilibrium conditions are concerned. In any event a floating electro-magnetic stirrer was used to agitate the liquid. Since, for argon, no difference in the measured α was found between runs with and without stirring, the stirrer was not used in the neon experiments; as a consequence, longer equilibration times were needed.

3·4. *Sampling and mass spectrometric analysis.* – After any desired constant temperature was reached, a lapse of time ranging from twenty minutes to one hour was allowed to secure isotopic equilibration. Then vapour samples of about 2 cm³ NPT were withdrawn through the capillary by the same procedure described in the first paper of this series (1).

The isotopic composition of the vapour samples was compared with the composition of the initial gas by means of a differential mass spectrometer, which reads directly the quantity

$$\delta_v = \frac{R \text{ vapour} - R \text{ initial}}{R \text{ initial}} , \tag{2}$$

R being the ratio of the less abundant over the more abundant isotopic species in each sample (*).

4. – Results.

In the present experiment the single stage separation factor α defined by (1) is not as simply related to the measured δ as assumed in the first paper, because now a substantial part of the weight of the system is in the vapour phase, particularly at the highest temperatures.

(*) The δ_v thus defined is identical with the δ used in the previous paper only when the lighter isotopic species is the less abundant. In the opposite case, as long as $\delta < 0.01$, one has $\delta = -\delta_v$ with good approximation, as it comes about for nitrogen and oxygen. However the condition $\delta < 0.01$ is not satisfied by neon.

It is convenient to introduce the quantity

$$\delta_{vl} = \frac{R_v - R_l}{R_l}, \tag{3}$$

related to α by

$$\delta_{vl} = \begin{cases} \alpha - 1 & \text{whenever } \delta_{vl} > 0, \\ \dfrac{1}{\alpha} - 1 & \text{whenever } \delta_{vl} < 0\,. \end{cases} \tag{4}$$

In (3) R is again the ratio of the less abundant over the more abundant isotopic species and the subscripts v and l refer to vapour and liquid phase.

As shown in the Appendix, the quantity δ_{vl} is related to the measured δ_v by

$$\delta_{vl} = \frac{n}{n_l}(\delta_v + \delta_{ct}), \tag{5}$$

where n/n_l is the ratio of the total number of molecules within the cell to the number of molecules in the liquid phase and δ_{ct} is a correction due to the tube connecting the cell with the room temperature valve J.

The results are presented in Table I and II for the isotopic pairs ^{36}A—^{40}A and ^{20}Ne—^{22}Ne respectively. The first digit of the sample numbers listed in the first column of both tables indicates different runs; the two following digits refer to progressive samples of the same run. In the second and third column, absolute temperatures and their reciprocals are given; the fourth column contains the experimental δ_v's; the fifth and sixth columns show the magnitude of the quantities contained in equation (5); in the seventh column, the δ_{vl}'s are given.

Since in the whole temperature range δ_{vl} is positive for argon and negative for neon, it follows from (4) that α is always positive, *i.e.* that the lighter isotopic species is always the more volatile, as it may be expected from general arguments (2).

Owing to the greater natural isotopic ratio and the higher isotopic effect, the precision reached by the mass spectrometer in the case of neon is about ten times larger than in the case of argon. For this reason, the differences observed from sample to sample for argon are mostly due to analysis, whereas for neon differences due to defective thermoregulation become apparent. One will notice that in both circumstances the experimental data are well reproducible on different runs and consistent with each other in the whole temperature range. Small systematic errors in the evaluation of the corrections (given by column 5 and 6 of Tables I and II) may somewhat affect the final results at the highest temperatures.

(2) K. F. HERZFELD and E. TELLER: *Phys. Rev.*, **54**, 912 (1938).

TABLE I. – *Argon results.*

Previous data						
	T (°K)	$\frac{1}{T}\cdot 10^2$				$\left[\ln \frac{p_A}{p_B}\right]_{av.}\cdot 10^3$
	84.4	1.185				6.6
	85.5	1.170				6.4
	87.0	1.149				6.1
New data						
Sample	T (°K)	$\frac{1}{T}\cdot 10^2$	$\delta_v\cdot 10^3$	$\delta_{ct}\cdot 10^3$	$\frac{n}{n_l}$	$\delta_{vl}=\alpha-1=\ln\frac{p_A}{p_B}\cdot 10^3$	$\left[\ln \frac{p_A}{p_B}\right]_{av.}\cdot 10^3$
101	88.2	1.135	5.9		1.03	6.0_5	5.8
102			5.4			5.5_5	
103			5.7			5.8_5	
104			5.7			5.8_5	
401	93.0	1.075	4.9_5		1.04	5.1_5	5.2_5
402			5.1_5			5.3_5	
403			5.1			5.3	
404			4.9_5			5.1_5	
301	99.2	1.008	3.9_5		1.07	4.2_5	4.2
302			3.8_5			4.1_5	
201	103.3	0.968	3.4_5		1.08	3.7	3.7
405	103.5	0.966	3.6		1.10	3.9_5	3.9
406			3.5_5			3.9	
303	107.4	0.931	2.6_5		1.14	3.0	3.2
304			2.9_5			3.3_5	
407	113.0	0.885	2.1_5	0.05	1.20	2.6_5	2.7_5
408			2.3			2.8	
409			2.2_5			2.7_5	
305	116.2	0.860	1.7_5	0.05	1.26	2.2_5	2.1
306			1.5_5			2.0	
410	118.7	0.842	1.6	0.05	1.30	2.1_5	2.1_5
411			1.5_5			2.1	
412			1.6_5			2.2	

TABLE II. – *Neon results.*

Sample	T (°K)	$\frac{1}{T}\cdot 10^2$	$\delta_v \cdot 10^2$	$\delta_{ot}\cdot 10^2$	$\frac{n}{n_1}$	$\delta_{vl}=\frac{1}{\alpha}-1$	$\ln\frac{p_A}{p_B}\cdot 10^2$	$\left[\ln\frac{p_A}{p_B}\right]_{av.}\cdot 10^2$
101			— 4.38			— 4.48	4.47	
102	24.8	4.03	— 4.32		1.02_2	— 4.42	4.41	4.44
103			— 4.35			— 4.45	4.44	
201			— 4.26			— 4.38	4.36	
202	25.02	3.998	— 4.29		1.02_9	— 4.41	4.39	4.38
203			— 4.29			— 4.41	4.39	
104	25.8	3.88	— 3.97		1.03_1	— 4.09	4.04	4.04
204	25.98	3.849	— 3.94		1.04_0	— 4.10	4.04	4.03
205			— 3.91			— 4.07	4.01	
105			— 3.56			— 3.71	3.63	
106	26.8	3.73	— 3.56		1.04_2	— 3.74	3.66	3.65
107			— 3.59			— 3.74	3.66	
206			— 3.53			— 3.72	3.64	
207	27.01	3.702	— 3.50		1.05_4	— 3.69	3.61	3.63
208			— 3.52			— 3.71	3.63	
301	27.79	3.598	— 3.15		1.07_4	— 3.38	3.28	3.29
302			— 3.17			— 3.40	3.30	
401			— 2.92			— 3.17	3.04	
402	28.74	3.479	— 2.86		1.08_7	— 3.11	2.98	3.05
403			— 3.00			— 3.26	3.13	
404			— 2.94			— 3.20	3.07	
303	30.21	3.310	— 2.44		1.14	— 2.78	2.61	2.61
501			— 2.36			— 2.74	2.56	
502	30.64	3.264	— 2.34		1.16	— 2.71	2.53	2.52
503			— 2.32			— 2.69	2.51	
504			— 2.31			— 2.68	2.50	
601	33.06	3.025	— 1.62		1.31	— 2.12	1.91	1.91
304	33.17	3.015	— 1.62	0.02	1.31	— 2.15	1.94	1.93
305			— 1.61			— 2.14	1.93	
602	35.15	2.845	— 1.05	0.03	1.54	— 1.66	1.46	1.46
603	37.62	2.658	— 0.49	0.06	2.20	— 1.21	1.02	1.02
604			— 0.49			— 1.21	1.02	
505			— 0.32			— 1.00	0.83	
506	38.58	2.592	— 0.31	0.07_5	2.54	— 0.98	0.80	0.84
507			— 0.33			— 1.03	0.86	
508			— 0.33			— 1.03	0.86	

5. – Discussion of the results.

At sufficiently high vapour pressures the single stage separation factor is not identical with the ratio p_A/p_B of the vapour pressures of the pure isotopes. A comparison with theory and with data obtained by different methods is actually easier if one uses the $\ln p_A/p_B$.

For any ideal mixture one may write, at any given temperature,

$$RT \ln \frac{(n_A/n_B)_v}{(n_A/n_B)_l} = RT \ln \alpha = \int_{p_A}^{p} (\tilde{V}_{Al} - \tilde{V}_{Av})\, \mathrm{d}p + \int_{p}^{p_B} (\tilde{V}_{Bl} - \tilde{V}_{Bv})\, \mathrm{d}p \tag{6}$$

as it can be easily derived by equating the chemical potentials; p is the total pressure of the mixture and $\tilde{V}_{Al}$, $\tilde{V}_{Av}$, $\tilde{V}_{Bl}$, $\tilde{V}_{Bv}$ are the molar volumes of the two components in the two phases.

It is easily seen that, as long as $\tilde{V}_l \ll \tilde{V}_v$ and the vapour behaves as a perfect gas, (6) becomes the currently used formula

$$\ln \alpha = \delta_{vl} = \ln \frac{p_A}{p_B} .$$

Such a formula is valid for argon in the whole temperature range explored so far, within the accuracy of measurements.

On the other hand, the vapour of neon cannot be treated as an ideal gas, particularly at the highest temperatures. In this case, keeping in account the second virial coefficient B, equation (6) yields

$$\ln \alpha = \ln \frac{p_A}{p_B} + \frac{B(p_A - p_B)}{RT} ;$$

other terms, arising from the difference in the second virial coefficients of ^{20}Ne and ^{22}Ne, can be shown to be negligible. Taking into account the relationship (4) between α and δ_{vl}, one finally gets for neon

$$\ln \frac{p_A}{p_B} = -\delta_{vl} + \frac{\delta_{vl}^2}{2} + \frac{B(p_A - p_B)}{RT} .$$

Values of $\ln (p_A/p_B)$ for argon and neon respectively are given in the last two columns of Tables I and II and plotted versus $1/T$ in Figs. 2 and 3, together with previous results. The present measurements on argon are seen to agree

very satisfactorily with those previously performed at temperatures below boiling-point (1) using a somewhat less refined experimental technique. On the other hand the agreement with the results of KEESOM and HAANTJES (3)

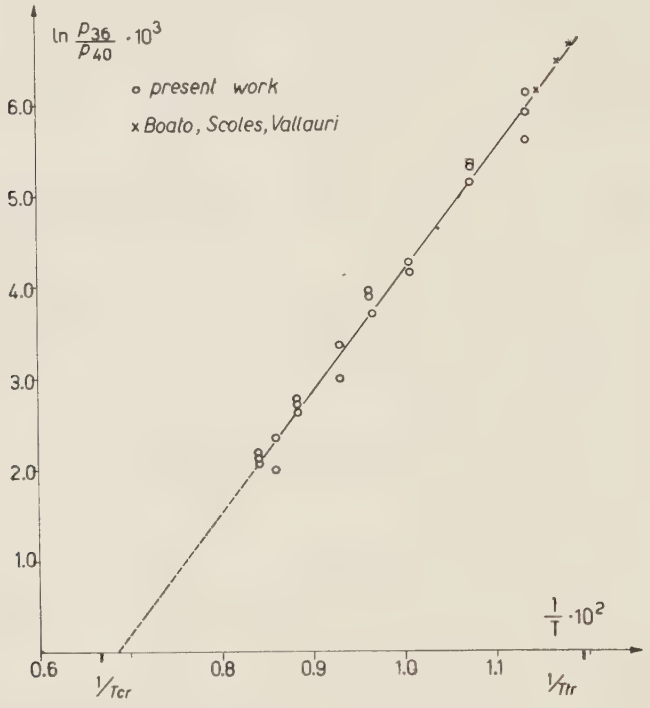

Fig. 2 – Argon: $\ln p_{36}/p_{40}$ *vs.* $1/T$.

on neon, obtained by a differential manometric method at pressure below one atmosphere, is good but not quite satisfactory: no evidence was found for an increase of $(\mathrm{d} \ln p_A/p_B)/\mathrm{d}(1/T)$ with $1/T$, as claimed by KEESOM and HAANTJES.

Both for argon and for neon, $\ln p_A/p_B$ appears to be a linear function of $1/T$ within the experimental error in the explored temperature range. By using the least squares method, the results are well represented by the equations

$$\ln \frac{p_A}{p_B} = 1.31 \frac{1}{T} - 8.95 \cdot 10^{-3}$$

(3) W. H. KEESOM and J. HAANTJES: *Physica*, **2**, 986 (1935).

for the isotopic pair $^{36}A—^{40}A$;

$$\ln \frac{p_A}{p_B} = 2.510 \frac{1}{T} - 5.673 \cdot 10^{-2}$$

for the isotopic pair $^{20}Ne—^{22}Ne$. The resulting straight lines, when extrapolated at higher temperatures, cross the abscissa in neighborhood of the critical temperature in both cases.

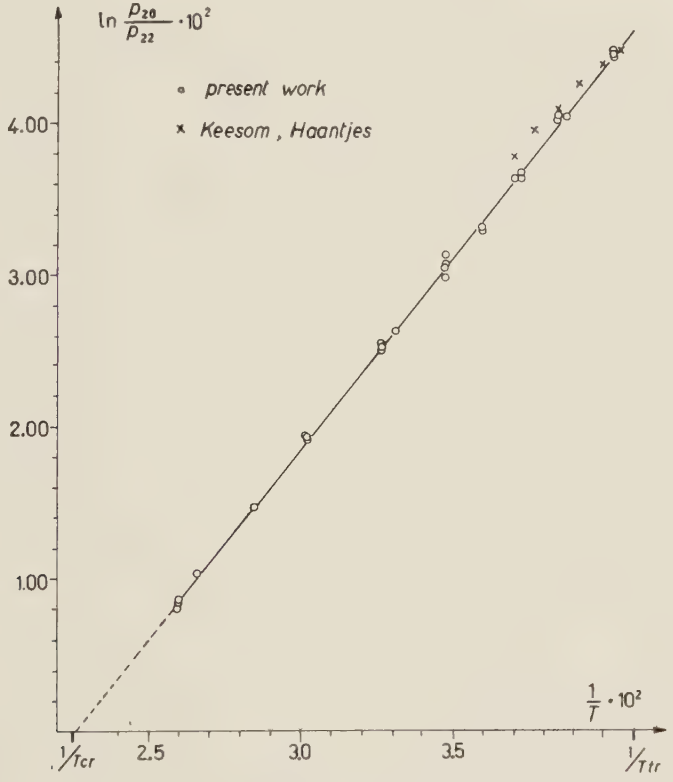

Fig. 3. – Neon: $\ln p_{20}/p_{22}$ *vs.* $1/T$.

One is tempted to give physical significance to this extrapolation, by postulating 1) a linear behaviour in the whole range of existence of the liquid, 2) the vanishing of $\ln (p_A/p_B)$ at the critical point (*). The linearity should be

(*) This would be very appealing. Unfortunately, a more detailed analysis, taking into account the differences in critical temperatures of two isotopic liquids, seems to lead to different conclusions.

related to the approximate linearity of $\ln p$ as a function of $1/T$ for Ne, A, Kr and Xe.

In order to compare the results relative to argon and neon with each other, the quantity $\ln (p_A/p_B)/(\Lambda_A^{*2} - \Lambda_B^{*2})$ has been plotted versus $1/T^*$, as shown in Fig. 4, Λ^* being defined as $h/\sigma\sqrt{m\varepsilon}$, and T^* as kT/ε, using the picture offered by the quantum theorem of corresponding states (see previous paper). It is shown by the theory that in such a plot all substances presenting small quantum effects ($\Lambda^* \ll 1$) would drop on the same curve, whereas deviations are to be expected when Λ^* is of the order of unity. It is seen from Fig. 4 that argon and neon behave similarly, but not identically, owing to the fact that for neon $\Lambda^* \simeq 0.6$ and therefore a contribution due to higher terms in the development of the partition function in powers of Λ^{*2} is present. From the above consideration, it has to be argued also that the isotopic effects on vapour pressure for krypton and xenon can be foreseen at best by using the argon curve in Fig. 4.

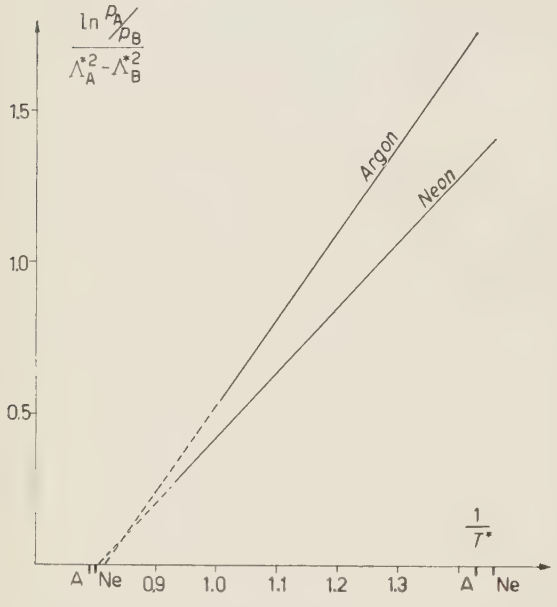

Fig. 4. – Corresponding isotopic effects in vapour-liquid equilibrium for A and Ne, as a function of the reciprocal of the reduced temperature. Reduced critical and triple points of A and Ne are shown.

A more detailed discussion of our results in the light of the theorem of corresponding states will be given in a forthcoming paper [1], together with an attempt at determining a self consistent set of molecular parameters σ and ε for Ne, A, Kr and Xe.

* * *

The present work was carried out with the financial help of the « Comitato per la Fisica del Consiglio Nazionale delle Ricerche ».

We would like to thank Dr. G. SCOLES for his collaboration during the crucial stage of the experiments. Thanks are due also to F. TRINCOSSI and R.

[1] G. BOATO and G. CASANOVA: to be published in *Journ. Chem. Phys.*

FILENI of the Physics Department in Genoa and to the crew of the Cryogenic Laboratory in Frascati for technical assistance.

We are glad to acknowledge the kindness of Prof. TACONIS and Dr. BEENAKKER of the Kamerlingh Onnes Laboratory for having given us helpful advice concerning the cryostat and for having supplied us with the pure neon necessary for this experiment.

APPENDIX

Evaluation of $\delta_{v'}$.

δ_{vl} defined by equation (4) can be related to the experimental δ_v as follows.

Let n_A and n_B be the total number of molecules of two isotopic species A and B, separated in f isotopic phases. Let n_{iA} and n_{iB} be the number of molecules of the two species in the i-th phase. If one defines

$$\delta_i = \frac{n_{Ai}/n_{Bi}}{n_A/n_B} - 1 \tag{A.1}$$

it follows immediately the general relation

$$\sum_1^f n_{Bi}\,\delta_i = 0\ ; \tag{A.2}$$

if now $n_A \ll n_B$, one can write simply

$$\sum_1^f n_i\,\delta_i = 0\ , \tag{A.3}$$

where $n_i = n_{Ai} + n_{Bi}$ is the total number of molecules in the i-th phase.

In our experiments we have actually to deal with more than two isotopic phases since, owing to the working conditions, the isotopic composition of the vapour in the tube connecting the cell with the room temperature valve J is different from the isotopic composition of the vapour in the cell. At the end of any run, a gas sample was taken from the room temperature side of the tube, which always yielded an isotopic composition (represented in the following by δ_t) different from that of the vapour at the last temperature reached. As the diffusion is sufficiently rapid at room temperature to mix thoroughly the gas, the vapour in the external tube was assumed to have a uniform isotopic composition, while for the tube laying inside the Dewar vessel was made the rather crude statement of a linear isotopic concentration gradient.

With these assumptions, equation (A.3) takes the form

$$n_l\delta_l + n_v\delta_v + n_t'\delta_t + \tfrac{1}{2}n_t'\delta_t = 0\ ,$$

where n_l and n_v are the number of molecules in the liquid and in the vapour inside the cell, and n'_t, n''_t are the same number in the external and in the internal section of the connecting tube, respectively; the δ's, defined by (A.1), are referred to the initial gas; δ_v and δ_l are measured quantities.

Making now use of the identity

$$\delta_{vl} = (\delta_v - \delta_l)(1 + \delta_v) \simeq \delta_v - \delta_l ,$$

the unknown δ_l can be eliminated, obtaining

$$\delta_{vl} = \frac{n}{n_l}\left[\delta_v + \frac{n'_t + \frac{1}{2}n''_t}{n}(\delta_l - \delta_v)\right] = \frac{n}{n_l}(\delta_v + \delta_{cl}) ,$$

which is equation (5).

The ratios between number of molecules may be calculated from the gas equation of state, which yields in our experimental condition:

$$\frac{n}{n_l} = \frac{1 - \dfrac{Mp}{\varrho RT}\dfrac{1}{1 + B/\tilde{V}}}{1 - \dfrac{p}{p_{in}}\left(\dfrac{V_c + V_t}{V_F}\dfrac{1}{1 + B/\tilde{V}} + \dfrac{V_{t0}}{V_F}\right)} ,$$

$$\delta_{cl} = (\delta_l - \delta_v)\frac{p}{p_{in}}\left(\frac{V_{t0}}{V_F} + \frac{1}{2}\frac{T_0}{T}\frac{V_t}{V_F}\right) ,$$

T is the working temperature, p the corresponding vapour pressure, T_0 the room temperature; p_{in} the difference between the initial pressure of the gas and the residual pressure after condensation (Section 3·2) in the storage flask; V_c is the cell volume, V_F the flask volume, V_t and V_{t0} the volume of the two sides of the connecting tube respectively within the Dewar vessel and at room temperature; M is the atomic mass, R the gas constant, B the second virial coefficient and $\tilde{V}$ the molar volume.

It has to be emphasized that the imperfection of the gas, represented by the ratio $B/\tilde{V}$, has a remarkable effect on the ratio n/n_l at the highest pressures reached in the experiments.

Note added in proof.

While this paper was in print, the authors were informed of a similar work carried out by ROTH and BIGELEISEN (*) at Brookhaven, by using separated isotopes.

Liquid neon was studied from triple point to 30 °K. The agreement between the results obtained by ROTH and BIGELEISEN and by us is scarce, the difference in the

(*) E. G. ROTH and J. BIGELEISEN: *Journ. Chem. Phys.*, **32**, 612 (1960).

$\ln (p_A/p_B)$ amounting to 4% at the triple point and to 20% at the highest temperature. A discussion with Dr. Roth and an exchange of letters with Prof. Bigeleisen could not explain up to now the reason of such a disagreement. In any event, we would like to point out that the measuring methods are fundamentally different.

RIASSUNTO

Con lo stesso metodo statico già usato in un precedente lavoro, abbiamo misurato il fattore di separazione α nell'equilibrio liquido-vapore di miscele isotopiche di liquidi semplici in un più ampio intervallo di temperatura. È stato costruito un apparecchio metallico che ci ha consentito di eseguire misure in miscele isotopiche naturali di argon e neon fino ad una tensione di vapore di 12 atm. L'apparecchio è stato mantenuto alle temperature richieste per mezzo di un criostato a bagno di vapore appositamente progettato. Dal valore di α abbiamo ricavato il logaritmo del rapporto delle tensioni di vapore degli isotopi puri, e abbiamo trovato che esso dipende linearmente, entro gli errori sperimentali, dall'inverso della temperatura, secondo le relazioni: $\ln (p_{36}/p_{40}) = 1.31(1/T) - 8.95 \cdot 10^{-3}$ per l'argon tra 83 °K e 120 °K, e $\ln (p_{20}/p_{22}) = 2.510(1/T) - 5.673 \cdot 10^{-2}$ per il neon tra 25 °K e 40 °K. Estrapolando verso le alte temperature i risultati ottenuti, si trova, al punto critico, un effetto pressochè nullo. La dipendenza lineare potrebbe pertanto sussistere con buona approssimazione in tutto il campo di esistenza dello stato liquido. I risultati sperimentali vengono brevemente discussi alla luce del teorema quantistico degli stati corrispondenti.

1543

Influence du développement sur la dimension transversale des traces d'ions lourds dans les émulsions ionographiques.

Ch. Gegauff et J. P. Lonchamp

Laboratoire de Physique Corpusculaire - Strasbourg

(ricevuto il 27 Gennaio 1960)

Résumé. — On étudie l'influence de divers révélateurs sur les dimensions transversales des traces d'ions $_2$He, $_6$C, $_7$N, $_8$O, $_{10}$Ne et $_{18}$A dans les émulsions ionographiques G-5, C-2 et L-4. La discrimination des traces d'ions lourds par la mesure de leur dimension transversale est dépendante de cette influence qui est très forte pour les révélateurs usuels (amidol, ID 19). On propose un contrôle du développement par la mesure de l'épaisseur de traces α. On démontre la difficulté d'application d'un facteur de correction simple tenant compte de l'influence du développement.

1. – Introduction.

Avant d'interpréter la structure des traces d'ions lourds et d'essayer de l'utiliser pour la discrimination entre ions de Z différents, il convient d'étudier les facteurs qui peuvent l'influencer.

Rappelons brièvement le mécanisme de la formation d'une trace de particule chargée dans l'émulsion ionographique. La particule pénètre dans l'émulsion avec une certaine énergie qu'elle perd essentiellement par interaction avec les électrons de ce milieu. Ces électrons acquièrent ainsi une énergie qui détermine leur parcours dans l'émulsion. Etant donné la grande concentration en BrAg (80 % en poids) des émulsions ionographiques, la majorité de ces électrons prennent naissance dans le microcristaux ou « grains » de BrAg traversés par la particule. Ceux, très nombreux, qui ont reçu une faible fraction de l'énergie passent dans la bande de conduction du microcristal et servent à la création de l'image latente sur les germes de sensibilité. D'autres ayant reçu une énergie suffisante pour leur permettre de sortir du grain, peuvent à leur tour créer

une image latente sur les grains voisins de ceux effectivement traversés par la particule. Ces électrons dénommé rayons δ ont un spectre d'énergie dont le maximum croît assez rapidement avec la vitesse de la particule.

En nous basant sur les hypothèses de P. Cüer [1] concernant la relation entre la dispersion et la dimension des amas argentiques de l'image latente des différentes radiations en fonction de l'énergie spécifique dépensée, nous pouvons admettre que nous nous trouvons en présence de deux types d'image latente après le passage de la particule.

En effet, dans le grain traversé par la particule, la perte d'énergie est très supérieure à celle dans un grain touché par un rayon δ. Ceci entraîne une différence dans le nombre d'électrons libérés par grain, et finalement, pour une même émulsion, les amas d'image latente des grains traversés par la particule seront plus importantes que ceux des grains traversés par les δ.

D'autre part, la sensibilité de l'émulsion, fonction de la répartition et du nombre des centres de sensibilité gouverne la formation de l'image latente.

C'est ce facteur qui détermine dans quelle mesure l'un et l'autre de ces deux types d'image latente seront enregistrés par les différentes émulsions.

Il en résulte que la structure de la trace dépend essentiellement des deux facteurs suivants:

a) La sensibilité de l'émulsion, c'est-à-dire sa réponse à la perte d'énergie que nous avons étudiée dans une précédente publication [2].

b) Le développement, c'est-à-dire la transformation de l'image latente en image visible.

Le développement est un phénomène complexe sur le compte duquel plusieurs théories s'affrontent que nous ne ferons qu'esquisser rapidement pour la compréhension de la partie expérimentale.

La transformation de l'image latente en image visible se fait par réduction de l'ion Ag^+ en argent métallique. Du point de vue thermodynamique, le développement est décrit par l'equation suivante:

$$\text{Red} + Ag^+ \leftrightharpoons \text{Ox} + Ag$$

qui n'est applicable qu'aux réactions réversibles, telles qu'elles se présentent pour les révélateurs inorganiques, du type $Fe^{++} - Fe^{+++}$.

Pour les révélateurs organiques non réversibles, le classement selon les

[1] R. Schmidt, M. Debeauvais-Wack et P. Cüer: *Wissenschaftliche Photographie Internationale Konferenz, Cologne* (1956), p. 96; P. Cüer: *Sci. et Ind. Phot.*, **18**, 321 (1947).

[2] J. P. Lonchamp et Ch. Gegauff: *Journ. Phys. et Rad.*, **20**, 797 (1959); Ch. Gegauff, J. P. Lonchamp et P. Cüer: *Compt. Rend. Acad. Sci.*, **247**, 1758 (1958).

potentiels redox ne représente qu'une grossière approximation; ceux-ci sont mieux décrits par leur niveau énergétique, notion qui ne fait pas intervenir la réversibilité. ABRIBAT [3] décrit le développement de cette manière en associant à chaque révélateur un niveau énergétique d'autant plus élevé que son pouvoir réducteur est plus grand. Le système constitué par le grain de BrAg, les germes de sensibilité et l'image latente, est caractérisé lui aussi par des niveaux énergétiques. Selon la position du niveau du révélateur par rapport à ceux du grain de BrAg, le passage des électrons est possible ou non, et la solution fonctionne ou non comme révélateur.

MITCHELL [4] décrit lui aussi le processus en termes de niveaux énergétiques dans sa théorie de la formation de l'image latente et du développement chimique. Il explique en plus les différences de cinétique de développement des grains de BrAg par la nature des germes qu'ils portent. En effet, un électron ne peut être transféré d'une molécule de réducteur à un germe de sous-image latente que lorsque le niveau de celui-ci est abaissé par adsorption d'un ion Ag^+. La durée de vie du germe de sous-image chargé étant très courte, la probabilité de capture d'un électron est faible et la période d'induction longue. Par contre, un germe d'image latente stable est toujours chargé positivement lorsqu'il est en équilibre thermique avec le cristal; le transfert de l'électron de la molécule réductrice au germe est toujours possible, et le développement s'amorce rapidement. En conséquence, plus les amas d'image latente seront gros, plus leur développement sera rapide, quel que soit le niveau énergétique du révélateur.

En conclusion, les deux facteurs importants pour l'étude de l'influence du développement sur l'épaisseur des traces sont, d'une part, la nature du révélateur, caractérisée par son potentiel redox ou son niveau énergétique et sa composition, et, d'autre part, la cinétique du développement en fonction de la taille de l'image latente.

Ceci s'applique à l'analyse des deux modes de développement qui sont:

1) Le développement chimique qui fait appel aux ions argent présents dans l'émulsion, réduits à partir des centres d'image latente à la surface des grains. Le révélateur dans son état initial contient un réducteur, mais pas de sels d'argent.

2) Le développement physique qui utilise les ions argent contenus dans le révélateur. Les ions argent du grain de BrAg ne participent pas au développement; le développement physique peut être effectué avant ou après fixage.

Remarquons que les deux types de développement peuvent coexister dans certains révélateurs.

---

[3] M. ABRIBAT: *Chimie Physique des couches sensibles photographiques*, p. 202.
[4] J. W. MITCHELL: *Sci. et Ind. Phot.*, **29**, 1 (1958).

2. - Etude de l'influence du développement chimique sur les dimensions transversales des traces α du polonium.

Une étude préliminaire du développement chimique a été faite sur des traces α du Po, le nombre de plaques nécessaires à ce travail rendant l'emploi des ions lourds prohibitif. Les expériences ont été effectuées à l'aide d'émulsions Ilford G-5, C-2 et L-4 de 10 μm et 50 μm d'épaisseur.

Les traces α d'une source de Polonium sont faciles à enregistrer à la surface de l'émulsion; il n'y a pas lieu de tenir compte d'un gradient de développement. Nous avons rejeté les méthodes d'imprégnation pour l'obtention des traces α car nous risquions de modifier les propriétés physicochimiques de l'émulsion par immersion dans les solutions d'imprégnation.

Les mesures ont été effectuées à l'aide du Poohstrolino ([5]). L'incertitude sur chaque point est représentée par la déviation standard de la distribution des moyennes. Il n'y a pas lieu de tenir compte de l'incertitude due à l'étalonnage, erreur systématique qui ne modifie pas l'allure des courbes.

Les germes utiles pour le développement sont ceux situés à la surface des grains et ceux mis à nu par un solvant du BrAg qui peut être contenu dans le révélateur.

Nous avons utilisé deux espéces de révélateurs: ceux dits totaux contenant un solvant du BrAg et ceux dits superficiels ne contenant pas de solvant du BrAg et nous avons examiné leur action en fonction du temps de développement. Leur niveau énergétique est suffisamment élevé pour que nous puissions admettre que les deux types d'image latente soient développés.

a) Influence du temps de développement des révélateurs totaux sur l'épaisseur des traces α. Les révélateurs utilisés sont classiques en technique ionographique. Ce sont l'amidol à pH 6.5 (formule de Bruxelles) et l'ID 19.

Nous avons essentiellement porté notre attention sur l'amidol, car c'est le révélateur le plus employé par les utilisateurs.

La courbe 1 (Fig. 1) représente la variation d'épaisseur des traces α en

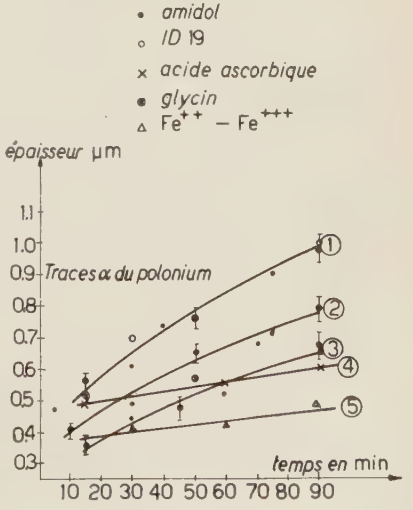

Fig. 1.

([5]) A. Bonetti, C. Dilworth, M. Ladu e G. Occhialini: *Lincei Rend. Sci. Fis. Mat. e Nat.*, **17**, 311 (1954).

fonction du temps de développement à l'amidol pour l'émulsion G-5; la courbe 2 est relative à l'émulsion C-2 et la courbe 3 à l'émulsion L-4. Les points correspondant au développement à l'ID 19 se rangent sur les courbes de l'amidol.

Pour la G-5, la variation d'épaisseur des traces α est de 0.5 μm pour des temps allant de 10 à 90 minutes, l'augmentation est régulière; elle est de 0.4 μm pour la C-2 et de 0.35 μm pour la L-4. A 45 minutes de développement qui est le temps nécessaire pour faire apparaître les β au minimum d'ionisation dans de bonnes conditions, l'épaisseur moyenne d'une trace α est de l'ordre de 0.75 μm dans la G-5; à 55 minutes, elle est de 0.80 μm.

Cette variation de l'épaisseur avec le temps de développement n'est pas négligeable si l'on veut utiliser la dimension transversale comme facteur de discrimination entre ions de charges différentes.

Les 3 courbes ont sensiblement la même allure. Il semble donc s'agir d'un même phénomène pour les trois émulsions; les différences en valeur absolue sont dues aux dimensions des grains. Il est possible que des grains de BrAg ayant reçu très peu d'énergie (image latente faible) soient développées bien après les autres, apportant tardivement leur contribution à l'épaisseur. D'autre part, JAMES [6] a signalé, pour les révélateurs contenant un solvant du BrAg, un dépôt d'Ag provenant d'un développement physique se surajoutant au développement chimique et qu'il a appelé « solution-physical développement » Ce développement physique, relativement lent, peut devenir important lorsque suffisamment d'Ag a passé en solution et lorsque le développement chimique a produit une surface d'argent métallique assez grande pour permettre le dépôt d'argent à partir de la solution. Il est vraisemblable que ces deux facteurs contribuent à l'augmentation de l'épaisseur des traces lorsque le temps de développement augmente.

b) Influence du temps de développement des révélateurs superficiels sur l'épaisseur des traces α. Pour les révélateurs superficiels, le développement physique est exclu puisqu'ils ne contiennent pas de solvant du BrAg.

Nous avons été amenés à examiner trois sortes de révélateurs superficiels pour l'émulsion G-5.

1) Le révélateur au génol-acide ascorbique de JAMES [6]

Formule:	acide ascorbique . . .	10	g	pour 1 000 cm³ H_2O
	génol	2.5	g	
	CO_3Na_2	80	g	
	BrK	2	g	

Sans être solvant pour le bromure d'argent comme le sulfite de sodium, l'acide ascorbique remplace celui-ci; son rôle est de protéger le réducteur de

[6] H. JAMES: *Phot. Sc. and Eng.*, **1**, 141 (1958).

l'oxydation aérienne et d'éliminer les produits d'oxydation du révélateur. Le pouvoir réducteur de ce révélateur est élevé. La courbe 4 (Fig. 1) représente l'allure de l'accroissement d'épaisseur des traces α. Cet accroissement est bien inférieur à celui causé par les révélateurs solvants; il n'est que de 0.1 μm entre 15 et 90 minutes.

2) Le révélateur au glycin sans sulfite de James

Formule:	glycin	10 g	pour 1000 cm³ H_2O
	CO_3Na_2	44 g	
	BrK	2 g	

Ce révélateur s'oxyde très rapidement à l'air à cause de l'absence de sulfite et d'acide ascorbique. Son usage n'est pas recommandé, car il perd rapidement ses propriétés développatrices. L'allure de l'accroissement d'épaisseur est comparable à celle du révélateur précédent (voir Fig. 1).

3) Le révélateur au ferro-oxalate qui est un révélateur inorganique superficiel.

Formule: 1 vol. d'une solution de SO_4Fe à 25% + + acide citrique à 0.3% + BrK 1‰, 3 vol. d'une solution d'oxalate de potassium à 25%.

L'accroissement d'épaisseur des traces α (courbe 5, Fig. 1) est comparable à celui occasionné par le révélateur au génol-acide ascorbique.

Ces trois types de révélateurs non solvants provoquent un accroissement d'épaisseur très faible pendant la durée d'action examinée: ceci peut être dû à une cinétique très lente du développement des grains ayant reçu une faible fraction d'énergie et très différente de celle du développement à l'aide de l'amidol.

La structure de l'Ag développé n'est certainement pas la même dans les deux cas (révélateur total ou superficiel). Des examens à l'aide du microscope électronique (7) ont montré un aspect filamentaux de l'argent provenant d'un développement rapide alors que le développement lent produit une masse d'argent plus compacte. Il est concevable qu'une telle différence puisse se répercuter sur l'épaisseur de traces.

---

(7) E. Klein: *Mitteilungen aus den Forschungslaboratorien der Agfa, Leverkusen, München*, Band III, p. 43.

c) Influence du temps de développement d'un révélateur au chlorure de titane sur l'épaisseur des traces α. Les propriétés de ce révélateur ont été démontrées par les travaux de RZYMKOWSKI [8], il nous a semblé intéressant de l'inclure dans cette étude.

Rappelons la formule proposée par RZYMKOWSKI:

5 cm³ Cl_3Ti à 15% (sol. commerciale) + 95 cm³ solution de réserve (composition: $C_2O_4K_2$ . . . . . 28 g
BrK . . . . . 1.7 g
auramine 1/2000 . 170 cm³
Compléter à 1 l.)

Ce révélateur donne en densitométrie des résultats très analogues au révélateur au méthol-hydroquinone; il est peu sensible à une variation de concentration de BrK et ne provoque pas de voile. Nous avons commencé à l'appliquer au développement des traces α du Polonium dans une émulsion G-5. L'épaisseur des traces α développées dans ce révélateur est superieure à celle des traces développées dans l'amidol ou l'ID 19 à temps égal. Nous nous trouvons en présence d'un révélateur intéressant dont nous nous proposons de poursuivre l'étude de façon systématique.

3. – Etude de l'influence du développement sur la dimension transversale des traces d'ions lourds ($Z > 2$).

Les mesures d'épaisseur ont été réalisées par la méthode photographique décrite précédemment [9].

a) Influence du temps de développement des révélateurs classiques en technique ionographique, révélateurs totaux. L'importance de l'accroissement d'épaisseur des traces α en fonction du temps de développement nous a amené à faire une étude systématique de ce facteur pour les ions lourds.

Nous disposions de deux types d'ions lourds: $_{10}Ne$ et $_{8}O$; enregistrés dans des plaques d'émulsion G-5 de 50 μm d'épaisseur. Les courbes représentent l'épaisseur moyenne, calculée à partir de 20 traces, en fonction du parcours résiduel. L'erreur portée sur ces courbes moyennes représente l'écart maximum entre les courbes relatives aux différentes traces individuelles.

---

[8] J. RZYMKOWSKI: *Arhiv. Kemiju*, **20**, 26 (1948).
[9] CH. GEGAUFF: *Thèse* (Strasbourg, 1959).

1) Fig. 2 – $_{10}$Ne – Développement à l'amidol à 22°:

Courbe (1)	20 minutes
Courbe (2)	40 minutes
Courbe (3)	60 minutes
Courbe (4)	80 minutes

Les courbes représentant un développement de 100 et de 120 minutes sont pratiquement confondues avec la courbe (4).

L'accroissement de l'épaisseur moyenne très important en chaque point, n'est pas uniforme tout le long des courbes. En effet,

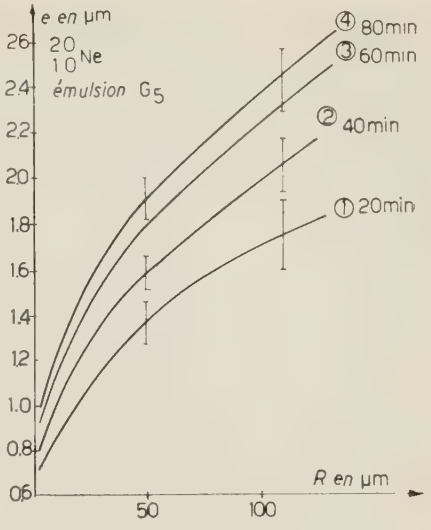

Fig. 2.

à 10 µm Δ (4) — (1) = 0.36 µm alors qu'à 120 µm, Δ (4) — (1) = 0.78 µm,

à 10 µm Δ (4) — (2) = 0.20 µm alors qu'à 120 µm, Δ (4) — (2) = 0.38 µm.

Cette série d'expériences semble prouver l'existence d'un palier se situant aux environs de 80 minutes de développement pour ce type d'ion et ce révélateur. Ce palier n'a pas été trouvé pour les traces α pour ces temps de développement, mais pourrait exister au-delà de 90 minutes.

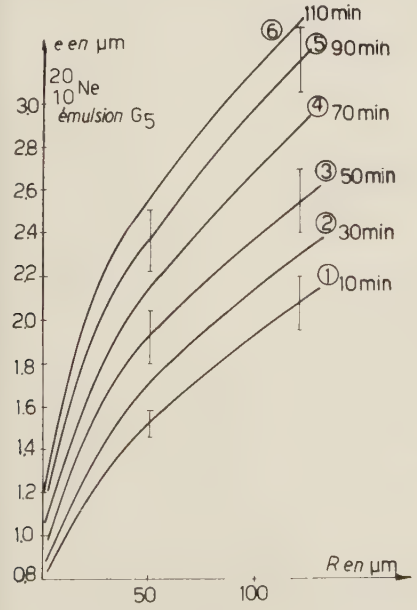

Fig. 3.

2) Fig. 3 – $_{10}$Ne – Développement à l'ID 19 dilution (1:6):

Courbe (1)	10 minutes
Courbe (2)	30 minutes
Courbe (3)	50 minutes
Courbe (4)	70 minutes
Courbe (5)	90 minutes
Courbe (6)	110 minutes

L'examen de ces courbes amène la même remarque que dans le cas du développement à l'amidol, à savoir que l'accroissement d'épaisseur est bien plus important pour les parties épaisses des

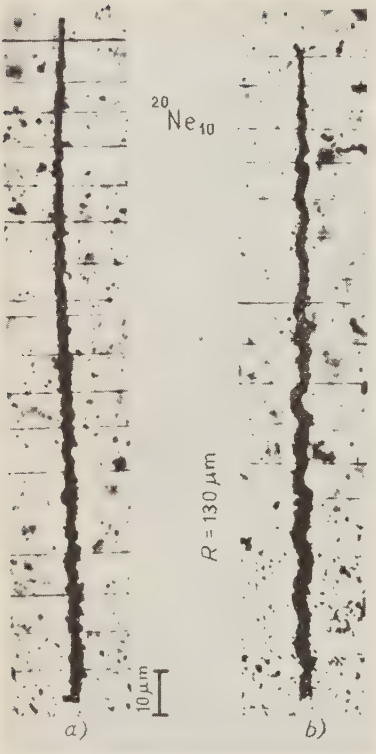

Fig. 4.

traces ou apparaissent les δ les plus énergiques, que pour les parties minces. Nous ne constatons plus de palier dans l'influence du développement. L'accroissement d'épaisseur se poursuit bien au-delà de 80 minutes.

Les valeurs de l'épaisseur des traces, à temps de développement égal, sont supérieures dans le cas du développement à l'ID 19. A partir de 70 minutes de développement à l'ID 19 (Fig. 4*b*), les traces prennent l'aspect en tirebouchon signalé par BARKAS [10]; cet aspect va en s'amplifiant lorsque le temps de développement augmente. Le développement à l'amidol ne fait pas apparaître ce phénomène (Fig. 4*a*, développement amidol 100 minutes), mais les valeurs de l'épaisseur restent toujours inférieures à celles correspondant à 70 minutes de développement dans l'ID 19. Il semble donc s'agir d'un effet de masse d'argent qui doit se faire place dans la gélatine à partir d'une certaine valeur. Nous avions déjà rencontré ce phénomène pour des traces α développées longuement dans un révélateur physique, c'est-à-dire là aussi dans un cas ou le dépôt d'argent était très important.

3) Fig. 5 – $_8O$ – Développement à l'amidol à 18 – 20° :

Courbe (1)	40 minutes
Courbe (2)	80 minutes

Même remarque que pour $_{10}Ne$; l'accroissement d'épaisseur est plus important pour la partie épaisse de la trace.

D'autre part, l'accroissement d'épaisseur est plus important pour $_{10}Ne$ que pour $_8O$ pour des temps de développement comparables. Il ne faut toutefois pas perdre de vue que ces ions sont enregistrés sur des plaques différentes et que ces plaques n'ont pas été traitées simultanément. De petites variations de sensibilité des émulsions et de petites variations de développement peuvent

[10] H. H. HECKMANN, B. L. PERKINS, W. G. SIMON, F. M. SMITH et W. N. BARKAS : *U.C.R.L.* 8763, Berkeley (1959).

exalter ce phénomène, de telle façon qu'il est impossible d'en tirer de loi générale.

L'ensemble de ces courbes tend à montrer que l'accroissement de l'épaisseur moyenne en fonction du temps de développement ne correspond pas à une translation des courbes représentant l'épaisseur en fonction du parcours.

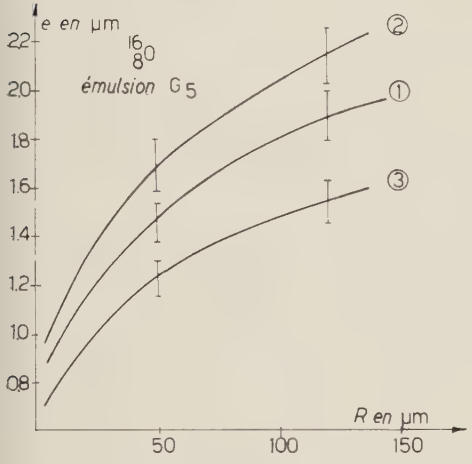

Fig. 5.

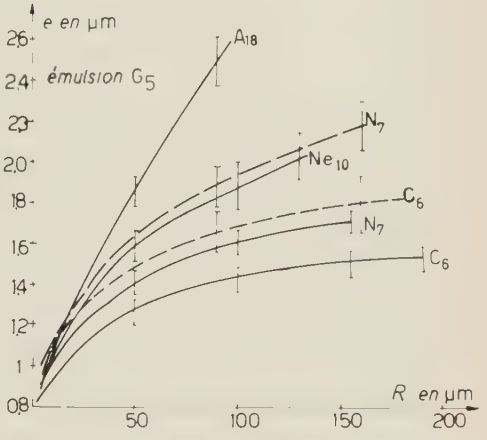

Fig. 6.

Cet accroissement paraît augmenter à mesure que l'on s'éloigne de l'origine ($R = 0$) surtout dans le cas du développement à l'ID 19. La correction de développement ne devrait donc pas se traduire par l'addition ou la soustraction d'un facteur constant tout le long de la courbe, ainsi que l'a proposé Della Corte ([11]).

Cette augmentation de l'accroissement de l'épaisseur, lorsque le parcours résiduel R croît, peut s'expliquer par une cinétique de développement plus lente des grains périphériques de la trace. Ces grains, affectés par les δ les plus énergiques, dont le nombre croit avec R, ont une image latente liée à une perte d'énergie faible, ce qui peut expliquer leur contribution plus tardive à l'épaisseur, comme pour les traces α à la Section précédente.

La Fig. 6 représente en traits pleins, les courbes relatives à $_{18}$A; $_{10}$Ne; $_{7}$N et $_{6}$C trouvés dans une même plaque et en tirets des courbes relatives à $_{7}$N et $_{6}$C, trouvés dans des plaques différentes qui ont été développées de façon plus poussée (ID 19: 45 minutes).

On remarque que l'influence du développement sur l'épaisseur moyenne peut dépasser l'influence du Z. Il est donc primordial de s'en tenir à des traces

([11]) P. G. Bizetti, M. G. Dagliana, M. Della Corte et L. Tocci: *Nuovo Cimento*, **10**, 388 (1958).

développées de façon comparable si l'on veut discriminer les ions lourds par leur épaisseur.

D'autre part, les courbes relative à $_{7}N$ et $_{6}C$ (développement fort) son pratiquement parallèles respectivement à celles du $_{10}Ne$ et à celles de $_{7}N$. Une correction de développement par translation entrainerait une grossière erreur dans ces cas.

Il nous a paru intéressant de trouver un critère permettant de déterminer le degré de développement des plaques, afin de pouvoir comparer des résultats émanant de plaques différentes. L'étude du développement des traces α nous a incité à les utiliser à cette fin. Il est, en effet, très facile d'ajouter des traces α du Po à toutes les plaques avant leur développement sans les détériorer. L'épaisseur de ces traces α, reportée sur la courbe 1, Fig. 1, permet de déterminer le degré de développement de la plaque.

Quelques essais effectués sur nos plaques G-5 ont vérifié cette hypothèse:

Epaisseur des traces α, contenues dans la plaque représentée par la courbe 1 (Fig. 5): $e_{\alpha} = 0.74$ µm. Cette valeur correspond à un développement de 40 minutes à l'amidol (voir Fig. 1); ce qui est conforme à la réalité.

(Fig. 6) courbes A, Ne, N, C, en traits pleins $e_{\wedge} = 0.61$ µm; temps de développement ~ 30 minutes.

b) *Influence du temps de développement des révélateurs superficiels.* Nous avons vu au paragraphe précédent, que les révélateurs superficiels avaient peu d'influence sur l'épaisseur des traces α dans un très grand domaine de temps. Il nous a paru intéressant d'appliquer ces résultats aux ions lourds. La courbe (3), Fig. 5, représente l'épaisseur moyenne de traces d'ion $_{8}O$ enregistrées dans une émulsion G-5 de 50 µm d'épaisseur et développées à l'aide du révélateur au génol-acide ascorbique pendant 25 minutes et 60 minutes.

Les deux courbes coïncident. Nous retrouvons ici un résultat déjà établi pour les α. L'accroissement du temps de développement est sans effet sur l'épaisseur au-delà d'une certaine limite certainement atteinte après 25 minutes de développement.

En valeur absolue, la courbe se situe en-dessous de celles relatives à l'amidol. Sa pente est moins forte.

Ce révélateur favorise la montée du voile par rapport au révélateur classique à l'amidol. Mais l'intérêt de cette méthode réside dans le fait que l'épaisseur moyenne est insensible à une variation du temps de développement. Il faudrait pouvoir l'étendre à un plus grand nombre d'ions différents avant de recommander son emploi.

c) *Le développement physique*, tel que nous l'avons décrit dans une précédente publication ([12]), ne présente que peu d'intérêt pour les ions lourds.

([12]) CH. GEGAUFF et J. P. LONCHAMP: *Wissenschaftliche Photographie, Internationale Konferenz* (Cologne, 1956), p. 322.

Ses propriétés discriminatoires entre α et β, conduisent à un nivellement entre les traces d'ions lourds de Z différents, puisqu'il néglige l'apport dû aux δ qui est le facteur de discrimination entre ces ions. Quelques essais effectués sur des fragments de fission de l'^{235}U nous ont conduits à un nivellement pour les émulsions C-2 et G-5, là ou le développement chimique permettait une discrimination entre le fragment lourd et le fragment léger par la mesure de l'épaisseur moyenne.

4. – Conclusion.

Ce travail démontre l'importance de l'influence du développement sur l'épaisseur des traces d'ions. Toute tentative de discrimination par l'épaisseur doit tenir compte des conditions du développement, ce qui montre la nécessité d'un contrôle de développement qui peut être constitué par la mesure de l'épaisseur des traces α du polonium comme nous l'avons démontré.

Il est impossible d'appliquer une correction simple tenant compte d'une différence de développement puisque cette différence varie d'un bout de la trace à l'autre.

Il reste à confirmer l'intérêt d'un révélateur superficiel pour les traces d'ions lourds qui permettrait peut-être d'éliminer cette influence du développement.

* * *

Ce travail a été exécuté au Laboratoire de Physique Corpusculaire de Strasbourg, grâce à l'appui matériel consenti par le CEA à qui nous exprimons ici même notre vive gratitude. Nous tenons à remercier vivement Monsieur le Professeur P. Cüer pour l'intérêt qu'il a bien voulu témoigner à ce travail. Nous exprimons notre très vive gratitude à Monsieur le Professeur Barkas de l'Université de Berkeley et à ses collaborateurs MM. H. Heckmann et F. Smith qui ont assuré l'irradiation des émulsions au Hilac. Nous remercions Mesdemoiselles Béatrice et Marthe Gerlinger pour leur collaboration technique.

RIASSUNTO (*)

Si studia l'influenza dei diversi rivelatori sulle dimensioni trasversali delle tracce degli ioni $_2He$, $_6C$, $_7N$, $_8O$, $_{10}Ne$ e $_{18}A$ nelle emulsioni ionografiche G-5, C-2 e L-4. La differenziazione delle tracce degli ioni pesanti a mezzo della misura delle loro dimensioni trasversali dipende da questa influenza che è molto forte nel caso dei rivelatori usuali (amidol, ID 19). Si propone un controllo dello sviluppo mediante la misurazione dello spessore delle tracce α. Si dimostra la difficoltà di applicare un fattore di correzione semplice che tenga conto dell'influenza dello sviluppo.

(*) *Traduzione a cura della Redazione.*

IL NUOVO CIMENTO Vol. XVI, N. 3 1° Maggio 1960

Quantum Effect on the Radial Distribution Function of Liquids.

F. P. Ricci

Comitato Nazionale Ricerche Nucleari - Roma

(ricevuto il 1° Febbraio 1960)

Summary. — The quantum effect on the radial distribution function of a liquid has been analyzed by means of the corresponding states principle. Also the best mode has been discussed for describing liquid Helium.

---

1. – Theoretical investigations of the quantum effects in the gas-phase properties give a satisfactory quantitative description of the phenomena. In the liquid phase, however, such refined theoretical results have not yet been obtained; consequently it is necessary to content ourselves with a semi-empirical investigation of the quantum effects in liquids based on the principle of corresponding states in quantum mechanics [1-3]. Along this way many applications concerning the critical constants, density and other equilibrium properties, have been done [1-3]. It is our aim to show in this work the influence of the quantum deviations on the radial distribution function, *i.e.* on the pseudo structure of the liquid.

2. – The radial distribution function [1] of a liquid system can be determined by means of the X-ray or slow neutron diffraction techniques. Even though the results show a general agreement, in this paper we will take into consideration only the results obtained by the neutron diffraction techniques. The main reason for this is that the neutron scattering amplitudes are isotropic

[1] J. de Boer: *Physica*, **14**, 139 (1948).
[2] J. de Boer and B. S. Blaisse: *Physica*, **14**, 149 (1948).
[3] J. de Boer and R. J. Lunbeck: *Physica*, **14**, 520 (1948).
[4] N. S. Gingrich: *Rev. Mod. Phys.*, **15**, 90 (1943).

in contrast with the angularly dependent X-ray amplitudes. This means that the outer-angles' features in the diffraction pattern become more significant for the determination of the structure.

In Fig. 1 we plotted the radial distribution function *vs.* the radial distance both in the reduced form for a classic liquid (Argon); a slightly quan-

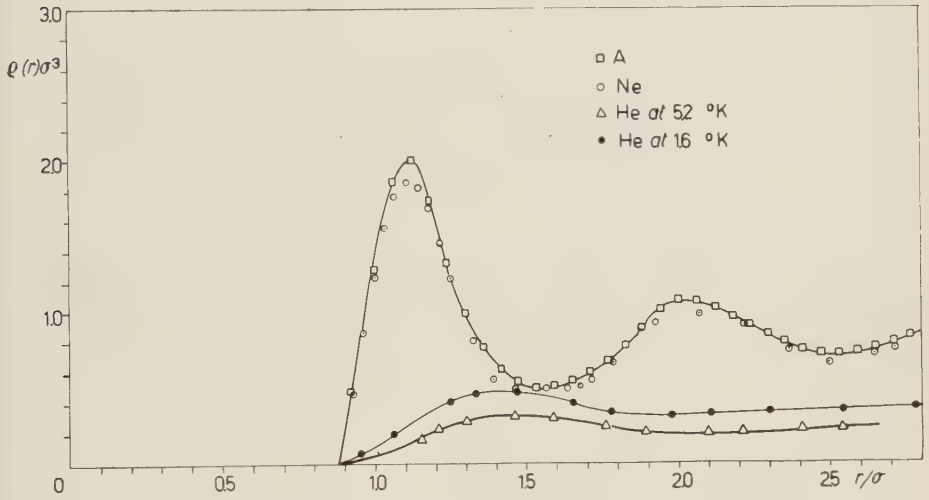

Fig. 1. – Radial distribution function in reduced units. Curves are stopped at $r/\sigma = 2.8$. In fact the radial distribution function loses its characteristics at distances larger than this value. The experimental data are taken from [9-11].

tistic liquid (Neon); a strongly quantistic liquid (Helium). We have the quantity $\varrho^* = \varrho\sigma^3$ on the ordinate axis and $r^* = r/\sigma$ on the abscissa (ϱ is the radial distribution function in atom/Å; r is the radial distance in Å, σ is the parameter of the $(6 \div 12)$ potential $\varphi = 4\varepsilon[(\sigma/r)^{12} - (\sigma/r)^6]$ (*)). We think that the reduced form we have chosen is more useful than the form $\varrho^* = \varrho/\varrho_0$ and $r^* = r/r_{\text{f.n.}}$ previously chosen by other authors [5]. In fact whether ϱ_0 or $r_{\text{f.n.}}$ are generally influenced by the same effects we wish to study (ϱ_0 is the mean atomic density and $r_{\text{f.n.}}$ is the mean radial distance of the first neighbours). If classical mechanics holds, we should have, in force of the corresponding state principle, that only one curve should be valid for all the three liquids, if the experimental measurements are referred to the states with the same reduced parameters.

(*) The values of ε and σ are taken from Table I ref. [1].

[5] J. A. Campbell and J. H. Hildebrand: *Journ. Chem. Phys.*, **11**, 334 (1943).

As far as Argon and Neon are concerned the experimental data are taken at $T^* = kT/\varepsilon \simeq 0.71$ and $p^* = p\sigma^3/\varepsilon \sim 0.003$; in the case of Helium we use the experimental data at 5.2 °K. A measurement at 7.2 °K and at a pressure of 20 cm Hg would be necessary, but this is obviously impossible. In the following analysis we will take into account such a difference, but in first approximation it is possible to consider all of the three liquids as being in corresponding states.

3. – The deviations from the classical curve, *i.e.* the curve of Argon, have to be ascribed to the inadequacy of classical mechanics, and therefore they give a measurement of the quantum effects for the particular liquid.

The Fig. 1 is self-explainatory as regards the importance of quantum effects in Neon and Helium.

These effects are negligible in the first case; in the second case they are so influent that the pseudo structure of the liquid Helium is more similar to that of a dense gas than of a liquid existing in the corresponding classical field.

In a more detailed examination we note that the following quantities are significant:

1) The cut-off point $r_{c.o.}$, of the $\varrho(r)$, which represents the minimum approach distance of two atoms.
2) Number of first neighbours, $n_{f.n.}$.
3) Mean distance of the first neighbours.
4) Width of the shell in which the first neighbours spread $\Delta r_{f.n.} = 2(r_{f.n.} - r_{c.o.})$.

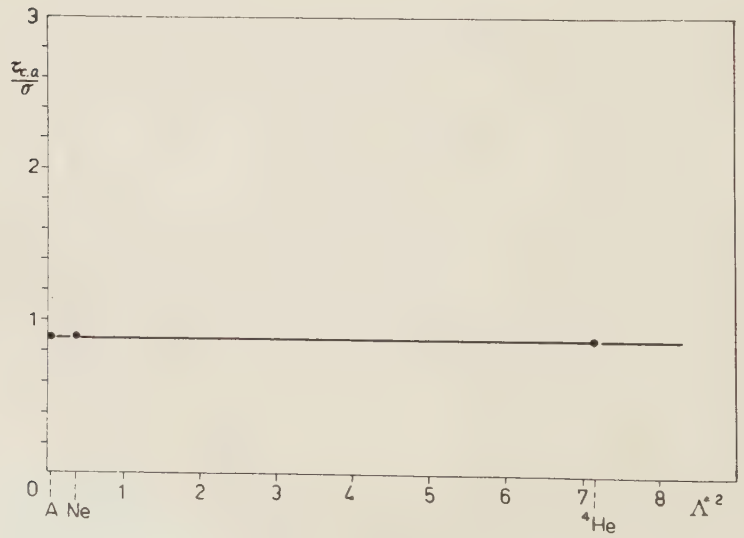

Fig. 2. – $r_{c.o.}/\sigma$ *vs.* Λ^{*2}.

In the diagrams of Figs. 2, 3, 4, 5 these quantities are plotted in reduced form *vs.* the quantum parameter, Λ^*, representing the reduced De Broglie wavelength.

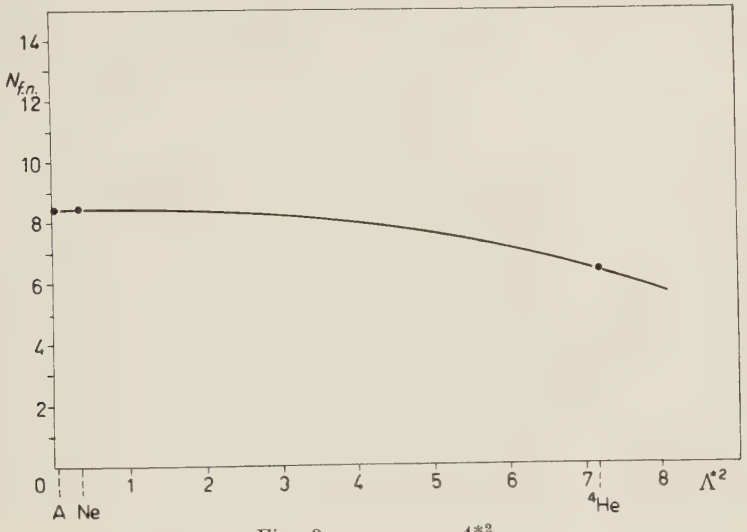

Fig. 3. – $n_{f.n.}$ *vs.* Λ^{*2}.

It appears from these diagrams that it is possible to summarize the quantum effects on the pseudo structure of a liquid as follows:

1) No effects exist on the minimum approach distance of two atoms; it should be possible to say that the repulsive part of the potential field is not considerably influenced.

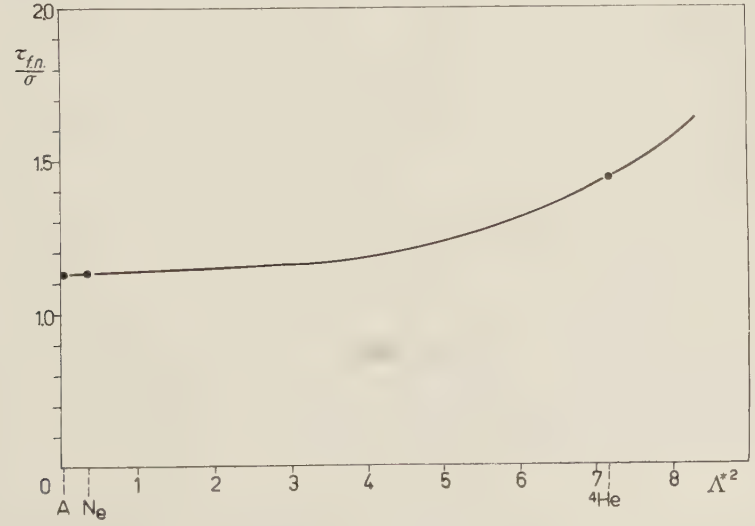

Fig. 4. – $r_{f.n.}/\sigma$ *vs.* Λ^{*2}.

2) A reduction of the number of the first neighbours.

3) An expansion of the first neighbours shell.

4) A very strong broadening of this shell.

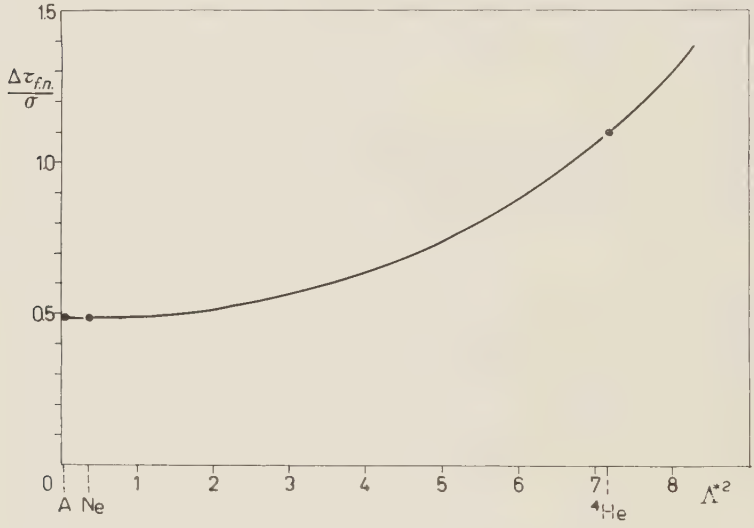

Fig. 5. – $\Delta r_{f.n.}/\sigma$ *vs.* Λ^{*2}.

If we take into account, in the case of Helium, the extrapolated values at $T^* \simeq 0.71$ and $\rho^* \simeq 0.003$, the points 2, 3, 4 would be considerably enhanced. As we want only to investigate in what direction the quantum effects appear, it is not necessary to introduce such extrapolation.

It is important to note that the radial distribution function of liquid Helium at 1.6 °K differs slightly from that at 5.2 °K if both of them are taken in reduced form, as in Fig. 1. The only difference concerns the number of first neighbours, which reaches the value of 8, the same number we have for the corresponding classic liquid. The properties mentioned in points 1, 3, 4 remain unchanged. Therefore, independently of the effective temperature we have a remarkable difference between the pseudo structure of liquid Helium and that of Argon.

We may conclude that the quantum effects appear as a progressive relaxation of the structure. This relaxation is similar to the relaxation we note when a liquid goes into a dense gas ([6]). In this case, however, the minimum approach distance between two atoms gradually decreases, in the case we are dealing with this distance remains constant.

([6]) A. Einstein and N. S. Gingrich: *Phys. Rev.*, **62**, 261 (1942).

Such a conclusion might be foreseen in a qualitative way from the zero point energy, which belongs to the various liquids, and from the dependence of their properties, such as transport properties, upon Λ^*.

However it is very significant that this relaxation derives so clearly from this analysis of the radial distribution functions, which is the most direct measurement of the pseudo structure.

4. – It is also interesting to examine the situation of Helium. Several times it has been discussed [7] about the opportunity of describing the liquid Helium properties starting from the ideal gas or solid state approach. Some experimental data (specific heat, thermal expansivity) seemed to suggest this last approach and much work has been done in this sense. Moreover the experimental measurements of the radial distribution function have always been discussed in terms of more or less complicated lattices [8-11].

On the contrary from our analysis it appears that the approach in the gas sense proposed by F. London and followed by other authors is more suitable, excepting for high values of the pressure. In this case liquid Helium should be more similar to the classic liquid, as from viscosity measurements [12-15].

5. – It is interesting to repeat again that a systematic use of the corresponding state principle allows to obtain an exact picture of the problem and a correct way for analysing the experimental results. It would be useful to have more experimental data, mainly it would be worth-while to know the radial distribution function of liquid ^{3}He in order to study the symmetry effects.

* * *

I wish to thank Prof. Careri for helpful discussions and Dr. Henshaw for sending me the experimental data.

[7] J. de Boer: *Progr. Low Temp. Phys.*, Vol. II, Ch. 1 (1957).
[8] D. G. Hurst and D. G. Henshaw: *Phys. Rev.*, **100**, 994 (1955).
[9] J. Reekie, T. S. Hutchison and C. F. A. Beaumont: *Proc. Phys. Soc.*, A **66**, 409 (1953); J. Reekie, and T. S. Hutchison: *Phys. Rev.*, **92**, 827 (1953); C. F. A. Beaumont and J. Reekie: *Proc. Roy. Soc.*, A **228**, 363 (1955).
[10] W. L. Gordon, C. H. Shaw and J. G. Daunt: *Phys. Rev.*, **96**, 1444 (1937).
[11] W. H. Keesom and K. W. Taconis: *Physica*, **4**, 28, 256 (1937); **5**, 270 (1938).
[12] F. London: *Superfluids*, Vol. II.
[13] D. G. Henshaw: *Phys. Rev.*, **105**, 976 (1957).
[14] D. G. Henshaw: *Phys. Rev.*, **111**, 1470 (1958).
[15] H. H. Tjekstra: *Physica*, **18**, 853 (1952).

Note added in proof.

Professor GINGRICH informed me that at the Argonne National Laboratory, Glen Clayton and Le Roy Heaton have just finished the measurements of the radial distribution function of liquid Kripton at various temperatures by means of the neutron diffraction. If we consider the experimental data at the temperatures and at the pressures of Fig. 1, they fit well the curve of Argon and Neon, as it was possible to foresee by means of the corresponding state principle. The data agree also with the value of A^* for Kripton.

RIASSUNTO

Mediante il teorema degli stati corrispondenti viene analizzato l'effetto quantistico sulla funzione radiale di distribuzione di un liquido. Si discute altresì il migliore modello da usare per descrivere l'Elio liquido.

IL NUOVO CIMENTO Vol. XVI, N. 3 1° Maggio 1960

A Test of Approximation Methods in Potential Scattering (*).

J. D. Bjorken and A. Goldberg

Institute of Theoretical Physics, Department of Physics
Stanford University - Stanford, Cal.

(ricevuto l'8 Febbraio 1960)

Summary. — Various approximation procedures fashionable in field theory for computing scattering amplitudes are tested on a soluble problem in potential theory — the s-wave scattering by an exponential potential. The methods include: 1) the Fredholm, or determinantal, expansion; 2) the Chew-Mandelstam procedure of constructing the scattering amplitude T_0 from analyticity properties and unitarity; 3) expansion of T_0 in powers of the potential strength λ (Born approximation); 4) expansion of tg δ_0 in powers of λ, and 5) expansion of ctg δ_0 in powers of λ. Each is carried out in first and second order of approximation and compared with the exact result. The results are displayed in effective-range plots of k ctg δ_0 *vs* energy. In addition, the energies of bound states as predicted by the approximations are compared with the exact result. Approximations 1), 2), and 5) in second order are comparable in accuracy, agree reasonably well with the exact result, and are appreciably better than 3) and 4). The binding energy of the first bound state is predicted well by method 2) in second order, and at best qualitatively by the other methods. All methods except 1) predict existence of bound states for repulsive potentials. In second order method 1) predicts no bound state for any value of λ.

1. – Introduction.

Quantum field theory has been plagued with mathematical difficulties sufficiently profound that no exact solutions to scattering problems have been obtained, and in the domain of strong coupling physics no proved reliable

(*) Supported in part by the United States Air Force through the Air Force Office of Scientific Research.

approximation scheme has been found. Various approximation schemes have been used, however, with various degrees of success, and it is the purpose of this paper to test some of these schemes on a soluble model in potential scattering. In particular, a new approximation procedure has been proposed by CHEW and MANDELSTAM [1], based upon a study of the analyticity properties of the scattering amplitude. It has been shown by several workers [2-4] that the analyticity properties in field theory are quite similar to those found in potential scattering. It is plausible, then, that approximation schemes which for some reason are valid in field theory should work in potential scattering, where the situation is simpler.

In particular we consider the s-wave amplitude

$$T_0 = \frac{1}{k} \exp [i\delta_0] \sin \delta_0 = \frac{1}{k \operatorname{ctg} \delta_0 - ik}, \tag{1}$$

for scattering of a particle of momentum k by an exponential potential. In this case the exact solution is known [5]. With this we compare the solutions obtained by (1) the FREDHOLM, or determinantal, expansion [6,7], 2) the expansion—considered by WILSON [8]—of $1/T_0$ in powers of the potential strength λ, 3) expansion of $\operatorname{tg} \delta_0$ in powers of λ, 4) Born approximation, and 5) the approximation scheme of CHEW and MANDELSTAM [1], which is described below. Our results are displayed in effective-range plots of $k \operatorname{ctg} \delta_0$ *versus* the energy. In addition, energies of bound states may also be obtained in these cases; they are also discussed.

2. – The approximation methods for the phase shift.

For an exponential potential of the form

$$V(r) = \lambda\mu^2 \exp [-\mu r], \tag{2}$$

[1] G. F. CHEW and S. MANDELSTAM: *University of California Report*, no.UCRL-8728 (unpublished).

[2] J. BOWCOCK and A. MARTIN: *Nuovo Cimento*, **14**, 516 (1959); J. BOWCOCK and J. D. WALECKA: *Nucl. Phys.*, **12**, 371 (1959).

[3] A. MARTIN: *Nuovo Cimento*, **14**, 403 (1959).

[4] R. BLANKENBECLER, J. GOLDBERGER, N. N. KHURI and S. B. TREIMAN: preprint. This paper contains many other references.

[5] H. A. BETHE and R. BACHER: *Rev. Mod. Phys.*, **8**, 111 (1936).

[6] R. JOST and A. PAIS: *Phys. Rev.*, **82**, 840 (1951).

[7] M. BAKER: *Ann. Phys.*, **4**, 271 (1958).

[8] K. WILSON: private communication.

the s-wave Schrödinger equation becomes

$$\left\{\frac{\mathrm{d}^2}{\mathrm{d}r^2} + \varepsilon - \lambda\mu^2 \exp[-\mu r]\right\} u(r) = 0\,, \tag{3}$$

where $u(r) = r\psi(r)$, $1/\mu$ measures the range of the potential, and $\varepsilon = \mu^2 s = -\mu^2 k^2$ is the energy, in the natural units $\hbar = 2m = 1$. λ is a dimensionless parameter which measures the strength of the potential, and m is the reduced mass of the scattering system. The solution of (3) is well known ([5]), and the scattering phase shift is expressible in terms of Bessel functions of imaginary argument and order. One finds

$$k \operatorname{ctg} \delta_0 = -\frac{1 + \sum_{n=1}^{\infty} \frac{\lambda^n}{n!} \sum_{m=1}^{n} \frac{(-1)^{m+1}}{(n-m)!\,(m-1)!} \frac{m}{m^2 + 4s}}{2 \sum_{n=1}^{\infty} \frac{\lambda^n}{n!} \sum_{m=1}^{n} \frac{(-1)^{m+1}}{(n-m)!\,(m-1)!} \frac{1}{m^2 + 4s}} = k \frac{\operatorname{Re} D}{\operatorname{Im} D}\,, \tag{4}$$

where

$$D = \frac{J_{2ik}(-2i\sqrt{\lambda})\,(-i\sqrt{\lambda})^{-2ik}}{\Gamma(1 - 2ik)}\,. \tag{5}$$

Having the exact expression, we may follow the rather unusual procedure of constructing from it the approximate solutions.

1) The first of the approximations is the Fredholm, or determinantal, method. It consists in expressing T_0 as the ratio of two power series in λ, each of which converges for all coupling strengths. Jost and Pais ([6]) have shown that the D which appears in (4) and (5) is identical with the Fredholm determinant. Hence through second order the Fredholm method yields

$$k \operatorname{ctg} \delta_0 = -\frac{1 + \frac{\lambda}{1+4s} + \frac{\lambda^2}{2}\left(\frac{1}{1+4s} - \frac{1}{2(1+s)}\right)}{\frac{2\lambda}{1+4s} + \frac{3\lambda^2}{4(1+4s)(1+s)}}\,. \tag{6}$$

2) The second approximation procedure is that proposed by Wilson, expanding $k \operatorname{ctg} \delta_0$ in a power series in λ. Through second order the Wilson prescription yields

$$k \operatorname{ctg} \delta_0 = -\left\{\frac{1+4s}{2\lambda} + \frac{1}{2} - \frac{3}{16}\frac{1+4s}{1+s}\right\}. \tag{7}$$

3) We next expand $\operatorname{tg} \delta_0$ in a power series in λ. To lowest order this is equivalent to Wilson's approximation. To second order we obtain from (4)

$$k \operatorname{ctg} \delta_0 = -\frac{1+4s}{2\lambda}\left[1 - \frac{\lambda}{1+4s} + \frac{3}{8}\frac{\lambda}{1+s}\right]^{-1}. \tag{8}$$

4) We turn to the celebrated Born approximation. This approximation is not unitary, and some prescription must be given to put it into the form of an effective range formula. A reasonable choice is to express

$$|T_0^{(1)} + T_0^{(2)}|^2 = \frac{1}{(k \operatorname{ctg} \delta_0)^2 + k^2} . \tag{9}$$

Through second order this procedure yields

$$[k \operatorname{ctg} \delta_0]^2 = \left\{ \left[\frac{2\lambda}{1+4s} + \frac{\lambda^2(s-\frac{1}{4})}{(1+s)(1+4s)^2} \right]^2 + \frac{16\lambda^4 s}{(1+4s)^4} \right\}^{-1} - s . \tag{10}$$

For $|\lambda| > 2$, this can lead to imaginary values of $k \operatorname{ctg} \delta_0$, which implies that $|T_0|$ has exceeded the limit allowed by unitarity.

5) Finally, we consider the Chew-Mandelstam method [1] of constructing the scattering amplitude, utilizing the analyticity properties of T_0, the energy s being extended into the complex plane. These analyticity properties have been described quite completely [9], and for our case the singularities of T_0 in the complex s-plane consist of a branch cut extending along the positive real axis and simple poles at the points

$$s_n = -\frac{n^2}{4} .$$

The n-th pole is contributed completely by n-th order Born approximation, and has residue

$$R_n = \frac{1}{2} \frac{(-\lambda)^n}{n!(n-1)!} . \tag{11}$$

The approximation consists of retaining only the first few singularities on the left, with the residues (in potential scattering) computed by Born approximation. Such an approximation can be expected to be best for small s. At low energy only the near poles are seen and they dominate the behavior of T_0. At higher energies the distant singularities become relatively more important.

The mathematical procedure necessary to construct a solution T_0 with a finite number of poles of prescribed residues and which satisfies unitarity on the positive real s-axis is described in references [1] and [4], and in the Ap-

[9] *E.g.* references [2], [3] and [4].

pendix. The result upon retaining only the first pole is

$$k \operatorname{ctg} \delta_0 = -\frac{(1+4s)(1-\lambda/2)+\lambda}{2\lambda}. \tag{12}$$

When the second pole is included, we obtain

$$k \operatorname{ctg} \delta_0 = \frac{1-\frac{\lambda}{2}+\frac{\lambda^2}{8}-\frac{\lambda^3}{144}+\left(1-\frac{\lambda^2}{24}\right)\frac{\lambda}{1+4s}-\left(1-\frac{\lambda}{6}\right)\frac{\lambda^2}{4(1+s)}}{-\left(1-\frac{\lambda^2}{24}\right)\frac{2\lambda}{1+4s}+\left(1-\frac{\lambda}{6}\right)\frac{\lambda^2}{4(1+s)}}. \tag{13}$$

3. – Bound states.

The existence of bound states is determined by any extra poles in the T-matrix for $s<0$. Such extra singularities occur at the energies of the bound states. It is only necessary to continue T_0 analytically to negative energies by the transformation $s=-\varkappa^2$, since T_0 is defined as the analytic function *above* the cut on the right,

$$T_0 = \frac{1}{k \operatorname{ctg} \delta_0 - ik} = \frac{1}{k \operatorname{ctg} \delta_0 + \varkappa}, \tag{14}$$

and the binding energies are determined by the solutions of the equation

$$k \operatorname{ctg} \delta_0 |_{s=-\varkappa^2} + \varkappa = 0. \tag{15}$$

Thus the expressions (5) through (13) for $k \operatorname{ctg} \delta_0$ may be used to solve for the binding energy $\varkappa^2$ as a function of λ. The exact solution yields the result

$$J_{2\varkappa}(2\sqrt{-\lambda}) = 0. \tag{16}$$

4. – Conclusions.

Our results are plotted in Figs. 1 through 9 for several values of λ. In most cases they speak for themselves. It should be kept in mind that a coupling strength of $\lambda=-1.5$ is sufficient to produce a bound state and that

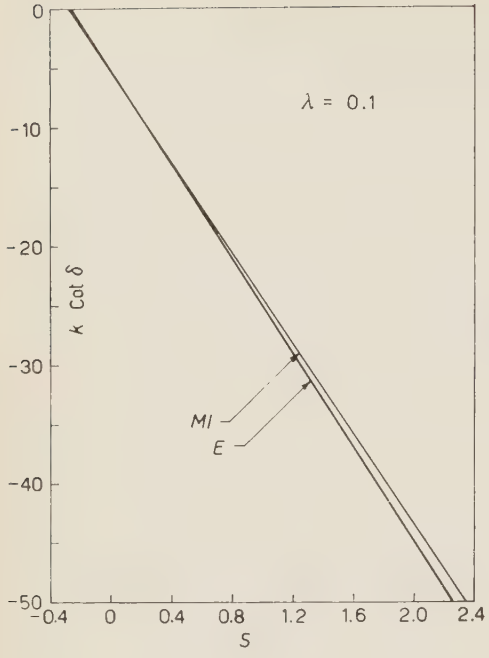

Fig. 1. – Effective range plot of k ctg δ_0 *vs* the energy s. All methods except $M1$ coincide with E. *Key*: E, exact; $M1$, first order Mandelstam; $D1$, first order determinantal (Fredholm); $T1$, first order expansion of tg δ_0 in powers of λ; $B1$, first order Born approximation; $W2$, second order expansion of ctg δ_0 in powers of λ; $D2 \equiv D11$, second order determinantal, etc. Positive λ implies a repulsive potential. The first bound state occurs for $\lambda = -1.5$.

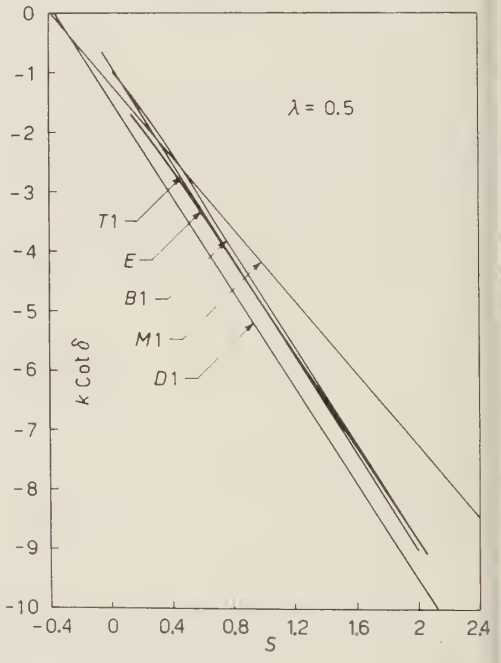

Fig. 2. – Effective range plot of k ctg δ_0 *vs*. the energy s. For the key, see the caption of Fig. 1.

the criterion for the validity of Born approximation is $|\lambda| \ll \sqrt{s}$. It should also be noted that the exponential potential is « smooth » (smoother than a Yukawa potential, for example), and that the scattering at high energy is small. Thus the various approximations probably converge better than for more singular (*e.g.* Yukawa) potentials. However, what we are primarily interested in is the relative merits of the approximations.

We see that the second order Chew-Mandelstam, determinantal (Fredholm), and Wilson approximations yield answers comparable in accuracy. The Chew-Mandelstam approximation appears to work quite well within its domain of applicability, but at least in first order fails rather badly when extended beyond this region. For instance, for $\lambda = 0.1$, only the first order Chew-Mandelstam answer differs appreciably from the exact result. It is to be emphasized that the Mandelstam method does not work for strong coupling, since the

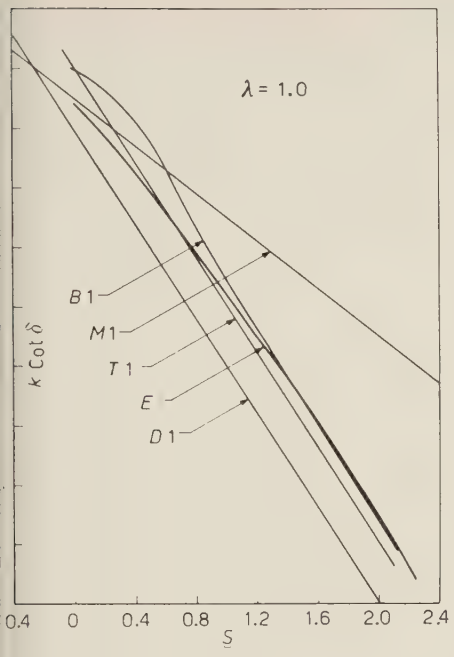

Fig. 3. – Effective range plot of k ctg δ_0 *vs.* the energy s. For the key, see the caption of Fig. 1.

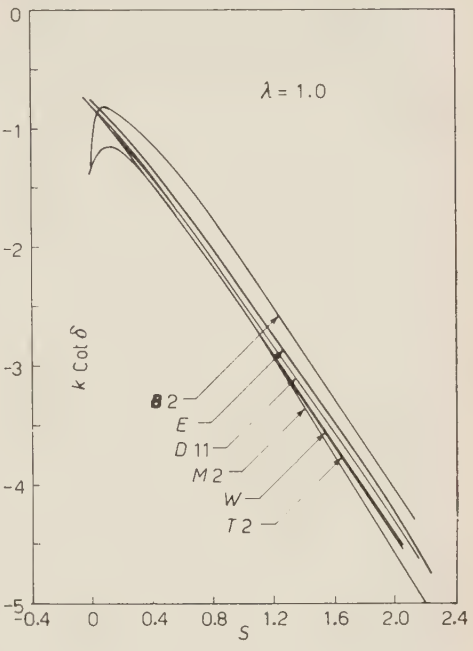

Fig. 4. – Effective range plot of k ctg δ_0 *vs.* the energy s. For the key, see the caption of Fig. 1.

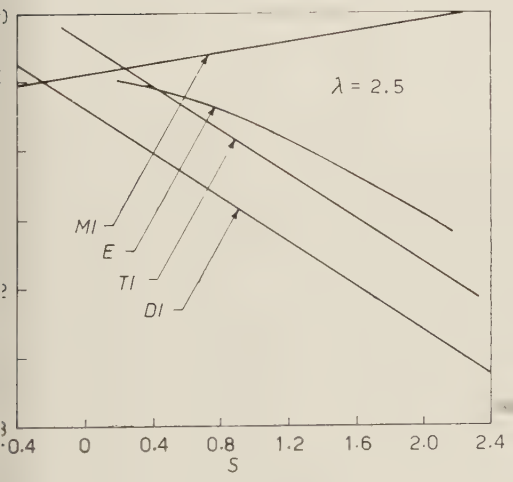

Fig. 5. – Effective range plot of k ctg δ_0 *vs.* the energy s. For the key, see the caption of Fig. 1.

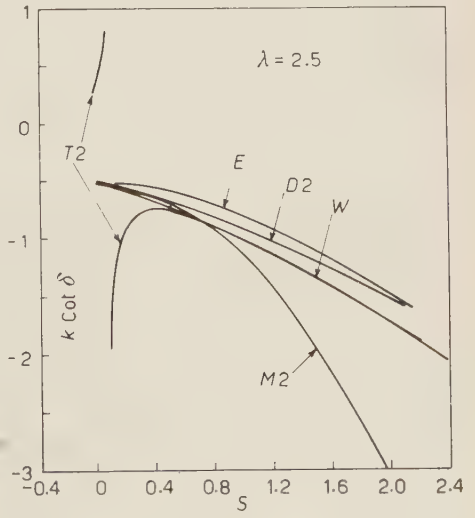

Fig. 6. – Effective range plot of k ctg δ_0 *vs.* the energy s. For the key, see the caption of Fig. 1.

residues of the neglected poles are $\sim (-\lambda)^n/n!(n-1)!$ [10]. This feature is true in general in potential scattering; the contribution to T_0 from the n-th singularity on the left is proportional to λ^n [11]. Again, the fact that $V(r)$ is

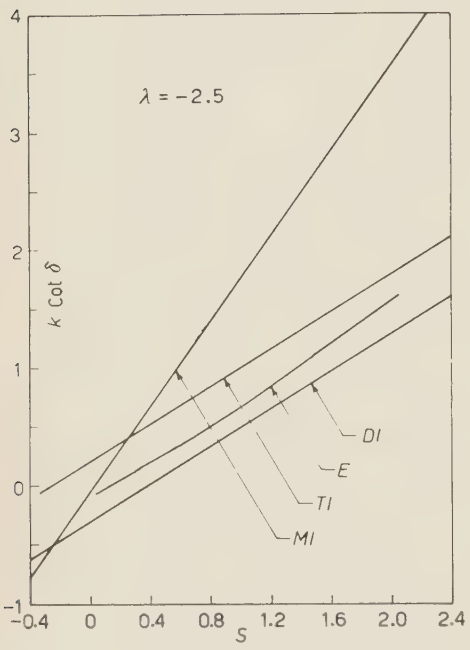

Fig. 7. – Effective range plot of k ctg δ_0 *vs.* the energy s. For the key, see the caption of Fig. 1.

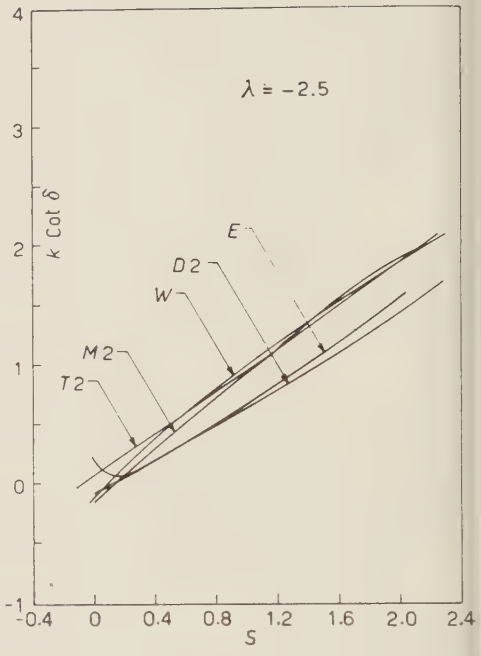

Fig. 8. – Effective range plot of k ctg δ_0 *vs.* the energy s. For the key, see the caption of Fig. 1.

« smooth » manifests itself in the factor $1/n!(n-1)!$ in the residues of the poles. It may be argued that this rapid convergence optimizes the chance of success of the Chew-Mandelstam procedure.

The Chew-Mandelstam method appears to work very well in predicting the energies of bound states; in contrast, the determinantal method in second order predicts no bound state whatsoever. Most of the approximations—with the exception of the determinantal—predict a « ghost state », *i.e.*, a bound state for strong repulsive potentials. This unphysical behavior serves as an

[10] This is also noted in reference [4].
[11] See, *e.g.*, BOWCOCK and WALECKA [2].

upper limit for the validity of the approximation procedure. For $\lambda \geq 4$ we can expect the second order Chew-Mandelstam result to break down badly, since the «ghost state» will produce non-existent resonances which can appear even at zero energy.

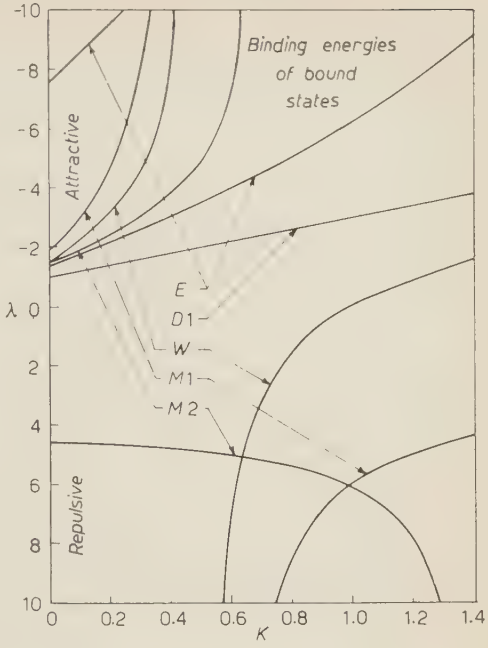

Fig. 9. – Energies of bound states, expressed in terms of coupling parameter λ *vs.* $\varkappa \equiv \sqrt{2m\varepsilon_B}$, with ε_B the binding energy. For the key, see the caption of Fig. 1.

* * *

We wish to thank Dr. Jean Pierre Lascoux for suggesting this problem and Dr. J. D. Walecka, F. Hadjioannou and Professors F. Zachariasen and M. Baker for helpful comments. We thank Professor L. I. Schiff and Professor S. D. Drell for reading the manuscript.

Appendix

The Chew-Mandelstam approximation.

The analyticity properties of T_0 may be inferred from the exact solution. The n-th order Chew-Mandelstam approximation retains the first n poles on the negative axis; their residues are given by (11). The method of construction assumes

$$T_0(s) = N(s)/D(s)\,,$$

where N is analytic except for poles on the left, and vanishes at $s=\infty$, and $D(s)$ is analytic except for a cut on the right and approaches unity as $s \to -\infty$. Hence

$$N(s) = \sum_{m=1}^{n} \frac{\alpha_m}{s + m^2/4}\,, \tag{17}$$

and thus

$$\alpha_m = \frac{1}{2}\,\frac{(-\lambda)^m}{m!(m-1)!}\,D\left(-\frac{m^2}{4}\right). \tag{18}$$

Unitarity requires that for $s > 0$

$$\text{Im } T_0 = k|T_0|^2 = k\frac{|N|^2}{|D|^2} = -\frac{N}{|D|^2}\,\text{Im } D\,. \tag{19}$$

Hence

$$\text{Im } D(s) = -kN(s)\,, \qquad s > 0\,. \tag{20}$$

We write a no-subtraction dispersion relation for $D(s)$ in the form

$$D(s) = 1 + \frac{1}{\pi}\int_0^\infty \frac{\text{Im } D(s')}{s' - s}\,\mathrm{d}s' = 1 - \frac{1}{\pi}\int_0^\infty \frac{N(s')\sqrt{s'}}{s' - s}\,\mathrm{d}s'. \tag{21}$$

Using the spectral representation (17) for N and carrying out the integral, we obtain

$$D(s) = 1 - \sum_{r=1}^{n} r\frac{2\alpha_r}{r + 2\sqrt{-s}}\,, \qquad s < 0\,. \tag{22}$$

Substitution of (22) into (18) yields a set of n linear equations for the α_m:

$$\alpha_m = \frac{1}{2}\frac{(-\lambda)^m}{m!\,(m-1)!}\left[1 - \sum_{r=1}^{n}\frac{2\alpha_r}{r+m}\right]. \tag{23}$$

Solution of these equations for $n=1$ and $n=2$ leads to eqs. (12) and (13) for $k\,\text{ctg}\,\delta_0$.

RIASSUNTO (*)

Si verificano, in un problema risolvibile della teoria del potenziale — lo scattering dell'onda s da parte di un potenziale esponenziale , vari procedimenti di approssimazione applicabili nella teoria dei campi per il calcolo delle ampiezze di scattering. I metodi comprendono: 1) lo sviluppo di Fredholm, o in determinanti; 2) il procedimento di Chew-Mandelstam di costruzione dell'ampiezza T_0 di scattering dalle proprietà di analiticità e di unitarietà; 3) sviluppo di T_0 in potenze dell'intensità di potenziale λ (approssimazione di Born); 4) sviluppo di $\text{tg}\,\delta_0$ in potenze di λ, e 5) lo sviluppo di $\text{ctg}\,\delta_0$ in potenze di λ. Con ogni metodo si sviluppano i calcoli sino al primo ed al secondo ordine di approssimazione ed i risultati si confrontano con quelli esatti. I risultati vengono esposti in diagrammi nell'intervallo effettivo di $k\,\text{ctg}\,\delta_0$ rispetto all'energia. In aggiunta, le energie degli stati legati quali vengono predette dai metodi di approssimazione vengono confrontate ai risultati esatti. Le approssimazioni 1), 2) e 5) nel secondo ordine sono di precisione comparabile, si accordano ragionevolmente con i risultati esatti, e sono apprezzabilmente migliori di 3) e 4). L'energia di legame del primo stato legato viene predetto bene dal metodo 2) nel secondo ordine, e quantitativamente meglio dagli altri metodi. Tutti i metodi eccettuato 1) predicono l'esistenza di stati legati per i potenziali repulsivi. Al secondo ordine il metodo 1) non predice alcuno stato legato per nessun valore di λ.

(*) *Traduzione a cura della Redazione.*

IL NUOVO CIMENTO Vol. XVI, N. 3 1° Maggio 1960

The Inelastic Scattering of Elementary Particles - II.

G. Feldman (*), P. T. Matthews and A. Salam

Imperial College - London

(ricevuto il 15 Febbraio 1960)

Summary. — An approximate scheme for calculating the inelastic scattering of elementary particles is proposed. The scheme fully incorporates the requirements of unitarity and partially includes causality. When applied to the simple problems of π-p and π-π scattering it reproduces very simply some well known results.

1. – Introduction.

In a previous paper (1) it has been shown how the requirements of unitarity in many channel scattering may be very simply incorporated in the inverse T-matrix. In this paper we consider the analytic properties of this matrix, when only two particle channels are included. We conjecture that in this case the matrix elements of T^{-1} for particular energy and angular momentum states satisfy dispersion relations, which depend on Born approximation and discontinuities on « left » and « right hand » cuts. The integral over the rigth hand cut is completely determined by unitarity.

If the approximation is made of neglecting the left hand cuts, an explicit solution is obtained, which depends only on a limited number of renormalized coupling constants. When applied to π-p and π-π scattering the method very simply reproduces the essential features of the approximate solutions due to Chew and Low (2) and Chew and Mandelstam (3). This approx-

(*) On leave of absence from The Johns Hopkins University, Baltimore, Md.

(1) P. T. Matthews and A. Salam: *Nuovo Cimento*, **13**, 381 (1959), referred to as (I).

(2) F. Low and G. F. Chew: *Phys. Rev.*, **101**, 1570 (1956).

(3) G. F. Chew and S. Mandelstam: *Phys. Rev.* (to be published).

imation has been developed with a view to expressing all the s-wave data on K-$\mathcal{N}$ and $\overline{\mathrm{K}}$-$\mathcal{N}$ scattering in terms of the four coupling constants $g_{\mathrm{K}\Lambda}$, $g_{\mathrm{K}\Sigma}$, $g_{\pi\Lambda}$, $g_{\pi\Sigma}$. This will be discussed in detail in a later paper.

2. – Unitarity.

In (I) the unitarity condition was given non-covariantly for s-wave scattering only. We now generalize the result. We define a T matrix in terms of the S-matrix by the relation

$$S = I + iT . \tag{2.1}$$

From the unitarity of S, it follows immediately that

$$T - T^{\dagger} = iTT^{\dagger} . \tag{2.2}$$

Multiplying left and right by T^{-1} and $(T^{\dagger})^{-1}$ respectively gives

$$\begin{aligned} 2\,\mathrm{Im}\,T^{-1} &= -1 \\ &= -\sum_{n} |n\rangle\langle n|, \end{aligned} \tag{2.3}$$

when $|n\rangle$ is a complete set of states. Now if P_{μ} is the energy-momentum operator and matrix elements of T^{-1} are taken in the space of this operator (in which T^{-1} is diagonal)

$$\langle p\,|\,T^{-1}\,|\,p'\rangle \equiv (2\pi)^4 \big(\delta(p - p')T_{p}^{-1} \tag{2.4}$$

and

$$\langle p\,|\,n\rangle = (2\boldsymbol{v})^4\,\delta(p - p_n) . \tag{2.5}$$

Thus, from (2.3)

$$2\,\mathrm{Im}\,T_{p}^{-1} = -\sum_{n} |n\rangle(2\pi)^4\,\delta(p - p_n)\langle n| . \tag{2.6}$$

For further considerations we work in the barycentric system for which

$$\boldsymbol{p} = 0 , \qquad p_0 = E .$$

The states $|n\rangle$ are defined as eigenstates of P_{μ}, and of some conserved operators C, which include the angular momentum J, and some other operators α, which, with P_{μ} and C, make up a complete commuting set. The

matrix T^{-1} is diagonal in the variables C, so we may define

$$T_{c'}^{-1}\delta_{c'c''} \equiv \langle c' | T_p^{-1} | c'' \rangle . \tag{2.7}$$

Then

$$2 \operatorname{Im} T_c^{-1} = (2\pi)^4 \sum_\alpha |\alpha(c')\rangle \, \delta(p - p_n) \langle \alpha(c') | , \tag{2.8}$$

where the summation is over a set of states belonging to the eigenvalues C'. Thus T_c^{-1} is a matrix in the space of the operators α, only. If states with more than two particles are involved in the summation the space α is still infinite-dimensional and the relation between T_c^{-1} and T_c is an integral equation of the first kind. However if the summation is restricted to two particle states, either exactly or as an approximation, the space α is finite-dimensional and simply specifies the nature of the particles in the channel. The matrix T is related to T^{-1} by a straightforward inversion of the matrix in channel space. To obtain T_c^{-1} from T_p^{-1}, the integration over the kinematic factors in any particular channel is,

$$\sum_{\text{spin}} \langle J | \boldsymbol{k}_1, \boldsymbol{k}_2, \text{spin} \rangle \frac{\mathrm{d}^4 k_1}{(2\pi)^3} \frac{\mathrm{d}^4 k_2}{(2\pi)^3} \theta(k_{10}) \theta(k_{20}) \delta(k_1^2 - m_1^2) \delta(k_2^2 - m_2^2) \cdot$$
$$\cdot (2\pi)^4 \delta(k_1 + k_2 - E) \langle \boldsymbol{k}_1, \boldsymbol{k}_2, \text{spin} | J \rangle = \frac{\eta_\alpha k_\alpha}{(2\pi)^2 E} \theta(E - E_\alpha) , \tag{2.9}$$

where: E_α is the threshold energy for the channel,

$$\eta_\alpha = \tfrac{1}{4} \qquad \text{for 2 boson states},$$
$$= \frac{m}{2} f \qquad \text{for 1 boson, 1 fermion states},$$
$$= m_1 m_2 \qquad \text{for 2 fermion states}.$$

k_α is the centre of mass momentum and m is the fermion mass. If we rename T_c by T_J, we have finally

$$\operatorname{Im} T_J^{-1} = \sum_\alpha |\alpha \frac{\eta_\alpha k_\alpha}{(2\pi)^2 E} \theta(E - E_\alpha) \langle \alpha | . \tag{2.10}$$

3. – Dispersion relations for T^{-1}.

For two-particle channels the Mandelstam conjecture leads to the conclusion [3] that $T_J(E)$ are themselves boundary values of analytic functions so

that dispersion relations of the following form can be written

$$\text{Re } T_J(S) = B_J(S) + \frac{1}{\pi}\int_{C_R, C_L} \frac{\text{Im } T_J(S')}{S' - S}\, \mathrm{d}'S, \tag{3.1}$$

where $S = E^2$ and $B_J(S)$ is Born approximation.

Consider first the case where there is only one channel, so that

$$T_J^{-1}(S) = (T_J(S))^{-1}, \tag{3.2}$$

and suppose that at some point S_B

$$B_J(S_B) = \infty . \tag{3.3}$$

We then conjecture that T^{-1} is also an analytic function with singularities

i) along the same cuts, C_R, C_L as T_J;

ii) corresponding to zeros of T_J, (which we ignore), and

iii) due to poles and branch points arising from $B(S)$.

We suppose further that $T_J(S)$ is equal to $B_J(S)$ whenever the latter is infinite. This leads to the equation

$$T_J^{-1} B_J(S) = 1 + \frac{S - S_B}{\pi}\int_{C_L, C_R} \frac{\text{Im}\,\{T_J^{-1} B_J(S')\}}{(S' - S + i\varepsilon)(S' - S_B)}\, \mathrm{d}S'. \tag{3.4}$$

Note that $B_J(S)$ is real in the physical region, so that this equation ensures that the imaginary part of T_J^{-1} is just as required by unitarity. Further the integral over the right hand cut is completely determined by (2.10) since Im $T^{-1}(S)$ involves a factor $\theta(E - E_{\text{th}})$ where E_{th} is the threshold energy, there is never any « unphysical » region over the right hand cut.

If Born approximation is zero or a constant we may express the amplitude in terms of its value at some unphysical point, E_0, where the amplitude is purely real:

$$T(S_0) = \lambda .$$

(It may be possible to interpret λ as a renormalized coupling constant associated with the process). Then the dispersion relation for T^{-1} becomes

$$\lambda T_J^{-1}(S) = 1 + \frac{S - S_0}{\pi}\int \frac{\text{Im}\,\{\lambda T_J^{-1}(S')\}}{(S' - S - i\varepsilon)(S' - S_0)}\, \mathrm{d}s'. \tag{3.5}$$

If Born approximation does not become infinite at any finite point we may assume that a no-subtraction relation holds for T_J and so $T_J \to B_J$ as $S \to \infty$ thus we write

$$T_J^{-1}(S)\, B_J(S) = 1 + \frac{1}{\pi}\int \frac{\mathrm{Im}\,\{T_J^{-1}\, B_J(S')\}}{S' - S - i\varepsilon}\, \mathrm{d}S', \tag{3.6}$$

and proceed as before.

We now proceed to the generalization of the method to multi-channel systems. We require the following lemma.

Lemma. If an element $B_{ik}(S)$ of a matrix is infinite at S_{ik},

$$B_{ik}(S_{ik}) = \infty\,, \tag{3.7}$$

then

$$B_{ik}^{-1}(S) = 0$$

for S_{lm} where either

$$l = i\,, \qquad m = 1, 2, \ldots, n$$

or

$$m = k\,, \qquad l = 1, 2, \ldots, n\,.$$

Proof. Let $\mathscr{B}_{ik}$ be the minor of B_{ik}. Then

$$B_{ik}^{-1} = \frac{\mathscr{B}_{ik}}{B_{i1}\mathscr{B}_{i1} + B_{i2}\mathscr{B}_{i2} + \ldots + B_{in}\mathscr{B}_{in}}\,. \tag{3.8}$$

Now $B_{i1}, B_{i2}, \ldots, B_{in}$ are not contained in $\mathscr{B}_{ik}$ so that if any of these numbers is infinite at a particular energy, B_{ik}^{-1} is zero at this energy. A similar argument applies if the determinant is expanded along the k-th column.

Using this Lemma the generalization of (3.4) is immediate. Define

$$F_{if}(S) = \prod_{r=1}^{n}\prod_{s=1}^{n}(S - S_{ir})(S - S_{sf})\,, \tag{3.9}$$

then

$$[T_J^{-1}\, B(S)]_{if} = \delta_{if} + F_{if}(S)\int_{c_L, c_R} \frac{\mathrm{Im}\,\{T_J^{-1} B_J(S')\}_{if}}{(S' - S - i\varepsilon)\, F_{if}(S')}\, \mathrm{d}S'. \tag{3.10}$$

If the approximation is made of neglecting the integral over the left hand cut, which should be reasonable for energies E which are close to threshold, the above is a completely explicit expression in terms of (2.10) and the appropriate Born approximation expression in terms of re-normalized coupling constants.

4. – Applications.

4·1. π-$\mathcal{N}$ *scattering.* – Born approximation for the $I = \frac{3}{2}\, J = \frac{3}{2}$ amplitude is

$$B(E) = -\frac{g^2}{4\pi}\,\frac{(\varepsilon + N)(E - N)}{8k^4 E}\left[-4k^2 + (2\varepsilon\omega - \mu^2)\log\frac{2\varepsilon\omega - \mu^2 + 2k^2}{2\varepsilon\omega - \mu^2 - 2k^2}\right], \tag{4.1}$$

where N and μ are the nucleon and pion masses, ε and ω the corresponding energies and k the centre of mass momentum. In the low energy limit this reduces to

$$B(\omega) \to f^2\,\frac{4k^2}{3\omega}\,, \qquad f^2 = \frac{g^2}{4\pi}\,\frac{1}{4N^2}\,. \tag{4.2}$$

Also

$$S = N^2 + \mu^2 + 2N\omega\,.$$

By (3.4) and (2.10), neglecting the left hand cut,

$$\frac{4f^2}{3}\,\frac{k^3\,\mathrm{ctg}\,\delta}{\omega} = 1 - \frac{4f^2}{3\pi}\,\omega\int\frac{k'^3\,\mathrm{d}\omega'}{\omega'^2(\omega' - \omega)}\,, \tag{4.3}$$

which is the Chew-Low [2] expression (neglecting crossing) for the resonance, the position of which is determined by the cut-off which has to be introduced in the final integral.

4·2. π-π *Scattering.* – For S-wave pion-pion scattering, renormalize so that

$$T(S_0) = 2a(4\pi)^2\,.$$

In the notation introduce above

$$S = 4\omega^2\,, \qquad S_0 = 4\omega_0^2$$

thus, by (3.5) and (2.10) with neglect of left hand cuts

$$\frac{k\,\mathrm{ctg}\,\delta}{\omega} = \frac{1}{a} + \frac{\omega^2 - \omega_0^2}{\pi}\int\frac{2k'\,\mathrm{d}\omega'}{(\omega'^2 - \omega_0^2)(\omega'^2 - \omega^2)}\,.$$

Introducing

$$k^2 = \nu\,,$$

and putting

$$\mu^2 = 1\,,$$

this reduces to

$$\left(\frac{\nu}{\nu+1}\right)^{\frac{1}{2}} \operatorname{ctg}\delta = \frac{1}{a} + \frac{\nu-\nu_0}{\pi}\int \frac{\nu'^{\frac{1}{2}}\,\mathrm{d}\nu'}{(\nu'+1)^{\frac{1}{2}}(\nu'-\nu_0)(\nu'-\nu)},$$

which is the explicit solution derived by CHEW and MANDELSTAM [3].

We have thus shown that the proposed approximation reproduces very simply the essential features of previous solutions of the pion-nucleon and pion-pion interactions. The method is not of much significance for these problems since it is not at all clear how the approximation could be improved upon. It has been developed primarily with a view to application to the K-nucleon and $\overline{\mathrm{K}}$-nucleon system for which the requirements of unitarity are already so complicated, that it seems improbable that any programme, even if it sets out to be more sophisticated, will be able, in fact, to include more than has been included here. An analysis of this interaction in terms fof our coupling constants $g_{\mathrm{K}\Lambda}$, $g_{\mathrm{K}\Sigma}$, $g_{\Lambda\pi}$, $g_{\Sigma\pi}$ will be the subiect of a separate publication.

* * *

One of us (G.F.) would like to thank the others and the D.S.I.R. for the hospitality of Imperial College.

RIASSUNTO (*)

Si propone uno schema approssimato per calcolare lo scattering anelastico delle particelle elementari. Lo schema incorpora pienamente le esigenze di unitarietà e comprende in parte le causalità. Applicato a semplici problemi dello scattering π-p e π-π riproduce in maniera semplice alcuni ben noti risultati.

(*) *Traduzione a cura della Redazione.*

On the Influence of Weak Interactions on Electromagnetic Properties of Fermions.

A. M. Brodski and D. Ivanenko

Physical Faculty of the Moscow University - Moscow

(ricevuto il 23 Febbraio 1960)

Summary. — Starting from the product of two currents for the description of Fermi-type interactions, one gets in the case of an external variable electromagnetic field a new specific effective kinematic magnetic moment in the equations of particles.

We sahll consider here electromagnetic properties of fermions which are due to universal Fermi-interaction, in the 1-st order in constants e and G. Let us concentrate our attention on nucleons, afterwards an obvious generalization to other fermions will follow immediately. It is well known that representing the interaction Lagrangian as a product of currents leads to terms of self-interaction type of the form

$$[p, n]^2 = \bar{p}\gamma_\mu(1+\gamma_5)n,\ \bar{n}\gamma_\mu(1+\gamma_5)p\,,$$

$$[\nu, \mu]^2 = \bar{\nu}\gamma_\mu(1+\gamma_5)\mu,\ \bar{\mu}\gamma_\mu(1+\gamma_5)\nu\,,\quad \text{etc.}$$

which after renormalization of the pseudo-vector current can be written in the form

$$\mathscr{L} = \frac{G}{\sqrt{2}}\{[\bar{p}\gamma_\mu(1+\lambda\gamma_5)n,\ \bar{n}\gamma_\mu(1+\lambda\gamma_5)p]_+ + \zeta[\bar{p}\gamma_\mu\gamma_5 n,\ \bar{n}\gamma_\mu\gamma_5 p]_+\}\,. \tag{1}$$

In absence of renormalization

$$\lambda = 1\,,\qquad \zeta = 0\,. \tag{2}$$

The last relation can be valid for leptons, but due to electromagnetic effects, then ζ is not exactly vanishing. Taking into account the commutation relation and Fierz's relations [1] we get instead of (1)

$$(3)\quad \mathscr{L} = -\frac{G}{\sqrt{2}}\left\{\frac{(1+\lambda)^2+\zeta}{4}[\bar{p}\gamma_\mu(1+\gamma_5)p,\ \bar{n}^c\gamma_\mu(1+\gamma_5)n^c + \right.$$

$$+ \bar{n}\gamma_\mu(1+\gamma_5)n,\ \bar{p}^c\gamma_\mu(1+\gamma_5)p^c] +$$

$$+ \frac{(1-\lambda)^2+\zeta}{4}[\bar{p}\gamma_\mu(1-\gamma_5)p,\ \bar{n}^c\gamma_\mu(1-\gamma_5)n^c + \bar{n}\gamma_\mu(1-\gamma_5)n,\ \bar{p}^c\gamma_\mu(1-\gamma_5)p^c] +$$

$$\left. + \frac{(1-\lambda)^2-\zeta}{2}[\bar{p}(1+\gamma_5)p,\ \bar{n}^c(1-\gamma_5)n^c + \bar{p}^c(1-\gamma_5)p^c,\ \bar{n}(1+\gamma_5)n]\right\}^2.$$

(We use $\psi^c = \gamma_5 C\psi^*$, $C\gamma_\mu = \gamma^* C$, $C^+ = C^{-1}$).

In Lagrangian (4) we see terms of the form

$$(4)\qquad \mathscr{K}\ \bar{\psi}_1 O^c \psi_1,\ \bar{\psi}_2 O^i \psi_2$$

($O^i = (1 \pm \gamma_5)$, $(1 \pm \gamma_5)\gamma_\mu$, $\mathscr{K}$; certain coefficients summing over implicit indices in O^i are understood).

Applying now considerations of our previous work [2] one is able to show that the supplementary term to the mass of the particle 1, due to the presence in the Lagrangian of a term of type (4), has the following form (in 1-st order in $\mathscr{K}$):

$$(5)\qquad \Delta\mathscr{M}^1(x, x') = i\mathscr{K} O^i \operatorname{Tr}[\mathscr{G}^2(x, x')O^i]\,\delta(x - x')\,.$$

Here $\mathscr{G}^2(x, x)$ is the casual propagator for the particle 2, depending generally from external fields. Then we get for the additional term to the expression of the field mass, *e.g.* of a neutron, due to an interaction of the type (3)

$$(6)\qquad \Delta\mathscr{M}^n(x, x') = -\frac{\mathscr{G}}{\sqrt{2}}\left\{\frac{(1+\lambda^2)+\zeta}{2}\gamma_\mu(1+\gamma_5)i\operatorname{Tr}[\mathscr{G}^p(x, x')\gamma_\mu(1+\gamma_5)] + \right.$$

$$- \frac{(1-\lambda)^2+\zeta}{2}\gamma_\mu(1-\gamma_5)i\operatorname{Tr}[\mathscr{G}^p(x, x')\gamma_\mu(1-\gamma_5)] -$$

$$\left. - \frac{(1-\lambda)^2-\zeta}{2}[(1+\gamma_5)i\operatorname{Tr}\mathscr{G}^p(x, x')(1-\gamma_5) + (1-\gamma_5)i\operatorname{Tr}\mathscr{G}^p(x, x')(1+\gamma_5)]\right\}\delta(x, x').$$

---

[1] M. Fierz: *Zeits. f. Phys.*, **107**, 553 (1937).

[2] A. Brodski and D. Ivanenko: *Compt. Rend. Dokl. Ac. Sci. USSR*, **120**, 995 (1958).

where $\mathscr{G}^{\mathrm{p}}(x, x')$ is the propagator for the proton. In the absence of external fields, the first two terms of (6) due to invariance conditions vanish and the last two terms lead to a divergent field mass term

$$\Delta\mathscr{M}^{\mathrm{n}} = \frac{\mathscr{G}}{(2\pi)^2\sqrt{2}}[(1-\lambda)^2-\zeta]\int\frac{(\mathrm{d}p)\,\mathscr{M}^{\mathrm{p}}}{p^2+(\mathscr{M}^{\mathrm{p}})^2}, \tag{7}$$

or after a cut-off at $\mathscr{M}$

$$\Delta\mathscr{M}^{n} \approx \mathscr{G}\cdot\mathscr{M}^2[(1-\lambda)^2-\zeta]\mathscr{M}^{\mathrm{p}}. \tag{7a}$$

It is essential that if the field mass induced by weak interaction happens to be equal for particles with different chirality, this does not lead to parity non-conservation for free particles.

Let us pass now to the case of the presence of an electromagnetic field, when appropriate field depending propagators must be substituted. First of all we see that a static magnetic moment (in the case of a constant electromagnetic field $F_{\mu\nu}$) induced by weak interactions does not exist; in virtue of gauge invariance at $x = x'$ in (6), and of fulfilment of the relations

$$\mathrm{Tr}\,\sigma_{\mu\nu} = \mathrm{Tr}\,\gamma_\alpha\cdot\sigma_{\mu\nu} = \mathrm{Tr}\,\gamma_5\gamma_\alpha\sigma_{\mu\nu} = 0\,, \qquad (\sigma_{\mu\nu} = i/2(\gamma_\mu\gamma_\nu-\gamma_\nu\gamma_\mu)).$$

One may remark that a static magnetic moment would arise only due to tensor Fermi coupling. The absence of such induced moment would be in harmony with exclusion of tensor coupling.

But for variable electromagnetic fields the fields depending terms induced by weak interactions ([1,2]) « in equations for fermions, (1) » coupled with fermions (2), do not vanish. Using in (6) expansions of fermionic, greenian (*i.e.* of Green's function) terms of the external field (cf. ([3])) one gets after some computations in Dirac's equation for particle 1 an additional term

$$\frac{e\mathscr{G}_F\mathscr{M}_2}{(4\pi)^2\sqrt{2}}[(1+\lambda+\zeta)+2\lambda\gamma_5]\int_{\mathscr{M}_2}^{\infty}\frac{\mathrm{d}s}{s}\exp[-\mathscr{M}_2^2 s]\cdot$$
$$\cdot\int_1^{+1}\frac{(1-r)^2\,\mathrm{d}r}{2}\int(2\pi)^{-2}\,\mathrm{d}^4k\,\exp[ikx]\exp\left[-s\,\frac{k^2(1-r)^2}{4}\,k_x\gamma_\beta F_{\alpha\beta}(k)\right]. \tag{8}$$

This term depends only slightly from the cut-off value $\mathscr{M}$ and is diverging logarithmically.

([3]) R. Karplus and A. Klein: *Phys. Rev.*, **85**, 972 (1952).

Such prediction of the new effective kinematic moment described by expression (8) can in principle be detected by observing the behaviour of a neutrino (particle 1 $\equiv \nu$; particle 2 $\equiv \mu, \nu$) or a neutron ($1 \equiv n$; $2 \equiv p$). One may separate the part of effect corresponding to violation of invariance at inversions (cf. (8)).

It is interesting to note that admitting the validity of expression (8) one must expect that the ordinary neutrino and the neutrino of muonic origin (neutretto) would possess different properties in the electromagnetic field. At the end we may remark that one arrives at an expression of the type (8) also if one starts from the non-linear interactions of fermions ([2]), in which case for Fermi's coupling constant must be substituted the constant of non-linear self-interaction and the particles 1 and 2 become identical.

RIASSUNTO (*)

Partendo dal prodotto di due correnti per descrivere interazioni del tipo di Fermi, si ottiene nelle equazioni delle particelle, nel caso di un campo elettromagnetico esterno variabile, un nuovo specifico momento magnetico cinematico effettivo.

(*) *Traduzione a cura della Redazione.*

On the Renormalization of the Axial Vector Coupling Constant in β-Decay.

J. Bernstein (*)

Faculté des Sciences - Orsay (S. et O.)

M. Gell-Mann (**)

Collège de France and Ecole Normale Supérieure - Paris

L. Michel

Faculté des Sciences - Orsay (S. et O.) (***)
Service de Physique Théorique, Groupe II - Orsay (S. et O.)

(ricevuto il 25 Febbraio 1960)

Summary. — The models of the axial vector current discussed by Gell-Mann and Lévy are examined further. Generalized Ward identities are derived for the axial vector weak vertex. It is then shown that in the σ model and the non-linear model the renormalization factor $-G_A/G$ may be expressed as a matrix element in the theory of strong interactions. Thus in the σ model, which is renormalizable, $-G_A/G$ is finite in every order. Since $-G_A/G$ exhibits divergences in the non-linear model, that model is not renormalizable in the usual sense.

1. – Introduction.

A conserved vector current [1,2] has been suggested in order to make the renormalization factor G_V/G of the weak vector current V_λ in β decay equal to unity. The quantity V_λ is taken to be a component of an isotopic vector $\boldsymbol{V}_\lambda$

(*) National Science Foundation Post-Doctoral Fellow.

(**) National Science Foundation Senior Post-Doctoral Fellow. Permanent address: California Institute of Technology, Pasadena, Cal.

(***) Postal address: Laboratoire de Physique Théorique et Hautes Energies, B.P. 12, Orsay (Seine et Oise).

(1) S. S. Gershtein and J. B. Zeldovich: *Žurn. Èksp. Teor. Fiz.*, **29**, 698 (1955).

(2) R. P. Feynman and M. Gell-Mann: *Phys. Rev.*, **109**, 193 (1958).

that is proportional to the isotopic spin current, so that its divergence vanishes.

In an accompanying article [3], a discussion is given of possible theories in which the analogous axial vector current P_α would have its divergence proportional to the pion field:

$$\partial_\alpha \boldsymbol{P}_\alpha = ia\boldsymbol{\pi}\,, \tag{1}$$

where a turns out to be equal to $-\mu_0^2/f_0$ in each case. Here, the theoretical renormalization factor $-G_A/G$ is not unity, and the experimental one is not either, having a value of about 1.25. We should like, of course, to be able to calculate this factor, and it is interesting to see how much we can learn about it by methods analogous to those that give the result $G_V/G = 1$ in the vector case. In particular, we shall be able to prove that in the second and third models considered in *A*, the quantity $-G_A/G$ is expressible as a matrix element of the pion field in the strong interaction theory. Thus in the second model (the σ model), which is renormalizable, the axial vector renormalization factor is finite in all orders. The third model (the non-linear one) gives a logarithmically divergent contribution in second order to $-G_A/G$ and therefore the corresponding theory of the pion strong interaction cannot be renormalizable in the usual sense.

In our work we shall make use of a «generalized Ward identity», which in the case of the conserved vector current gives immediately [4] the result that $G_V/G = 1$. The identity may be derived by a gauge transformation [5] and we shall use the same method to derive the analogous identity for the axial vector current in the models of article *A*. (Generalization to other theories of the axial vector current is not difficult). In the Appendix, the same «generalized Ward identities» for axial vector currents are derived by another method.

2. – The identities.

In the vector case, we have generated the current $\boldsymbol{V}_\alpha$ by means of the infinitesimal gauge transformations of eq. (A.22), such that:

$$N(x) \to (1 + i\boldsymbol{\tau}\cdot\boldsymbol{u}(x))\, N(x) \tag{2}$$

[3] M. Gell-Mann and M. Lévy: to be referred to as A. We shall employ the notation of that article and we shall quote equations from it as (A.1) (A.2), etc.

[4] S. Okubo: *Nuovo Cimento*, **13**, 292 (1959).

[5] R. Utiyama, S. Sunakawa and T. Imamura: *Progr. Theor. Phys.*, **8**, 77 (1952).

and

$$\mathscr{L} \to \mathscr{L} - i\boldsymbol{V}_\alpha \cdot \partial_\alpha \boldsymbol{u} \,. \tag{3}$$

Now the unrenormalized nucleon propagator $S'_F(p)$ is proportional to the Fourier transform of:

$$S'_F(x-y) = \langle T(N(x)\bar{N}(y))\rangle_0 \,, \tag{4}$$

where we have taken the expectation value in the physical vacuum of the T-product of two Heisenberg operators. We may now alter the nucleon fields as in eq. (2) and we can calculate the corresponding change in the propagator (4) by adding a first order perturbation to the Lagrangian, as given in (3). Thus we have:

$$i\boldsymbol{\tau}\cdot\boldsymbol{u}(x)\, S'_F(x-y) - i\, S'_F(x-y)\,\boldsymbol{\tau}\cdot\boldsymbol{u}(y) = \Delta S'_F(x-y) \,, \tag{5}$$

where $\Delta S'_F(x-y)$ is the change induced by the perturbation in (3). If we now go over to momentum space and if we define $\boldsymbol{\Gamma}_\alpha(p', p)$ to be the unrenormalized vertex function corresponding to the current $\boldsymbol{V}_\alpha$, we have:

$$i\boldsymbol{\tau}S'_F(p) - i\, S'_F(p')\boldsymbol{\tau} = -\, S'_F(p')\, k_\alpha \boldsymbol{\Gamma}_\alpha(p', p)\, S'_F(p) \,, \tag{6}$$

where $k = p' - p$. Dividing on the left by $S'_F(p')$ and on the right by $S'_F(p)$, we obtain:

$$i[S'_F(p')]^{-1}\boldsymbol{\tau} - i\boldsymbol{\tau}[S'_F(p)]^{-1} = -\, k_\nu \boldsymbol{\Gamma}_\nu(p'p) \,. \tag{7}$$

We may now transform to renormalized quantities, by multiplying both sides by $-iZ_2$:

$$S_{FC}^{-1}(p')\boldsymbol{\tau} - \boldsymbol{\tau}\, S_{FC}^{-1}(p) = i k_\nu \hat{\boldsymbol{\Gamma}}_\alpha(p', p) \,. \tag{8}$$

Here $\hat{\boldsymbol{\Gamma}}_\nu = Z_2\boldsymbol{\Gamma}_\alpha$ is the effective value of the vertex, often written as:

$$\hat{\boldsymbol{\Gamma}}_\alpha = \frac{Z_2}{Z_1}\boldsymbol{\Gamma}_{\alpha C} \,, \tag{9}$$

where $\boldsymbol{\Gamma}_{\alpha C}(p, p)$ between free spinors of equal momentum acts like $\boldsymbol{\tau}\gamma_\alpha$ with coefficient unity, and Z_2/Z_1 is the renormalization factor G_V/G. In other words, we have, for free nucleons:

$$\bar{u}_f(p)\,\hat{\boldsymbol{\Gamma}}_\alpha(p, p)\, u_i(p) = \bar{u}_f\boldsymbol{\tau}\gamma_\alpha u_i \frac{G_V}{G} \,. \tag{10}$$

From the « generalized Ward identity » (8) it is trivial to see that $G_v/G = 1$. We let $p' \to p$ or $k \to 0$ on each side and to first order in k we have, since $\boldsymbol{\tau}$ commutes with S'_F, the result of Ward:

$$\boldsymbol{\tau} \frac{\partial}{\partial p_\alpha} S_{FO}^{-1}(p) = i \hat{\boldsymbol{\Gamma}}_\alpha (p, p) . \tag{11}$$

But near the mass shell $S_{FO}^{-1}(p) = i\gamma \cdot p + m + O(i\gamma \cdot p + m)^2$, so that:

$$\overline{u}_f(p)\, \hat{\boldsymbol{\Gamma}}_\alpha(p, p)\, u_i(p) = \overline{u}_f \boldsymbol{\tau} \gamma_\alpha u_i , \tag{12}$$

and hence by (10) the renormalization factor is unity. (It should be noticed that if we simply take eq. (8) between free states directly we learn only that $0 = 0$).

Now let us obtain the analogous results for the axial vector current in the second and third models of A. The gauge transformations are those of eq. (A.39) and have the properties:

$$\begin{cases} N \to (1 + i \boldsymbol{\tau} \cdot \boldsymbol{v}\, \gamma_5) N , \\ \mathscr{L} \to \mathscr{L} - i \boldsymbol{P}_\lambda \cdot \partial_\alpha \boldsymbol{v} + a \boldsymbol{\pi} \cdot \boldsymbol{v} . \end{cases} \tag{13}$$

Instead of (8) we get the generalized Ward identity (6):

$$S_{FO}^{-1}(p')\boldsymbol{\tau}\gamma_5 + \boldsymbol{\tau}\gamma_5 S_{FO}^{-1}(p) = i k_\alpha \hat{\boldsymbol{\Gamma}}_{\alpha 5}(p', p) - a\sqrt{Z_3}\, g_1 \frac{\hat{\boldsymbol{\Gamma}}_5(p', p)}{k^2 + m_\pi^2} d_\pi(k^2) , \tag{14}$$

where $\hat{\boldsymbol{\Gamma}}_5$ is the effective pion vertex and the other quantities are defined as in (A.10). The plus sign on the left hand side of eq. (14) results from the anticommutation of $\boldsymbol{\tau}\gamma_5$ with the matrix β in $\overline{N}$.

In the gradient coupling model, the gauge transformations are those of (A.30) and give:

$$\begin{cases} N \to N , \\ \mathscr{L} \to \mathscr{L} - i \boldsymbol{P}_\lambda \cdot \partial_\lambda \boldsymbol{v} + a \boldsymbol{\pi} \cdot \boldsymbol{v} , \end{cases} \tag{15}$$

so that instead of (14) we have:

$$0 = i k_\alpha \hat{\boldsymbol{\Gamma}}_{\alpha 5}(p', p) - a\sqrt{Z_3}\, g_1 \hat{\boldsymbol{\Gamma}}_5(p', p) \frac{d_\pi(k^2)}{k^2 + m_\pi^2} . \tag{16}$$

(6) Identities of this type have been studied in the limit of a conserved axial vector current by S. Weinberg (private communication to J. Bernstein).

In contrast to the vector case, we get a non-trivial result if we just take the matrix element of (14) or (16) between free nucleons, namely:

$$(17) \qquad 0 = ik_\alpha \bar{u}_f(p') \hat{\mathbf{\Gamma}}_{\alpha 5}(p', p) \bar{u}_i(p) - a\sqrt{Z_3} g_1 \frac{d_\pi(k^2) F_\pi(k^2)}{k^2 + m_\pi^2} \bar{u}_f(p') \boldsymbol{\tau} \gamma_5 u_i(p) .$$

But this is an equation that we could have derived directly from (1). In fact, it is obvious from eq. (A.10) and the discussion preceding that equation.

Our weak current being invariant under $GP = CP \exp[i\pi I_y]$, we may write (7):

$$(18) \qquad \bar{u}_f(p') \hat{\mathbf{\Gamma}}_{\alpha 5}(p', p) u_i(p) = -\frac{G_A}{G} \bar{u}_f \boldsymbol{\tau} \gamma_\alpha \gamma_5 u_i \alpha(k^2) + i \bar{u}_f \boldsymbol{\tau} \gamma_5 u_i k_\alpha \beta(k^2) ,$$

where $\alpha(0) = 1$. We then have, from (17) and (18), the important formula:

$$(19) \qquad 2m \left(-\frac{G_A}{G} \right) \alpha(k^2) + k^2 \beta(k^2) = -a\sqrt{Z_3} g_1 \frac{d_\pi(k^2) F_\pi(k^2)}{k^2 + m_\pi^2} ,$$

which contains some familiar results. When $k = 0$ we just get eq. (A.11):

$$(20) \qquad -\frac{G_A}{G} = -a\sqrt{Z_3} \frac{f_1}{m_\pi^2} d_\pi(0) F_\pi(0) .$$

Near the pole, which can occur only in β and not in α, since it comes from a virtual pion, we have:

$$(21) \qquad \beta(k^2) \approx \frac{a\sqrt{Z_3}}{m_\pi^2} g_1 \frac{1}{k^2 + m_\pi^2} ,$$

and since $a\sqrt{Z_3}$ is related to the pion decay amplitude by eq. (A.7), this is just the result of GOLDBERGER and TREIMAN (8) on the induced pseudoscalar interaction. They assume that the pole term dominates even at the value $k^2 = m_\mu^2$ relevant to muon capture; such a result is made plausible by dispersion calculations.

So far we have not really used our generalized Ward identities (14) and (16).

3. – Use of the identities and results.

Let us now consider the identity (14) characteristic of the second and third models and extract new information from it. We put $p^2 = p'^2 = -m^2$, but we do not take matrix elements between free spinors. The GP invariance then

(7) S. WEINBERG: *Phys. Rev.*, **112**, 1375 (1958).
(8) M. L. GOLDBERGER and S. B. TREIMAN: *Phys. Rev.*, **111**, 354 (1958).

allows us to write the two vertex functions in the following way:

$$\hat{\Gamma}_{\alpha 5} = \tau \{\gamma_\alpha \gamma_5 F_1(k^2) + \gamma \cdot k \gamma_5 k_\alpha F_2(k^2) + i\gamma_5 k_\alpha F_3(k^2) + \tag{22}$$
$$+ [\gamma_\alpha, i\gamma \cdot l]\gamma_5 F_4(k^2) + [\gamma \cdot k, i\gamma \cdot l] k_\alpha \gamma_5 F_5(k^2) + \gamma \cdot l \gamma_5 l_\alpha F_6(k^2)\},$$

$$\hat{\Gamma}_5 = \tau \left\{\gamma_5 i\gamma \cdot k \frac{\xi(k^2)}{2m} + \gamma_5 \eta(k^2) + [i\gamma \cdot l, i\lambda \cdot k]\gamma_5 \frac{\zeta(k^2)}{k^2 + 4m^2}\right\}, \tag{23}$$

where $l = (p+p')/2$. With $p^2 = -m^2$, we may write:

$$S_{FO}^{-1}(i\gamma \cdot p) = (i\gamma \cdot p + m)C, \tag{24}$$

where

$$C = (2m)^{-1} S_{FO}^{-1}(i\gamma \cdot p = +m). \tag{25}$$

We may now compute $ik_\alpha \hat{\Gamma}_{\alpha 5}$ as follows:

$$ik_\alpha \hat{\Gamma}_{\alpha 5} = \tau \{i\gamma \cdot k \gamma_5 (F_1 + k^2 F_2) + \gamma_5 (-k^2 F_3) + [i\gamma \cdot k, i\gamma \cdot l]\gamma_5 (F_4 + k^2 F_5)\}. \tag{26}$$

The identity (14) then yields three equations:

$$C = F_1(k^2) + k^2 F_2(k^2) - X(k^2)\,\xi(k^2), \tag{27a}$$

$$2mC = -k^2 F_3(k^2) + 2mX(k^2)\,\eta(k^2), \tag{27b}$$

$$0 = F_4(k^2) + k^2 F_5(k^2) - \frac{2m}{4m^2 + k^2} X(k^2)\,\zeta(k^2), \tag{27c}$$

where

$$X(k^2) = -\frac{a\sqrt{Z_3} g_1}{2m} \frac{d_\pi(k^2)}{k^2 + m_\pi^2} = \frac{\mu_0^2}{k^2 + m_\pi^2} \frac{f_1}{f_0} \sqrt{Z_3} d_n(k^2); \tag{28}$$

we have used the fact that $a = -\mu_0^2/f_0$.

In particular, for $k^2 = 0$, we have:

$$C = F_1(0) - X(0)\,\xi(0), \tag{29a}$$

$$-C = -X(0)\,\eta(0), \tag{29b}$$

$$0 = 2m F_4(0) - X(0)\,\zeta(0). \tag{29c}$$

In order to apply these results, we note that by taking matrix elements of (22) and (23) between free spinors we obtain:

$$-\frac{G_A}{G} = F_1(0) + 2mF_4(0)\,, \tag{30}$$

$$F_\pi(k^2) = \xi(k^2) + \eta(k^2) + \zeta(k^2)\,. \tag{31}$$

By considering the vertex $\hat{\mathbf{\Gamma}}_5$ in the general form (23), we have split the pion form factor F_π into three parts; between free spinors only the sum is important, since all three matrices in (23) look like γ_5 when taken between free nucleons.

If we sum the three relations (29), we simply get back eq. (20). But if we use them separately, we can evaluate the axial vector renormalization factor in terms of the nucleon propagator and the pion vertex:

$$-\frac{G_A}{G} = C\frac{F_\pi(0)}{\eta(0)} = C\frac{F_\pi(0)}{F_\pi(0) - \xi(0) - \zeta(0)}\,. \tag{32}$$

Thus if our strong interaction theory is renormalizable, as in the σ model, the quantity $-G_A/G$ is *finite in every order*. For example, up to second order, we may put: $C = 1 + C_2$, $F_\pi(0) = 1 + F_{\pi_2}$, $\xi(0) = \xi_2(0)$, $\zeta(0) = \zeta_2$. We find $\xi_2 = 0$ and:

$$-\frac{G_A}{G} = 1 + C_2 + \zeta_2 = 1 + \frac{1}{\pi}\frac{g_1^2}{4\pi} + \ldots\,, \tag{33}$$

with m_π and m_σ put equal to zero for simplicity. (As $m_\pi > 0$, both C_2 and ζ_2 have infrared divergences, but they cancel in the sum). It is easy to see that the power series (33) is not much use for calculation, even though the coefficients are finite.

It is also true that if $-G_A/G$ exhibits a divergence in second order, as in the non-linear model, then the corresponding strong interaction theory cannot be renormalizable in the usual sense. In that model, the culprit in second order is ξ_2, which is logarithmically divergent and comes from corrections to the pion vertex due to the term $2f^2 m_0 \tau^2 \bar{N} N$ in the expansion of the Lagrangian $\mathscr{L}_3$ of eq. (A.46).

In the gradient coupling model, the Ward identity (16) leads to equations just like (29) with C replaced by zero, but they tell us nothing new.

Appendix

An alternate method of deriving (14) and (16) may be sketched as follows ([6,9]). If $J_\alpha(y)$ is any current then we may define the vertex $\Gamma_\alpha(u, u', y) = \Gamma_\alpha(u-y, y-u')$ by the equation:

$$\text{(A.1)} \quad \langle T(\bar{N}(x) N(x') J_\alpha(y))\rangle_0 \equiv -\int \mathrm{d}^4u\, \mathrm{d}^4u'\, S'_F(x-u)\, \Gamma_\alpha(u-y, y-u')\, S'_F(u'-x') \,.$$

The notation is as in (4) of the text.

Now it follows from well-known properties of the T symbol that:

$$\text{(A.2)} \quad \frac{\partial}{\partial y_\alpha} \langle T(N(x)\, \bar{N}(x') J_\alpha(y))\rangle_0 = \left\langle T\left(\frac{\partial}{\partial y_\alpha} J_\alpha(y)\, N(x)\, \bar{N}(x')\right)\right\rangle -$$

$$- \delta(x_0 - y_0) \langle T(\bar{N}(x')[N(x), J_0(x)])\rangle_0 - \delta(x'_0 - y_0) \langle T(N(x)[\bar{N}(x'), J_0(y)])\rangle_0 \,.$$

In the familiar case of electrodynamics, and hence also in the case of the vector β-decay current $\boldsymbol{V}_\alpha$, one may write:

$$\text{(A.3)} \qquad \boldsymbol{V}_\alpha = \bar{N}\boldsymbol{\tau}\gamma_\alpha N + \boldsymbol{G}_\alpha \,,$$

where $\boldsymbol{G}_\alpha$ is a function of fields other than the nucleon field, which commutes with the nucleon field at equal times. Hence the equal time commutators in (A.2) may be evaluated explicitly.

Using the definition of $S'_F(x-x')$ and the relation $\partial_\alpha \boldsymbol{V}_\alpha = 0$ we are led at once to (6) when we transform (A.1) and (A.2) into momentum space.

For the second and third models of A we may also write:

$$\text{(A.4)} \qquad \boldsymbol{P}_\alpha = \bar{N}\boldsymbol{\tau}\gamma_\alpha\gamma_5 N + \boldsymbol{G}_{\alpha 5} \,,$$

where $\boldsymbol{G}_{\alpha 5}$ commutes, as above, with N. In this case the equal time commutations give the plus sign noted in (14) and $\partial_\alpha \boldsymbol{P}_\alpha = ia\boldsymbol{\pi}$ gives the last term on the right hand side of (14).

In the pseudovector model we have:

$$[\boldsymbol{G}_{05}, N] \neq 0 \,,$$

at equal times. This is a familiar property of the gradient coupling. However, in the model under consideration we have:

$$\text{(A.5)} \qquad \boldsymbol{P}_\alpha = \bar{N}\boldsymbol{\tau}\gamma_\alpha\gamma_5 N - \frac{i}{f_0}\, \partial_\alpha \boldsymbol{\pi}$$

([9]) Y. Takahashi: *Nuovo Cimento*, **6**, 371 (1957).

and it is easy to see from the pseudovector Lagrangian that the component P_4 is proportional to the field mometum canonical to π. Thus the equal time commutators in (A.2) simply vanish in virtue of the canonical commutation relations and one is led to (16).

RIASSUNTO (*)

Si esaminano ulteriormente i modelli della corrente vettoriale assiale discussi da FEYNMAN, GELL-MANN e LÉVY. Si derivano identità generalizzate di Ward per il vertice debole del vettore assiale. Si mostra poi che nel modello σ e nel modello non lineare il fattore di rinormalizzazione $-G_A/G$ può essere espresso come un elemento di matrice nella teoria delle interazioni forti. Così nel modello σ, che è rinormalizzabile, $-G_A/G$ è finito in ogni ordine. Poichè $-G_A/G$ presenta divergenze nel modello non lineare, questo modello non è rinormalizzabile nel senso usuale.

(*) *Traduzione a cura della Redazione.*

LETTERE ALLA REDAZIONE

(La responsabilità scientifica degli scritti inseriti in questa rubrica è completamente lasciata dalla Direzione del periodico ai singoli autori)

Remarks on the Paper by K. Stiegler: "On the Mechanical Foundation of the Theory of Special Relativity."

(*Nuovo Cimento*, **13**, 873 (1959)).

Z. Janković
Faculty of Science - Zagreb

(ricevuto il 7 Gennaio 1960)

Reading this paper, I found, among other things, that starting with the basic relation (24), the details of the subsequent proof and conclusions up to the end of the paper, can all be found in my thesis published ten years ago: *Prilog izgradnji mehanike* (Odnos klasične mehanike i specijalne teorije relativnosti) - *A Contribution to the Development of Mechanics* (Relation between the Classical Mechanics and Special Theory of Relativity), Zagreb, 1950, the corresponding notations being different in this way: a_1, a_2, b_1, b_2, u, c_1, c_2, A (thesis); a_{11}, a_{12}, a_{21}, a_{22}, v, C, C', α (paper).

Supercurrent and Energy Gap.

R. Suzuki and M. Akano

Department of Physics, Tokyo College of Science - Tokyo

(ricevuto il 12 Gennaio 1960)

The characteristic properties of superconducting states are that the superconductors have no measurable electric resistance below a critical temperature (infinite conductivity) and the macroscopic superconductors are perfectly diamagnetic, *i.e.* no magnetic field can exist inside them (Meissner effect). It has been shown by many authors that these properties are described by means of the energy gap model, and especially with the recent works of BCS [1] and BTS [2] it has been established that the electron-phonon interaction leads to an energy gap in the excitation energy spectrum of systems under condensation. We investigate the existence of a supercurrent from the viewpoint of the energy gap model by means of Bogoljubov's mathematical method, and its derivation is given by the collision operator [3], taking *account of* the multiple scattering of phonons by quasi-particles in intermediate states.

The current density operator in the second order of electric charge is *given from* the transition operator obtained by solving the Møller's wave matrix. However, it must be borne in mind that in solving the wave matrix the electron-phonon and electron-photon interactions are not dealt with as small perturbations simultaneously. Then, we have to investigate the expectation value of the following operator, in view of the London equation, for the unperturbed Bogoljubov ground state:

$$(1) \qquad J = -\frac{1}{V}\frac{\delta T}{\delta A} = -\frac{1}{V}\left\{H_g \frac{1}{a}\frac{\delta}{\delta A}\left((H_{AA} + H_A \frac{1}{a} H_A\right)\frac{1}{a - L} H_g + \right.$$

$$\left. + H_g \frac{1}{a - L} H_g \frac{1}{a}\frac{\delta}{\delta A}\left(H_{AA} + H_A \frac{1}{a} H_A\right) + H_g \frac{1}{a}\frac{\delta}{\delta A}\left(H_A \frac{1}{a - L} H_g \frac{1}{a} H_A\right)\right\},$$

$$a \equiv E_0 - H_0 + i\varepsilon\,,$$

[1] J. Bardeen, L. N. Cooper and J. R. Schriffeer: *Phys. Rev.*, **108**, 1175 (1957).

[2] N. N. Bogoljubov, V. V. Tolmachev and D. V. Širkov: *A New Method of in the Theory of Superconductivity* (Moscow, 1958).

[3] K. A. Brueckner and K. M. Watson: *Phys. Rev.*, **92**, 1023 (1953).

where H_g is the electron-phonon interaction, H_A and H_{AA} the magnetic energy (terms linear and quadratic in the vector potential, respectively), H_0 the energy of free electron and phonon gas, and E_0 the energy of the system. These quantities, of course, are expressed in terms of Bogoljubov's variables α_{ki}, α^*_{ki}. $L \quad H_g(1/a)H_g$ may be interpreted as a potential for the scattering of phonons which is produced by the right H_g and absorbed by the left H_g.

The expectation value of the current density operator is divided into two parts, *i.e.* ordinary term and exchange term according to WENTZEL's [4] nomenclature. The former is not explicitly so dependent on the energy gap as the latter, which vanishes in the limit of zero energy gap, that is to say it is absent in the ordinary perturbation theory. Then, it gives rise to a supercurrent, and finally we have in the limit of zero photon momentum

$$\lim_{\varrho\to 0} J_{AA}^{\text{exch}} = \frac{3\pi}{32}\left[\frac{C}{Sk_F} R \log \frac{\sqrt{c^2+(\xi^2)}+\bar{\xi}}{\sqrt{c^2+(\bar{\xi}^2)}-\bar{\xi}}\right]\frac{1}{2}\varrho J_W \equiv J_s \tag{2}$$

where $\bar{\xi}$ is a mean value of $\xi(=E_k - E_F)$ in the region of $c/2 \leqslant \xi \leqslant c$, and c is the energy gap in the excitation spectrum of the superconductor. R is a resonant function which appears as a trial function in solving the scattering matrix, J_W the London or BCS values for the supercurrent, ϱ Bogoljubov's parameter, $g^2(mk_F/2\pi^2)$, and S the sound velocity in metal

$$R = \begin{cases} \dfrac{1}{1-\frac{1}{2}g^2F(\beta)} = R_0 : & c \to 0 , \\ \dfrac{1}{1-g^2F(\beta)} = R_{\max} : & c = \bar{\xi} , \\ \dfrac{1}{1-\frac{1}{2}g^2F(\beta)} = R_0 : & c \to \infty . \end{cases} \tag{3}$$

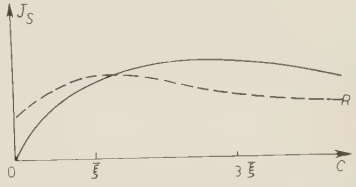

Fig. 1. – While R has a maximum value at $\bar{\xi}$, J_s is maximum at $(2\sim 3)\bar{\xi}$.

$F(\beta)$ is a positive definite function of the cut-off momentum β of the phonon, in the order of magnitude of the electron mass.

As expressed in the above equation, our supercurrent depends essentially on the energy gap, and further it involves the resonant function which has a striking property as indicated in Fig. 1. Therefore, the supercurrent vanishes as $c \to 0$, increases to a maximum value gradually with increasing c, and then decreases slowly owing to the feature of R. MOREVER, there is no contribution to the supercurrent from J_A, *i.e.* the diamagnetic currents do not result from the only iteration of H_A, but rather from H_{AA}. This fact would correspond to the statement of London that the supercurrent is the same state as the diamagnetic current. Further, that the supercurrent have a maximum value in a finite region of the energy gap would mean its metastability. A full discussion will be given in a subsequent paper.

(4) G. WENTZEL: *Phys. Rev.*, **111**, 1488 (1958).

The Canonical Theory of Motion of Charged Particles in External Electromagnetic Fields.

T. Taniuti (*)

Institute for Theoretical Physics, University of Copenhagen

(ricevuto il 14 Gennaio 1960)

In this note we are dealing with the canonical theory of motion of charged particles in external electromagnetic fields. Consider a system of n identical particles with charge e and mass m. When we assume that the motion is subjected mainly to external fields, both the Coulomb interaction and the interaction between the particles and the radiation field may be neglected. Hence, the zero-th order Hamiltonian can be given by

$$\mathscr{H} = \left(\frac{1}{2m}\right)\sum_{k=1}^{n} (\boldsymbol{P}_k - (e/c)\boldsymbol{A}(\boldsymbol{x}_k))^2 + e\sum_{1=k}^{n} V(\boldsymbol{x}_k)\,, \tag{1}$$

where $\boldsymbol{x}_k$ is the position vector of the k-th particle and $\boldsymbol{P}_k$ is the conjugate momentum; $\boldsymbol{A}$ is an external vector potential and V is an external scalar potential. Moreover, in the following discussion, it will be assumed that the magnetic field $\boldsymbol{H}$ has a z-component only and its magnitude is independent of z, and that the electric field $\boldsymbol{E}$ is in the plane perpendicular to $\boldsymbol{H}$, *i.e.*,

$$\boldsymbol{H} = \boldsymbol{e}_z H(x, y)\,, \qquad \boldsymbol{H} \perp \boldsymbol{E}\,.$$

Under the above specialized configuration, the motion governed by the Hamiltonian $\mathscr{H}$ becomes essentially a two-dimensional one. For simplicity, we assume that the particles are moving in the xy-plane. The orbit theory [1] shows that the motion can be separated approximately into two parts, the drift of the guiding center and the gyration about it, if the following conditions for the external field are valid:

$$\begin{cases} |(\boldsymbol{r}_H\cdot\nabla)H| \ll H\,, & |(\boldsymbol{r}_H\nabla)\boldsymbol{E}| \ll |\boldsymbol{E}|\,, \\ |\omega_H^{-1}\,\mathrm{d}H/\mathrm{d}t| \ll H\,, & |\omega_H^{-1}\,\mathrm{d}\boldsymbol{E}/\mathrm{d}t| \ll |\boldsymbol{E}|\,, \end{cases} \tag{2}$$

(*) On leave from Kobe University, Kobe, Japan.

(1) H. Alfvén: *Cosmical Electrodynamics* (Oxford, 1950).

where r_H is the radius of the gyration and ω_H is its frequency. This separation will be done on the basis of a canonical transformation.

Suppose that all n identical particles are gyrating around the same guiding center. Introduce a collective coordinate [2] $\boldsymbol{\xi}$ and its conjugate momentum $\boldsymbol{\pi}$ satisfying the following subsidiary condition:

$$\boldsymbol{\pi} = 0 \,. \tag{1'}$$

Let us first introduce a canonical transformation through a generating function Ω_1 given by the equation

$$\Omega_1 = (\boldsymbol{\pi}' - \sum_k^n \boldsymbol{P}_k') \cdot \boldsymbol{\xi} + \sum_k^n \boldsymbol{x}_k \cdot \boldsymbol{P}_k' \,;$$

then, the subsidiary condition is

$$\boldsymbol{\pi}' = \sum \boldsymbol{P}_k' \,. \tag{3'}$$

By virtue of the relations (2) and (3') we have the transformed Hamiltonian $\mathscr{H}'$ given by the equation

$$\mathscr{H}' = \mathscr{H} = \overline{\mathscr{H}}_0 - (e/mc)\,\boldsymbol{\pi}' \cdot \boldsymbol{A} + (e^2/mc^2) \sum_k^n D_k \boldsymbol{A} \cdot \boldsymbol{A} + (e^2/2mc^2) \sum_k^n D_k^2 \boldsymbol{A} \cdot \boldsymbol{A} + \tag{3}$$

$$+ (ne^2/2mc^2)\,\boldsymbol{A}^2 + enV + e \sum_k^n (D_k V + \tfrac{1}{2} D_k^2 V) + 0(|\nabla H|^2, |\nabla \boldsymbol{E}|^2) \,,$$

in which all field variables $\boldsymbol{A}$ and V are functions of $\boldsymbol{\xi}$ and t, independent of $\boldsymbol{x}_k'$, and D_k and $\mathscr{H}_0$ are defined as follows:

$$D_k = (\boldsymbol{x}_k' \cdot \nabla_\xi) \,,$$

$$\overline{\mathscr{H}}_0 = (1/2m) \sum_k^n (\boldsymbol{P}_k' - (e/c) D_k \boldsymbol{A}(\boldsymbol{\xi}, t) - (e/2c) D_k^2 \boldsymbol{A}(\boldsymbol{\xi}, t))^2 \,.$$

We now introduce the second canonical transformation through a generating function Ω_2 given by the equation

$$\Omega_2 = \sum_k^n (\boldsymbol{P}_k'' - \boldsymbol{\alpha}(\boldsymbol{\xi}, t)) \cdot \boldsymbol{x}_k' + \boldsymbol{\pi}'' \cdot \boldsymbol{\xi}' \,,$$

where $\boldsymbol{\alpha}$ is a vector, each component of which is a function of $\boldsymbol{\xi}$ and t. The explicit functional form of $\boldsymbol{\alpha}$ will be specified later so that $\boldsymbol{\xi}$ becomes the position vector of the guiding center. Performing this transformation and omitting primes, we

---

[2] D. TER HAAR: *Introduction to the Physics of Many Body Problem* (New York, 1958), § 6·4.

obtain the new subsidiary condition

$$\sum_k^n \boldsymbol{P}_k = \boldsymbol{\pi} + n\boldsymbol{\alpha} - \sum_k^n \nabla_\xi(\boldsymbol{\alpha}\cdot\boldsymbol{x}_k)\,, \tag{4'}$$

and the transformed Hamiltonian $\mathscr{H}$ given by the equation

$$\mathscr{H} = \mathscr{H}' + \partial\Omega_2/\partial t = \mathscr{H}_p + \mathscr{H}_d - (e/2c)\sum_k^n \boldsymbol{u}\cdot D_k^2\boldsymbol{A} - \tag{4}$$

$$- (e/2mc)\sum_k^n (\boldsymbol{P}_k - (e/c)D_k\boldsymbol{A})\cdot D_k^2\boldsymbol{A} + (e/2)\sum_k^n D_k^2 V + \sum_k^n \boldsymbol{F}\cdot\boldsymbol{x}_k\,,$$

where $\boldsymbol{F}$, $\boldsymbol{u}$, $\mathscr{H}_p$ and $\mathscr{H}_d$ are defined by the following equations:

$$\boldsymbol{F} = m(\partial/\partial t + (\boldsymbol{u}\cdot\nabla))\boldsymbol{u} - e\{\boldsymbol{E} + (1/c)[\boldsymbol{u}\times\boldsymbol{H}]\}\,, \tag{5}$$

$$\boldsymbol{u} = -(1/m)(\boldsymbol{\alpha} + (e/c)\boldsymbol{A})\,, \tag{6}$$

$$\mathscr{H}_p = (1/2m)\sum_k^n (\boldsymbol{P}_k - (e/c)D_k\boldsymbol{A})^2\,, \tag{7}$$

$$\mathscr{H}_d = -(mn/2)\boldsymbol{u}^2 - (ne/c)\boldsymbol{u}\cdot\boldsymbol{A} + enV + \boldsymbol{u}\cdot\boldsymbol{\pi}\,. \tag{8}$$

It should be noted that all the quantities $\boldsymbol{\pi}$, $\boldsymbol{u}$, $\boldsymbol{A}$ and V are functions of $\boldsymbol{\xi}$ and t. The velocity of the guiding center is given by the equation

$$\mathrm{d}\boldsymbol{\xi}/\mathrm{d}t = \partial\mathscr{H}/\partial\boldsymbol{\pi} = \boldsymbol{u}\,.$$

If both $\boldsymbol{E}$ and $\boldsymbol{H}$ are constant, and $\boldsymbol{\alpha}$ is specified as a solution of the equation $\boldsymbol{F}=0$, *i.e.* $\boldsymbol{E}+(1/c)[\boldsymbol{u}\times\boldsymbol{H}]=0$, then $\mathscr{H}$ becomes a sum of $\mathscr{H}_p$ and $\mathscr{H}_d$. $\mathscr{H}_p$ is obviously that part of the Hamiltonian which corresponds to the gyration around the guiding center or $\mathscr{H}_p$ may be considered as representing internal degrees of freedom of particles, $\mathscr{H}_d$ is the Hamiltonian of the guiding center. If $\boldsymbol{H}$ is not constant, then the third and the fourth terms in (4) give the interaction between the gyration specified by $\mathscr{H}_p$ and the drift by $\mathscr{H}_d$. However, the effect of the interaction can easily be renormalized as an additional drift. Introducing a vector $\boldsymbol{G}$, each component of which is a function of $\boldsymbol{\xi}$ and t, we can rewrite (4) as follows:

$$\mathscr{H} = \mathscr{H}_p + \mathscr{H}_d - (e/2mc)\sum_k^n (\boldsymbol{P}_k - (e/c)\boldsymbol{A})D_k^2\boldsymbol{A} - (e/2c)\sum_k^n \boldsymbol{u}\cdot D_k^2\boldsymbol{A} + \tag{9}$$

$$+ (e/2)\sum_k^n D_k^2 V + \sum_k^n \boldsymbol{G}\cdot\boldsymbol{x}_k + \sum_k^n (\boldsymbol{F}-\boldsymbol{G})\cdot\boldsymbol{x}_k\,.$$

If we now put the equation

$$\boldsymbol{F} - \boldsymbol{G} = 0\,, \tag{10}$$

then the equation of motion for the internal degrees of freedom becomes

$$(11) \quad m\,\mathrm{d}\boldsymbol{v}_k/\mathrm{d}t = (e/c)[\boldsymbol{v}_k \times \boldsymbol{H}(\boldsymbol{\xi}, t)] + (e/c)[\boldsymbol{v}_k + D_k\boldsymbol{H}] + (e/c)\,D_k[\boldsymbol{u}\times\boldsymbol{H}] + eD_k\boldsymbol{E} - \boldsymbol{G}\,.$$

In the above equation, the 2nd, the 3rd, and the 4th terms on the right-hand side can be considered as representing a perturbation force. Substituting for $\boldsymbol{v}_k$ and $\boldsymbol{x}_k$ in these terms the zero-th order solutions, and averaging over one period of gyration, we get

$$m\,\mathrm{d}\boldsymbol{v}_k/\mathrm{d}t \doteqdot (e/c)[\boldsymbol{v}_k \times \boldsymbol{H}] - \mu\boldsymbol{\nabla}_{\xi} H - \boldsymbol{G}\,,$$

in which μ is the magnetic moment [1].

Therefore, if we assume the following form of $\boldsymbol{G}$,

$$\boldsymbol{G} = -\mu\boldsymbol{\nabla}H\,,$$

then the total Hamiltonian $\mathscr{H}$ may be given effectively by the equation

$$\mathscr{H} \doteqdot \mathscr{H}_p + \mathscr{H}_d\,,$$

so far as the motion averaged over a time interval ω_H^{-1} is considered. The drift velocity of the guiding center is given by the equation

$$\mathrm{d}\boldsymbol{\xi}/\mathrm{d}t = \boldsymbol{u}\,.$$

The velocity $\boldsymbol{u}$ is of course given by a solution of the field equation

$$m(\partial/\partial t + \boldsymbol{u}\cdot\boldsymbol{\nabla})\boldsymbol{u} = e\{\boldsymbol{E} + (1/c)[\boldsymbol{u}\times\boldsymbol{H}]\} - \mu\boldsymbol{\nabla}H\,.$$

However, as is obvious from our assumptions, $\boldsymbol{u}$ should change slowly over the distance r_H and the time ω_H^{-1}. Hence, we have to restrict our solutions to those satisfying these conditions. In the present canonical formalism, the adiabatic invariance of the magnetic moment results as a consequence of the general theorem [3].

---

[3] H. C. Corben and P. Stehle: *Classical Mechanics* (New York, 1950), § 72.

Lie Relations Associated with Relativistic Rotators and Bilocal Theory.

F. Halbwachs and J. P. Vigier
Institut Henri Poincaré - Paris

(ricevuto il 18 Gennaio 1960)

In a recently published paper (1) we have developed a classical model of relativistic rotating fluid droplet whose global behaviour is summarized by the evolution laws of a linear momentum G_μ and a proper angular momentum $S_{\mu\nu}$ localized at a definite point Y_μ of the droplet (center of matter density) (2). The corresponding evolution laws can be derived from a Lagrangian depending on vector variables b_μ^ξ (the so-called Einstein-Kramer variables) and their derivatives with respect to the proper time of the point Y_μ: $\dot{b}_\nu^\xi$. These vectors, which build an orthonormal tetrad, are bound to the unitary velocity of the point Y_μ, which is colinear to the fourth one b_μ^4. Then the invariance of the Lagrangian $L(\dot{Y}_\mu, b_\mu^\xi, \dot{b}_\mu^\xi)$ under an infinitesimal inhomogeneous Lorentz transformation yields, according to a well known procedure (3), a set of tensor relations for two tensor quantities:

$$G_\mu = \frac{\partial L}{\partial \dot{Y}_\mu}, \qquad S_{\mu\nu} = b_\mu^\xi \frac{\partial L}{\partial \dot{b}_\nu^\xi} - b_\nu^\xi \frac{\partial L}{\partial \dot{b}_\mu^\xi},$$

which are just the above mentionned linear and angular momenta, namely:

$$\dot{G}_\mu = 0 \qquad \text{and} \qquad \dot{S}_{\mu\nu} = G_\mu \dot{Y}_\nu - G_\nu \dot{Y}_\mu .$$

Now it is suitable to take under consideration the fundamental algebraic relations of the invariance group, namely the Lie commutation formulae, which govern the generating operators of the infinitesimal inhomogeneous Lorentz group, $\mathscr{P}_{\mu(\text{op})}$ and $\mathscr{M}_{\mu\nu(\text{op.})}$. We have:

$$\text{(I)} \qquad \begin{cases} [\mathscr{P}_\mu, \mathscr{P}_\nu] = 0 , \\ [\mathscr{M}_{\mu\nu}, \mathscr{P}_\alpha] = \delta_{\alpha\mu}\mathscr{P}_\nu - \delta_{\alpha\nu}\mathscr{P}_\mu , \\ [\mathscr{M}_{\mu\nu}, \mathscr{M}_{\alpha\beta}] = \delta_{\mu\alpha}\mathscr{M}_{\nu\beta} + \delta_{\nu\beta}\mathscr{M}_{\mu\alpha} - \delta_{\nu\alpha}\mathscr{M}_{\mu\beta} - \delta_{\mu\beta}\mathscr{M}_{\nu\alpha} . \end{cases}$$

(1) F. Halbwachs, P. Hillion and J. P. Vigier: *Nuovo Cimento*, **15**, 209 (1960).
(2) D. Bohm and J. P. Vigier: *Phys. Rev.*, **109**, 1882 (1958).
(3) F. Halbwachs and J. P. Vigier: *Compt. Rend. Acad. Sci.*, **248**, 490 (1959).

The application of the usual correspondence principle implies a connection between the latter operators and tensor quantities constant in time. If we assume that to $\mathscr{P}_{\mu(\text{op.})}$ corresponds the linear momentum $G_\mu = \partial L/\partial \dot{Y}_\mu$ and to $\mathscr{M}_{\mu\nu\text{op.})}$ corresponds the *total* angular momentum $M_{\mu\nu} = q_\mu^{(r)}(\partial L/\partial \dot{q}_\nu^{(r)}) - q_\nu^{(r)}(\partial L/\partial \dot{q}_\mu^{(r)})$ (the $q_\mu^{(r)}$ are all the variables), we get:

$$M_{\mu\nu} = Y_\mu \frac{\partial L}{\partial \dot{Y}_\nu} - Y_\nu \frac{\partial L}{\partial \dot{Y}_\mu} + b_\mu^\xi \frac{L\partial}{\partial \dot{b}_\nu^\xi} - b_\nu^\xi \frac{\partial L}{\partial \dot{b}_\mu^\xi} = Y_\mu G_\nu - Y_\nu G_\mu + S_{\mu\nu},$$

according to the above recalled general formalism.

Let us recall that: $\dot{G}_\mu = 0$ and $\dot{S}_{\mu\nu} = G_\mu \dot{Y}_\nu - G_\nu \dot{Y}_\mu$. We can then establish the remarkable result that the classical Poisson brackets between G_μ and $M_{\mu\nu}$ satisfy relations (1). In order to show this, let us use the canonical momenta calculated in our above quoted paper [1]. Besides $G_\mu = \partial L/\partial \dot{Y}_\mu$, we have the four-momenta: $\beta_\mu^\xi = \partial L/\partial \dot{b}_\mu^\xi$, so that the canonical expression of our functions are:

$$G_\mu = G_\mu, \qquad M_{\mu\nu} = Y_\mu G_\nu - Y_\nu G_\mu + b_\mu^\xi \beta_\nu^\xi - b_\nu^\xi \beta_\mu^\xi.$$

Then the three sets of Poisson brackets become indeed:

$$(2) \qquad \begin{cases} [G_\mu, G_\nu] = 0, \\ [M_{\mu\nu}, G_\alpha] = \delta_{\alpha\mu} G_\nu - \delta_{\alpha\nu} G_\mu, \\ [M_{\mu\nu}, M_{\alpha\beta}] = \delta_{\mu\alpha} M_{\nu\beta} + \delta_{\nu\beta} M_{\mu\alpha} - \delta_{\nu\alpha} M_{\mu\beta} - \delta_{\mu\beta} M_{\nu\alpha}, \end{cases}$$

which establishes the fact that the Poisson bracket relations between the tensor functions have exactly the same form as the algebraic Lie relations concerning the commutators between the generating operators of the invariance group.

As L. de Broglie often emphasized [4], a quantity like $M_{\mu\nu}$ which contains the coordinates Y_μ of a physical point with respect to an arbitrary origin, has no physical meaning, and it is more suitable to refer the total angular momentum to another physical point travelling along with the droplet, an idea which transfers us very naturally into the frame of a « bilocal » model. Such a point is just provided by the so-called « center of gravity » X_μ [1], which moves parallel to G_μ with a constant velocity. The vector R_μ joining X_μ to Y_μ is known to be [5]:

$$R_\mu \equiv Y_\mu - X_\mu = \frac{1}{M^2 c^2} S_{\mu\nu} G_\nu,$$

where M is a constant given by: $-M^2 c^2 = G_\mu G_\mu$; thus we have to introduce a third angular momentum

$$\mathscr{M}_{\mu\nu} = S_{\mu\nu} + R_\mu G_\nu - R_\nu G_\mu = M_{\mu\nu} - X_\mu G_\nu + X_\nu G_\mu,$$

---

(4) L. de Broglie: *Théorie des particules de spin* $\frac{1}{2}$ (Paris, 1952), chap. IV.
(5) F. Halbwachs: *Théorie relativiste des fluides à spin* (Paris, 1960), chap. II.

which splits in a very natural way into the « proper » momentum and an « orbital » momentum with respect to X_μ, and has thus a clear physical meaning. $\mathcal{M}_{\mu\nu}$ is also a constant, because $\dot{\mathcal{M}}_{\mu\nu} = -\dot{X}_\mu G_\nu + \dot{X}_\nu G_\mu$ and $\dot{X}_\mu$ is colinear to G_μ.

Now $\mathcal{M}_{\mu\nu}$ easily appears as a linear combination of the ten fundamental constants G_μ and $M_{\mu\nu}$, with constant coefficients: let θ be the proper time of point X_μ: We have:

$$\frac{\mathrm{d}}{\mathrm{d}\theta} X_\mu = \frac{G_\mu}{M} \qquad \text{and hence:} \qquad \frac{\mathrm{d}^2}{\mathrm{d}\theta^2} X_\mu = 0 .$$

Thus X_μ takes the form:

$$X_\mu = \frac{G_\mu}{M}\theta + B_\mu ,$$

B_μ being a constant vector, and $\mathcal{M}_{\mu\nu}$ becomes:

$$\mathcal{M}_{\mu\nu} = M_{\mu\nu} - \left(\frac{G_\mu}{M}\theta + B_\mu\right) G_\nu + \left(\frac{G_\nu}{M}\theta + B_\nu\right) G_\mu = M_{\mu\nu} - B_\mu G_\nu + B_\nu G_\mu .$$

If we carry this expression in relation (2), and take into account the distributivity properties of Poisson brackets, we get:

$$(3) \qquad \begin{cases} [G_\mu, G_\nu] = 0 , \\ [\mathcal{M}_{\mu\nu}, G_\alpha] = \delta_{\alpha\mu} G_\nu - \delta_{\alpha\nu} G_\mu , \\ [\mathcal{M}_{\mu\nu}, \mathcal{M}_{\alpha\beta}] = \delta_{\mu\alpha}\mathcal{M}_{\nu\beta} + \delta_{\nu\beta}\mathcal{M}_{\mu\alpha} - \delta_{\nu\alpha}\mathcal{M}_{\mu\beta} - \delta_{\alpha\beta}\mathcal{M}_{\nu\alpha} , \end{cases}$$

that is once more a set of relations formally analogous to those of Lie, with Poisson brackets replacing commutators. This set relates the most physically meaningful quantities.

The present result may be easily applied to the relativistic Nakano rotator whose rotation energy takes the « hyperspherical » form: $T = \frac{1}{4} I \omega_{\mu\nu}\omega_{\mu\nu} = \frac{1}{4} I \dot{b}_\mu^\xi \dot{b}_\mu^\xi$ considered in our quoted paper, and which we have developed in many subsequent papers [6,7].

[6] F. HALBWACHS: *Compt. Rend. Acad. Sci.*, **249**, 2293, 2500 (1959); L. DE BROGLIE, P. HILLION and J. P. VIGIER: *Compt. Rend. Acad. Sci.*, **249**, 2225 (1959); F. HALBWACHS, P. HILLION and J. P. VIGIER: *Formalisme hamiltonien associé au rotateur de Nakano, Compt. Rend. Acad. Sci.*: **250**, 471 (1960).

[7] D. BOHM, P. HILLION, T. TAKABAYASI and J.-P. VIGIER: *Relativistic rotators and bilocal theory*, in print in *Progr. Theor. Phys.*

IL NUOVO CIMENTO Vol. XVI, N. 3 1° Maggio 1960

Antwort auf die Bemerkungen von Z. Janković zu meiner Abhandlung: "On the Mechanical Foundation of the Theory of Special Relativity."

(*Nuovo Cimento*, **13**, 873 (1959))

K. Stiegler
München

(ricevuto il 28 Gennaio 1960)

Hinsichtlich der Bemerkungen von Z. Jancović zu meiner oben genannten Abhandlung muß ich folgende wesentliche Tatsachen erwähnen: Das Axiomensystem in meiner Abhandlung und dasjenige auf dem der genannte Verfasser in seiner Abhandlung "*Über die Beziehung der klassischen Mechanik und der speziellen Relativitätstheorie*" (Z. Jancović: *Doktor-Dissertation*, Zagreb, 1950), seine Betrachtungen gründet *unterscheiden sich wesentlich*. In meiner oben erwähnten Abhandlung sind die grundlegenden Formeln der speziellen Relativitätstheorie für die Masse, und Energie der materiellen Korpuskeln in Bewegung, die Existenz der Grenzgeschwindigkeit sowie das Prinzip der Konstanz der Grenzgeschwindigkeit die logischen Folgerungen des am Anfang der Abhandlung gegebenen Systems von fünf Axiomen, wobei die Masse eines materiellen Teilchens in Ax. 2 und Ax. 3 eine noch ganz *unbestimmte* Funktion der Geschwindigkeit bedeutet. (Siehe S. 874 und 875 meiner Abhandlung).

Ich muß an dieser Stelle noch einige wesentliche Momente hervorheben und zwar *erstens*, daß das Axiomensystem des genannten Verfassers die *explizit* gegebene Formel der speziellen Relativitätstheorie für die Masse eines Materiellen Teilchens in Bewegung als ein Axiom der Mechanik enthält, und daß *er zweitens behauptet*, daß die Beziehung

$$(*) \qquad \frac{\mathrm{d}m(\dot{x})\dot{x}}{\mathrm{d}t} = \frac{\mathrm{d}m(\dot{x}')\dot{x}'}{\mathrm{d}t'} \ ,$$

(das ist in meiner Abhandlung das Ax. 5 bzw. die Formel (7)) eine notwendige Folgerung des speziellen Relativitätsprinzips ist, aus welcher er dann, mit Hilfe der linearen Transformationen für die Raum und Zeit-Koordinaten und seines Massenaxioms, d.h. der expliziten speziellrelativistischen Formel für die Masse der materiellen Teilchen in Bewegung, die Beziehung welche in meiner Abhandlung mit (24) bezeichnet ist, ableitet.

Es ist vollkommen klar, daß die Beziehung (*) nicht aus dem speziellen Relativitätsprinzip hervorgeht, da aus diesem Prinzip, wenn wir es auf das Newtonsche Grundgesetz der Mechanik anwenden, *nur die Gleichheit der analytischen Form* des Gesetzes in allen Inertialsystemen hervorgeht, d.h. daß wenn die x-Komponente der Kraft im System S,

$$X_s = \frac{\mathrm{d}m(\dot{x})\dot{x}}{\mathrm{d}t}$$

ist, dann im S' die entsprechende Komponente der Kraft dieselbe analytische

Form haben muß, also, daß dann auch

$$X_{s'} = \frac{\mathrm{d}m(\dot{x}')\dot{x}'}{\mathrm{d}t'},$$

ist und weiter nichts. Es folgt aus diesem Prinzip noch keine Gleichheitsbeziehung zwischen den genannten Komponenten d.h. aus dem speziellen Relativitätsprinzip (bei mir das Ax. 4) *geht nicht* die Beziehung (∗) hervor. Auf diese wichtige Tatsache hat mich noch im Jahre 1951 der verstorbene Professor Wolfgang Pauli in einem Briefe vom 6. November aufmerksam gemacht (1). Diese Gleichheit muß man postulieren als ein selbstständiges Axiom was ich schon in meiner Abhandlung *Sur les rapports entre le principe de Maupertuis-Lagrange et celui de Fermat d'une part et la théorie de la Relativité restreinte et la Mécanique ondulatoire d'autre part* (*Ac. Roy. Belgique, Bull. Cl. Sci.*, Sér. 5, T. 39, pp. 1052-63, Bruxelles, 1953) getan habe.

In der genannten Doktordissertation von Z. Janković ist die Grenzgeschwindigkeit der materiellen Teilchen eine von *vornherein* gegebene Voraussetzung, welche in seinem Massenaxiom, d.h. in seiner als Axiom gegebenen speziellrelativistischen Formel für die Masse der materiellen Teilchen in Bewegung, schon enthalten ist.

In meiner Theorie ist die Existenz der Grenzgeschwindigkeit die notwendige Folgerung aus der Formel (12) für die Masse der materiellen Teilchen in Bewegung, welche aus dem Ax. 2 (dieses besteht nicht bei Z. Janković) und Ax. 3 hervorgeht.

Da die Beziehung (24) in meiner Abhandlung, auf welcher Z. Janković seine Bemerkungen aufbaut, bei mir die notwendige Folgerung des Ax. 1, Ax. 2, Ax. 3 und Ax. 4 ist, wird auch die grundlegende Beziehung (40)

$$C = C',$$

(d.h. das Prinzip der Konstanz der Grenzgeschwindigkeit) welche aus (24) hervorgeht, wieder die notwendige Folgerung dieser Axiomen (2).

Die Beziehung (24) wird bei dem genannten Verfasser mittels der linearen Transformationen für die Raum- und Zeit-Koordinaten, der expliziten als Axiom gegebenen speziellrelativistischen Formel für die Masse eines materiellen Teilchens in Bewegung sowie der Beziehung (∗) abgeleitet, also *ganz anders* als in meiner Abhandlung.

Es ist auch der gegenseitige Zusammenhang der Konstanz der Masse mit der absoluten Zeit Newtons in meiner Abhandlung eine notwendige logische und physikalische Folgerung der Beziehung (36), Ax. 1 und des Ax. 5, welches im Axiomensystem von Z. Janković *nicht besteht*. Da bei Z. Janković die Formel (∗) als notwendige Folgerung des speziellen Relativitätsprinzips gedeutet wird, geht auch der Zusammenhang der gegenseitigen Abhängigkeit der Konstanz der Masse mit der absoluten Zeit als notwendige Folgerung aus diesem Prinzip hervor, was in Wirklichkeit, wie wir schon oben erwähnt haben, eine fehlerhafte Schlußfolgerung darstellt (3).

Auf Grunde von allen diesen hervogehobenen Verschiedenheiten in der Art der logischen und physikalischen Folgerungen aus den zwei gegebenen wesentlich verschiedenen Axiomensyste-

(1) Die Photokopie des Briefes von W. Pauli befindet sich bei der Redaktion von *Il Nuovo Cimento*.

(2) Vergleiche meine Abhandlungen: *Proc. Phys. Soc.* (*London*), **71**, 512 (1958); *Il Nuovo Cimento*, **8**, 922 (1958); *Compt. Rend. Ac. Sci.*, **234**, 1250 (1952).

(3) Auf diese fehlerhafte Schlußweise von Z. Janković hat schon M. Hegedušić in seiner Kritik der Doktordissertation des genannten Verfassers aufmerksam gemacht (Siehe: *Naučna Misao*, Bilten br. 2, Zagreb, 1954; Der wissenschaftliche Gedanke, Bulletin no. 2). Auf diese Kritik von M. Hegedušić hat Z. Janković nie eine Antwort Gegeben.

men geht klar hervor, daß sich die Kette der physikalischen Folgerungen in meiner Abhandlung als Ganzheit betrachtet, *wesentlich* von derjenigen in der Doktordissertation von Z. JANKOVIĆ unterscheidet, obwohl sie, wenn *oberflächlich und isoliert* betrachtet, in diesem Teile, welchen Z. JANKOVIĆ in seinem Briefe erwähnt, mit denjenigen in seiner Doktordissertation gegebenen, als identisch erscheinen könnte.

Das Ziel der axiomatischen Untersuchungen besteht in der *Entdeckung der inneren Struktur* einer auf einem gegebenen Axiomensystem gegründeten Theorie und *der subtilen Zusammenhänge* welche zwischen verschiedenen Axiomen und einzelnen Theoremen bestehen, das heißt in der bewußten Erkenntnis der inneren logischen Gegebenheiten. Axiomatisch denken heißt mit Bewußtsein, das heißt wissenschaftlich, denken und nur in diesem Sinne hat die axiomatische Methode ihre volle Berechtigung.

On Mesonic Decays of the Hypernucleus $^3H_\Lambda$.

D. Ivanenko and V. Lulka

Physical Faculty of the Moscow University - Moscow

(ricevuto il 20 Febbraio 1960)

Investigations of various decay channels of the hypernuclei can yield valuable information on the hyperon-nucleon forces as well as on the spins of such nuclei. Picasso and Rosati [1-3] pointed out that the ratio of the decay rates through the channels $^3H_\Lambda \to {}^3He + \pi^-$ and $^3H_\Lambda \to d + p + \pi^-$ indicates a spin value $\frac{1}{2}$ for $^3H_\Lambda$, but the agreement with experiment was not fully satisfactory.

We show that if one takes into account that final state interaction, whose effects were not considered in [1], one gets a far better agreement with experimental results. The interaction of the π^- with the other decay products is small at the energies of interest, and the effect is essentially connected with the final state interaction between proton and deuteron.

The amplitude for Λ decay in the hypernuclei has the form:

$$M = g_S + g_P \frac{(\boldsymbol{\sigma}, \boldsymbol{k})}{k_0},$$

where k_0 is the impulse of the π^- in the decay of a free Λ-particle (~ 101 MeV/c). The square of the matrix elements for the decay $^3H_\Lambda \to p + d + \pi^-$ will depend on the spin j of the hypernucleus $^3H_\Lambda$ and after averaging over spins we get (for the p-d system we have choosen the wave functions given in [4]):

$$(1) \qquad \begin{cases} |M_{if}|^2 = \left(g_S^2 + \frac{1}{9} g_P^2 \frac{k^2}{k_0^2}\right) |I^d|^2 + \frac{8}{9} g_P^2 \frac{k^2}{k_0^2} |I^q|^2, & (j = \tfrac{1}{2}), \\ |M_{if}|^2 = \frac{4}{9} g_P |I^d|^2 + \left(g_S^2 + \frac{5}{9} g_P \frac{k^2}{k_0^2}\right) |I^q|^2, & (j = \tfrac{3}{2}). \end{cases}$$

(1) L. E. Picasso and S. Rosati: *Nuovo Cimento*, **11**, 711 (1959).
(2) M. Leon: *Phys. Rev.*, **113**, 1604 (1959).
(3) R. H. Dalitz: *Phys. Rev.*, **112**, 605 (1958).
(4) R. A. A. Buckingham and H. S. W. Massey: *Proc. Roy. Soc.*, A **1791**, 23 (1942).

where:

$$I^{q,a} = \int \psi^{q,a^+}_{\boldsymbol{k}_f}(\boldsymbol{r}_\Lambda, \boldsymbol{r}_\mathrm{P}, \boldsymbol{r}_\mathrm{n}) \exp\left[-i\,\frac{2}{3}\,\boldsymbol{k}\boldsymbol{\rho}\right] \psi_{^3\mathrm{H}_\Lambda}(\boldsymbol{r}_\Lambda, \boldsymbol{r}_\mathrm{P}, \boldsymbol{r}_\mathrm{n})\, \mathrm{d}\boldsymbol{r}_\Lambda\, \mathrm{d}\boldsymbol{r}_\mathrm{P}\, \mathrm{d}\boldsymbol{r}_\mathrm{n}\,,$$

$$\psi^{a,q}_{k_f} = \exp\left[i\boldsymbol{k}_f\boldsymbol{\rho}\right] + \frac{\exp\left[-ik_f\varrho\right]}{k_f\varrho} \sum_l (-1)^l(2l+1) \exp\left[-i\delta^{q,a}_l\right] \sin\delta^{a,q}_l\, P_l(\cos\theta)\,.$$

Here $\delta^{q,a}_l$ are the phase-shifts in the spin states $\frac{1}{2}$ and $\frac{3}{2}$ ([5]), $\overline{k}$ is the impulse of the π^-, $\overline{k}_f$ the relative impulse of proton and deuteron, and

$$\boldsymbol{\rho} = \boldsymbol{r}_\Lambda - \tfrac{1}{2}(\boldsymbol{r}_\mathrm{P} + \boldsymbol{r}_\mathrm{n})\,.$$

We have taken into account only S and P states in the system p-d, since at the energies of interest the phase-shifts for $l \geqslant 2$ are small.

The final state interaction leads to a dependence of the decay probability for $^3H_\Lambda \to p+d+\pi^-$ from the spin of $^3H_\Lambda$. If this interaction were absent, then $I^q = I^a$, and from (1) we would get a result independent from the spin of the $^3H_\Lambda$, as in ([1]). For the decay in the channel $^3H_\Lambda \to {}^3He+\pi^-$, the matrix elements are given by:

$$(2)\qquad \begin{cases} |M_{if}|^2 = \dfrac{1}{12}\left(9\,g_S^2 + g_P^2\,\dfrac{k^2}{k_0^2}\right)|I|^2\,, & (j=\tfrac{1}{2}),\\[2ex] |M_{if}|^2 = \dfrac{1}{3}\,g_P^2\,\dfrac{k^2}{k_0^2}\,|I|^2\,, & (j=\tfrac{3}{2}),\\[2ex] I = \displaystyle\int \psi^+_{^3\mathrm{He}}(\boldsymbol{r}_\Lambda\,\boldsymbol{r}_\mathrm{P}\,\boldsymbol{r}_\mathrm{n}) \exp\left[-i\boldsymbol{k}\boldsymbol{r}_\Lambda\right] \psi^3_{^3\mathrm{H}_\Lambda}(\boldsymbol{r}_\Lambda\,\boldsymbol{r}_\mathrm{P}\,\boldsymbol{r}_\mathrm{n})\, \mathrm{d}\boldsymbol{r}_\Lambda\, \mathrm{d}\boldsymbol{r}_\mathrm{P}\, \mathrm{d}\boldsymbol{r}_\mathrm{n}\,. \end{cases}$$

Then one can evaluate the ratio of the decay rates for the two channels for each of the two possible values of the spin of the $^3H_\Lambda$.

The effect of Coulomb interaction was taken into account following ([6]). It seems plausible to take $x = g_S^2/g_P^2$ between the limits $1 \leqslant x \leqslant 5$.

Depending on the value of x, the ratio W, defined as

$$W^{(j)} = \frac{\tau(^3\mathrm{H}_\Lambda \to {}^3\mathrm{He}+\pi^-)}{\tau(^3\mathrm{H}_\Lambda \to \mathrm{d}+\mathrm{p}+\pi^-)}\,,$$

will have values between the limits:

$$0.67 \geqslant W^{(\frac{1}{2})} \geqslant 0.53\,; \qquad 1.42 \leqslant W^{(\frac{3}{2})} \leqslant 5.31\,,$$

according to the spin value: $\frac{1}{2}$ or $\frac{3}{2}$.

For a spin value of $\frac{1}{2}$, W is in satisfactory agreement with the experimental

([5]) H. S. W. Massey: *Progr. Nucl. Phys.*, **3**, 263 (1953).
([6]) Y. C. Tang: *Nuovo Cimento*, **10**, 780 (1958).

value, which indicates $W \leqslant 1$. The agreement is better than in previous calculations [1], where values of $W^{\frac{1}{2}}$ greater than one were obtained.

* * *

We express our thanks to Mrs. N. ILINA for the help in numerical calculations.

Note added in proof.

Taking into account interactions in final state at the decay

$$^4\mathrm{He}_\Lambda \to {}^3\mathrm{He} + \mathrm{p} + \pi^-$$

one of us (V. L.) has obtained a very satisfactory agreement with experimental data for angular distributions and energy spectrum.

On the Energy Dependence of the α_{33}-Phase-Shift.

G. Höhler

Institut für theoretische Physik der Universität - München

(ricevuto il 2 Marzo 1960)

The energy dependence of α_{33} is usually discussed in a diagram showing $q^3 \operatorname{ctg} \alpha_{33}/\omega$ as a function of ω (Chew-Low-plot) and it turns out that this function is approximately linear up to $\omega \approx 1.8$. ω is the total energy minus the nucleon mass and q the pion momentum, both in the C.M. system. Above resonance the deviations from the straight line

$$(1) \qquad \frac{q^3}{\omega} \operatorname{ctg} \alpha_{33} = \frac{3}{4f^2}\left(1 - \frac{\omega}{\omega_r}\right),$$

grow very fast, therefore the two-parameter formula (1) cannot be used for a quantitative description of the first resonance, it is only useful on the left wing.

Several authors used a three-parameter Breit-Wigner-formula

$$(2) \quad \operatorname{tg} \alpha_{33} = \frac{\Gamma}{2(\omega_0 - \omega)}; \quad \Gamma = \frac{2(qa)^3}{1 + (qa)^2}\gamma^2.$$

But again, it is not possible to have a good fit for the low and the high energy data at the same time. Furthermore, (2) leads to difficulties with the dispersion relation for the 3-3-amplitude [1].

We are working now on the prediction for the energy dependence of the s- and p-scattering phases according to the dispersion relations of Chew, Goldberger, Low and Nambu [2] without the $1/M$ approximation. The expression $\sin^2 \alpha_{33}/q^3$ occurs frequently in these calculations and we found that its energy dependence is given by a simple formula which is valid inside the limits of error for all measurements above 189 MeV up to 525 MeV [3]:

$$(3) \qquad \frac{\sin^2 \alpha_{33}}{q^3} = A \exp\left[-\frac{\omega}{\sigma}\right],$$

$$A \approx 47.5, \quad \sigma \approx 0.397.$$

Theoretical arguments leading to (3) are not yet known.

The new straight line plot, proposed in this note, has several applications. Fig. 1 shows that always one of the solutions given by the authors at 525, 500, 420 and 333 MeV lies on the straight

---

[1] K. Dietz and G. Höhler: *Zeits. f. Phys.*, **157**, 362 (1959).

[2] G. F. Chew, M. L. Goldberger, F. E. Low and Y. Nambu: *Phys. Rev.*, **106**, 1337 (1957).

[3] For (220 ÷ 333) MeV the phase shifts calculated by Zinov, Korenchenko, Polumordvinova and Tentjukova have been used. I am much indebted to Prof. Pontecorvo for sending me a preprint. 150, 170 MeV: H. Y. Chiu and E. Lomon: *Ann. of Phys.*, **6**, 50 (1959). 420, 525 MeV: M. E. Blevins, M. M. Block and J. Leitner: *Phys. Rev.*, **112**, 1287 (1958). 500 MeV: W. J. Willis: *Phys. Rev.*, **116**, 753 (1959).

line and the other one is excluded. At 500 MeV we have taken the only solutions for which the sign of the

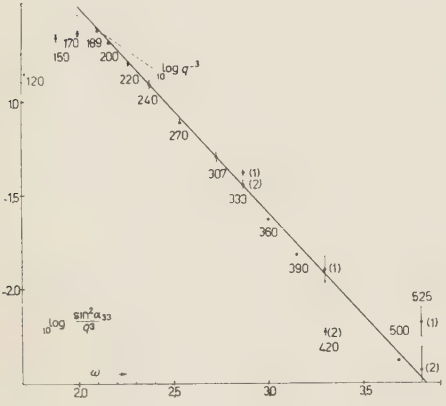

Fig. 1.

D-phases corresponds to the results reported by PONTECORVO [4] at lower energies.

An estimation of the resonance energy leads to values a little below $\omega = 2.10$.

The best way to generalize (3) for all energies is probably to start from

$$(4) \qquad q^{-}(\omega) = A \cdot \frac{\sin^2 \alpha_{33}}{q^3} \exp\left[\frac{\omega}{\sigma}\right].$$

calculated with the experimental α_{33}-values, which shows an almost sharp cut-off at $\omega \approx 2.1$ and is equal to A at threshold.

It is possible now to continue our earlier investigation of the dispersion relation for the 3-3-amplitude [1], because the principal value integral can be evaluated also above resonance if (3) is used. An iteration procedure should lead either to a contradiction between the experimental values and the dispersion relation or to a good interpolation formula for all energies. (3) is also of interest for the closely related question how to describe the resonance quantitatively by a simple model. The resonance follows from a pole of the matrix element of the resolvent in the 2nd sheet of the complex energy plane [5]: $f(z)/(z - z_0)$ and $f(z)$ depends on $\alpha_{33}(E)$.

Finally our formula simplifies all quantitative applications of the isobar model, because the properties of the isobar are given by its quantum numbers and by $\alpha_{33}(E)$.

* * *

I am indebted to K. DIETZ for some calculations.

[4] B. PONTECORVO: *Kiev Conference* (1959).

[5] Cf. the application of Zumino's method by G. HÖHLER: *Zeits. f. Phys.*, **152**, 546 (1958).

On the Anisotropy of Inertia.

S. T. Epstein

The Brace Laboratory of Physics, University of Nebraska - Lincoln, Nebr.

(ricevuto il 28 Marzo 1960)

1. – Recently there has been considerable interest ([1-3]) in the possibility of an anisotropy of inertia, and an upper limit has been placed on the magnitude of such an anisotropy ([3]). However this upper limit has been determined by assuming a specific model, and it is therefore of interest to examine the « model dependence » of such estimates.

In particular it has been assumed that the anisotropy appears only in the kinetic energy terms in the Hamiltonian. However it would seem plausible that the potential energy terms should then also be anisotropic since they are produced by the exchange of quanta, now presumed to have anisotropic inertial properties. Indeed in the next section we will sketch a simple model in which, though the kinetic energy terms and potential energy terms are separately anisotropic, there is an exact cancellation and the total Hamiltonian exhibits no anisotropy. Thus depending on what one assumes concerning the potential energy terms, it would seem that one can get a great variety of predictions.

2. – We start with the Dirac Hamiltonian $\alpha_i p_i + m\beta$ (here we have put $c=1$ and we sum over repeated indices $i, j, \ldots$, the indices running from 1 to 3). A natural generalization to include a possible anisotropy is

$$\alpha_i \Omega_{ij} p_j + m\beta\,, \qquad \Omega_{ij} = \Omega_{ji}\,.$$

Squaring this we obtain as the generalization of the Klein-Gordon operator

$$(1) \qquad p_i \Omega_{ij} \Omega_{jk} p_k + m^2\,,$$

from which the non-relativistic expression for the kinetic energy becomes

$$(p_i \Omega_{ij} \Omega_{jk} p_k)/2m\,,$$

which is the form suggested by Cocconi and Salpeter ([1]).

However (1) further suggests that forces mediated by quanta of mass μ should be derived from the Klein-Gordon operator

$$(2) \qquad p_i \Omega_{ij} \Omega_{jk} p_k + \mu^2\,,$$

([1]) G. Cocconi and E. Salpeter: *Nuovo Cimento*, **10**, 646 (1958).

([2]) A. Carrelli: *Nuovo Cimento*, **13**, 853 (1959).

([3]) G. Cocconi and E. Salpeter: *Phys. Rev. Lett.*, **4**, 176 (1960).

and hence we are led to the potential (the Green's function for (2))

$$V \sim \int \mathrm{d}^3 p \, \frac{\exp\left[i p_j R_j\right]}{p_j \Omega_{sk} \Omega_{kL} p_L + \mu^2},$$

which, by the change of variables $\Omega_{kL} p_L \to p_k$ is seen to be of the form $V = V(\Omega_{rj}^{-1} R_j)$.

Putting all this together we have for the N-particle Hamiltonian of our model

$$\sum_{\alpha=1}^{N} \frac{p_i^{(\alpha)} \Omega_{ri} \Omega_{jk} p_k^{(\alpha)}}{2 m_\alpha} + \\ + \sum_{\alpha,\beta=1}^{N} V_{\alpha\beta}(\Omega_{ij}^{-1} R_j^{\alpha} - \Omega_{ij}^{-1} R_j^{\beta}),$$

which would appear to be extremely anisotropic. However in fact it is not since by the unitary transformation

$$\Omega_{ik} p_k^{(\alpha)} \to p_i^{(\alpha)}, \qquad \pi_i^{(\alpha)} \to \Omega_{ik} R_k^{(\alpha)},$$

it is transformed into

$$\sum_{\alpha=1}^{N} \frac{p_i^{(\alpha)} p_i^{(\alpha)}}{2 m_\alpha} + \sum_{\alpha,\beta=1}^{N} V_{\alpha\beta}(R_i^{(\alpha)} - R_i^{(\beta)}),$$

which is clearly isotropic q.e.d.

We conclude with the following remarks:

(i) Since our N particles could include those of any external sources which may be present, our model implicitly contains the possibility of external fields. However because it is only meant as an illustrative model we will not attempt to refine it by introducing vector (magnetic field) interactions.

(ii) We chose the same Ω_{ij} for the quanta as for the particles, and the same Ω_{ij} for each kind of particle. Any deviation from equality would, of course, yield deviations from exact cancellation

(iii) We have neglected any possible spatial dependence of Ω_{ij}.

LIBRI RICEVUTI E RECENSIONI

Libri ricevuti.

A. Beer: *Vistas in Astronomy*, vol. III, Pergamon Press, London, 1960; pp. 345, £ 6.

L. Brillouin: *Wave Propagation and Group Velocity*; Academic Press, New York, 1959; pp. xi+154. $ 16.00.

R. M. Fano, Lan Yen Chu and R. B. Adler: *Electromagnetic Field, Energy and Forces*; John Wiley and Sons Inc., New York, 1960; pp. xv+520, $ 12.00.

R. Resnick and D. Halliday: *Physics for Students of Science and Engineering*, part I; John Wiley and Sons Inc., New York, 1960; pp. xiv+594, $ 6.00.

Studies in Theoretical Physics - Proceedings in the Summer School of Theoretical Physics, I; Government of India, Ministry of Scientific Research, New Dehli, 1959; pp. v+185, senza prezzo.

Studies in Theoretical Physics - Proceedings in the Summer School of Theoretical Physics, II; Government of India, Ministry of Scientific Research, New Dehli, 1959; pp. i+152, senza prezzo.

Recensioni.

The Lloyd William Taylor Manual of Advanced Undergraduate Experiments in Physics. Sponsored by the American Association of Physics Teachers. T. B. Brown Editor-in-Chief. Addison-Wesley, 1959. 550 pp., 244 figg., prezzo non indicato.

Il crescente interesse mostrato dai giovani per lo studio della fisica in questi ultimi anni ha creato problemi sempre più seri a coloro che sono preposti all'insegnamento ed alla organizzazione dei corsi universitari.

In particolare, i corsi di esercitazioni di laboratorio presentano difficoltà a carattere contingente di spazio e di tempo e di attrezzature, ed altre intrinseche relative alla scelta di temi che siano istruttivi e moderni. Per queste ragioni registriamo con piacere la pubblicazione di questo manuale — dedicato alla memoria di un illuminato insegnante di fisica americano, il prof. L. W. Taylor, scomparso nel 1948 — scritto col principale intento di agevolare la pianificazione di un corso di esercitazioni pratiche.

Le fonti di questo libro sono svariate: il materiale per esso è stato infatti raccolto durante dieci anni da un'apposita commissione che, oltre a spigolare tra le riviste, ha consultato qualche centinaio di istituti di fisica e di privati sottoponendo a ciascuno un questionario.

Il manuale svolge, in forma sintetica, argomenti di esercitazione relativi a tutti i principali rami della fisica. Meccanica, termologia, acustica, ottica ed elettricità e magnetismo occupano altrettanti capitoli; altri tre capitoli sono dedicati ad elettronica, fisica atomica e fisica nucleare; uno, il primo, riassume le regole fondamentali per una corretta analisi dei

dati di osservazione. In questi capitoli il lettore potrà trovare, sfogliando qua e là, giroscopi, oscillatori non lineari, radiazione del corpo nero, punto di Curie, microfoni, filtri acustici, effetto Kerr, ottica delle microonde, transistori, effetto Raman, sonde di Langmuir, sezione d'urto per neutroni ed autoradiografia mescolati a moltissimi altri esercizi più convenzionali.

Può sorprendere come tanti argomenti possano trovare posto in un volume di dimensioni normali: diremo allora che il manuale è concepito in modo da avere una elevata densità di informazione: infatti gli esercizi più ovvi o più noti sono solo richiamati brevemente (ed il lettore è rimandato alla letteratura adatta per maggiori particolari); e solo per alcuni si può trovare una vera descrizione, completa eventualmente di disegni e di grafici. Un'altra ragione che limita la mole del libro è l'aver raccolto le sole esercitazioni ad un certo livello — si veda il sottotitolo — il cui equivalente italiano è, approssimativamente, il terzo anno di fisica. Naturalmente nel manuale si possono trovare molte esercitazioni adatte al primo biennio ed altre, ad esempio quelle di radioattività, che qui vengono per lo più svolte al quarto anno.

Nel complesso ci sembra che l'opera abbia pienamente raggiunto lo scopo e, specie per la sua ricca bibliografia, riuscirà assai utile ad insegnanti e studenti.

R. Cervellati

J. E. Hooper and M. Scharff – *The Cosmic Radiation*. London, Methuen's Monographs on Physical Subjects, 1958.

Un libro semplice, chiaro e generalmente preciso, anche se talvolta la completezza della informazione o dell'analisi é sacrificata al desiderio di brevità e a una certa schematizzazione. Nell'insieme, un'opera utile e, nei limiti propri alla collana cui appartiene, completa.

Una breve introduzione storica introduce i fenomeni essenziali e tipici dovuti alla radiazione cosmica: gli effetti di transizione, quelli geomagnetici, ecc. Sono poi analizzate le tecniche usate nello studio della radiazione cosmica, dopo una rapida ma accurata esposizione della teorica del passaggio di particelle cariche attraverso la materia: contatori, camere ad espansione, emulsioni nucleari. La radiazione primaria è poi studiata in dettaglio, e sono riportati i risultati ottenuti mediante l'uso delle tecniche precedentemente introdotte; la natura della primaria, lo spettro energetico e di carica delle particelle incidenti e la loro intensità, i problemi relativi alla origine della radiazione primaria sono discussi. I successivi capitoli trattano i processi elettromagnetici di alta energia (con un accenno alle teorie sulla cascata elettrofotonica), la degradazione della primaria attraverso l'atmosfera, gli effetti a livello del mare e sotterranei, e infine gli effetti di temperatura e quelli barometrici. Una esauriente bibliografia completa il volumetto, che contiene anche alcune utili tavole sulle relazioni percorso-energia.

B. Vitale

F. Cap – *Physic und Technik der Atomreaktoren*. Pagg. XXIX-487; 100 figure nel testo. Editore Springer-Verlag, Wien, 1957.

L'Autore di questo volume, prende le mosse da una concisa descrizione dei fondamenti di fisica atomica, per coprire in nove densi capitoli tutto il campo che va dalla teoria, costruzione e funzionamento dei reattori nucleari, sino ai problemi di sicurezza che l'uso di tali macchine impone.

I singoli capitoli sono scritti in maniera molto concisa e, crediamo, rendono

il libro particolarmente utile come manuale di consultazione. Tuttavia, poichè il filo logico della esposizione è sempre rigorosamente mantenuto, esso può certamente essere usato anche come libro di studio.

Il capitolo ottavo dà un panorama, aggiornato al principio dell'anno 1957, dei reattori di ricerca e di potenza installati nei vari paesi. Vi viene anche brevemente trattato il problema economico del costo dell'energia elettrica prodotta con i vari tipi di reattori nucleari.

Nel capitolo nono vengono trattati i problemi relativi all'impiego dei reattori, sia per ricerca che per produzione di radioisotopi e per altre applicazioni industriali.

Completa il libro una molto estesa bibliografia, che viene presentata divisa razionalmente per argomenti.

Tabelle, grafici, figure, esempi numerici, rendono il volume particolarmente utile e ne semplificano l'impiego per la consultazione.

I. F. QUERCIA

1958 Annual International Conference on High Energy Physics at CERN. Edited by B. FERRETTI. Stampato dal CERN Scientific Information Service, Ginevra, prezzo 45 Fr. sv.

L'edizione 1958 della conferenza « di Rochester » si è tenuta a Ginevra e si è svolta seguendo il metodo dei rapporteurs. Con questo metodo si ottiene senza dubbio una notevole compattezza di esposizione accompagnata, bisogna dirlo, da quella attenzione che suscitano i grandi nomi della fisica di oggi.

La conferenza è divisa in nove parti: 1) Nucleon structure; 2) e 3) The nucleon and its interaction with pions, photons, nucleons and antinucleons; 4) Fundamental theoretical ideas; 5) e 6) Strange particle interactions; 7) Special theoretical topics; 8) e 9) Weak interactions.

Una decima parte è rappresentata dai « Concluding remarks » di J. R. Oppenheimer. Un'appendice racchiude argomenti sparsi; infine in un'ultima appendice vengono dati, per ogni singola parte, degli opportuni suggerimenti bibliografici.

Le relazioni sono tutte di grande interesse, come ci si poteva aspettare. Tuttavia ci sembra che il nocciolo di questo volume stia quasi nelle discussioni, fedelmente riportate da lodevolissimi segretari. Infatti, è da queste discussioni che si ricava una quantità di idee, dati, opinioni, confrontabili con quelle che si avrebbero in un gran numero di scambi personali, senza la fatica di doverli stimolare. Alcune di queste discussioni hanno addirittura un tono acceso e polemico quale non ci si aspetterebbe in una conferenza scientifica.

Il volume, benchè messo in circolazione a breve distanza di tempo dalla conferenza, si presenta in bella veste tipografica e con pochi errori di stampa.

C. BERNARDINI

G. RAOULT – *Les ondes centimetriques*. Masson et Cie, Editeurs, 120, Boulevard Saint-Germain, Paris, VI^{e}, 1958.

Il libro *Les ondes centimétriques* del Prof. G. Raoult presenta un panorama conciso e praticamente completo nel campo delle applicazioni delle onde centimetriche.

Sia nella presentazione che nella successione degli argomenti trattati, questo libro si stacca notevolmente da altre pubblicazioni (sostanzialmente in lingua inglese) che trattano lo stesso tema. Per esempio le guide d'onda vengono trattate prima delle linee di trasmissione su filo, ecc.

In generale i problemi vengono esaminati sia teoricamente sia praticamente e in molti casi si scende anche nei dettagli costruttivi.

La trattazione matematica è contenuta entro limiti (tranne che nel capitolo dedicato alle antenne) molto elementari, mentre l'enfasi è sempre posta sul lato fisico delle varie questioni.

Credo quindi che l'autore abbia raggiunto lo scopo propostosi e dichiarato nella prefazione di illuminare, e non di approfondire, tutti o quasi i campi della vasta e complessa materia, ricorrendo piuttosto all'intuizione che agli sviluppi analitici.

Particolarmente interessanti ci sono sembrati i capitoli riguardanti la « rivelazione » che comprende anche un poco della teoria dei semi conduttori, e quello sulla radio-astronomia; argomenti questi che in genere non vengono trattati in libri di questo genere.

Manca e sarebbe stato interessante qualche cenno sui problemi che riguardano la tecnologia e parte della teoria dei circuiti a micro-onde di grande potenza; come per esempio i klystron di potenza; gli acceleratori lineari, ecc.

In conclusione si può affermare che questo libro può essere un'utile guida per tutti coloro che, anche senza una certa preparazione matematica, vogliano avere una inquadratura panoramica e precisa nel vasto campo delle applicazioni delle micro-onde.

M. Puglisi

Direttore responsabile: G. POLVANI Tipografia Compositori - Bologna

Questo Fascicolo è stato licenziato dai torchi il 28-V-1960